# Combining Inertial Sensing and Predictive Modeling for Biomechanical Exposure Assessment in Specific Material Handling Work

by

Sol Ie Lim

A dissertation submitted in partial fulfillment
of the requirements for the degree of
Doctor of Philosophy
(Industrial and Operations Engineering)
in the University of Michigan
2019

Doctoral Committee:

Assistant Professor Clive D'Souza, Chair
Professor Thomas Armstrong
Professor Judy Jin
Professor Albert Shih

Sol Ie Lim
solielim@umich.edu
ORCID iD:0000-0001-5569-9312

© Sol Ie Lim 2019

# ACKNOWLEDGMENTS

Above all, I would like to express my deepest gratitude to my advisor Dr. Clive D'Souza for his advice, support, and patience along the way. This work would not have been possible without his support. His excellence and passion in research have helped to shape my interest in research and my decision to pursue a career in ergonomics research. Foremost, he always has a belief in me and my potential as a researcher, which has motivated me to stay focused on research even in difficult times. I also would like to thank the members of my dissertation committee, Dr. Thomas Armstrong, Dr. Judy Jin, and Dr. Albert Shih, for supporting me throughout this process, and for providing their time, expertise, and constructive feedback to improve this dissertation.

I am also grateful to Dr. Bernard Martin, Dr. Sheryl Ulin, Dr. Nadine Sarter, and Dr. Paul Green, for their mentoring and support. I am also appreciative of the excellent staff and administration within the Department of Industrial and Operations Engineering (IOE) and Center for Ergonomics. I thank Eyvind Claxton, Charles Wolley, Christopher Konrad, Olof (Mint) Minto, and Rodney Capps for their gracious technical assistance through all phases of my research projects, and Teresa Maldonado for her generous support.

I want to thank my friends and colleagues who supported me throughout my graduate studies. Firstly, my lunch buddy, Dr. Justin Haney, for his resilience coping with me for the last four years. I am proud that we could successfully finish our degrees at about the same time. I would also like to thank the Center for Ergonomics family - Dr. Ke Liu, Dr. Yuzhi Wan, Yue Luo, Yadrianna Acosta-Sojo, Yidu Lu, Albert Fu, Na Du, Kevin Lieberman, Yifan Li, Kamolnat Tabattanon, and all my students - for their support and encouragement.

This work was funded by the National Institute for Occupational Safety and Health, Centers for Disease Control and Prevention under the training Grant T42-OH008455 and the National Institute on Disability, Independent Living, and Rehabilitation Research under the grant 90IF0094-01-00, and a Rackham Graduate Student Research Grant.

Last, but first in my heart, I would like to thank my parents and family for their unconditional love and support. Finishing my dissertation with my little love, Jason Lee was a bit challenging. With the help of my parents and husband, Sang Won Lee, I was able to keep my smiles throughout the process. I am especially grateful to Sang for being my best friend and mentor all the time.

# TABLE OF CONTENTS

**Acknowledgments** . . . . . **ii**

**List of Figures** . . . . . **vii**

**List of Tables** . . . . . **xii**

**List of Appendices** . . . . . **xv**

**List of Abbreviations** . . . . . **xvi**

**Abstract** . . . . . **xvii**

**Chapter**

**1 Introduction** . . . . . **1**

1.1 Overview . . . . . 1
1.2 Background . . . . . 2
1.2.1 Exposure Assessment in Non-repetitive Jobs . . . . . 2
1.2.2 Wearable Inertial Sensing for Exposure Assessment . . . . . 4
1.3 Research Objectives . . . . . 5
1.4 Conceptual Model . . . . . 7
1.5 Dissertation Outline . . . . . 9

**2 A Review of Inertial Sensing in Biomechanical Exposure Assessment** . . . . . **12**

2.1 Introduction . . . . . 12
2.1.1 Inertial Sensing Technologies . . . . . 13
2.1.2 Modeling−Sensing−Analysis−Assessment−Intervention (MSAAI) Framework . . . . . 14
2.2 Methods . . . . . 17
2.2.1 Search Strategy . . . . . 17
2.2.2 Exclusion Criteria . . . . . 17
2.2.3 Data Extraction and Analyses . . . . . 18
2.3 Results . . . . . 19
2.3.1 Modeling . . . . . 22
2.3.2 Sensing . . . . . 22
2.3.3 Analysis . . . . . 28
2.3.4 Assessment . . . . . 36
2.3.5 Intervention . . . . . 37

2.4 Discussion . . . 37
2.4.1 Modeling, Sensing and Sensor Placement . . . 38
2.4.2 Analysis: Quantifying Exposures and the Use of Predictive Modeling . . . 40
2.4.3 Assessment of Work-related Musculoskeletal Disorder (WMSD) Risk . . . 41
2.4.4 Intervention: Real-time Feedback . . . 41
2.4.5 Study Limitations . . . 42
2.5 Conclusion . . . 42

**3 Quantifying Effects of Load carriage on Gait Kinematics Using Wearable Inertial Sensors . . . 45**

3.1 Introduction . . . 45
3.2 Methods . . . 48
3.2.1 Study Participants . . . 48
3.2.2 Experiment Procedures . . . 48
3.2.3 Instrumentation . . . 50
3.2.4 Data Processing and Dependent Measures . . . 50
3.2.5 Statistical Analyses . . . 53
3.3 Results . . . 54
3.3.1 Temporal Gait Parameters . . . 54
3.3.2 Torso and Pelvis Postural Sway and Coordination . . . 58
3.4 Discussion . . . 62
3.4.1 Analysis of Two-Handed Side Carry . . . 64
3.4.2 Analysis of Two-Handed Anterior Carry . . . 65
3.4.3 Methodological Considerations and Limitations . . . 66
3.5 Conclusion . . . 68

**4 Statistical Classification of Load Carriage Mode and Magnitude from Inertial Sensor Derived Gait Kinematics . . . 69**

4.1 Introduction . . . 70
4.2 Methods . . . 73
4.2.1 Study Participants . . . 73
4.2.2 Experiment Procedures . . . 73
4.2.3 Instrumentation . . . 75
4.2.4 Algorithm to Classify Carrying Mode and Load Level . . . 75
4.2.5 Evaluating Model Performance . . . 80
4.2.6 Interpreting the Classification Model . . . 81
4.3 Results . . . 81
4.3.1 Bayesian Inference Update vs. Averaging . . . 82
4.3.2 Model Performance . . . 82
4.4 Discussion . . . 87
4.4.1 Methodological Contributions . . . 89
4.4.2 Study Limitations . . . 94
4.4.3 Application and Relevance . . . 95

4.5 Conclusion . . . 96

**5 Investigating Generalized Algorithms for Statistical Classification of Load Carriage and Lifting-Lowering Exposures . . . 98**

5.1 Introduction . . . 99
5.1.1 Lifting-lowering and Low Back Disorder Risk . . . 99
5.2 Methods . . . 102
5.2.1 Study Participants . . . 102
5.2.2 Experiment Procedures . . . 103
5.2.3 Instrumentation . . . 105
5.2.4 Algorithm to Classify Carrying Mode and Load Level . . . 106
5.2.5 Algorithm to Classify Lifting-Lowering Height, Hand Mode, and Load Level . . . 109
5.2.6 Evaluating Model Performance . . . 114
5.3 Results . . . 114
5.3.1 Model Performance: Carrying Mode and Load Level . . . 114
5.3.2 Model Performance: Lifting and Lowering Height, Hand Mode, and Load Level . . . 115
5.4 Discussion . . . 118
5.4.1 Statistical Classification of Carried Load Intensity . . . 118
5.4.2 Statistical Classification of Lifting and Lowering Intensity . . . 122
5.4.3 Study Limitations . . . 123
5.4.4 Contributions and Implications for Practice . . . 124
5.5 Conclusion . . . 126

**6 Inertial Sensor-Based Biomechanical Exposure Assessment: Preliminary Framework Implementation . . . 128**

6.1 Introduction . . . 129
6.2 Methods . . . 130
6.2.1 Study Participants . . . 130
6.2.2 Experiment Procedures . . . 131
6.2.3 Instrumentation and Data Segmentation . . . 131
6.2.4 Algorithmic Framework for the Inertial Sensor-Based Biomechanical Exposure Assessment . . . 133
6.2.5 Statistical Analysis . . . 137
6.3 Results . . . 138
6.3.1 Exemplar Output from a Low vs. High Intensity Job Cycle . . . 138
6.3.2 Aggregate Performance Across Low vs. High Intensity Job Cycles 139
6.3.3 Manual Material Handling (MMH) Task Detection . . . 139
6.3.4 MMH Task Condition Classification . . . 145
6.4 Discussion . . . 145
6.5 Conclusion . . . 147

**7 Conclusion . . . 148**

7.1 Summary of Findings . . . 148

7.2 Theoretical Contributions . . . . . 150
7.3 Limitations and Future Research Direction . . . . . 152
7.4 Concluding Remarks . . . . . 154

**Appendices** . . . . . **156**

**Bibliography** . . . . . **181**

# LIST OF FIGURES


1.1 Overview of the proposed framework relating biomechanical principles and empirical findings, wearable inertial sensing, and predictive modeling for quantifying biomechanical exposures associated with low back disorder risk in non-repetitive material handling work. . . . . 5

1.2 Overview of the conceptual model relating the effects of external loads, environment, person variables, and manual material handling task conditions on internal biomechanical loads and measured posture kinematics. Boxes shaded in gray are the primary focus of this research. Elements in bold text were directly manipulated and/or measured, while other elements were held constant or not directly measured. Measured posture kinematics are used for estimating cumulative spinal loads as an indicator of health outcomes, specifically occupationally-relevant low back disorder risk. Fatigue, though not explicitly modeled, is considered to have a mediating effect on posture kinematics, estimated cumulative spinal load, and health outcomes. . . . . 9

1.3 Schematic of the dissertation outline. . . . . 10

2.1 Conceptual framework for biomechanical exposure assessment using wearable inertial sensors spanning Modeling, Sensing, Analysis, Assessment, and Intervention (MSAAI). . . . . 15

2.2 Flowchart summarizing the phases of the document search and selection process. 18

2.3 Summary of the review results in terms of the number of studies by publication year between 1998 and 2017 (a), by field study site where the data collection was performed (b), and by component of the Modeling-Sensing-Analysis-Assessment-Intervention (MSAAI) framework addressed (c). . . . . 20

2.4 Body locations of the inertial sensors across the reviewed studies (n=67). . . . 25

3.1 Images showing the two carrying modes evaluated in this study: (a) two-handed side carry, (b) two-handed anterior carry, along with the location of (c) six inertial sensors attached on the body at T6, S1, thigh (Right, Left), and shank (Right, Left). . . . . 49

3.2 Mean (± standard error) thoracic sway angle (top panel), pelvic sway angle (middle panel) and thoracic-pelvic coordination angle (bottom panel) in the *coronal* plane obtained from the average gait cycle data from N = 9 participants. The figure compares two-handed side carry (left panel) and two-handed anterior carry (right panel) in two of the four load levels, namely, no-load (grey) and High load level at 13.6 kg (colored blue and red for side and anterior carry, respectively). Dotted lines and adjacent numerical values (deg.) in the bottom panel represent the mean relative phase angle averaged over the gait cycle duration, with lower values implying more in-phase or synchronized movements. . . . . 59
3.3 Mean (± standard error) thoracic sway angle (top panel), pelvic sway angle (middle panel) and thoracic-pelvic coordination angle (bottom panel) in the *transverse* plane obtained from the average gait cycle data from N = 9 participants. The figure compares two-handed side carry (left panel) and two-handed anterior carry (right panel) in two of the four load levels, namely, no-load (grey) and High load level at 13.6 kg (colored blue and red for side and anterior carry, respectively). Dotted lines and adjacent numerical values (deg.) in the bottom panel represent the mean relative phase angle averaged over the gait cycle duration, with lower values implying more in-phase or synchronized movements. . . . . 61
3.4 Mean (± standard error) thoracic sway angle (top panel), pelvic sway angle (middle panel) and thoracic-pelvic coordination angle (bottom panel) in the *sagittal* plane obtained from the average gait cycle data from N = 9 participants. The figure compares two-handed side carry (left panel) and two-handed anterior carry (right panel) in two of the four load levels, namely, no-load (grey) and High load level at 13.6 kg (colored blue and red for side and anterior carry, respectively). Dotted lines and adjacent numerical values (deg.) in the bottom panel represent the mean relative phase angle averaged over the gait cycle duration, with lower values implying more in-phase or synchronized movements. . . . . 63

4.1 Images showing the four carrying modes performed in this study: (a) one-handed right hand carry (1H-R), (b) one-handed left hand carry (1H-L), (c) two-handed side carry (2H-Side), (d) two-handed anterior carry (2H-Anterior) along with the location of four inertial sensors attached on the body at T6, S1, and shank (R, L). . . . . 74
4.2 Overview of the carrying mode and load level classification algorithm developed in the study. The right panel shows example classification results for three consecutive gait cycles at a two-handed anterior carry with 50% Maximum Acceptable Weight of Carry (MAWC) load condition. . . . . 76

4.3 Example results from the random forest classification to predict carrying mode for fifteen consecutive gait cycles from a two-handed anterior carry walk trial without (top-panel) and with (bottom-panel) Bayesian inference applied. In each gait cycle, the mode with the highest predicted probability is labeled as the classification result for that gait cycle. In this example, without Bayesian inference applied (top-panel) 3 of the 15 gait cycles were misclassified as either 1H-L (gait cycle #1) or no-load (gait cycle #9 and #10). In the bottom graph, Bayesian inference was applied to the same data and updated the posterior probability of the gait cycle based on prior gait cycles cumulatively. The probability of the data predicted as the correct class (i.e., two-handed anterior carry in this case) exceeded 0.9 after four gait cycles and converged to 1.0 in subsequent cycles. . . . . 83
4.4 Posterior probabilities of the target carrying mode in each walk trial depicted by gait cycles. Misclassified classes are marked as red dotted lines. . . . . 85
4.5 Relative importance (%) of the predictor variables computed as the mean decrease in the Gini index relative to the maximum (100%) for each of the five classification models, namely, for carrying mode (panel A) and for load level (panels B-1 to B-4). . . . . 88

5.1 Overview of the experiment procedures for simulated MMH tasks. . . . . 104
5.2 Sample images in a 1-handed right lifting condition at knee height depicting the three different symmetricity conditions evaluated in the experiment: (a) asymmetric, counter-clockwise (-45 deg.), (b) symmetric, and (c) asymmetric, clockwise (+45 deg.). The distance between the center of the original box location to the middle of the participants' right and left anterior shoe-tip was a constant 40 cm. . . . . 106
5.3 Images showing the four inertial sensors attached on the body at T6, S1, thigh (Right), and shank (Right). . . . . 107
5.4 Hierarchical structure of the classification model for lifting and lowering intensity. Separate classification models were developed for each stage. For example, model-H for classifying height condition (floor vs. knee) and model M1 was developed for classifying hand mode (1H vs. 2H) for a predicted lifting height at floor-level. Load magnitudes of 0 kg (no-load) and and 4.5 kg were categorized as a Low load level, while the 13.6 kg and 22.7 kg load magnitudes were categorized as a High load level. . . . . 110
5.5 Graphical representation of the classification model for load carriage mode and load level for the algorithm with highest prediction accuracy (i.e., *Rel-NL*). Numbers next to each box represent sensitivity (%, above) and precision (%, below) in distinguishing that outcome class from the parent model (i.e., circles labelled M, L1 to L4). Sensitivity and precision values below 70% are indicated in red. . . . . 117

5.6 Graphical representation of the lifting and lowering classification results in terms of sensitivity and precision from the algorithm using *Original* variables. Numbers near each box represent sensitivity (%, top) and precision (%, bottom) in distinguishing that class from the preceding model (denoted using circles). Sensitivity or precision values below 70% are colored in red. . . . . 121
5.7 Probability of each measurement belonging to the high load level in a two-class random forest model (Low vs. High), when lifting (top panel) and lowering (bottom panel) from/to floor height in a one-handed hand mode. Two decision boundaries (0.375 and 0.625, red lines) were drawn to create a medium load level between the low ($p < 0.375$) and high ($p > 0.625$) level outcome classes. . . . . 125

6.1 Plan view of the experiment set-up for performing simulated continuous MMH job cycles described in Table 6.2. . . . . 132
6.2 Flowchart showing the algorithmic framework for the MMH task detection and task condition classification. . . . . 134
6.3 Example screenshot of the Elan software used for annotating the start and end of MMH tasks and task conditions. Upper left videos show the participant performing a two-handed lifting task at knee height. . . . . 137
6.4 An example MMH task detection and task condition classification results for a low intensity job cycle. For Step 2 on classifying task intensity (middle panel) blocks colored red indicate misclassified load levels. Li = Lifting. Lo = Lowering. . . . . 140
6.5 An example MMH task detection and task condition classification results for a high intensity job cycle. For Step 2 on classifying task intensity (middle panel) blocks colored red indicate misclassified load levels. Li = Lifting. Lo = Lowering. . . . . 141
6.6 Cumulative spinal compression force, $F_c$, estimated for low (top) vs. high (bottom) intensity job cycle. "Internal" corresponds to $F_c$ attributed to the postural load due to mass of the head, arms and torso. "External" corresponds to $F_c$ attributed to the predicted external load. *True* corresponds to $F_c$ computed using reference data from video analysis, i.e., without misclassifications. . . . 143

7.1 Revised conceptual framework depicting the inertial sensor-based biomechanical exposure assessment investigated in the research. . . . . 151

C.1 Graphical overview of the algorithm for detecting temporal gait events, applied to right and left legs separately. Sample profile of the sagittal angular velocity (rad/s) from the right and left shank sensors are depicted for one complete gait cycle (100%) recorded during empty-handed condition. . . . . 164

D.1 Graphical summary of the double pendulum model (adapted from Aminian et al.) used for estimating the stride lengths from sagittal angular velocity (rad/s) data of the right shank and right thigh during right stance and swing phases separately. . . . . 168

E.1 Overview of the algorithm for computing mean thoracic-pelvic relative phase angle using one exemplar participant data from the no-load condition in the coronal plane. . . . . 173

F.1 Graphical overview of the algorithm for detecting start and end of lowering and lifting phases. Sample profile of the sagittal angle (°) and angular velocity (°/s) from the upper back (T6) sensor are depicted for one complete bending and lifting trial recorded during a two-handed anterior lifting condition. . . . . 175

G.1 Low-back biomechanical model based on inverse kinematics for calculating low-back compression forces ($F_c$) as a function of posture, internal ($W_{HAT}$) and external ($W_L$) loads and corresponding moment arms, $b$ and $h$. . . . . 177

G.2 Low-back biomechanical model based on inverse kinematics for calculating low-back compression forces ($F_c$) when the torso is in upright posture during two-handed anterior carry of load. . . . . 180

# LIST OF TABLES


2.1 Summary of biomechanical modeling techniques used in the reviewed studies (n = 8). . . . . 23

2.2 Summary of predictive modeling techniques used in the reviewed studies (n = 9). . . . . 31

2.3 Summary of the 46 studies reviewed that reported exposure characteristics of intensity, duration, and/or repetition calculated using inertial sensor-derived data. The fifth column (Task-based) represents whether the exposure characteristics were summarized either for specific tasks (T) or aggregated over the entire work duration irrespective of task (A). . . . . 33

3.1 List and definitions of gait parameters calculated from inertial sensor data. In each row, location of sensors used for calculating the parameters are indicated by '•' with relevant source reference. Connected dots indicate pairs of sensors used together. . . . . 51

3.2 Summary results from the mixed effects analyses for the main and interaction effects of carrying mode and load level on temporal gait measures. Significant pair-wise Bonferroni comparisons ($p < 0.05$) are provided for main and interaction effects that were significant at $p < 0.05$ indicated by *. NL = No-load (empty-handed), L = Low load at 4.5 kg, M = Medium load at 9.1 kg, H = High load at 13.6 kg. . . . . 55

3.3 Summary results from the mixed effects analyses for the main and interaction effects of carrying mode and load level on torso and pelvis postural sway and thoracic-pelvic coordination measures in the coronal, transverse, and sagittal planes. Significant pair-wise Bonferroni comparisons ($p < 0.05$) are provided for main and interaction effects that were significant at $p < 0.05$ indicated by *. NL = No-load (empty-handed), L = Low load at 4.5 kg, M = Medium load at 9.1 kg, H = High load at 13.6 kg. . . . . 56

3.4 Estimated marginal mean $\pm$ standard error for the No-load condition, and the average mean differences relative to no-load condition by carrying mode and load level, at average values of centered gait cycle duration and centered stride length. . . . . 57

4.1 List and definitions of gait parameters calculated from the inertial sensor data for each gait cycle. Excluding stance right and left leg (%) and swing right and left leg (%), all of the remaining 12 parameters were used as predictors in the classification model. . . . . 78

4.2 Confusion matrix showing the classification result for carrying modes from each walk trial data: No-load = empty-handed reference condition, 1H-R = one-handed right carry, 1H-L = one-handed left carry, 2H-Side = two-handed side carry, 2H-Anterior = two-handed anterior carry. . . . . 84
4.3 Confusion matrices summarizing the classification results for load level for each predicted carrying mode. . . . . 86

5.1 Average (standard deviation) age, stature, body mass, BMI, and low-back lifting strength for the study sample stratified by gender and age category (N = 27). . . . . 103
5.2 List and definitions of kinematic parameters calculated from the inertial sensor data for each lifting and lowering phase. Lifting-lowering parameters were selectively used in different classification models, namely, models H, M1, M2, L1 to L4 in Figure 5.4) and identified by a ✓. . . . . 112
5.3 Summary of the carrying mode and load level classification accuracy (%) comparing three different generalized algorithms. Results from the twenty repetitions of the hold-out validation tests were averaged for each model (N=27). . . 115
5.4 Confusion matrix summarizing the classification result for carrying modes across all of the walk trials in the *Rel-NL* model (N=27), where No-load = empty-handed reference condition, 1H-R = one-handed right carry, 1H-L = one-handed left carry, 2H-Side = two-handed side carry, 2H-Anterior = two-handed anterior carry. . . . . 116
5.5 Confusion matrices summarizing the classification results for load level for each predicted carrying load level in *Rel-NL* model (N=27): Low = 4.5 kg, High = 13.6 kg and 22.7 kg. . . . . 116
5.6 Summary of the lifting and lowering height, hand mode, and load level classification accuracy (%) comparing three different generalized algorithms. Results from twenty repetitions of the hold-out validation tests were averaged for each model (N=26). . . . . 118
5.7 Confusion matrices summarizing the classification results for height, hand mode, and load level for lifting using the classification algorithm with *Original* variables (N = 26), where 1H = 1-handed right and left combined, 2H = 2-handed anterior, Low = no-load and 4.5 kg, and High = 13.6 kg and 22.7 kg. load magnitudes. . . . . 119
5.8 Confusion matrices summarizing the classification results for height, hand mode, and load level for lowering using the classification algorithm with *Original* variables (N = 26), where 1H = 1-handed right and left, 2H = 2-handed anterior, Low = no-load and 4.5 kg, and High = 13.6 kg and 22.7 kg. load magnitudes. . . . . 120

6.1 Gender, age, stature, body mass, BMI, and low-back lifting strength for each of the 8 participants in the study sample. . . . . 131
6.2 Task sequence and conditions performed in two simulated job cycles comprising carrying, lifting, and lowering performed either at low load intensity (4.5 kg load) or high intensity (22.7 kg load). . . . . 132

6.3 Example task detection and task condition classification results for low (refer to Figure 6.4) vs. high (refer to Figure 6.5) intensity job cycles. Correct classifications are indicated in green, while misclassified conditions are highlighted in red with the *true* task condition in parenthesis. . . . . 142
6.4 Summary performance measures of the Load carriage, lifting, and lowering detection and task condition classification (N=8). . . . . 144

A.1 Summary of studies in the literature review. . . . . 157

B.1 Example commercial inertial sensors used across different studies with product specifications. . . . . 162

# LIST OF APPENDICES


Appendix A Summary of studies in the literature review. . . . . 156
Appendix B Type of commercial inertial sensors . . . . . 162
Appendix C Computing temporal gait parameters from angular velocity of the shank and thigh recorded by inertial sensors . . . . . 163
Appendix D Estimating stride length from angular velocity of the right shank and thigh recorded by inertial sensors . . . . . 167
Appendix E Algorithm for calculating the mean thoracic-pelvic relative phase angle . . 171
Appendix F Detecting lowering and lifting from thoracic angular displacement and velocity recorded by inertial sensor located at T6 . . . . . 174
Appendix G Algorithm for calculating low back compression force ($F_c$) . . . . . 176

# LIST OF ABBREVIATIONS

**CoM** Center of Mass

**IH** Index of Harmonicity

**IMUs** Inertial Measurement Units

**MAWC** Maximum Acceptable Weight of Carry

**MMH** Manual Material Handling

**MSAAI** Modeling−Sensing−Analysis−Assessment−Intervention

**ROM** Range of Motion

**RMS** Root-mean-squared

**WMSD** Work-related Musculoskeletal Disorder

## ABSTRACT

Occupationally-relevant low back disorders are an important health concern in the workplace. Measuring workers exposure to biomechanical risk factors such as non-neutral postures and high force exertions is an important step for managing and mitigating the risk of such cumulative disorders. Accurate and precise quantification of exposures to biomechanical risk factors in non-repetitive material handling present unique challenges, particularly in jobs where the magnitude of hand loads vary during the workday and/or are difficult to measure directly (e.g., warehousing, construction). Wireless wearable inertial sensors offer new opportunities to acquire continuous posture data *in situ* and has received considerable interest in ergonomics research. This research explores several emerging issues and opportunities afforded by body-worn inertial sensing technology for quantifying biomechanical exposures and low back disorder risk particularly in relation to non-repetitive Manual Material Handling (MMH) jobs.

The specific goal of this research was to develop, implement, and assess a framework that combines occupational biomechanics principles and empirical findings, wearable inertial sensing, and predictive modeling for quantifying biomechanical exposures associated with low back disorder risk in non-repetitive MMH work. The research specifically targeted manual load carriage, lifting and lowering, which represent common MMH tasks associated with an increased risk of low back disorders.

A series of four laboratory studies were conducted. The first study quantified the effects on manual load carriage mode and load magnitude on gait kinematics measured using body-worn inertial sensors. Load carriage was found to induce systematic alterations in gait patterns and pelvic-thoracic coordination. Leveraging this information, the second study

developed and assessed a statistical prediction algorithm for classifying carrying mode and normalized hand-loads using specific inertial sensor-based kinematic features as predictors. The third study extended the statistical classification model to different task conditions in load carriage and lifting-lowering. The fourth study incorporated the developed algorithms into a framework implementation for quantifying biomechanical exposures in manual load carriage, lifting, and lowering by leveraging continuous inertial sensor-based kinematic information and predictive modeling. A quantitative evaluation of the implemented framework based on empirical data from simulated manual load carriage, lifting, and lowering indicated promising results for detecting load carriage tasks (>97.0% on average) and for classifying the carrying mode (>83.1% on average) and load level (>86.2% on average). Prediction accuracy in the lifting and lowering task for classifying height and mode were also high, though accuracy was comparatively less when classifying load level (>43.1% on average).

Overall, this research makes important contributions towards our theoretical understanding of adaptations in gait and posture resulting from transient loads and task conditions. It also demonstrates the potential for combining biomechanical information, wearable inertial sensing, and predictive modeling to quantify physical exposures associated with low back disorder risk in non-repetitive MMH work. Inertial sensing in ergonomics has largely been limited to characterizing the intensity, repetitions and duration of postures. The ability to extract information about work content from motion data is underutilized. Likewise, the application of predictive modeling techniques in ergonomics remains underexplored. The presented research substantially expands the applications and opportunities afforded by body-worn inertial sensing technology and predictive modeling techniques in ergonomics.

# CHAPTER 1

# Introduction

## 1.1 Overview

Accurate and precise quantification of exposures to biomechanical risk factors in non-repetitive material handling present unique challenges, particularly in jobs where the magnitude of hand loads vary during the workday and/or are difficult to measure directly (e.g., warehousing, construction). Miniaturized, wireless wearable inertial sensors offer new opportunities to acquire continuous posture data *in situ* and has received considerable interest in ergonomics research. This research explores several emerging issues and opportunities afforded by body-worn inertial sensing technology for quantifying biomechanical exposures and low back disorder risk particularly in relation to non-repetitive MMH jobs. The ergonomics field also lacks methods and software tools that leverage the up-and-coming discipline of predictive modeling for biomechanical exposure assessment and improving worker health more broadly. To that end, this research develops, implements, and evaluates an algorithmic framework that combines biomechanical information and empirical findings, wearable inertial sensing, and predictive modeling for quantifying physical exposures associated with low back disorder risk in non-repetitive material handling work.

## 1.2 Background

Prior epidemiological studies provide strong evidence of a biomechanical pathway between MMH work and the increased risk of low back disorders [1, 2, 3, 4]. The cumulative trauma model provides one explanation for the occupational relevance of musculoskeletal disorders specifically due to repeated and long durations of external load handling and/or forceful exertions performed throughout the workday. The cumulative trauma model assumes injury results from the accumulated effect of transient external loads that in isolation may be not exceed internal tissue tolerances. Exposures from repetitive and/or prolonged duration cause cumulative compressive and shear loading on the spine such that the internal tolerances of tissues are eventually exceeded.

Accurate, precise and cost-effective quantification of exposures to biomechanical risk factors is an important step to identify problematic tasks, and develop effective risk prevention and reduction programs [5]. Biomechanical exposures during physical work are often characterized by three main dimensions: *intensity* (e.g., load magnitudes, extent of non-neutral postures), *repetition* (frequency or number of force exertions and motions), and *duration* (the time the physical activity is performed, sustained non-neutral postures) [6]. Biomechanical exposure are assessed by sampling work to estimate either all or a subset of the three main exposure dimensions. These estimates are typically then extrapolated to a longer time period (e.g., workday or shift) to quantify the cumulative biomechanical exposure.

### 1.2.1 Exposure Assessment in Non-repetitive Jobs

Strong associations between biomechanical factors (e.g., load magnitude, load moment or load location, duration and repetitions) and the risk of low back disorder are evident in non-repetitive material handling jobs such as patient handling [7, 8, 9, 10], material handling in construction sites [11], distribution centers and ware-housing operations [12], and team lift-

ing [13]. Non-repetitive jobs are defined as jobs that display *variation* and *diversity* in terms of work element frequency, duration, or content [14, 15]. Non-repetitive jobs may contain repetitive elements or fundamental cycles [16], but the intensity, repetitions, and duration of the task varies over time and between workers. Biomechanical exposure assessment in non-repetitive material handling work is challenging because any evaluation performed on a small sample of workers or using discrete-interval work sampling may not represent the work content and resulting exposures compared to occupations with repetitive work tasks [17]. This implies the work assessment may need to be performed across multiple workers over long work periods to capture a representative profile of physical exposures.

Traditional exposure assessment techniques have multiple limitations when applied to field evaluations of biomechanical exposures in non-repetitive work. Direct observational methods such as the Owako Working Posture System (OWAS) [18, 19], Rapid Upper Limb Assessment (RULA) [20], and Rapid Entire Body Assessment (REBA) [21] can be used for assessing the non-repetitive work, but a large number of observations are needed in order for the sampling to be representative. This can be time and labor intensive. Direct measurement methods allow for long durational data collection, and are considered advantageous in terms of performance (e.g., accuracy, precision) and cost [6]. However, instrumentation can be bulky and potentially interfere with worker movements and work performance. Examples of direct instrumentation used for field measurement of work postures include electronic goniometers [22], the lumbar motion monitor [23], and inclinometers [24]. Examples of force measurement instrumentation *in situ* are pressure mapping insoles [25], instrumented force shoes [26], instrumented gloves [27], and electromyography (EMG) for estimating the magnitude of force exertion from muscle activity [28]. These types of methods also rely on trained ergonomists for measurement and analysis. For these reasons, field-based direct quantification methods are needed that can be utilized for multiple workers over extended work period with less effort and cost.

### 1.2.2 Wearable Inertial Sensing for Exposure Assessment

Wearable inertial sensors, also known as Inertial Measurement Units (IMUs), have garnered much attention for human motion measurement in both laboratory and naturalistic settings [29]. Much of this interest has stemmed from improvements in the miniaturization and reduced weight of the sensor hardware, decreased manufacturing cost [30], advancement in wireless connectivity and data processing software, and increased battery life and storage capacity which allows for continuous monitoring over long durations (e.g., an 8-hour work shift). The resulting hardware portability and limited interference with a worker's natural work postures [31] have also made body-worn inertial sensors a suitable alternative for direct measurement of dynamic movements and postures in ergonomics studies over laboratory-based motion tracking systems (e.g., optical motion capture).

The use of inertial sensing is particularly promising in the assessment of biomechanical exposures in non-repetitive material handling jobs. To capture the variations in work content, repetitions and duration, direct measurements are often complemented with additional methods such as work log, activity report, self-reported ratings, questionnaires, or observations to understand the context of the job and its influence on exposure characteristics. The long-term monitoring of workers' movements using the inertial sensors can be an adequate solution to overcome the limitations of the traditional methods.

Despite the growing interest in wearable inertial sensing technologies for ergonomics research, its adoption in occupational settings still lags. A recent survey of ergonomics practitioners in the US attributed this slow uptake to concerns about employee data privacy and compliance, sensor durability, information validity, and efficacy [32]. Efficacy in this context includes the usefulness and practicality of the exposure-related information conveyed to the wearer (i.e., instrumented worker) or to the ergonomist/practitioner, for instance about cumulative workload, work-related injury risk, or about priorities for job modification based on the type and severity of the exposure level [5]. Beyond generating accurate and reliable data, wearable sensor-based exposure assessment tools would need

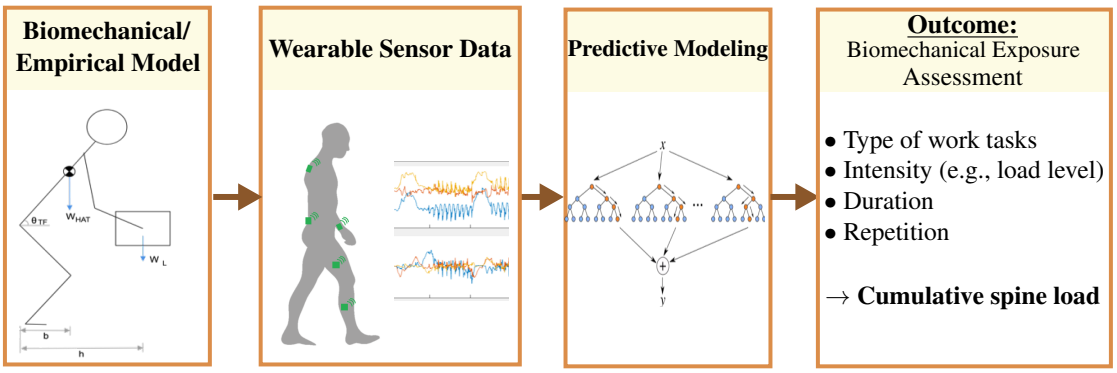



Figure 1.1: Overview of the proposed framework relating biomechanical principles and empirical findings, wearable inertial sensing, and predictive modeling for quantifying biomechanical exposures associated with low back disorder risk in non-repetitive material handling work.

to convey actionable but straightforward information about cumulative exposures and/or musculoskeletal disorder risk to help prioritize intervention targets [5]. Furthermore, wireless inertial sensing technologies connected to web services (i.e., cloud-based) have the potential to compute and communicate such information in near real-time. A review on the current state of the science on inertial sensing technologies applied to ergonomics is needed to help inform research on inertial sensor-based exposure assessment tools.

## 1.3 Research Objectives

The overarching goal of this research is to advance the science of biomechanical exposure assessment in non-repetitive work by leveraging wearable inertial sensing technologies and predictive modeling techniques. To this end, this research creates and evaluates a framework that combines occupational biomechanics principles and empirical findings, wearable inertial sensing, and predictive modeling for quantifying biomechanical exposures associated with low back disorder risk in non-repetitive material handling work. Figure 1.1 presents a graphical overview relating these components and scope this research.

The specific research objectives are to:

(1) Quantify empirically the relationships between effects of hand load and carrying mode in manual load carriage on inertial sensor-based posture kinematics.

- *Hypothesis*: Magnitude and mode of manual load carriage jointly influence posture and gait kinematics relative to unloaded gait.

(2) Develop and assess a statistical prediction algorithm that uses posture kinematics calculated from body-worn inertial sensors to classifying material handling mode and load level.

- *Hypothesis*: Load carriage mode and load level can be predicted from inertial sensor-derived kinematic adaptations in gait.
- *Hypothesis*: Lifting and lowering load level can be predicted from inertial sensor-based postural kinematics.
- *Hypothesis*: Adjusting for between-person variability by normalizing predictors relative to reference motions and postures will improve the accuracy of statistical prediction.

(3) Implement and empirically assess an algorithmic framework for quantifying biomechanical exposures during load carriage and lifting-lowering by leveraging outcomes from Objectives 1 and 2, including, inertial sensing and predictive modeling techniques.

- *Hypothesis*: Mode, repetition (occurrences), duration, and intensity level of load carriage and lifting-lowering can be quantified from inertial sensor-based postural kinematics.

This research makes theoretical contributions in terms of:

(1) improving our understanding about the biomechanical effects of load magnitudes during material handling on gait and posture,

(2) creating an algorithmic framework that combines biomechanical and empirical findings, wearable inertial sensing, and predictive modeling to quantify biomechanical exposures associated with low back disorder risk in non-repetitive material handling work, and

(3) demonstrating the potential for leveraging wearable inertial sensing and predictive modeling techniques to improve the accuracy of quantifying biomechanical exposures in ergonomics applications.

The practical outcomes of this research include:

(1) a review of emerging issues and opportunities afforded by body-worn inertial sensing technology for ergonomics applications,

(2) a preliminary inertial sensor-based software application for quantifying biomechanical exposures in non-repetitive material handling jobs, specifically load carriage and lifting-lowering, and

(3) demonstrating the practical use for wearable inertial sensing and predictive modeling techniques to potentially improve biomechanical exposure assessment and the ability of workers, managers and ergonomists to measure and mitigate low back disorder risk, and thereby improve worker health and well-being.

## 1.4 Conceptual Model

Informed by prior research literature and the objectives of this research, a conceptual model depicted in Figure 1.2 is proposed that summarizes the key factors considered to influence

posture kinematics in load carriage and lifting-lowering. The main focus of this research is to quantify relationships between external load factors, person variables, and task parameters during load carriage and lifting-lowering to posture kinematics and estimated spinal compressive force.

Broadly, three categories of factors consisting of the environment, external load characteristics, and person variables are considered to influence task conditions in manual load carriage and lifting-lowering. **Environmental factors**, such as the location, flooring conditions, and weather (temperature, humidity) have an impact on human movement and workload in MMH tasks. These factors were treated as constants in a laboratory setting. Factors pertaining to the **external load** such as the load magnitude and location of the load center of mass were manipulated to examine their effects on posture kinematics (**Objective 1**). To simplify the problem, load characteristics such as size dimensions and hand-handle coupling were treated as constants. **Person variables** such as gender and age were considered in the sampling of participants, while individual anthropometry and functional strength were treated as covariates in the analysis where relevant.

**Task conditions**, namely, task type (load carriage and lifting-lowering), mode (e.g., one vs. two handed), and load intensity level during load carriage and lifting-lowering were hypothesized to influence internal biomechanical loading, which leads to adaptations in posture kinematics, for example, gait kinematics during load carriage, or torso kinematics during lifting-lowering. Specific to this research, posture kinematics measured using body-worn inertial sensors were used for extracting information about task conditions using predictive modeling (**Objective 2**). Information about posture and predicted task conditions were used as inputs to an algorithm for estimating cumulative low back compressive force as a measure of low back disorder risk (**Objective 3**). Task duration and repetitions were controlled to minimize fatigue, which was not explicitly modeled in this research and is a topic of future investigation. However, fatigue is included in the figure in the interest of completeness, and considered to have a mediating effect on posture kinematics, estimated

cumulative spinal load, and occupationally relevant health outcomes.

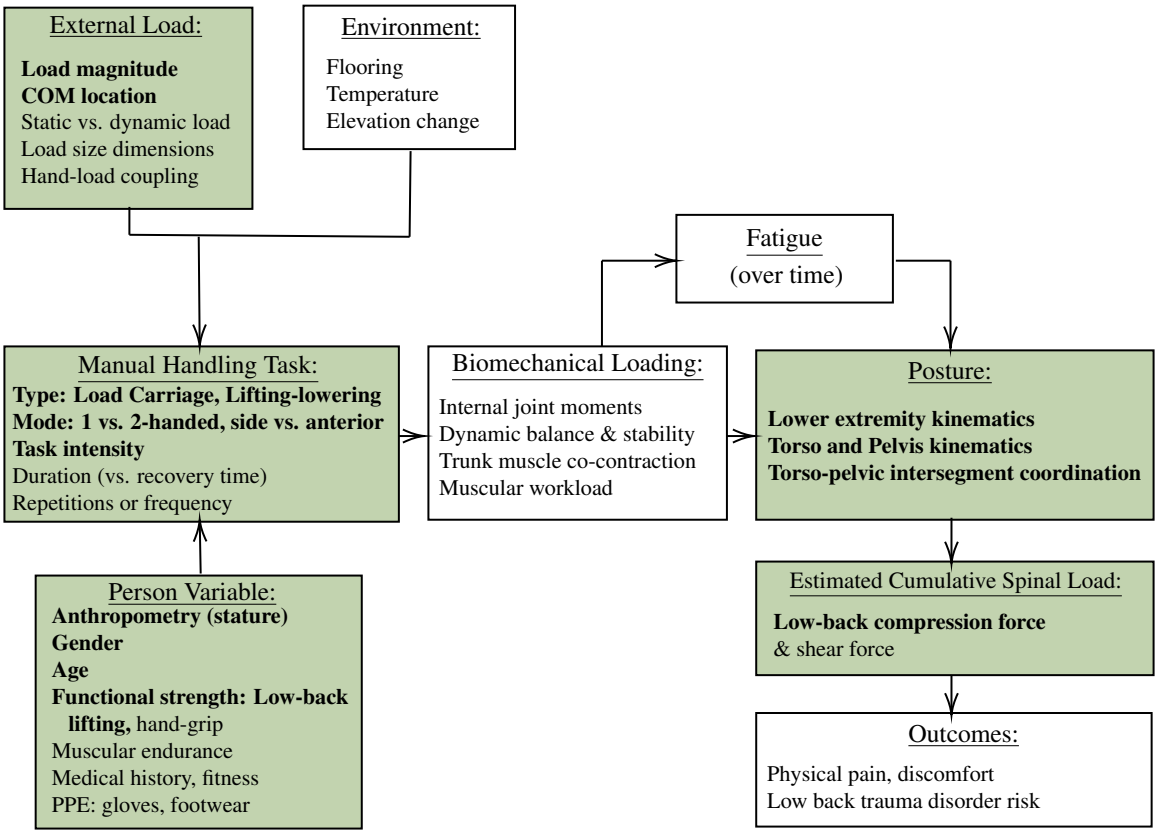



Figure 1.2: Overview of the conceptual model relating the effects of external loads, environment, person variables, and manual material handling task conditions on internal biomechanical loads and measured posture kinematics. Boxes shaded in gray are the primary focus of this research. Elements in bold text were directly manipulated and/or measured, while other elements were held constant or not directly measured. Measured posture kinematics are used for estimating cumulative spinal loads as an indicator of health outcomes, specifically occupationally-relevant low back disorder risk. Fatigue, though not explicitly modeled, is considered to have a mediating effect on posture kinematics, estimated cumulative spinal load, and health outcomes.

## 1.5 Dissertation Outline

Figure 1.3 provides an overview of the structure of this dissertation document by chapter. **Chapter 1** provides an introduction to the research. **Chapter 2** reviews the current

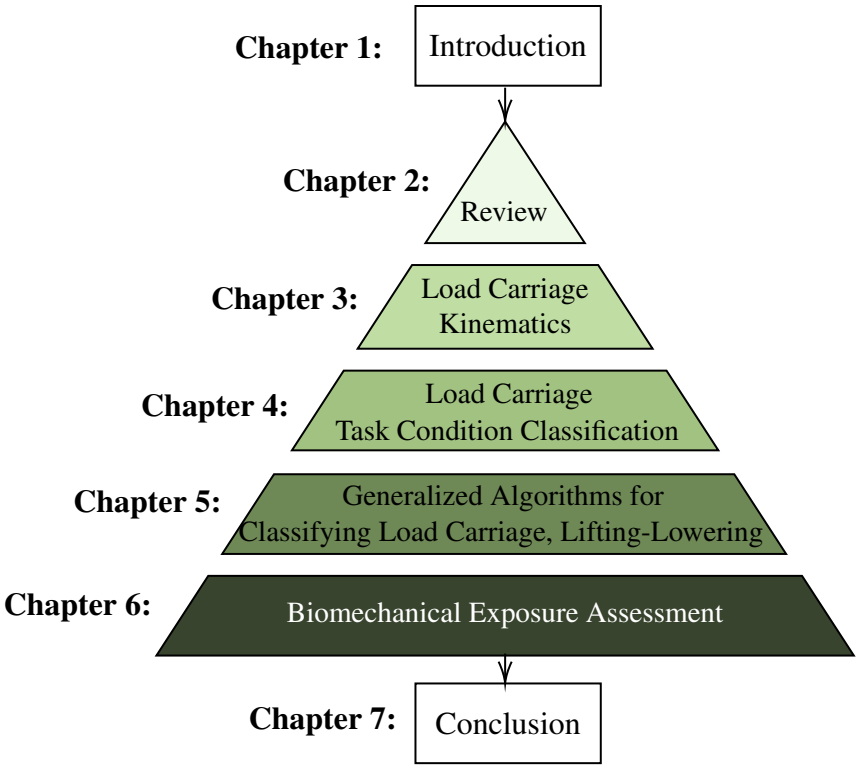



Figure 1.3: Schematic of the dissertation outline.

state-of-the-science of wearable inertial sensing technologies in biomechanical exposure assessment in order to contextualize the research objectives and eventual contributions of this research.

**Chapter 3** presents a study quantifying the effects on manual load carriage mode and load magnitude on gait kinematics measured using body-worn inertial sensors. The study focuses on postural gait adaptations in the torso and pelvis due to biomechanical loads. Based on findings from this chapter, the subsequent **Chapter 4** describes an initial study to develop and assess a statistical prediction algorithm for classifying carrying mode and normalized hand-loads using specific inertial sensor-based kinematic features as predictors.

**Chapter 5** extends the statistical prediction algorithm to analyze three specific MMH tasks, namely, load carriage, lifting, and lowering, in order to classify task mode and intensity in a diverse cohort of men and women. **Chapter 6** integrates the preceding statistical

algorithms into a framework for biomechanical exposure assessment for estimating cumulative spinal compression loads from continuous inertial sensor data. The framework is implemented in a prototype software application and evaluated for prediction performance in a laboratory study on MMH.

**Chapter 7** summarizes the key contributions and significance of this research, its broader implications for ergonomics research and practice, current limitations and future research directions.

# CHAPTER 2

# A Review of Inertial Sensing in Biomechanical Exposure Assessment[1]

Miniaturized, wireless wearable inertial sensors offer opportunities to acquire directly-measured posture data. This technology has generated new interest in biomechanical exposure assessment in real-world occupational settings. The objectives of this review were to: (1) examine the current state-of-the-science of wearable inertial sensing technologies applied to biomechanical exposure assessment, and (2) identify research gaps and opportunities for leveraging wearable inertial sensing for real-time biomechanical exposure assessment. The review helps to contextualize the objectives and eventual contributions of this dissertation research on combining inertial sensing and predictive modeling for biomechanical exposure assessment in MMH work.

## 2.1 Introduction

The objectives of this review were to: (1) examine the current state-of-the-science of wearable inertial sensing technologies applied to biomechanical exposure assessment, and (2) identify research gaps and opportunities for leveraging wearable inertial sensing for real-time biomechanical exposure assessment. Specifically, this study presents results from a review of inertial sensing based approaches to quantifying worker's prolonged exposures

[1] Portions of this chapter appear in [33]

to awkward postures, repetitive movements, and forceful exertions for the purpose of measuring and mitigating work-related musculoskeletal injury risk.

This review begins with a brief introduction to inertial sensing technologies, a conceptual ergonomics-based framework to scope the review, followed by the review methodology, findings, and implications for research.

### 2.1.1 Inertial Sensing Technologies

Inertial sensing refers to sensing technologies that use the property of inertia. This dissertation uses the term inertial sensing to include accelerometers, inclinometers, gyroscopes, and inertial measurement units (IMUs) which are a combination of accelerometers, gyroscopes, and/or magnetometers. A brief description of each type of sensor is provided below.

#### 2.1.1.1 Accelerometers or Inclinometers

A single axis accelerometer measures the linear acceleration of the sensor's reference frame relative to the earth's gravitational field vector [34]. Accelerometers, ranging from uniaxial to triaxial, also function as inclinometers when used for measuring inclination or tilt angles of the sensor relative to the earth's gravitational field vector [35]. In ergonomics applications, gravity-based inclinometers are used to measure orientations (e.g., flexion/extension or elevation angle) of a specific body segment. However, the orientation estimates can be unstable when one of the rotation axes is aligned with gravity since accelerometers are insensitive to rotation about the earth's gravitational field vector [34].

#### 2.1.1.2 Gyroscopes

A gyroscope measures angular velocity in response to rotation of the sensor with respect to the inertial frame, i.e., the Coriolis force [36]. Integrating the gyroscope sensor data provides angular displacement about the sensor frame, so it can be used to estimate the

rotation angle of the sensor axis. However, the integrated sensor results drift over time due to the accumulation of noise and offsets in the raw signal. Consequently, filtering techniques are applied to compensate for drift, or the integration is limited to short durations (e.g., < 5s). Gyroscope and accelerometer data are often combined for calculating sensor rotation angles.

#### 2.1.1.3 IMUs

IMUs consist of a triaxial accelerometer and a gyroscope to measure 3D acceleration and angular velocity of the sensor with respect to gravity [35]. Appendix B summarizes the make, model, and technical specifications of some of the commercially-available inertial sensors used in ergonomics research studies. Calculating 3D rotations using both accelerometer and gyroscope signals has advantages over using any one individual signal since each sensor data can compensate for the limitations of the other [37] with the use of sensor data fusion algorithms such as a Kalman filter or complimentary filter. For instance, the effects of drift error introduced by integrating gyroscope data can be corrected by the accelerometer-based orientation estimates. The orientation error which is affected by earth's gravity in the accelerometer can be corrected by gyroscope-based rotation estimates. Often, IMUs also include a triaxial magnetometer to measure the geomagnetic field to estimate the heading of the sensor relative to the earth's magnetic polarity. Magnetometers provide heading information that neither accelerometers nor gyroscopes provide. Sensor fusion algorithms in most commercial IMUs are proprietary and thus not inspectable.

### 2.1.2 MSAAI Framework

To scope this review and adequately synthesize the contemporary uses of inertial sensing in ergonomics research, a "Modeling-Sensing-Analysis-Assessment-Intervention" (MSAAI) framework was proposed [33] as depicted in Figure 2.1. This conceptual framework draws upon the reviewed studies to depict the typical role of wearable inertial sensing and sensor

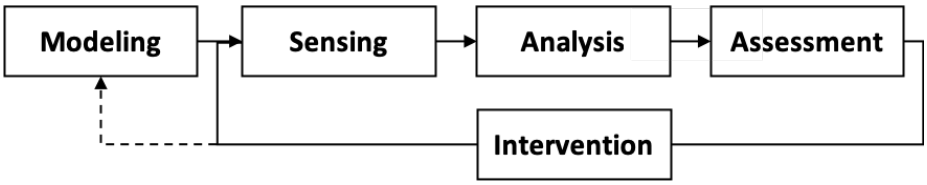



Figure 2.1: Conceptual framework for biomechanical exposure assessment using wearable inertial sensors spanning Modeling, Sensing, Analysis, Assessment, and Intervention (MSAAI).

data for biomechanical exposure assessment. Each component of the MSAAI framework is briefly described.

The use of inertial sensing is typically preceded by some form of biomechanical **modeling**, either through explicit analyses or implicit assumptions in order to represent the relationships between critical elements of the person-equipment-task system and to inform the sensing phase. **Sensing** includes decisions on the types of measures and sensors to use, the locations for sensor attachment, and the process of measuring worker postures and movements. The **analysis** component refers to the myriad approaches to analyzing sensor data spanning descriptive and inferential statistical analysis, and more recently using predictive modeling (i.e., machine learning) techniques to obtain relevant measures of physical exposures. Descriptive statistics are typically used to summarize key dimensions of physical exposures, namely, intensity (e.g., extent of non-neutral postures, magnitude of motions, joint loads), duration (e.g., time spent in a particular posture or on a task, time to complete a movement), and repetition (i.e., frequency of motions) [6]. Inferential statistics include hypothesis testing such as ANOVA to compare exposures between conditions (e.g., between task types or equipment) or to quantify associations between inertial sensor-based physical exposure measures and ergonomics outcomes (e.g., injury prevalence, productivity). Certain exposure characteristics such as force exertions are often not directly available from inertial sensor data, hence additional methods (e.g., direct observation, indirect video-based observations, work diaries) get used in conjunction.

**Assessment**, very broadly, implies that the quantified exposures are either compared

to previously established "*absolute*" limits and thresholds to assess workload and/or injury risk (e.g., NIOSH Lifting Index, RULA or OWAS scores) or compared in "*relative*" terms. Examples of the latter include comparisons between different occupations, task conditions, types of equipment design, or pre- vs. post-intervention (e.g., workplace modification) to assess relative differences in biomechanical exposures and/or the risk of WMSDs.

The assessment of exposures (either absolute and relative) and cumulative disorder risk help to inform and prioritize **interventions**, i.e., actions aimed at modifying work content in order to augment task performance, reduce the risk of work-related cumulative trauma and injury, and/or improve worker well-being. Interventions in ergonomics can take many forms, including lowering of task demands by changing work equipment/tool or the environment, by augmenting worker capacity using assistive technologies, or by means of worker training and worker selection. In the context of wearable inertial sensing, the present review of interventions is limited to direct feedback strategies in the workplace that are near real-time (e.g., using prompts or alerts from wearable devices) aimed at either altering or reinforcing certain actions/behaviors in contrast to the aforementioned interventions that are asynchronous and post priori. The closed feedback loop in the conceptual framework indicates that the biomechanical exposures are assessed across time (i.e., longitudinally, or pre- and post-intervention), or compared between conditions (i.e., cross-sectional A-B designs) towards some salutary goal. The modeling component can be updated based on comparisons between the expected (i.e., modeled or hypothesized) behavior and actual (i.e., measured or observed) behavior of the system (Figure 2.1, indicated by a dotted line pointing to the biomechanical modeling in a closed feedback loop).

## 2.2 Methods

### 2.2.1 Search Strategy

This review follows the PRISMA (Preferred Reporting Items for Systematic Reviews and Meta-Analyses) methodology for conducting and reporting systematic reviews in health sciences [38, 39]. For the review, three databases (i.e., Web of Science, PubMed, and ProQuest) were searched for articles printed through February, 2018 in the initial search performed on January 22nd. A second search was performed on June 20th to include articles through June, 2018. Search keywords to identify studies on inertial sensing in biomechanical exposure assessment includes ['work*' or 'Ergonomic*' or 'Biomechanic*' or 'Occupation*'] and ['Exposure' or 'Assessment' or 'Evaluat*' or 'Posture'] and ['inertia*' or 'acceler*' or 'inclino*' or 'gyro*' or 'wearable']. Any peer-reviewed journal articles or conference proceedings including the search keywords in the document title, abstract, or keywords were selected. Only studies written in English were searched. The search process and exclusion criteria are summarized in Figure 2.2.

### 2.2.2 Exclusion Criteria

The initial search identified a total of 491 studies based on title, abstract, and keywords, and after discarding duplicate papers. Review articles were excluded unless the document also contained an empirical case-study originating from the authors' own research. Selected studies (n = 491) were reviewed in their entirety based on the title and abstract (*Step 1* in Figure 2.2) and full text (*Step 2* in Figure 2.2) and were excluded from further analysis if the article described a study that:

- did not include human subjects; or
- used inertial sensing for applications other than measuring some aspect of body posture or postural kinematics. For example, studies using accelerometers to measure

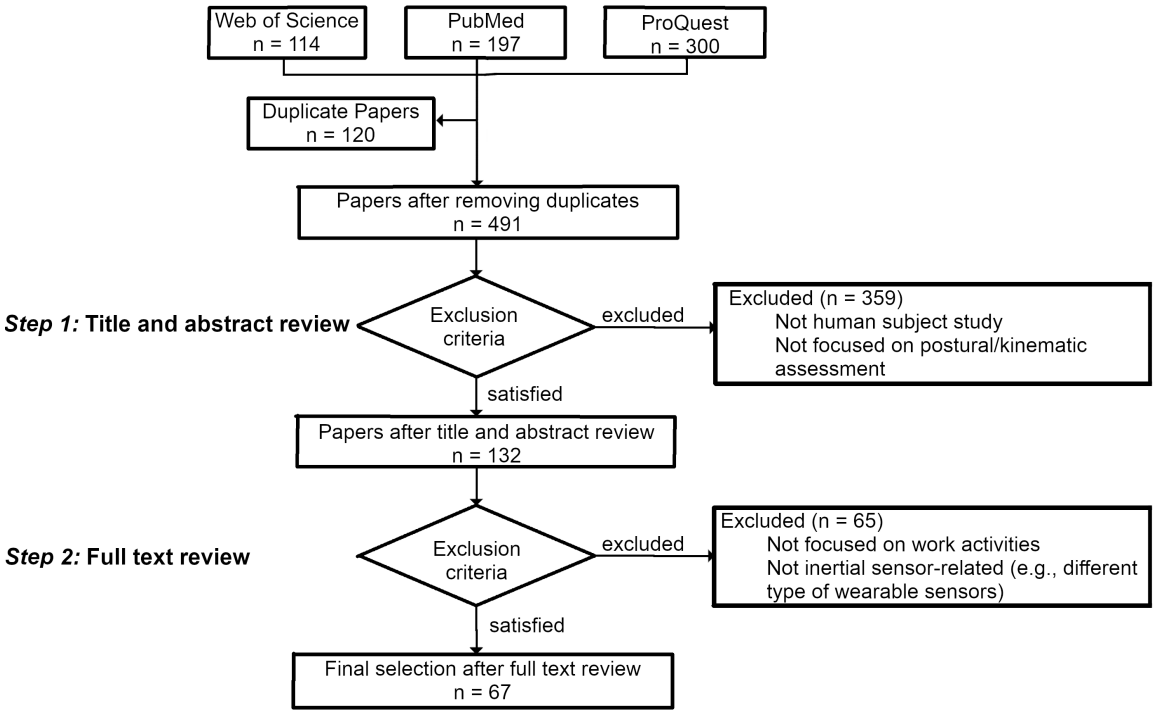



Figure 2.2: Flowchart summarizing the phases of the document search and selection process.

movement or vibration of an inanimate object or equipment were excluded; or

- did not focus on occupational (work) activities. For example, studies focusing activities of daily living, fitness, sports, athletics, and clinical rehabilitation were excluded.

### 2.2.3 Data Extraction and Analyses

A total of 67 studies met all criteria after the full-text review (Step 2 in Figure 2). These were analyzed and coded according to the PRISMA methodology and MSAAI framework (Figure 2.1). Extracted data entries included the following:

- *General information:* Author(s), year of publication, title, journal, study objective, study sample size and composition (i.e., participant characteristics), study setting (e.g., lab vs. field), and type of study site (i.e., job type) if it were a field study.

- *Modeling:* Formal recognition of using biomechanical modeling [yes/no], biomechanical model details, main purpose or objective for the model, method for model validation, and key finding(s).

- *Sensing:* Sensor attachment location(s), sensor pairs if used for measuring inter-segment or joint kinematics, and additional methods used to record the type of work tasks performed.

- *Analyze:* Physical exposure characteristics (intensity, duration, repetition), type of statistical technique used for analysis (i.e., descriptive statistics, inferential statistics, or predictive modeling), specific technique used, main purpose/objective of the analysis, model assessment and findings if predictive modeling was used.

- *Assessment:* Relative vs. absolute assessment, specific criteria used for the assessment if an absolute assessment was performed.

- *Intervention:* Type of intervention used, content and modality if real-time feedback was used, and whether biomechanical exposures were re-examined post-intervention either in a cross-sectional or longitudinal manner.

## 2.3 Results

Appendix A summarizes general information on the 67 studies reviewed including each study's sample composition and size, study design (e.g., whether the study was performed in a lab or field setting), types of occupational activities examined, number of sensors attached on the subject, and the specific analysis and assessment methods used. Review results indicated that the number of ergonomics-related research studies that employed inertial sensors for physical exposure assessment has steadily increased in the past decade. Over 50% of the studies reviewed (n = 35 of 67) were published in the previous 3 years ($2015 - 2017$; Figure 2.3a).

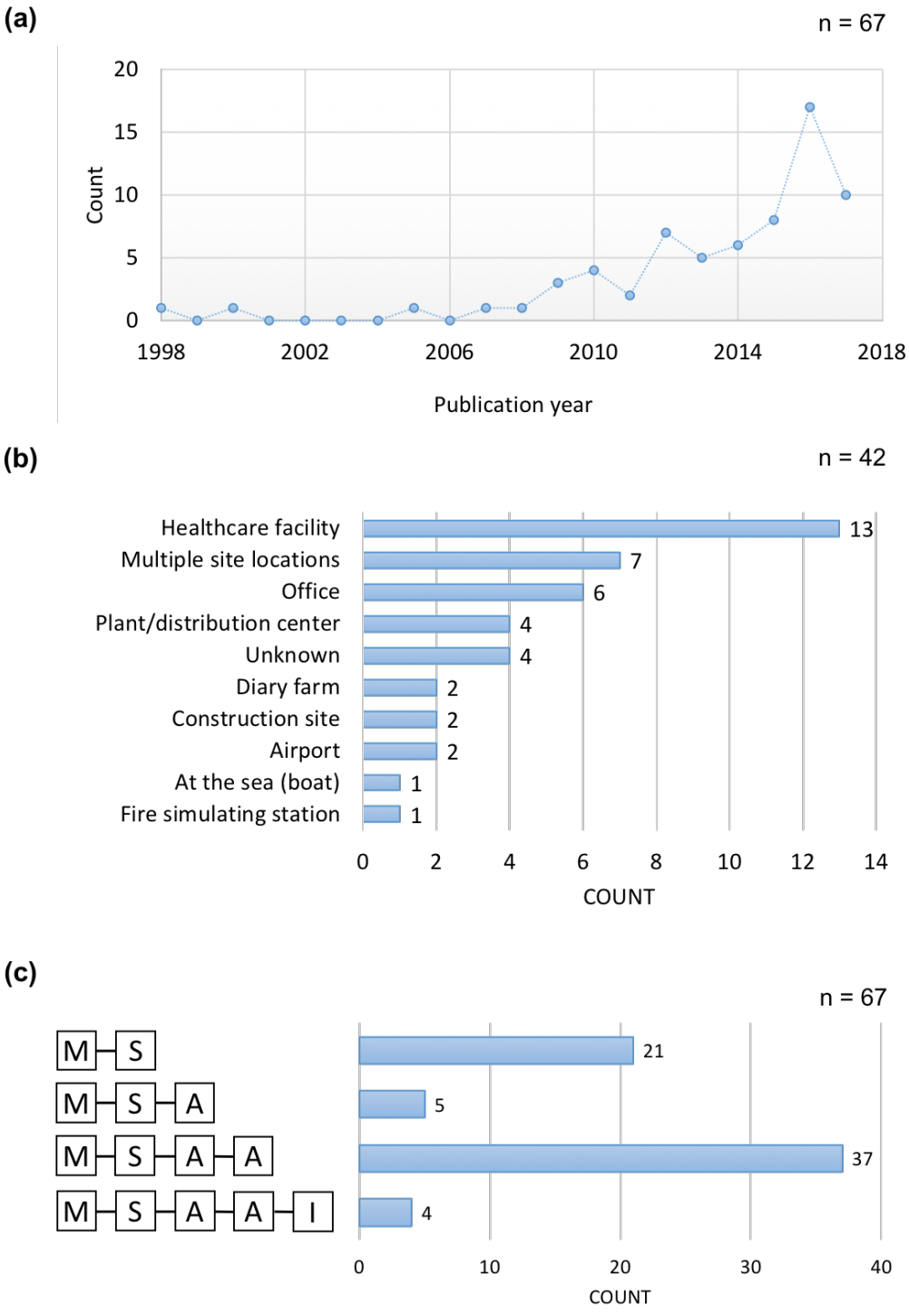



Figure 2.3: Summary of the review results in terms of the number of studies by publication year between 1998 and 2017 (a), by field study site where the data collection was performed (b), and by component of the Modeling-Sensing-Analysis-Assessment-Intervention (MSAAI) framework addressed (c).

Four of the 67 studies performed data collection in both field and laboratory settings, 38 (56.7%) were conducted in field settings, while 25 (37.3%) were performed in a laboratory environment (Figure 2.3b). Health-care facilities (e.g., hospitals, dentistry clinics, operating rooms, and long-term care facilities) were the most frequently studied work sites (13 of the $38 + 4 = 42$ field-based studies, 31.0%). Offices comprising white-collar work were the primary study site in 6 of the 42 (14.3%) field-based studies. Seven of the 42 field-based studies (16.7%) investigated multiple site locations mostly to compare biomechanical exposures between job types. For example, Teschke et al. [40] used measurements of angular displacement and velocity from a triaxial inclinometer attached at the thoracic vertebra (T6) to compare the magnitude of non-neutral torso postures (i.e., flexion/extension and lateral bending) over a work shift in workers across forestry, wood and paper products, transportation, warehousing, and construction jobs.

With reference to the proposed framework, only four studies spanned all five components of the framework with the intervention including real-time feedback (M-S-A-A-I in Figure 2.3c). Over half of the reviewed studies (n = 37 out of 67, 55.2%) included the four components of modeling, sensing, analysis, and assessment of biomechanical exposures (M-S-A-A in Figure 2.3c). Thirty-three of these studies were performed in field settings. About one-third of the reviewed studies (n = 21 of 67) included only modeling and sensing as the sole focus to validate the accuracy or reliability of the inertial sensor-based kinematic measures, i.e., the study did not compare measured exposures to any known limits and thresholds or between measured tasks, occupations, or interventions.

The subsequent sections summarize prominent themes organized by each framework component, i.e., modeling (M), sensing (S), analysis (A), assessment (A) and feedback intervention (I), identified from the analysis and synthesis of the 67 studies reviewed.

### 2.3.1 Modeling

The review results on modeling approaches are limited to 8 of the 67 studies (11.9%) that explicitly used biomechanical models to estimate joint loads and moments. Table 2.1 summarizes the type of biomechanical models used across the studies, along with the modeling purpose, approaches to validation, and key findings. Examples of modeling approaches used spanned inverse dynamics models (e.g., [41, 42, 43, 44, 45]), and musculoskeletal finite element-based models [46]. Across the 8 studies, inertial sensor-derived posture angles were used as an input to the biomechanical model along with information from other instrumentation such as ground reaction forces from force plates [43] or in-shoe pressure sensors [43], or estimated locations of body or segmental Center of Mass (CoM) [41]. The locations for inertial sensor attachment in these studies were guided by the specific segment postures or joint angles needed for calculating joint loads and moments in the biomechanical model (refer Section 2.3.2 for details). The accuracy of estimated joint loads and moments were validated by comparing these inertial sensor derived estimates to corresponding measures computed using data from optoelectronic motion capture and force plates. Valero et al. (2016) proposed an additional step by using a deterministic postural angle-based threshold model to distinguish different lifting strategies (i.e., stoop, squat, or combined) from inertial sensor-based postural angles [47]. Trunk and leg inclination angles were used as criteria to discriminate between lifting strategies, for example, a trunk inclination angle $\leq$ 20° and shank inclination angle between 0° and 30° was used to characterize a stoop lift [47].

### 2.3.2 Sensing

#### 2.3.2.1 Sensor Attachment Locations

The number of inertial sensors used per study ranged from 1 to 17, with a median of 3 sensors per study. Figure 2.4 depicts the total number of times an inertial sensor was attached at

Table 2.1: Summary of biomechanical modeling techniques used in the reviewed studies (n = 8).

| Study | Purpose | Validation | Key findings |
|---|---|---|---|
| **Inverse dynamic model** | | | |
| Faber et al., 2016 [41] | To estimate the L5/S1 moment from the estimated CoM location | Compared with optical motion capture and force plate-derived L5/S1 moments calculation | RMSE < 10 Nm (L5/S1 moment) |
| Holmes et al., 2010 [42] | To estimate the L4/L5 joint loadings and moments | | |
| Kim & Nussbaum, 2013 [43] | To estimate the joint moments at the knees, hips, L5/S1, and shoulders | Compared with optical motion capture and force plate-derived joint moments | Peak Absolute Errors (PAE) < 14.4 Nm (L5/S1 moment), PAE < 11.2 Nm (hip moments) |
| Faber et al., 2012 [44] | To estimate the knee, hip, and L5/S1 joint loadings and moments | Compared with optical motion capture and force plate-derived joint moments | RMSE% < 4% (knee moments), RMSE% < 14 % (L5/S1 moment) |
| Shojaei et al., 2016 [45] | To estimate the L5/S1 compressive and shear loads and moments | | |
| **Musculoskeletal finite element model** | | | |
| Gholipour et al., 2016 [46] | To estimate the L5/S1 compressive and shear loads from the estimated 3D rotation of trunk postures, given load, and link length | Compared with optical motion capture-derived L5/S1 loadings | RMSE = 173 N (L5/S1 compression load), RMSE = 35N (L5/S1 shear load) |
| **Single-segment inverted pendulum model** | | | |
| Nocerino et al., 2011 [48] | To estimate the CoM location | | |
| **Deterministic postural angle-based threshold model** | | | |
| Valero et al., 2016 [47] | To discriminate different lifting strategies (stoop, squat, or a combination of both) | Compared with the video-based analysis | |

a particular body location (denoted by circles) yielding 175 total sensor placements across the 67 studies reviewed. Sensors were placed bilaterally in 128 out of 175 sensor placement locations (73.1%). When a sensor was placed unilaterally, either the right side or the dominant side was chosen more often (38 out of 175, 21.7%) than either the left or non-dominant side in the remaining 9 out of 175 (5.1%) studies. The upper arm was the most frequently used location for attaching an inertial sensor (32 out of 67 studies, 47.8%), followed by the thoracic vertebrae (between T1 to T12) in 20 of the 67 studies (29.9%), and the hip in 19 of the 67 studies (28.4%).

Lines connecting two circles in Figure 2.4 denote pairs of sensors used in conjunction such as for computing the joint angle between a proximal and distal body segment or movement coordination (e.g., lumbarpelvis ratio calculated as the ratio of lumbar flexion to pelvic rotation) [45] between two segments. The shoulder and knee were the two most frequently investigated joints, namely, in 8 out of 67 studies (11.9%) each. In general, studies used different pairs of sensor locations to derive joint angle kinematics such as at the neck, shoulder, trunk, and hip, suggesting a lack of standardization in joint description.

For example, rotations at the shoulder (glenohumeral) joint (i.e., flexion/extension, abduction/adduction, internal rotation) were calculated by combining data from a sensor attached on the upper arm and either the scapula, chest/sternum, or thoracic spine, with the scapula being the most frequent choice (4 out of 8, 50.0%). For measuring neck posture, pairs of sensors were attached either on the head and thoracic vertebra [49, 50], or forehead and cervical vertebra [51, 52], or head and chest or sternum [53, 54].

#### 2.3.2.2 Evaluating Sensor Performance

Studies validating inertial sensor measurements for accuracy and precision in ergonomics applications were all performed in lab settings. Accuracy was evaluated by statistical comparison of kinematic measures obtained using inertial sensing to corresponding measures obtained from a reference ”gold standard” instrumentation system. Examples of the latter

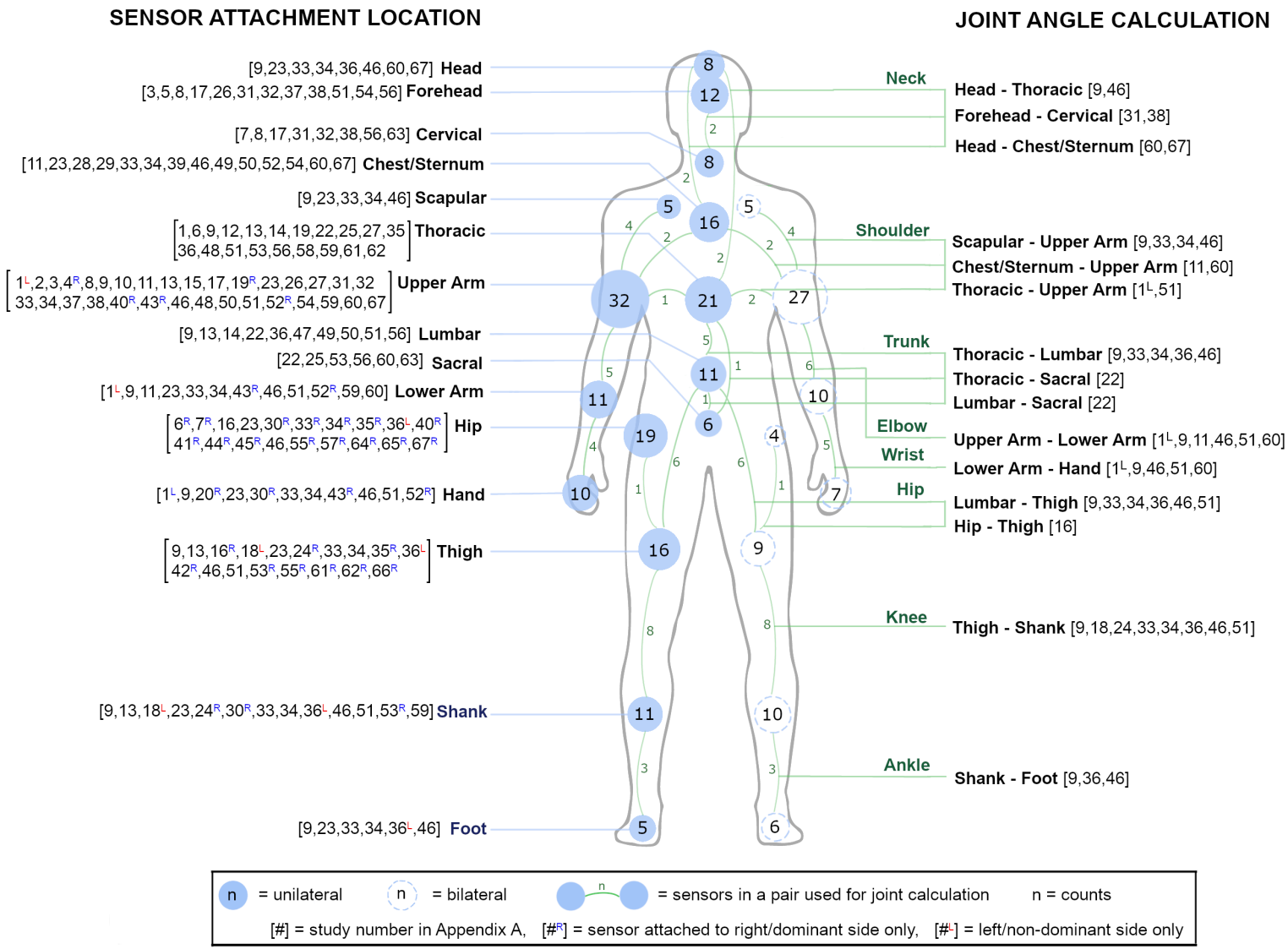



Figure 2.4: Body locations of the inertial sensors across the reviewed studies (n=67).

included optoelectronic motion capture [41, 43, 50, 55, 56, 57], magnetic motion tracking [58, 59], ultrasound-based motion capture [60], lumbar motion monitor [61], and previously validated accelerometers (Logger Teknologi HB) [62]. Kinematic and kinetic compared for validation purposes included segment or joint angular displacement, velocity, and acceleration, Range of Motion (ROM), and joint moments. Statistical measures typically used for assessing the accuracy of inertial sensor-derived measures compared to reference (gold standard) instrumentation measures included correlation coefficients, paired and independent sample t-tests, and summary statistics on root mean squared errors (RMSE), mean absolute errors, peak absolute errors (PAE), mean peak errors, and Bland-Altman bias and limits of agreement.

Two studies validated kinetic measures derived using inertial sensor data. Faber et al. [41] used IMU-derived joint position estimates to compute CoM positions which were subsequently used for calculating 3D L5/S1 moments. Kim and Nussbaum [43] computed joint moments at the L5/S1, shoulders, hips, and knees during lifting and lowering, carrying, and pushing and pulling tasks using a combination of IMUs for posture and in-shoe pressure measurement system for measuring vertical force component at the ground [43]. In both studies, the difference in L5/S1 joint moments calculated using optoelectronic motion capture and force plates to inertial sensor derived estimates were found to be comparable with a RMSE < 10 Nm [41] and PAE < 14.4 Nm [43], respectively.

Precision of sensor measurements was evaluated by assessing inter-rater repeatability and intra-rater repeatability, respectively. To examine inter-rater reliability, multiple examiners took turns attaching sensors to the same participant and with the participant repeating the same movement each time [63, 64]. Intra-rater repeatability was typically examined by having the same examiner attach sensors to the same participant multiple times and the resulting measurements compared [58, 59, 61, 65].

A direct comparison of inertial sensor accuracy and precision across the different studies reviewed was hindered by differences in experimental design that influence estimated

errors. Examples include differences in the location of sensor attachment, type of kinematic and kinetic measures compared, the reference gold standard instrumentation used, type of reference tasks performed, duration of the measurement, signal processing techniques used, and type of error estimates reported, and the type of statistical test performed on the error estimates. However, findings in general reported that comparisons of segment orientations had smaller error magnitudes than joint angle estimates [56], long complex task produced larger errors than short duration movements (e.g., manual material handling task performed over 32 mins vs. short functional movements such as flexion/extension at head, trunk, upper arms, and upper legs [50]), movement velocity in dynamic tasks influences sensor accuracy (e.g., motions performed between 50°/s and 75°/s showed better accuracy than motions above these angular velocities) [56], and differences in the biomechanical models used contributed more to the error in outcome measures than the inherent instrumentation error of the sensor itself [50].

#### 2.3.2.3 Relationships between Inertial-based Direct vs. Subjective Measurements

Seven studies (10.4%) investigated associations between inertial-sensor derived direct postural measures and subjective measures of workload such as self-reported questionnaires (e.g., [66]). A sub-set of these studies used commercial software to classify different postures from inertial sensor data across time (e.g., activePAL, Acti4, and ActiLife 6). The time spent in the different postures were compared to durations obtained from self-reported questionnaires such as the Occupational Sitting and Physical Activity [66, 67] or the Multicontext Sitting Time Questionnaire [68]. Results showed that the total duration of walking obtained from self-reported methods were overestimated by 4.6-12.4% [66, 68] compared to durations obtained from an inertial sensor-based posture classification algorithm. Standing was either not significantly different [66] or underestimated by 4.6% [68] in self-reported methods compared to the inertial sensor-based classification. Teschke et al. [40] compared inertial sensor measured torso flexion/extension and lateral bending angle

to direct observations using the Back Exposure Sampling Tool (Back-EST) [69] and also with a structured questionnaire on the level of physical exposures similar to questions in the Back-EST. In that study, observations and self-reported questionnaire responses were found to account for 30-61% and 33-40% of the variance in inertial sensor measurement, respectively. Overall, these studies demonstrated advantages of using direct inertial sensing measurements over observation and questionnaire based methods, which are time and labor intensive. Continuous inertial sensing data were also amenable to leveraging statistically-based posture classification algorithms to identify postures and durations in specific work activities such as standing, walking, and MMH tasks.

### 2.3.3 Analysis

#### 2.3.3.1 Type of Analysis Methods

All of the studies reviewed provided descriptive statistics of the measured or processed sensor data in some form (e.g., mean, median, standard deviation, range, percentiles) calculated either for the entire data collection duration or stratified by condition for comparison (e.g., by job category, task types, equipment used, or before vs. after intervention) (refer Appendix A for details). A few studies were limited to reporting descriptive statistics (e.g., [70, 71, 72]). Over half the reviewed studies (n = 25 out of 46 studies, 54.3%) used inferential statistics such as ANOVA or repeated mixed-effects either to contrast physical exposure characteristics between conditions, or to examine associations between work-related musculoskeletal disorders and biomechanical exposures [73, 74].

Importantly, 9 of the reviewed studies (19.6%) used **predictive modeling (i.e., machine learning)** techniques either to classify postures and type of work task performed from the inertial sensor data, or to predict inertial-sensor derived postures from different incomplete sources of information (e.g., hand position, observation). Table 2.2 summarizes these 9 studies in terms of the type of predictive model used, modeling purpose/objective, model validation and key findings. Six studies used inertial sensor data as predictors for classify-

ing tasks and/or postures. Three of the 6 studies relied on commercial posture classification software, e.g., SenseWear Professional 6.1 [75], ADL Monitor software [76], and ActiLife 6 [67] to identify work-related activities such as walking, sitting, standing, and reclined resting. These three studies did not perform any validation of the classification algorithm of their own in the study, neither was the algorithm inspectable. However, if the validations were available elsewhere, the results and references were also included in Table 2.2.

Three studies proposed their own predictive model for classifying work tasks or postures with inertial-derived kinematic data as predictors. Brandt et al. [77] used accelerometer-based measurements of torso flexion and lateral bending angles recorded while participants performed "high-risk lifting" (i.e., 16, 18 and 20 kg loads) vs. "low-risk lifting" (i.e., 22, 24 kg at short distance, 8, 12 and 16 kg asymmetric, and 16 kg with long reaching distance lifting) as input to a statistical classification algorithm. On average, the measured postural angles correctly separated 65% of the high vs. low-risk lifting tasks. Classification accuracy increased to 76% when the accelerometer-derived predictor variables were supplemented with Root-mean-squared (RMS) electromyography activity of the upper trapezius and erector spinae muscles [77]. In a laboratory study of simulated MMH, Kim and Nussbaum [78] compared the performance of three different predictive modeling techniques to classify work tasks such as walking, carrying, lifting, lowering, pushing, and pulling using continuous data from 10 body-worn IMUs. The precision of classification exceeded 90% in all of the work tasks, while the duration of work tasks were underestimated by 14% [78]. Peppoloni et al. [79] developed a machine learning-based segmentation algorithm to identify the start and end of different hand activities including neutral posture, reaching, grasping, and moving in a study simulating the repetitive hand motions of supermarket cashiers. Posture deviations from the neutral of upper limb, neck, trunk, and leg during the segmented activities were used to calculate the RULA score for each activity. The study reported an accuracy of 94.8% within each activity cycle for RULA scores obtained from the algorithm compared to a human coder [79].

Three other studies implemented predictive modeling techniques to predict postures and movements obtained from inertial sensors using task variables and/or person attributes as predictors. Gholipour and Arjmand [46] successfully demonstrated the use of Artificial Neural Networks (ANN) with individual stature and position of the hand load as inputs to predict 3D spinal posture measured by IMUs attached at S1, T12 and T1, with an overall RMSE $< 11^{\circ}$ and $R^2 < 0.95$. In a study of workers in a paper mill, Heiden et al. [80] used a combination of administrative data (e.g., worker's demographics, work shifts such as the shift type, number of staff on shift, number of paper rolls produced), worker's subjective ratings before and after each shift using a Borg CR-10 scale [81] and video-based observational data to predict the trunk and arm inclination angles measured by accelerometers. Results indicated that the coefficient of determination for predicting trunk and arm inclination angles was the highest in the case of direct observation ($R^2 < 56\%$) compared to worker's subjective ratings ($R^2 < 36\%$) and administrative data ($R^2 < 15\%$). Nath et al. [82] demonstrated the use of raw acceleration data obtained from a smart phone worn on the upper arm as feature vectors in a linear predictive model to estimate the range of trunk and shoulder flexion angles during a simulated construction task.

#### 2.3.3.2 Measured Physical Exposure Characteristics

Inertial sensors were exclusively used for quantifying the intensity, repetition, and/or duration of extreme motions or postures. Table 2.3 provides a summary for the 46 studies that reported on inertial sensor-derived exposure characteristics in terms of these three dimensions. Exposure characteristics measured using methods other than inertial sensors (e.g., observer-based) were excluded from the table. **Intensity** of extreme motions and postures was expressed in three ways. First, by ordinal categories based on threshold. For example, thresholds for arm elevations of 30°, 60°, and 90°were typically used to calculate either the duration and/or repetition of movement in the range of $0^{\circ}$ to $30^{\circ}$, $30^{\circ}$ to $60^{\circ}$, $60^{\circ}$ to $90^{\circ}$, and $\geq 90^{\circ}$of arm elevation, with larger deviations from neutral ($0^{\circ}$) implying

Table 2.2: Summary of predictive modeling techniques used in the reviewed studies (n = 9).

| Study | Model | Purpose | Validation | Result |
|---|---|---|---|---|
| **Task/posture classification** | | | | |
| Brandt et al., 2018 [77] | Linear Discriminant Analysis (LDA) | To classify the low and high-risk lifting based on the guidelines of the Danish Working Environment Authority | Monte-Carlo cross validation (random sampling of training and test set repeated 100 times) | 65.1-65.5% accuracy |
| Breidahl et al., 2015 [75] | Proprietary, unspecified (used SenseWear Professional 6.1 software) | To classify postures: sleep, supine position; and steps taken | | |
| Busser et al., 1998 [76] | Proprietary, unspecified (used ADL Monitor software) | To classify postures: locomotion, standing, sitting, and lying | Compared the classified physical activities with the video-based task analysis | Accuracy of 89-96.5% were reported in [87] |
| Kim & Nussbaum, 2014 [78] | Linear Discriminant Analysis (LDA), k-nearest neighbor (k-NN), Multilayer feedforward neural network (MFNN) | To classify task types: walking, carrying, lifting, lowering, pushing and pulling | Three fold cross-validation | Precision of > $\tilde{9}$0% and recall of 80% |
| Peppoloni et al., 2016 [79] | State machine | To classify task types: neutral pose, reach, grasp, and move | Strain Index and RULA score calculated with the measured postures within the identified task duration were compared with human evaluator's ratings | Accuracy of 94.8% for RULA action level, 44.8% for Strain Index |
| Wick et al., 2016 [67] | Decision tree (used ActiLife 6 software) | To classify postures: sitting, standing, and walking | | Sensitivity of 99% and specificity of 100% were reported in [88] using the same algorithm |
| **Posture prediction** | | | | |
| Gholipour & Arjmand, 2016 [46] | Artificial Neural Networks (ANN) | To predict the 3D spinal posture (x, y, z rotation angle at T1, T12, S1) by using hand position (x, y, z) and body height as inputs | 70%-15%-15% (training, validation, testing data set) | RMSE < 8° between the measured angles from the inertial sensors and the predicted angles validation |
| Heiden et al., 2017 [80] | Linear mixed model | To estimate the trunk and arm inclination postures from the other sources (administrative data, worker ratings, observation) | Resampling validation using bootstrapping (500 virtual datasets drawn with replacement from the original dataset) | Model fit ($R^2$) < 15% (administrative data), < 36% (worker ratings), and < 56% (observation) |
| Nath et al., 2017 [82] | Linear model | To extract the feature vector from the raw acceleration data that reliably represents the observed postural angles | | Absolute error in trunk and shoulder flexion < 7°. |

greater postural load or intensity. Threshold levels were decided either based on previously validated absolute limits or study-specific thresholds (see details in Section 2.4.3). Second, the intensity of the exposure was expressed in terms of absolute magnitude such as by calculating an average or cumulative summary statistic such as average arm accelerations (m/s$^2$), cumulative joint loading, or cumulative activity counts. Multiple studies used physical activity level on the job measured as cumulative activity counts to convey intensity [68, 83, 84, 85, 86], with activity being identified as any movement with accelerations above a pre-defined threshold (0.016 m/s$^2$) [84]. Third, exposure intensity was conveyed using percentile (e.g., 10th, 90th, 95th) calculated from the cumulative distribution of posture angles, angular velocities and accelerations over the measurement duration. Most studies used a threshold-based approach (27 out of 46, 58.7%) compared to percentiles (11 out of 46, 23.9%) and average/cumulative magnitude (9 out of 46, 19.6%).

**Duration** characterized sustained postures and motions represented as an absolute time spent in certain postures or activities or as percent time normalized to total measurement time. Measures of percent time were used more often (16 out of 26, 61.5%) than absolute time (10 out of 26, 38.5%). **Repetition** was quantified either as the number of posture changes across a pre-defined threshold per time duration (counts/min) [54, 83] or by using frequency analysis such as a Fourier transformation to estimate motion repeatability in repetitive tasks [72, 89].

Exposure characteristics were computed either over the entire duration of data collection (22 out of 46, 47.8%) or stratified by specific tasks or activities (24 out of 46, 52.2%) (Table 2.3). For the latter, studies (21 out of 24, 87.5%) used information from additional methods such as direct or video-based observations to annotate and segment sensor data with the start and end of tasks and task type (10 out of 24 studies, 41.7%), diaries or work-logs (6 out of 24 studies, 25.0%) to record the time and duration of work vs. non-work (e.g., sleep, leisure) activities especially for data collection sessions spanning multiple days [73, 74, 90], and self-reported questionnaires for estimating the approximate duration

Table 2.3: Summary of the 46 studies reviewed that reported exposure characteristics of intensity, duration, and/or repetition calculated using inertial sensor-derived data. The fifth column (Task-based) represents whether the exposure characteristics were summarized either for specific tasks (T) or aggregated over the entire work duration irrespective of task (A).

| Reference | Physical exposure characteristics | | | Task-based | Additional Methods |
|---|---|---|---|---|---|
| | Intensity | Duration | Repetition | | |
| [91] | Threshold-based (arm elevation > 30°, > 60°, > 90°), Percentile (50th, 90th, 99th of arm elevation angle and velocity) | %time | | A | |
| [92] | Percentile (1st, 50th, and 90th of head flexion and lateral flexion, upper arm elevation angle and velocity) | | | T | Diary |
| [89] | Threshold-based | %time | Frequency analysis | A | |
| [83] | Threshold-based (trunk flexion < -10°, -10° to 20°, 20° to 45°, > 45°, Activity count <100 counts/min, 101-759 counts/min, 760-1952 counts/min, 1953-5724 counts/min, >5725 counts/min) | Time | Count (bends/hour) | A | |
| [84] | Threshold-based (trunk flexion < -10°, -10° to 20°, 20° to 45°, > 45°, Activity count <100 counts/min, 101-759 counts/min, 760-1952 counts/min, 1953-5724 counts/min, >5725 counts/min) | Time | Count (bends/hour) | A | |
| [70] | Percentile (1st, 10th, 50th, 90th, and 99th of wrist flexion, head flexion, upper arm elevation angle and velocity) | | | A | |
| [49] | Threshold-based (varies depending on the selected method) | Time | Count | T | Direct observation |
| [93] | Threshold-based (arm elevation > 60°, or < 20° and movement velocity < 5°/s) | %time | | A | Diary, video-based task analysis |
| [71] | Magnitude (average elbow/shoulder flexion angle, and shoulder abduction/adduction angle) | | | A | |
| [94] | N/A | | | T | Video-based task analysis |
| [77] | Threshold-based (high vs. low risk lifting based on the guidelines of the Danish Working Environment Authority) | | | T | |
| [75] | Magnitude (energy expenditure/hour) | | | T | Self-reported questionnaire |
| [76] | Threshold-based (trunk flexion > 50°) | %time | Count (bends/hour) | T | Video-based task analysis |
| [72] | Threshold-based (shoulder elevation < 20°, > 45°, > 60°), Percentile (10th, 50th, 90th of shoulder elevation) | Time | Frequency analysis | A | |
| [95] | Magnitude (average arm acceleration) | | | T | Work load |
| [46] | Magnitude (average flexion angle and L5-S1 compression and shear loadings) | | | A | |
| [96] | Percentile (10th, 50th, 90th, and 99th of head flexion, upper arm elevation) | | | A | |
| [80] | Threshold-based (trunk flexion 0-20°, upper arm inclination <20°) | Time | Count (uninterrupted neutral posture/min) | A | Video-based task analysis |

**Table 2.3 – continued from previous page**

| Reference | Physical exposure characteristics | | | Task-based | Additional Methods |
|---|---|---|---|---|---|
| | Intensity | Duration | Repetition | | |
| [97] | Percentile (1st, 10th, 50th, 90th, and 99th of trunk flexion angle, angular velocity, and angular acceleration) | | | T | Video-based task analysis |
| [42] | Magnitude (peak and cumulative joint loading, lateral and anterior-posterior shear loading at lumbar) | | | T | Direct observation |
| [98] | Threshold-based and Magnitude (hip, ankle, wrist acceleration counts) | | | A | |
| [51] | Percentile (10th, 50th, and 90th of head flexion and lateral flexion, neck flexion and lateral flexion, arm elevation angle and velocity) | | | T | Direct observation |
| [99] | Percentile (50th of head flexion, trunk flexion, upper arm elevation angle and velocity) | | | T | Video-based task analysis |
| [78] | | Time | | T | |
| [73] | Threshold-based (trunk flexion > 30°, > 60°, > 90°) | %time | | T | Diary |
| [100] | Threshold-based (head flexion and arm elevation > 30°) | %time | | A | Video-based task analysis |
| [52] | Threshold-based (arm elevation > 60°, > 90°), percentile (1st, 10th, 50th, 90th, and 99th of arm elevation, head flexion, neck flexion angle) | %time | | T | Direct observation |
| [101] | Magnitude (average relative acceleration between the equipment and a person) | | | A | |
| [82] | Threshold-based (trunk flexion/elbow flexion 0° to 30°, 30° to 60°, 60° to 90°, >90°, trunk lateral bend 0° to 15°, 15° to 30°, 30° to 45°, shoulder flexion/abduction 0°- 30°, 30° to 60°, 60° to 90°, 90° to 120°, > 120°) | | | T | Direct observation |
| [79] | Threshold-based (wrist extension < 10°, 11Âř- 25°, 2°Âř -4°, 41°- 55°, >60°, wrist flexion <5°, 6°- 15°, 16°- 30°, 31°- 50°, > 50°, ulnar deviation <10°, 11°- 15°, 16°- 20°, 21°- 25°, >25°) | %time | | T | Self-reported questionnaire |
| [102] | Threshold-based (trunk flexion > 30°, > 45°, > 60°) | %time | Count (> 5s over the threshold) | A | |
| [103] | N/A | | | A | |
| [104] | Percentile (10th, 50th, and 90th of trunk flexion and lateral bending) | | | A | |
| [105] | Percentile (10th, 50th, and 90th of trunk flexion, arm elevation), threshold-based (trunk flexion and upper arm elevation < 20°, > 45°, > 60°, velocities < 5°/s, > 90°/s) | %time | Count (3s period in neutral trunk or arm posture with velocity < 5°/s per min) | A | |
| [106] | Threshold-based (same as RULA) | | | A | Video-based task analysis |
| [107] | Threshold-based (neck flexion 0° to 10°, 10° to 20°, >20°, neck extension > 0°, trunk flexion at 0°, 0° to 20°, 20° to 60°, > 60°, shoulder elevation 0° to 20°, 20°to 45°, 45° to 90°, >90°) | %time | | A | |
| [85] | Threshold-based (activity count <100 counts/min, 101-1952 counts/min, 1953-5724 counts/min, >5725 counts/min) | Time | | T | Diary |

**Table 2.3 – continued from previous page**

| Reference | Physical exposure characteristics | | | Task-based | Additional Methods |
|---|---|---|---|---|---|
| | Intensity | Duration | Repetition | | |
| [47] | Threshold-based (trunk flexion < 20° and shank inclination 0° to 30°, >30°) | Time | Cound(bends/hour) | T | |
| [53] | Threshold-based (same as RULA) | %time | | A | |
| [74] | Threshold-based (trunk flexion > 30°) | Time | | T | Diary |
| [90] | Threshold-based (trunk flexion levels expressed as a percentage with a 10% increment) | Time | | T | Diary |
| [108] | N/A | | | T | Direct observation |
| [86] | Threshold-based (activity count <150 counts/min, 150-2019 counts/min, 2020-5999 counts/min, >5999 counts/min) | %time | | T | Self-reported questionnaire |
| [68] | Threshold-based (activity count <100 counts/min) | %time | | T | Self-reported questionnaire |
| [67] | Magnitude (percentage time spend on each posture) | %time | | T | Self-reported questionnaire |
| [54] | Threshold-based (neck flexion > 10°, trunk flexion > 20°, shoulder elevation > 45°), magnitude (mean and ROM of neck, torso flexion and shoulder elevation) | %time | | A | |

of work and non-work activities (5 out of 24 studies, 20.8%). In 3 studies, the exposure characteristics were stratified by tasks by first identifying the duration and type of specific work tasks using more objective techniques such a deterministic posture thresholds for classifying lifting strategy (i.e., stoop, squat, or combined) [47] and predictive modeling such as Linear Discriminant Analysis (LDA) [77, 78].

### 2.3.4 Assessment

Measured exposure characteristics were assessed using either "relative" vs. "absolute" assessment criterion. **Relative** assessments involved comparing measured biomechanical exposure characteristics (i.e., intensity, duration, and repetition of tasks or motions) within each study to determine increased vs. decreased WMSD risk between type of task performed [42, 51, 52, 54, 75, 92, 97, 99, 108], job category [76, 85], equipment used [71, 101, 107, 108], environmental conditions (e.g., load location, workstation set-up) [70, 98, 100, 104], level of social support [74], and effects of ergonomics training [104]. Alternatively, inertial sensor-based biomechanical exposures were compared with previously established or validated "**absolute**" thresholds to create an ordinal scale of WMSD risk. For example, Arias et al. [83] and Arias et al. [84] used thresholds derived from prior epidemiological studies on low-back disorders [3, 4, 109] to categorize low-back disorder risk from torso flexion exposures into three ordinal levels: 1) low risk: trunk flexion $< 15^{\circ}$ during 86% of the work shift, 2) high risk: trunk flexion $> 20^{\circ}$ during 33% of the shift, and 3) medium risk: all other exposure values. Bergsten et al. [93] used thresholds for exposures describing '*time in extreme*' and '*time in neutral*' developed using findings reported by Wahlström et al. [110]. In a study of mill workers, Heiden et al. [80] categorized trunk and arm postural exposures obtained from inclinometry using limits for neutral vs. non-neutral working postures specified in the European Standard '*Evaluation of working postures and movements in relation to machinery*' [111]. Others have assessed inertial sensor-derived postural exposures using ordinal risk scores analogous to observation-based

coding methods such as RULA and OWAS (e.g., [49, 53, 79, 106, 107]).

### 2.3.5 Intervention

Only four studies of the reviewed studies used real-time direct feedback as a method of intervention [47, 49, 69, 79]. Visual display was the most common feedback modality used, typically depicting graphical representations of highlighted or color-coded high risk motions and postures identify from the exposure analysis [47, 49, 69, 79]. In a study of manufacturing workers, Vignais et al. [53] used a head-mounted display to highlight joints and segments exceeding a threshold level from an inertial-based RULA assessment. Auditory feedback such as a warning beep when the postural angle exceeds a threshold level [47, 53] and vibrotactile feedback [47] were also used in combination with visual displays. When real-time feedback was provided directly to the worker instrumented with inertial sensors to instantly modify their work postures, auditory and vibrotactile feedback were found to be more effective (e.g., prompt, less obtrusive) since workers could attend to it in parallel with visually-dominant work task, compared to the visual display that interferes with work [47].

## 2.4 Discussion

Body-worn inertial sensor technology provides a number of opportunities to advance the safety and health of workers engaged in physical work. This research reviewed 67 references in the ergonomics literature on inertial sensing-based biomechanical exposure assessment to examine the current state of the science and potential gaps in different areas of sensor use based on a proposed MSAAI framework. The subsequent sections discuss key themes and gaps identified with an eye towards informing future research on wearable inertial sensing-based tools for biomechanical exposure assessment.

### 2.4.1 Modeling, Sensing and Sensor Placement

Choosing where to place sensors on the body is a critical decision when considering the use of body-worn inertial sensors for novel ergonomics applications. Sensor locations in most studies were primarily informed by either implicit or explicit biomechanical modeling criteria related to that study's focal research question, i.e., the relevant segments or joints that were being modelled. Some studies relied on up to 17 body-worn inertial sensors, which can be obtrusive and time-consuming, and affect wearability. Clearly, minimizing the number of sensors would be advantageous. Trade-offs between the number of sensors and user comfort are rarely documented in the ergonomics literature. A study by Mokhlespour and Nussbaum [112] reported that respondents rated the ankle, wrist, waist, thigh, and foot as the most preferred location for inertial sensor placement compared to the neck, torso, elbow, fingers. Beeler et al. reported that sensors attached on the upper arm, hip, and back were rated relatively higher in comfort and acceptability compared to the chest location which was rated the lowest [113]. Interestingly, the number and anatomical locations of the sensors differed across studies even when investigating the same type of joint or movement. This review also identified a need for consistency in the reporting of joint angular motions in the anatomical or segment reference frame such as flexion/extension, abduction/adduction, or internal/external rotation to aid the interpretation of results compared to using the sensor frame of reference (e.g., roll, pitch, and yaw).

#### 2.4.1.1 Sensor Performance

Studies validating inertial sensor performance (e.g., accuracy, reliability, and repeatability) largely focused on determining whether the inertial sensor-derived kinematic or kinetic information were accurate and precise compared to traditional lab-based methods. While metrics of sensor performance were not directly comparable across different studies due to the differences in study design and factors affecting estimated errors, the overall trend showed consensus that inertial sensors are accurate and reliable for measuring hu-

man movement in practical applications relevant to ergonomics. However, several issues pertaining to inertial sensor performance remain unanswered or under-explored despite the many validation studies. For example, few validation studies have examined the effects of different biomechanical modeling methods on the performance of inertial sensor based exposure metrics [43, 50, 57]. The focus of most validation studies to date was on investigating the inherent instrumentation error rather than the comparison between different biomechanical modeling methods. However, two studies in particular demonstrated that differences in biomechanical models contributed more to the accuracy of the kinematic data compared to the inherent instrumentation error [43, 50]. Also, sensor durability, reliability, and repeatability can become a critical issue when the data collection span long-term durations, such as across multiple days wherein users themselves or different researchers need to reattach the sensors on the user each time. Also, if sensors are not directly attached to the skin using adhesive tape (e.g., by using straps), subtle changes in the sensor locations over time are unavoidable.

Multiple studies required that one of the sensor axes was aligned with the anatomical axis of the body, so that linear and angular movement of the sensor can be directly mapped to segment kinematics. However, it can be difficult to perfectly align a sensor axis to the anatomical axis of the body segment, especially when the user (e.g., worker) has to attach the sensor themselves. Data processing algorithms that are robust to account for small misalignment would be ideal. Alternately, improved dynamic calibration methods may provide a more practical solution to minimize effects of small deviations in sensor placement (i.e., using a calibration pose or reference movements) than assuming that sensor locations remain unchanged over time. Some studies employed such static or dynamic calibration methods to correct for misalignment between the sensor axis and the anatomical axis [59, 91]. In a study measuring the upper arm elevation angle, Acuna and Karduna [91] performed a static calibration by asking participants to align their arm perpendicular to the floor by laterally bending their trunk while maintaining in a seated upright posture

and holding a 1-kg weight. Favre et al. [59] developed a dynamic calibration method involving hip abduction and adduction movement to align two IMUs attached on thigh and shank segments. Wearable sensors incorporated into clothing fabric (e.g., [114]) and body-worn equipment such as exoskeletons and personal protective devices (e.g., back support belts) that have specific location and orientation could altogether alleviate some of these misalignment concerns.

### 2.4.2 Analysis: Quantifying Exposures and the Use of Predictive Modeling

Quantifying biomechanical exposures and identifying high-risk work conditions requires knowing the specific work context [115, 116, 117]. Most studies that examined biomechanical exposures by task (21 out of 24, 87.5%) incorporated additional methods (e.g., direct observations, self-reported measures) to identify task type and duration (i.e., start and end of specific tasks) since such information is not readily apparent from inertial sensor data alone. However, direct observation and video-based task analysis are time and labor intensive, and not feasible in some field environment for privacy and logistical reasons. Self-reported questionnaires, diaries, and work logs can be subjective and susceptible to systematic bias [66, 68] and often cannot provide the specific time-frame of work activities unless workers are asked to log their activities over very short time interval (< 1 min).

As an alternative, predictive modeling techniques have shown strong potential for extracting rich contextual information from inertial-sensor based kinematic data in non-occupational domains. For example, activity recognition in daily activities [118, 119] and detecting falls [120, 121, 122] have gained much research attention in health-care, smart homes and assisted living, and sports/kinesiology applications. In contrast the application of predictive modeling techniques in biomechanical exposure assessment remains under-explored. A few of the studies reviewed [67, 75, 76] used commercial software to detect different work postures. However biomechanical exposure assessment requires informa-

tion beyond just postures to identifying the specific tasks performed, durations (i.e., start and end times), repetitions, and intensity (e.g., magnitude of loads carried). In this regard, studies on classifying work-relevant tasks [78, 79] and task intensity [77, 123, 124, 125] from inertial sensor data though limited in task conditions were comparable in performance to traditional methods for exposure assessments (e.g., direct observations) with the benefit of less time and cost. Collectively these studies show potential for combining inertial sensor data with predictive modeling techniques in developing work activity and intensity classification algorithms for use in biomechanical exposure assessment.

### 2.4.3 Assessment of WMSD Risk

Reviewed studies that were focused on exposure assessment followed traditional observation-based methods by substituting observed categorical posture codes with inertial sensor-based posture angles into assessment tools (e.g., RULA and OWAS scores, Strain Index). Since these traditional methods were developed assuming that human observers visually code posture angles categorically each time, the coding scheme and the resulting WMSD risk scales are very simple. Research is needed to develop more valid and sensitive measures of WMSD risk relying of directly measured exposure data.

### 2.4.4 Intervention: Real-time Feedback

Most commercial wearable inertial sensors have the capability to stream data to a web server (cloud) or remote computer in real-time (e.g., APDM Inc.). This allows for recording, processing and reviewing sensor data online and in near real-time affording new opportunities for quick feedback about work postures to workers (e.g., to prompt changes in work postures) or to supervisors and ergonomists (e.g., about durations and repetitions of worker postures over time). However, few studies in this review utilized such real-time feedback functionality. Leveraging this capability will require developing software algorithms that receive, process, and calculate biomechanical exposure metrics or risk levels in real-time.

Research studies in the subsequent chapters describe initial steps in this direction.

### 2.4.5 Study Limitations

The current review was limited to the use of inertial sensing technologies for continuous monitoring of biomechanical exposures. Applications combining inertial sensing with other wearable technologies for collecting data on human performance and physiology (e.g., wireless surface electromyography, heart rate, galvanic skin response) and ambient work conditions (e.g., temperature, air particulates, etc.) are also fast developing although were not explored in this research review. However, these wearable technologies present similar concerns as those raised in this study related to modeling, sensing, analysis, assessment, intervention, and usability (i.e., wearability, privacy, user adoption). Wearable inertial sensing in ergonomics is a rapidly evolving field and as such, this review is only a small part of a larger conversation about realizing the full potential of wearable sensors in ergonomics research and practice.

## 2.5 Conclusion

This chapter reviewed the current state of the science on wearable inertial sensors for biomechanical exposure assessment within an ergonomics framework, i.e., modeling, sensing, analysis, assessment, and intervention. Findings suggest a growing body of knowledge pertaining to wearable inertial sensing in ergonomics, however most studies remain relegated to laboratory studies to validate inertial sensor data compared to "gold standard" motion capture measures, or to fields studies for measuring motions and postures instead of observational methods. As such, wearable inertial sensors have largely held appeal as new "research" tool. Translating inertial sensing technologies to biomechanical exposure assessment in real world settings still lags. The biggest contribution of this emerging technology to ergonomics is in the ability to increase the quality and quantity of biomechanical

exposure data towards identifying and mitigating the risk of cumulative trauma disorders. To this effect, a few key conclusions and directions for future research are provided:

- *Modeling & sensing*: Since misalignment in sensor placement are unavoidable, posture analysis techniques using inertial sensing need to be robust to minor misalignment, or involve calibration postures or movements that are simple enough for practitioners to administer.

- *Modeling*: Quantifying inertial sensor "measurement error" is important but has been overemphasized in previous research. For example, when quantifying low-back disorder risk, the effect of modeling assumptions used in calculating internal low-back biomechanical loads (e.g., a single-vector back extensor muscle when calculating low-back compressive forces) exceeds the influence of inertial sensor "error" in measuring torso flexion angle [43, 50]. It is important that research involving new emerging sensing technologies not lose perspective of the end goal, namely, reducing the risk of cumulative trauma disorders.

- *Assessment*: Related to the previous point, algorithmic frameworks are needed that relate wearable inertial sensing with biomechanical exposure assessment and WMSD risk. Currently, studies continue to rely on observational-based risk scores such as RULA and OWAS to summarize WMSD risk from inertial sensor derived postural stress (e.g., [79]).

- *Analysis*: Analysis of inertial sensor data was largely limited to characterizing the intensity, repetitions and duration of postures. The ability to extract information about work content from motion data is underutilized. Two approaches from this review appear promising:

  - deterministic threshold-based methods to activity classification, particularly when clear criteria for separating tasks from posture information (e.g., standing, vs. walking vs. sitting; [47, 83, 84]) can be identified, and

  - statistical prediction techniques to identify tasks or behaviors (e.g., lifting strategy, load carrying mode [77, 78]), particularly when subtle changes in multiple sensor data features are involved.

- *Sensing*: Alongside the modeling requirements, wearability issues associated with the number and location of body-worn sensors needs to be considered . With some studies requiring up to 17 body-worn inertial sensors it is clear that the trade-offs between the number/location of sensors and wearability are often ignored [78].

- *Intervention:* Wearable inertial sensing (including other physiological sensors) present unprecedented opportunity for feedback about biomechanical exposures. Early studies indicate that auditory and vibrotactile feedback modalities are more effective when real-time feedback derived from inertial sensor kinematic data is provided directly to the worker (e.g., to instantly modify their work postures [53]). Visual displays may be more effective when the viewer is not the worker, but rather a work-supervisor, manager, or ergonomist reviewing a workers' cumulative biomechanical load exposures across time (e.g., spinal compression loads at the end of a work-shift). Research is needed to understand the content and modality of information provided, and identify appropriate use-cases for such real-time feedback capability.

The subsequent chapters represent initial steps to address some of these research gaps towards new wearable inertial sensor-based approaches for biomechanical exposure assessment in non-repetitive work.

# CHAPTER 3

# Quantifying Effects of Load Carriage on Gait Kinematics Using Wearable Inertial Sensors[1]

The objective of this study was to quantify the effects of mode of load carriage and load magnitude on gait parameters using 2 body-worn inertial sensors. Nine participants performed walk trials at self-selected speeds while carrying hand loads in two modes (two-handed side vs. anterior) at four load levels (empty-handed, 4.5 kg, 9.1 kg, and 13.6 kg). Six temporal gait parameters, six postural sway parameters, and three measures of thoracic-pelvic coordination were calculated from data recorded by six body-worn inertial sensors for 540 gait cycles. Results demonstrated that gait patterns characterized by inertial sensor-derived temporal and kinematic gait parameters changed systematically by the mode of load carriage and load magnitude, after adjusting for gait cycle duration and stride length. Measures of thoracic-pelvic coordination and sway in the coronal and transverse planes showed trends of significant practical relevance and may provide sufficient information to typify alterations in gait across two-handed side vs. anterior load carriage of different magnitudes.

## 3.1 Introduction

Load carriage is common in daily activities. People often choose to carry loads in their hands anteriorly or laterally for convenience over short distances or for intermittent peri-

[1]Portions of this chapter appear in [126]

ods. Manual load carriage is also prevalent and inevitable in many occupations such as military [127], firefighting [128], and construction work [129], and MMH in manufacturing, warehousing, packaging, and distribution. Routine load carriage is associated with an increased risk of MSDs in the low-back [2, 130]. Low-back injuries such as back strain or spinal discs trauma were frequently reported in soldiers [131]. Prior studies associate the increase of hand loads to increased torso and hip moments [132, 133, 134], increased back and abdominal muscle activity to improve spinal stability [135, 136, 137] and increased compressive and shear loads on the lumbar spine [129, 138, 139, 140].

Beyond temporal aspects of duration and repetition, the risk from load carriage to the musculoskeletal system also depends on the load magnitude and the mode or manner by which the load is carried [140, 141]. The latter alters the position of the load relative the spine to affect spinal loads. Prior studies have used analytical models to estimate spinal loads as a means of quantifying the risk of spinal disorders from load carriage. McGill et al. [138] estimated that compressive loads on the spine are significantly more when carrying weights in one hand compared to using both hands. Rose et al. [140] investigated compressive and shear loading in the lumbar spine in various modes of load carriage including one-handed side carry, shoulder carry, two-handed anterior carry, and posterior carry. Their study concluded that for the same load level, two-handed anterior carry resulted in the largest increase in anterior-posterior shear loading and thereby posed the greatest relative risk to low back injury [140]. Rohlmann et al. [142] estimated that lumbar compression force with respect to standing was nearly twice as high for carrying a weight in front of the body compared to carrying it laterally.

Human gait encapsulates movement with the arms, head, legs, and torso, and while each may be seem variable and arbitrary but are, in fact, repeatable and predictable. This is particularly true of kinematic adjustments for maintaining postural stability in response to external hand loads while walking. Effects of posterior loads from carrying a backpack or rucksack on gait patterns [143, 144, 145, 146] has received the most attention

in ergonomics due to its relevance to military soldiers [147, 148], firefighters [128] and school children [149, 150]. Increasing backpack load was associated with a decrease in swing duration [151], single support duration [146], and stride length [143], and an increase in double support duration [146] and stride frequency [143]. Increasing posterior loads also produced changes in postural kinematics such as increased mean torso inclination [145, 146, 148], decreased torso angular acceleration [132], and decreased transverse torso and pelvis rotation [143].

Biomechanical loading from load carriage also affects the way people move their torso and pelvis when walking. The relative phase angle, described by the phase difference or relative phase between two oscillating segments, provides a measure of coordination between multiple body segments or joints during complex and repetitive multi-joint movements [152]. In conventional gait analyses, relative phase angles are used as a measure of rotational thoracic-pelvic coordination [134, 143, 153, 154, 155]. Graham et al. [156] used variability in thoracic-pelvic relative phase angles as a measure of postural stability in comparing posterior vs. anterior load carriage. However, all of the prior studies using inter-segment relative phase angles relied on optical motion tracking with participants walking at precise speeds on a treadmill, and thus do not directly extend to applied work settings.

Wearable inertial sensors or IMUs have gained considerable attention in biomechanics research as an inexpensive and less obtrusive form of bioinstrumentation [157]. The portability and low power consumption of inertial sensors make them very suitable for monitoring outdoor ambulation over long durations [158, 159]. Multiple studies have demonstrated the validity and reliability of commercial, body-worn inertial sensors and related data processing algorithms combining data from rate gyroscopes (i.e., angular velocity) and linear accelerometers to analyse able-bodied and pathological gait [160, 161, 162, 163, 164]. In comparison, the application of body-worn inertial sensors to analyze ambulatory occupational tasks such as manual material handling and load carriage is still emerging.

The aim of this study was to quantify the effects of hand loads during two-handed side

and anterior load carriage on temporal and postural gait parameters obtained from body-worn inertial sensors. The study hypothesized that the magnitude and mode of load carriage would jointly influence temporal gait parameters, torso and pelvic sway, and thoracic-pelvic coordination during load carriage relative to unloaded gait at a self-selected walking speed. The study implemented a previously-validated algorithm by Aminian et al. [160] to identify gait events and extract temporal gait parameters using data from a gyroscope mounted on the lower-leg (i.e., shank).

## 3.2 Methods

### 3.2.1 Study Participants

The study sample comprised nine healthy male individuals aged between 18 to 35 years old recruited from the university population. The study was approved by the university's institutional review board. Prior to participation, participants provided written informed consent and were screened for pre-existing back injuries or chronic pain with a body discomfort questionnaire adapted from the body mapping exercise developed by NIOSH [165]. Age, gender, and health restrictions were applied in order to minimize potential inter-subject variability in gait patterns from these sources in the interest of obtaining a homogeneous sample.

### 3.2.2 Experiment Procedures

A laboratory experiment was conducted that required participants to carry a weighted box down a levelled corridor (26.2 m length x 1.6 m width) for a distance of 24 m in two carrying modes, namely, a two-handed side carry and two-handed anterior carry (Figure 3.1). Four levels of box weights were evaluated in each mode: no-load (i.e., unloaded reference condition), 4.5 kg, 9.1 kg, and 13.6 kg. The two-handed anterior carry was performed using

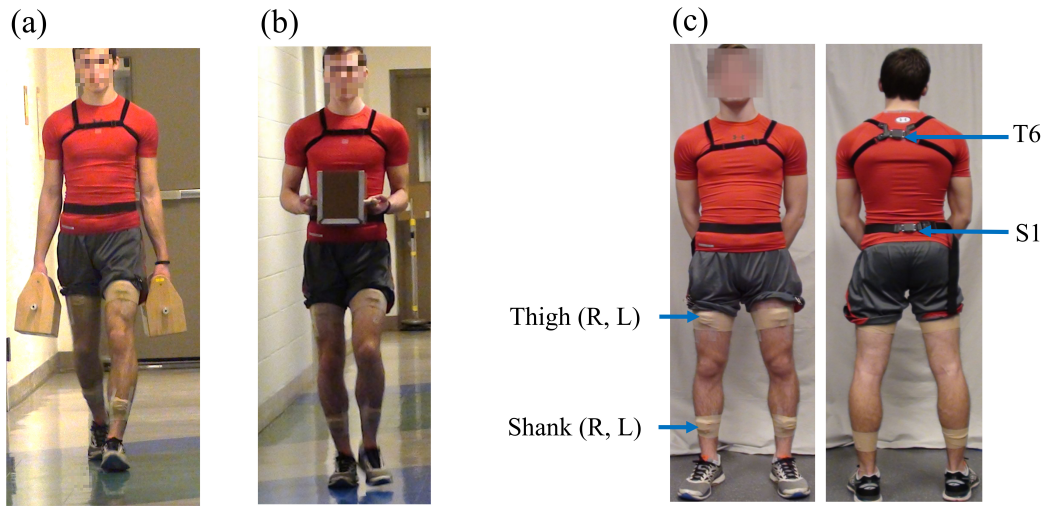



Figure 3.1: Images showing the two carrying modes evaluated in this study: (a) two-handed side carry, (b) two-handed anterior carry, along with the location of (c) six inertial sensors attached on the body at T6, S1, thigh (Right, Left), and shank (Right, Left).

one box with two handles on the sides (177.8 mm width x 228.6 mm depth x 203.3 mm height). The two-handed side load carriage was performed using a box in each hand with a handle on the top (152.4 mm width x 177.8 mm depth x 127 mm height). To maintain symmetry in hand-loads the combined weight in the anterior carry was equally divided between the right and left hand in the two-handed side carry.

Two walk trials in the no-load condition were performed at the beginning of the experiment. Subsequently, each participant performed two consecutive walk trials with hand loads in each combination of carrying mode and load level, presented in random order. Participants were instructed to self-select a walking speed for each condition that could be comfortably maintained over both walk trials. In the two-handed anterior condition participants were instructed to hold the box close to their torso with their elbow flexed 90 degrees. In order to minimize carryover effects of fatigue, participants were provided two-minute rest breaks between each condition and were allowed additional rest breaks at anytime if they requested.

### 3.2.3 Instrumentation

During the walk trials, kinematic data were continuously recorded using six commercial inertial sensors (Opal, APDM Inc., Portland, OR, USA). Two inertial sensors were attached over the sixth thoracic vertebra (T6) and the first sacral vertebra (S1) using elastic Velcro straps, respectively (Figure 3.1). Two sensors were positioned along the superior aspect of the right and left thigh midway between the hip and lateral femoral epicondyles, and two sensors on the superior aspect of the right and left shank midway between the lateral femoral and malleolar epicondyles, and attached using double-sided hypoallergenic tape and medical tape wrap. Sensors were attached with one of the sensor axes (i.e., x-axis) aligned with the proximal-distal axis of the body segment and pointing inferiorly.

### 3.2.4 Data Processing and Dependent Measures

The six inertial sensors synchronously recorded triaxial accelerometer, gyroscope, and magnetometer data at a sampling frequency of 80 Hz. The data was filtered using a second-order low-pass zero-lag Butterworth filter with a cut-off frequency of 2-Hz. Gyroscope data was integrated to obtain angular displacement, and subsequently filtered using a second-order high-pass filter with a cut-off frequency of 0.75 Hz to reduce the effect of drift [166].

Next, a custom software algorithm implemented in MATLAB (MATLAB R2016b, The MathWorks Inc., Natick, MA, USA) was used for computing two covariates, namely, gait cycle duration and stride length, and fifteen gait parameters as dependent measures from the inertial sensor data for each recorded gait cycle. Table 3.1 provides definitions and sensor locations used for computing each parameter. These gait parameters, identified by a comprehensive review of the gait literature, comprise six temporal measures of the gait phases, six measures of torso and pelvis postural sway, and three measures of thoracic-pelvic coordination in the form of relative phase angles in the coronal, transverse, and sagittal planes. Procedures for computing these measures from inertial sensor data for each gait cycle are briefly described below.

Table 3.1: List and definitions of gait parameters calculated from inertial sensor data. In each row, location of sensors used for calculating the parameters are indicated by '•' with relevant source reference. Connected dots indicate pairs of sensors used together.

| Parameter | | Definition | Inertial Sensor Location | | | | | | Source |
|---|---|---|---|---|---|---|---|---|---|
| | | | T6 | S1 | R. thigh | R. shank | L. thigh | L. shank | |
| **Spatio-temporal parameters** | | | | | | | | | |
| 1 | Gait cycle duration (sec) | The duration of one gait cycle (one right plus left step duration) | | | | • | | • | [160] |
| 2 | Stride length (cm) | The length moved from right heel-strike to the next right heel-strike during one gait cycle | | | • | • | | | [160] |
| 3,4 | Stance, Right and Left Leg (%) | The percentage of the gait cycle in which the right or left foot is on the ground. | | | | • | | • | [160] |
| 5,6 | Swing, Right and Left Leg (%) | The percentage of the gait cycle in which the right or left foot is not on the ground. | | | | • | | • | [160] |
| 7 | Initial double support (%) | The percentage of the gait cycle in which both feet are on the ground after a right foot heel strike. | | | | • | | • | [160] |
| 8 | Terminal double support (%) | The percentage of the gait cycle in which both feet are on the ground after a left foot heel strike. | | | | • | | • | [160] |
| **Torso and pelvis postural sway** | | | | | | | | | |
| 9,10 | Coronal ROM at T6 & S1 (deg.) | Range of rotation angle in coronal plane: Max (integrated angular velocity, z-axis) - min (integrated angular velocity, z-axis) | • | • | | | | | [143] |
| 11,12 | Transverse ROM at T6 & S1 (deg.) | Same calculation as above in transverse plane: x-axis | • | • | | | | | |
| 13,14 | Sagittal ROM at T6 & S1 (deg.) | Same calculation as above in sagittal plane: y-axis | • | • | | | | | |
| **Thoracic-pelvic coordination** | | | | | | | | | |
| 15 | Coronal mean relative phase angle between T6 and S1 (deg.) | Average (pelvic phase angle - thoracic phase angle). Phase angle (t) = arctan (normalized angular velocity, z-axis (t)/normalized integrated angular velocity, z-axis (t)) | •——• | | | | | | [143, 152, 169] |
| 16 | Transverse mean relative phase angle between T6 and S1 (deg.) | Same calculation as above in transverse plane: x-axis | •——• | | | | | | |
| 17 | Sagittal mean relative phase angle between T6 and S1 (deg.) | Same calculation as above in sagittal plane: y-axis | •——• | | | | | | |

#### 3.2.4.1 Spatio-temporal parameters

First, heel-strike (i.e., when the foot first touches the floor) and toe-off events for both feet were detected using the filtered angular velocity data obtained from gyroscopes on the right and left shank using an algorithm adapted from Aminian et al. [160] and validated in multiple prior studies e.g., [167, 168]. Two consecutive right heel-strikes were denoted as one gait cycle. Using these event markers, durations for six key phases of the gait cycle namely, right and left stance phase, right and left swing phase, initial double support, and terminal double support were computed and expressed as a percentage (%) of a gait cycle duration. This algorithm is summarized in Appendix C, and was repeated for all gait cycles.

Stride length (cm) was estimated using the double segment gait model by Aminian et al. [160] summarized in Appendix D. The double segment gait model estimates stride length by modelling the thigh and shank as a double pendulum during the swing phase, and likewise as an inverted double pendulum during the stance phase with the assumption of symmetry between both legs [160].

#### 3.2.4.2 Torso and Pelvis Postural Sway

For each gait cycle, six measures of torso and pelvic postural sway were calculated as the peak-to-peak range of motion (ROM) angles in the coronal, transverse, and sagittal planes at the thoracic (inertial sensor at T6) and pelvic (inertial sensor at S1) segment location, respectively. The angular displacements were calculated by integrating the filtered gyroscope data again within each gait cycle ( 1 s) to minimize the effect of drift.

#### 3.2.4.3 Thoracic-Pelvic Coordination

Thoracic-pelvic coordination was measured using the mean relative phase angle [152] computed at each data-frame and averaged over a gait cycle (refer Appendix E). A higher mean relative phase angle implies an out-of-phase or uncoordinated movement between the thorax and pelvis segments compared to more in-phase (i.e., synchronized and coordinated

movements) for lower mean relative phase angles.

### 3.2.5 Statistical Analyses

The nine participants averaged 13.5 $\pm$ 1.8 gait cycles in each of the two repetitions of walk trials per condition. Ten gait cycles per condition were extracted for analysis by selecting 5 gait cycles from the middle portion, typically 5th to 9th gait cycle, from each of the two walk trial repetitions per condition in order to minimize the effects of acceleration and deceleration near the start and end of the walk trials. Fifteen gait parameters were computed for a total of 540 gait cycles (i.e., 9 participants x 8 conditions x 10 gait cycles per condition).

Statistical analyses were conducted in two stages. First, descriptive statistics and Pearson correlation coefficients for the 15 gait parameters over 10 gait cycles per condition were calculated. Second, mixed effects models [170] implemented in SPSS v. 23 (IBM Inc., New York, USA) were used to quantify the effects of within-subject variables, viz., carrying mode (two-handed side carry vs. two-handed anterior carry) and load level (no-load, 4.5 kg, 9.1 kg, and 13.6 kg) and their two-way interaction effect on each of the 15 gait parameters. In each mixed effects model, centered gait cycle duration and centered stride length were included as covariates (i.e., set as fixed effect and random effect parameters in the mixed effects model) to adjust for changes in walking speed and stride length between participants and test conditions. Gait cycle count (1-10) was included as a repeated measure. Significant main and interaction effects ($p < 0.05$) were examined using Bonferroni post hoc tests which adjusts for Type-I error rates to analyze paired comparisons between carrying mode at each level of load level and vice versa. Estimated marginal means and standard errors for the 15 gait parameters obtained from the mixed effects models were tabulated, stratified by carrying mode and load level, at the average values of centered gait cycle duration and centered stride length.

## 3.3 Results

The nine participants had an average ($\pm$ standard deviation, SD) age of 22.0 $\pm$ 3.0 years, stature 1.75 $\pm$ 0.05 mm, and weight 77.11 $\pm$ 9.98 kg. Average gait cycle duration and stride length across all gait cycles were 1.05 $\pm$ 0.05 s (range: 0.93 - 1.16 s) and 110 $\pm$ 12 cm (range: 81 - 156 cm), respectively. Five pairs of temporal gait parameters were highly correlated with a Pearson's correlation coefficient of $|R| > 0.8$, namely, initial double support and swing left ($R$ = -0.87), terminal double support - stance right ($R$ = 0.87), terminal double support - swing right ($R$ = -0.86), stance right - swing right ($R$ = -0.98), stance left - swing left ($R$ = -0.97). Correlation coefficients between pairs of spatial parameters and sway parameters were below 0.49.

Results from the mixed effects analyses of carrying mode and load level on temporal gait parameters and postural sway parameters are summarized in Table 3.2 and Table 3.3, respectively. Table 3.4 provides the estimated marginal means for the 15 gait parameters with statistically significant ($p < 0.05$) effects of carrying mode and load level relative to the no-load condition, at average values of the covariates, namely, centred gait cycle duration and centred stride length. Significant trends are discussed in the subsequent section.

### 3.3.1 Temporal Gait Parameters

Statistically significant main effects of carrying mode were found for all six temporal parameters (Table 3.2). Right stance, left stance, initial double support, and terminal double support durations were significantly longer in the side carry compared to the anterior carry condition. Conversely, right and left leg swing durations were significantly shorter in the side carry compared to the anterior carry. No significant main effect of load levels on temporal parameters was observed.

A significant interaction effect was observed for five temporal parameters. In the side carry condition, durations for right and left leg stance and terminal double support increased

Table 3.2: Summary results from the mixed effects analyses for the main and interaction effects of carrying mode and load level on temporal gait measures. Significant pair-wise Bonferroni comparisons ($p < 0.05$) are provided for main and interaction effects that were significant at $p < 0.05$ indicated by *. NL = No-load (empty-handed), L = Low load at 4.5 kg, M = Medium load at 9.1 kg, H = High load at 13.6 kg.

| | | | | **Covariates** | |
|---|---|---|---|---|---|
| | **Carrying Mode** | **Load Level** | **Carrying Mode x Load Level** | **Gait Cycle Duration Centered (s)** | **Stride Length Centered (cm)** |
| Stance, Right Leg (%) | $F(1, 336) = 13.72$, $p < 0.001$ * Side > Anterior | $F(3, 141) = 2.40$, $p = 0.070$ | $F(3, 113) = 8.02$, $p < 0.001$ * Side: (H, M) > (L, NL) H, M: Side > Anterior | $F(1, 44) = 13.96$, $p = 0.001$ * | $F(1, 5) = 0.05$, $p = 0.835$ |
| Stance, Left Leg (%) | $F(1, 394) = 46.82$, $p < 0.001$ * Side > Anterior | $F(3, 226) = 0.53$, $p = 0.661$ | $F(3, 185) = 15.71$, $p < 0.001$ * Side: M > NL Anterior: NL > (M, H) H, M, L: Side > Anterior | $F(1, 26) = 0.34$, $p = 0.565$ | $F(1, 20) = 0.01$, $p = 0.999$ |
| Swing, Right Leg (%) | $F(1, 332) = 13.75$, $p < 0.001$ * Anterior > Side | $F(3, 143) = 2.0$, $p = 0.117$ | $F(3, 113) = 7.89$, $p < 0.001$ * Side: (NL, L) > H H, M: Anterior > Side | $F(1, 39) = 12.89$, $p = 0.001$ * | $F(1, 6) = 0.04$, $p = 0.850$ |
| Swing, Left Leg (%) | $F(1, 356) = 9.92$, $p = 0.002$ * Anterior > Side | $F(3, 186) = 2.22$, $p = 0.087$ | $F(3, 148) = 3.76$, $p = 0.012$ * Side: NL > (M, H) H, M: Anterior > Side | $F(1, 27) = 24.46$, $p < 0.001$ * | $F(1, 14) = 0.01$, $p = 0.998$ |
| Initial double support (%) | $F(1, 316) = 9.0$, $p = 0.003$ * Side > Anterior | $F(3, 179) = 1.62$, $p = 0.187$ | $F(3, 151) = 2.15$, $p = 0.096$ | $F(1, 30) = 14.79$, $p = 0.001$ * | $F(1, 18) = 0.01$, $p = 0.994$ |
| Terminal double support (%) | $F(1, 325) = 20.78$, $p < 0.001$ * Side > Anterior | $F(3, 195) = 1.28$, $p = 0.283$ | $F(3, 144) = 9.68$, $p < 0.001$ * Side: H > (L, NL) H, M: Side > Anterior | $F(1, 329) = 20.07$, $p < 0.001$ * | $F(1, 11) = 0.17$, $p = 0.685$ |

Table 3.3: Summary results from the mixed effects analyses for the main and interaction effects of carrying mode and load level on torso and pelvis postural sway and thoracic-pelvic coordination measures in the coronal, transverse, and sagittal planes. Significant pair-wise Bonferroni comparisons ($p < 0.05$) are provided for main and interaction effects that were significant at $p < 0.05$ indicated by *. NL = No-load (empty-handed), L = Low load at 4.5 kg, M = Medium load at 9.1 kg, H = High load at 13.6 kg.

| | | | | Covariates | |
|---|---|---|---|---|---|
| | **Carrying Mode** | **Load Level** | **Carrying Mode x Load Level** | **Gait Cycle Duration Centered (s)** | **Stride Length Centered (cm)** |
| **Coronal plane** | | | | | |
| ROM at T6 (deg.) | $F(1, 483) = 45.77$, $p < 0.001$ * Anterior > Side | $F(3, 220) = 45.74$, $p < 0.001$ * NL > L > (M, H) | $F(3, 192) = 13.15$, $p < 0.001$ * Side: NL > L > (M, H) Anterior: (NL, L) > (H, M) H, M, L: Anterior > Side | $F(1, 24) = 2.30$, $p = 0.142$ | $F(1, 6) = 0.01$, $p = 0.996$ |
| ROM at S1 (deg.) | $F(1, 468) = 8.70$, $p = 0.003$ * Side > Anterior | $F(3, 258) = 77.07$, $p < 0.001$ * (H, M) > L > NL | $F(3, 281) = 19.92$, $p < 0.001$ * Side: H > M > L > NL Anterior: (H, M, L) > NL H: Side > Anterior | $F(1, 54) = 0.12$, $p = 0.731$ | $F(1, 9) = 0.01$, $p = 0.971$ |
| Mean relative phase angle (deg.) | $F(1, 379) = 466.74$, $p < 0.001$* Side > Anterior | $F(3, 121) = 5.95$, $p = 0.001$ * NL > L | $F(3, 119) = 78.93$, $p < 0.001$ * Side: H > M > (L, NL) Anterior: NL > (L, M) > H H, M, L: Side > Anterior | $F(1, 343) = 8.14$, $p = 0.005$ * | $F(1, 10) = 0.01$, $p = 0.957$ |
| **Transverse plane** | | | | | |
| ROM at T6 (deg.) | $F(1, 475) = 1.32$, $p = 0.251$ | $F(3, 237) = 1.53$, $p = 0.208$ | $F(3, 224) = 4.12$, $p = 0.007$ * Side: L > NL L: Side > Anterior | $F(1, 422) = 0.05$, $p = 0.817$ | $F(1, 6) = 0.01$, $p = 0.972$ |
| ROM at S1 (deg.) | $F(1, 445) = 271.78$, $p$ <0.001* Side > Anterior | $F(3, 250) = 6.87$, $p < 0.001$ * (H, M, L) > NL | $F(3, 254) = 59.34$, $p < 0.001$ * Side: (H, M, L) > NL Anterior: NL > (L, M, H) H, M, L: Side > Anterior | $F(1, 254) = 2.60$, $p = 0.108$ | $F(1, 9) = 0.01$, $p = 0.992$ |
| Mean relative phase angle (deg.) | $F(1, 469) = 94.9$, $p < 0.001$ * Anterior > Side | $F(3, 240) = 46.45$, $p < 0.001$ * NL > L > (M, H) | $F(3, 210) = 13.55$, $p < 0.001$ * Side: NL > (L, M, H) Anterior: NL > (L, M) > H H, M, L: Anterior > Side | $F(1, 331) = 0.15$, $p = 0.702$ | $F(1, 10) = 0.01$, $p = 0.997$ |
| **Sagittal plane** | | | | | |
| ROM at T6 (deg.) | $F(1, 527) = 78.83$, $p$ <0.001 * Side > Anterior | $F(3, 265) = 4.50$, $p = 0.004$ * (H, L) > NL | $F(3, 257) = 8.95$, $p < 0.001$ * Side: (H, M, L) > NL H, M, L: Side > Anterior | $F(1, 345) = 5.21$, $p = 0.023$ * | $F(1, 8) = 0.01$, $p = 0.995$ |
| ROM at S1 (deg.) | $F(1, 453) = 22.09$, $p < 0.001$ * Anterior > Side | $F(3, 271) = 25.25$, $p < 0.001$ * (H, M) > L > NL | $F(3, 285) = 9.51$, $p < 0.001$ * Side: M > (H, L, NL) Anterior: H > (M, L) > NL H, L: Anterior > Side | $F(1, 26) = 0.20$, $p = 0.658$ | $F(1, 11) = 0.01$, $p = 0.997$ |
| Mean relative phase angle (deg.) | $F(1, 488) = 27.31$, $p < 0.001$ * Side > Anterior | $F(3, 262) = 3.28$, $p = 0.021$ * NL > H | $F(3, 247) = 5.63$, $p = 0.001$ * Anterior: (NL, L) > (M, H) H, M: Side > Anterior | $F(1, 316) = 0.57$, $p = 0.451$ | $F(1, 9) = 0.01$, $p = 0.998$ |

Table 3.4: Estimated marginal mean ± standard error for the No-load condition, and the average mean differences relative to no-load condition by carrying mode and load level, at average values of centered gait cycle duration and centered stride length.

| | | Side carry | | | Anterior carry | | |
|---|---|---|---|---|---|---|---|
| | **No-Load** | **Low (4.5 kg)** | **Medium (9.1 kg)** | **High (13.6 kg)** | **Low (4.5 kg)** | **Medium (9.1 kg)** | **High (13.6 kg)** |
| **Temporal parameters** | | | | | | | |
| Stance, Right Leg (%) | 58.1 ± 0.8 | - | + 0.3 | + 0.5 | - | - | - |
| Stance, Left Leg (%) | 57.8 ± 6.7 | - | + 1.0 | - | - | - 0.9 | - 0.9 |
| Swing, Right Leg (%) | 41.9 ± 0.9 | - | - | - 0.4 | - | - | - |
| Swing, Left Leg (%) | 42.3 ± 3.9 | - | - 0.7 | - 0.9 | - | - | - |
| Initial double support (%) | 7.9 ± 4.2 | - | - | - | - | - | - |
| Terminal double support (%) | 8.3 ± 0.4 | - | - | + 0.7 | - | - | - |
| **Postural Sway, Coronal plane** | | | | | | | |
| ROM at T6 (deg.) | 5.2 ± 1.5 | - 1.2 | - 1.9 | - 1.6 | - | - 0.8 | - 0.6 |
| ROM at S1 (deg.) | 8.0 ± 0.8 | + 0.9 | + 1.3 | + 1.7 | + 0.7 | + 0.8 | + 0.5 |
| Mean relative phase angle (deg.) | 110.7 ± 3.7 | - | + 11.1 | + 17.4 | - 15.7 | - 18.9 | - 26.4 |
| **Postural Sway, Transverse plane** | | | | | | | |
| ROM at T6 (deg.) | 5.3 ± 0.3 | + 0.6 | - | - | - | - | - |
| ROM at S1 (deg.) | 8.0 ± 0.9 | + 2.3 | + 2.4 | + 2.2 | - 0.8 | - 0.4 | - 1.0 |
| Mean relative phase angle (deg.) | 100.7 ± 6.3 | - 25.8 | - 33.0 | - 31.8 | - 6.7 | - 11.7 | - 19.6 |
| **Postural Sway, Sagittal plane** | | | | | | | |
| ROM at T6 (deg.) | 2.9 ± 0.1 | + 0.6 | + 0.5 | + 0.5 | - | - | - |
| ROM at/S1 (deg.) | 4.1 ± 1.2 | - | + 0.7 | - | + 0.5 | + 0.6 | + 0.9 |
| Mean relative phase angle (deg.) | 79.3 ± 5.7 | - | - | - | - | - 11.1 | - 13.4 |

significantly with increasing load levels, while right and left leg swing duration decreased with increasing load. In the anterior load carrying condition, only left leg stance duration decreased significantly with increasing load.

### 3.3.2 Torso and Pelvis Postural Sway and Coordination

#### 3.3.2.1 Coronal Plane

Figure 3.2 depicts the mean (± standard error) thoracic and pelvic sway angles, and thoracic-pelvic relative phase angle in the coronal plane obtained from the average gait cycle data from all participants (N = 9). Thoracic rotation in the coronal plane was significantly more in the anterior carry compared to the side carry condition (Table 3.3). This difference was also statistically significant within the high, medium, and low load conditions. In the side carry, thoracic coronal plane rotation was significantly more in the no-load vs. low load level, which in turn was more than the medium and high load conditions. In the anterior carry condition, thoracic coronal plane rotation was significantly more in the no-load and low load level compared to the medium and high load conditions.

In the coronal plane, the range of pelvic rotation differed from thoracic rotation (middle panel in Figure 3.2). Pelvic coronal plane rotation was significantly more in the side carry compared to the anterior carry condition. This difference was also significant within the high load condition. In the side carry, pelvic coronal rotation was significantly more in the high load vs. medium load level, which in turn was more than the low and no-load conditions. In the anterior carry condition, pelvic coronal plane rotation was significantly more in each of the loaded conditions (i.e., high, medium and low load) compared to the no-load condition.

Mean coronal relative phase angle decreased significantly in the anterior carry vs. side carry condition, suggesting more in-phase thoracic-pelvic movement in the anterior carry condition (bottom panel in Figure 3.2). This difference between carrying modes was sig-

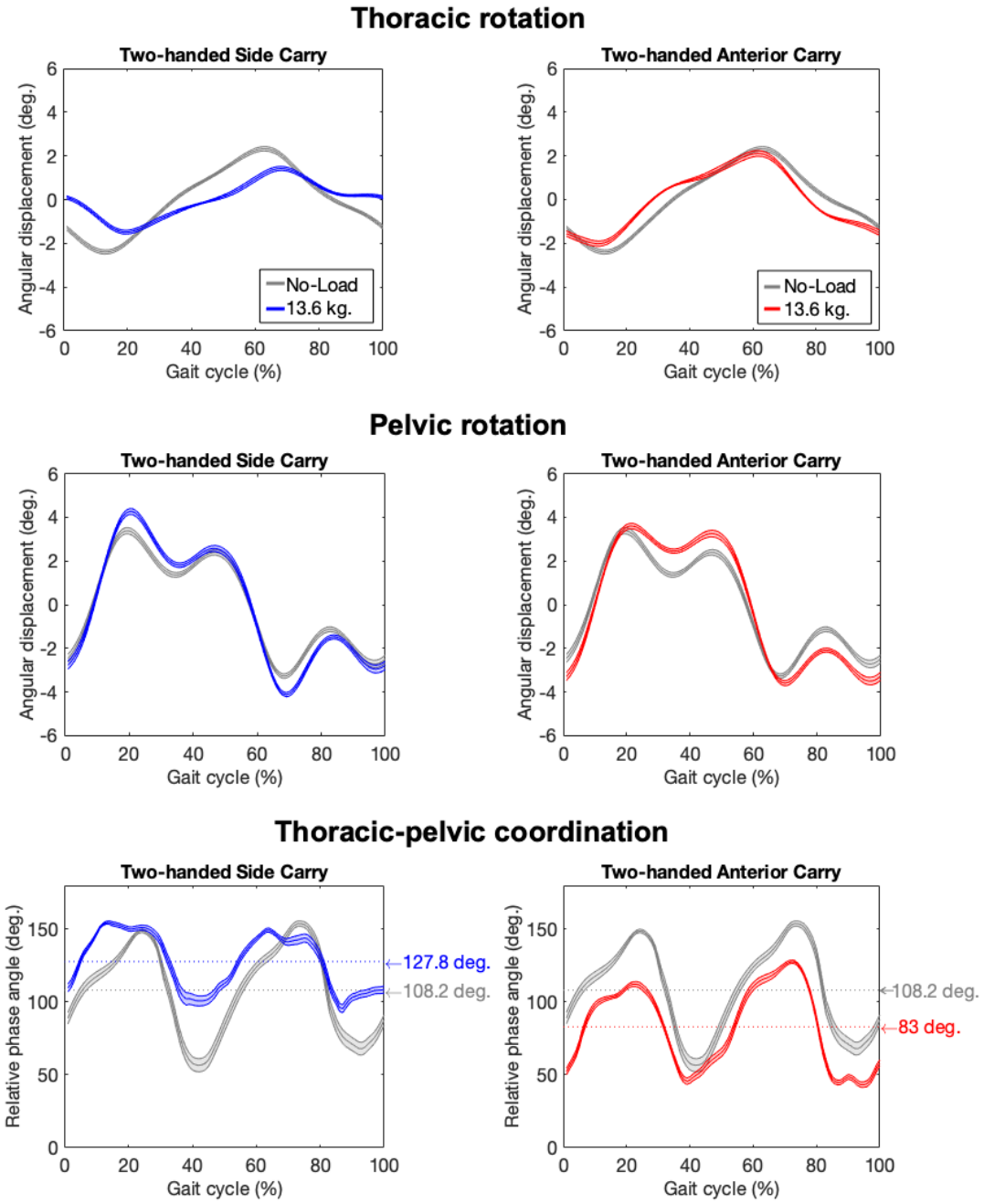



Figure 3.2: Mean ($\pm$ standard error) thoracic sway angle (top panel), pelvic sway angle (middle panel) and thoracic-pelvic coordination angle (bottom panel) in the *coronal* plane obtained from the average gait cycle data from N = 9 participants. The figure compares two-handed side carry (left panel) and two-handed anterior carry (right panel) in two of the four load levels, namely, no-load (grey) and High load level at 13.6 kg (colored blue and red for side and anterior carry, respectively). Dotted lines and adjacent numerical values (deg.) in the bottom panel represent the mean relative phase angle averaged over the gait cycle duration, with lower values implying more in-phase or synchronized movements.

nificant within the low, medium and high load conditions separately. In the side carry condition the mean sagittal relative phase angle was significantly more in high load condition vs. the medium load condition, which in turn was significantly more than in the low load and no-load conditions. In the anterior carry condition, the mean sagittal relative phase angle was significantly greater in the no-load condition compared to the low load and medium load conditions, which in turn were more than in the high load condition.

#### 3.3.2.2 Transverse Plane

Figure 3.3 depicts the mean ($\pm$ standard error) thoracic and pelvic sway angles, and thoracic-pelvic relative phase angle in the transverse plane obtained from the average gait cycle data from all participants (N = 9). Analysis for the range of thoracic transverse rotation revealed a significant interaction between carrying mode and load level (Table 3.3). At the low load level, thoracic transverse rotation was significantly more in the side carry compared to the anterior carry condition and the no-load condition. None of the other paired comparisons were significant.

Transverse rotation at the pelvis was significantly more in the side carry compared to the anterior carry within the low, medium and high load conditions separately. In the side carry condition, transverse pelvic rotations increased significantly in the loaded vs. unloaded condition. Conversely, in the anterior carry, transverse pelvic rotations decreased significantly in the loaded vs. unloaded condition. In all three loaded conditions, transverse pelvic rotations increased significantly in the side carry vs. anterior carry condition.

The mean relative phase angle in the transverse plane decreased in all of the loaded vs. unloaded conditions. This trend was significant in both, the side carry and anterior carry modes. Within the low, medium and high load conditions, the mean transverse relative phase angle was significantly less in the side carry vs. anterior carry conditions, implying more in-phase thoracic-pelvic movements in the side carry condition.

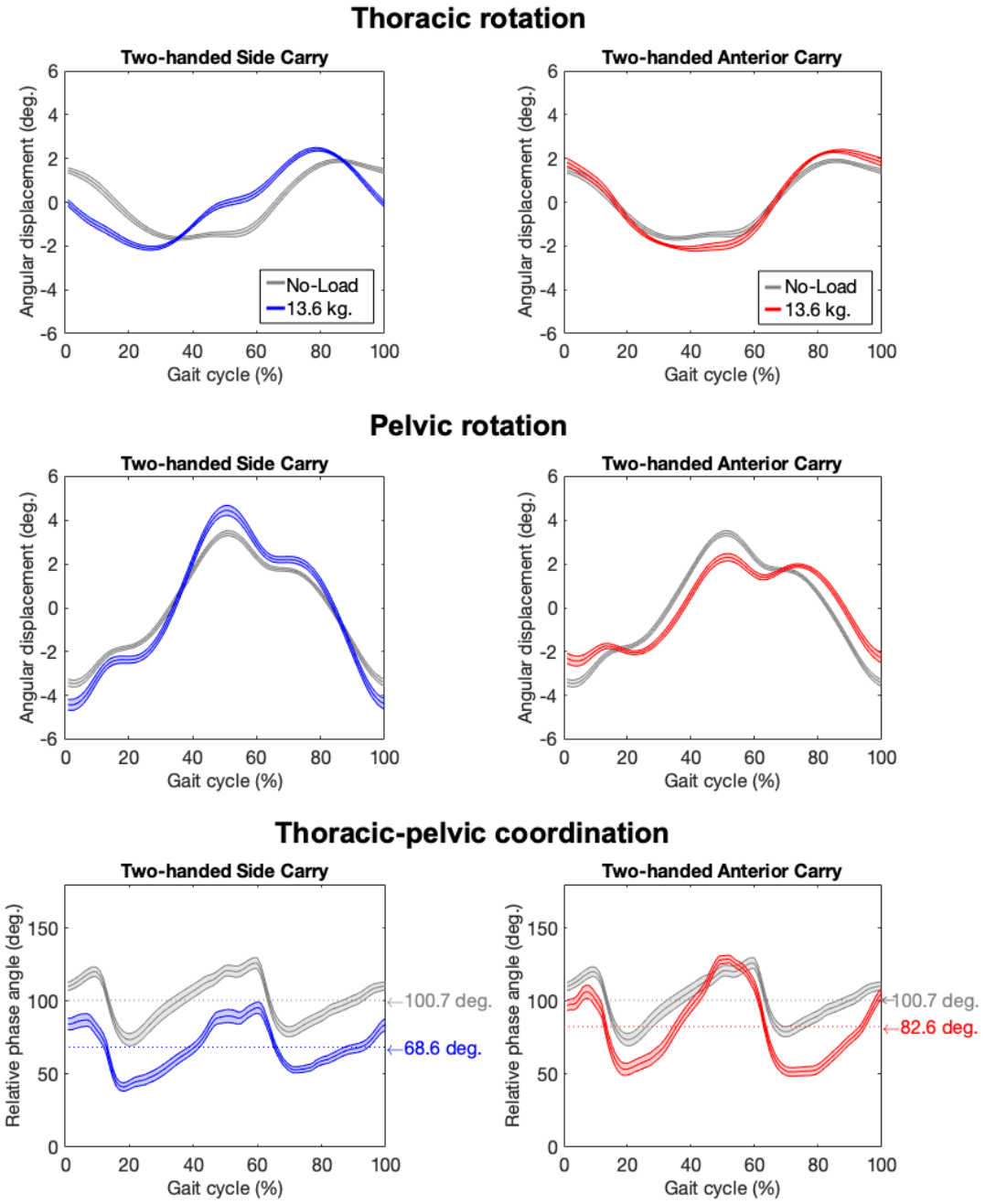



Figure 3.3: Mean (± standard error) thoracic sway angle (top panel), pelvic sway angle (middle panel) and thoracic-pelvic coordination angle (bottom panel) in the *transverse* plane obtained from the average gait cycle data from N = 9 participants. The figure compares two-handed side carry (left panel) and two-handed anterior carry (right panel) in two of the four load levels, namely, no-load (grey) and High load level at 13.6 kg (colored blue and red for side and anterior carry, respectively). Dotted lines and adjacent numerical values (deg.) in the bottom panel represent the mean relative phase angle averaged over the gait cycle duration, with lower values implying more in-phase or synchronized movements.

#### 3.3.2.3 Sagittal Plane

Figure 3.4 depicts the mean (± standard error) thoracic and pelvic sway angles, and thoracic-pelvic relative phase angle in the sagittal plane obtained from the average gait cycle data from all participants (N = 9). Thoracic sagittal rotation was significantly more in the side carry vs. anterior carry mode. This difference was significant in the low, medium and high load conditions separately. Trends in the range of pelvic sagittal rotation deferred from that of the thoracic sagittal rotation. Pelvic sagittal rotation was significantly more in the anterior vs. side carry conditions for the high and low load level. Pelvic sagittal rotation was also significantly more in the loaded vs. no-load conditions.

Mean sagittal relative phase angle was significantly less in the anterior carry vs. side carry mode, suggesting more in-phase thoracic-pelvic movements in the anterior carry condition. In the anterior carry condition, the mean sagittal relative phase angle was significantly less in the medium and high load conditions compared to the no-load and low load conditions.

## 3.4 Discussion

This study aimed to quantify the effects of hand loads during two-handed side and anterior load carriage on temporal and postural gait parameters obtained from body-worn inertial sensors. Results indicate that two-handed side and anterior load carriage relative to unloaded walking produce systematic influences on temporal gait patterns, torso and pelvis sway, and thoracic-pelvic coordination computed from inertial sensors data after adjusting for gait cycle duration and stride length.

Prior studies have investigated biomechanical adaptations in gait due to the magnitude and position of hand loads [128, 144, 145, 147, 148, 151]. However, these studies have primarily involved either walking on treadmills at controlled speeds or on ground without accounting for walking speed. Moreover, the various studies examined different carrying

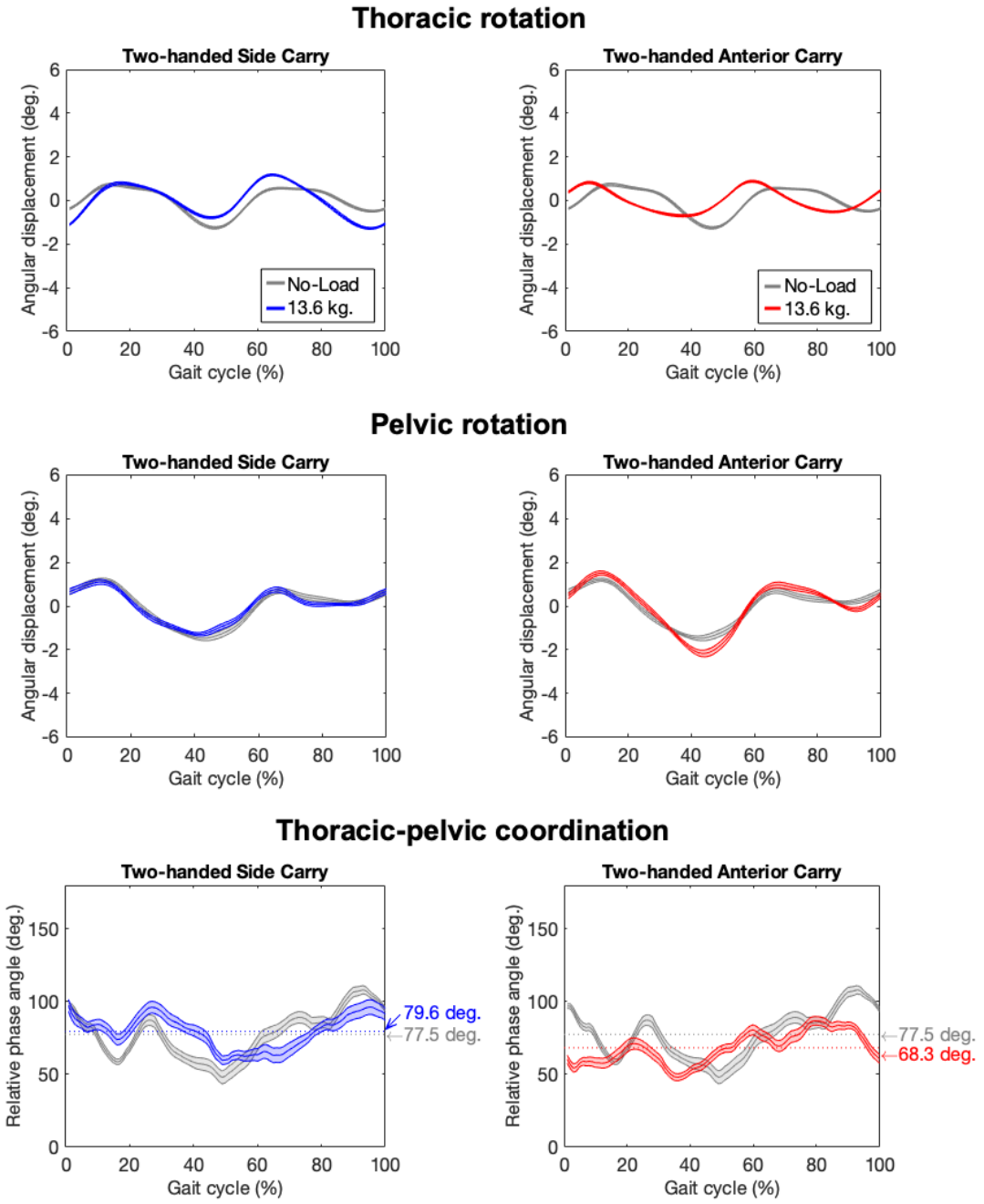



Figure 3.4: Mean ($\pm$ standard error) thoracic sway angle (top panel), pelvic sway angle (middle panel) and thoracic-pelvic coordination angle (bottom panel) in the *sagittal* plane obtained from the average gait cycle data from N = 9 participants. The figure compares two-handed side carry (left panel) and two-handed anterior carry (right panel) in two of the four load levels, namely, no-load (grey) and High load level at 13.6 kg (colored blue and red for side and anterior carry, respectively). Dotted lines and adjacent numerical values (deg.) in the bottom panel represent the mean relative phase angle averaged over the gait cycle duration, with lower values implying more in-phase or synchronized movements.

modes and magnitudes of load including a fixed amount, or loads normalized to percentage of body weight. As a result, direct comparisons with the present study are not possible. However, the trends in direction of change in gait and postural kinematics obtained in the present study are supported by findings from prior studies and are briefly discussed here.

This study found small changes in temporal parameters from the external loads. Side carry was associated with an increased single stance and double support duration and decreased swing duration compared to anterior load carriage and unloaded conditions. Trends in temporal parameters with the increasing load magnitude during the side carry were similar to earlier studies on posterior load carry [146, 151].

Importantly, the effects of carrying mode and load magnitude on gait were more evident in the measures of postural sway and thoracic-pelvic coordination. Side load carriage was characterized by an increase in pelvic sway in the coronal and transverse planes, an increase in thoracic sway in the sagittal plane, and a decrease in thoracic sway in the coronal plane. Coordination between thoracic-pelvic segments were more out-of-phase in the coronal plane, and more in-phase in the transverse plane. Anterior load carriage was characterized by an increase in pelvic sway in the coronal and sagittal planes, and a decrease in pelvic sway in the transverse plane. In addition, there was more in-phase coordination between thoracic-pelvic segments in the coronal, transverse, and sagittal planes relative to unloaded gait patterns. The magnitude of intersegment coordination increased with increasing load levels. These trends in postural sway and thoracic-pelvic coordination across carrying modes and load magnitudes can be explained by changes in body dynamics, specifically, angular momentum [143] and location of the CoM [147] as follows.

### 3.4.1 Analysis of Two-Handed Side Carry

During the swing phase, the upper torso including the arms counter-rotates relative to the pelvis in the transverse plane to reduce the net angular momentum [171]. In a side carry with the external load equally divided between the right and left hand, there is a net increase

in the moment of inertia and the angular momentum in the transverse plane from loads located laterally [172]. Consequently, the angular momentum of the rest of the body needs to increase in the opposite direction to reduce the net angular momentum. This increase is accomplished by synchronizing the transverse rotation of the torso and pelvic segments, and evinced as increased pelvic sway and more in-phase coordination between thoracic-pelvic segments in the transverse plane relative to unloaded gait.

Hand loads in a side carry lowers the location of the CoM of the upper body in the coronal and the sagittal planes. Consequently, there is an increase in the moment of inertia and angular momentum of the torso in coronal plane. Angular momentum of the upper body in the coronal plane with the increasing load levels is controlled by limiting thoracic coronal sway. Pelvic sway in the coronal plane was found to increase with increasing load levels to compensate for this reduced rotation of the trunk. Furthermore, the trunk and pelvis tend to counter-rotate in the coronal plane in order to decrease the net angular momentum between the torso and pelvis, which was recorded as more out-of-phase coordination between thoracic-pelvic segments with increasing load levels.

### 3.4.2 Analysis of Two-Handed Anterior Carry

Rotation of the arms is restricted in a two-handed anterior carry since the torso, arms and hand load are coupled and move together [129, 153, 173]. In order to reduce the net angular momentum in the transverse plane while walking, the upper body including the arms and the trunk counter-rotate relative to the lower body. The need for increased postural stability due the anterior load is achieved by co-contracting the trunk muscles and limiting rotational movement in the upper body [137] and by a concomitant decrease in pelvic sway in the transverse plane with increasing anterior loads. This decreased pelvic transverse rotation during load carriage is compensated by a simultaneous increase in hip excursion [143] and reflected in an increase in pelvic sway that was recorded in the coronal plane.

During anterior load carriage, coordination between the thoracic-pelvic segments was

more in-phase or synchronized in the loaded conditions vs. no-load in all three planes indicating the close coupling between the torso and pelvis. Thoracic-pelvic coordination in the transverse plane during anterior carry followed a similar trend to the side carry, but the magnitude of change was much smaller compared to the side carry, i.e., a 19.6 deg. decrease in the mean relative phase angle with the high load condition in the anterior carry relative to the no-load condition vs. 31.8 deg. decrease in the side carry relative to no-load. Since the load is located medially in the transverse and coronal planes during anterior load carriage in contrast to the laterally positioned loads in a side carry, the moment of inertia and angular momentum in the coronal plane at the torso is less in the anterior carry [172]. Thus the need for counter-rotating the upper vs. lower body to reduce the net angular momentum between the segments is relatively lower compared to the side carry. This difference in angular momentum and trunk movements between modes produced diverging trends in thoracic-pelvic coordination in the anterior carry (i.e., more in-phase) compared to the side carry (i.e., more out-of-phase) with increasing load magnitude.

### 3.4.3 Methodological Considerations and Limitations

The present study specifically focused on body-worn inertial sensors due to their applicability in applied settings. Prior studies on posture and gait during load carriage have typically used optical motion tracking while participants walked on a treadmill at a precise speed. The present study had walk trials performed in more naturalistic conditions with participants walking at a self-selected speed in a sufficiently long and levelled corridor. This was done in order to observe the natural adaptation in gait patterns associated with carrying mode and load level without imposing any external constraint on gait speed. Earlier studies support the notion that walking speeds and stride length do slightly change depending on the loads carried [143, 148, 174]. The present study used estimates of gait cycle duration and stride length from inertial sensor data as covariates to account for between and within-participant differences in walking speeds. Even with this statistical treatment it is possible

that some of the postural parameters were influenced by changes in gait cycle duration and stride length besides load intensity and carrying mode.

Only two carrying modes were considered in this study. A shift in the centre of mass posteriorly such as while wearing a backpack [132, 140, 143, 146, 151] or laterally with a load in one hand or on one shoulder [135, 137, 138, 151] may result in gait adaptations different from those produced in this study. However, our findings on postural sway and intersegment coordination during the anterior carry were similar to findings on the effects of posterior load carriage reported by LaFiandra et al. [143] wherein a loaded backpack carry decreased transverse thoracic and pelvic rotation and the mean relative phase angle between thoracic and pelvic segments, suggesting similar effects on gait kinematics. The load magnitudes used in the present study were lower than some previous studies (e.g., 40% of the body weight) [143] and focused on a relatively short duration of walking. With increased load magnitudes, the metabolic cost of load carriage is expected to increase leading to fatigue onset and causing even further alterations in muscle activation patterns, posture, and gait kinematics [175, 176].

As an initial investigation the present study was limited to a relatively small, homogeneous sample of participants with multiple gait cycles analyzed per condition and participant, resulting in 540 gait cycles analyzed. Subsequent studies would need to consider diversity in age, strength, and gender among other known sources of variability in gait patterns. Despite the limited generalizability in subjects and test conditions, postural sway and pelvic-thoracic coordination measures in the present study demonstrated significant and plausible differences in carrying mode and magnitude of load suggesting consistent kinematic adaptations.

The findings from the present study suggest that information about both carrying mode and load magnitude may be obtained from a combination of temporal measures of the gait phases, torso and pelvis postural sway, and thoracic-pelvic coordination. These findings along with the presented data processing algorithms have potential for informing ap-

proaches to assessing exposures from load carriage in work settings where the intensity, durations, frequency, and mode of load carriage varies over time, such as in construction work, warehousing, packaging, and distribution. Field-based studies of biomechanical exposure assessment typically require instrumentation for force measurement such as surface electromyography for muscle activation levels and force platform for measuring ground reaction forces at the foot that is conspicuous, cumbersome, and potentially interferes with workers movements and task performance. Wearable inertial sensors may provide a low-cost and less obtrusive alternative for classifying load levels in manual material handling.

## 3.5 Conclusion

This study demonstrates the use of body-worn inertial sensors to measure changes in gait kinematics with different hand loads in two-handed load carriage. The study found statistically significant differences in temporal and kinematic gait parameters by carrying mode and load level, after adjusting for gait cycle duration and stride length. These differences reflect temporal and postural adjustments to maintain postural stability under external load conditions. Postural sway of the torso and pelvis and rotational movement coordination between the torso and pelvis measured as relative phase angles in the coronal, transverse and sagittal planes were particularly insightful to assess the modifying effects of hand-load magnitude and carrying mode on walking. This study found that relative phase angles measured in the coronal and transverse planes may provide sufficient information to describe changes in gait posture and kinematics induced by the magnitude of hand-load and carrying mode. Findings from this study serve as a foundation for subsequent studies using wearable inertial sensors to measure posture adaptations and workers' exposures to manual load carriage. The subsequent Chapter 4 investigates this topic in further detail.

# CHAPTER 4

# Statistical Classification of Load Carriage Mode and Magnitude from Inertial Sensor Derived Gait Kinematics[1]

Load carriage induces systematic alterations in gait patterns and pelvic-thoracic coordination. Leveraging this information, the objective of this study was to develop and assess a statistical prediction algorithm that uses body-worn inertial sensor data for classifying load carrying modes and load levels. Nine men participated in an experiment carrying a hand load in four modes: one-handed right and left carry, and two-handed side and anterior carry, each at 50% and 75% of the participant's MAWC, and a no-load reference condition. Twelve gait parameters calculated from inertial sensor data for each gait cycle, including gait phase durations, torso and pelvis postural sway, and thoracic-pelvic coordination were used as predictors in a two-stage hierarchical random forest classification model with Bayesian inference. The model correctly classified 96.9% of the carrying modes and 93.1% of the load levels. Coronal thoracic-pelvic coordination and pelvis postural sway were the most relevant predictors although their relative importance differed between carrying mode and load level prediction models. This study presents a preliminary algorithmic framework for combining inertial sensing with statistical prediction with potential use for quantifying physical exposures from load carriage.

[1]Portions of this chapter appear in [124, 125]

## 4.1 Introduction

Prolonged exposure to manual load carriage is a known risk factor for low back disorders [2, 130]. Epidemiological findings suggest an increased odds of developing a prolapsed lumbar disc from frequently carrying objects more than 11.3 kg (25 lbs.) [177]. Heavy and frequent load carriage may accelerate spinal degeneration due to an increased loading on the spine and would damage spinal tissues in the vertebral column [7]. While minimizing the repetition and intensity of manual load carriage is ideal, such tasks are still common and inevitable in non-routinized work such as in construction [129], firefighting [128], and manufacturing [178]. Accurate measurement of exposures to biomechanical risk factors is an important step to develop effective musculoskeletal injury prevention and risk reduction programs [5]. Measuring the duration, repetition, and magnitude of hand loads longitudinally is an essential step for assessing the biomechanical impacts to the musculoskeletal system and identifying strategies for intervention.

Measuring longitudinal exposures to load carriage in field settings presents unique challenges. Traditional exposure assessment techniques that rely on direct observations have limitations in non-repetitive job conditions where the work tasks vary considerably in duration, frequency, or intensity levels [14]. Direct measurement of task durations and load magnitudes in applied settings would require instrumentation system that is wireless and portable and unrestricted by changes in a worker's location. In addition to load magnitude, the biomechanical effects of load carriage are influenced by the mode of load carriage (e.g., two-handed anterior, one-handed side). A study by Rose et al. [140] demonstrated that carrying the same load with different carrying modes generates a significant difference in the anterior-posterior shear loading at L2/L3. Carrying a two-handed anterior load of 11.3 kg was sufficient to produce an average shear load of 856 N, which exceeded the recommended exposure limits of 700 N [179] and can potentially damage spinal tissues. The same load carried in a backpack produced a lower average shear load of 345 N [140]. Thus, methods for direct measurement of such exposures need to identify and quantify

both dimensions, namely, carrying mode and load magnitude, besides temporal aspects of duration and frequency.

Wearable inertial sensors (or inertial measurement units, IMUs) have gained attention in ergonomics research [47] for field-based direct measurement of worker postures. Inertial sensors are light-weight, portable, less obtrusive, and have on-board power and data storage capacity that allows for data collection over a long work period [29, 157]. Typical use of wearable inertial sensors in ergonomics studies to date have focused on posture measurement in occupational tasks (e.g., lifting and pushing/pulling) to estimate the orientation of a body segment or joint angle between segments [47, 61, 82, 95] relative to a neutral posture (i.e., typically upright standing) in order to quantify the extent and proportion of time spent in non-neutral postures. During load carriage, the postural deviation relative to an upright standing posture is subtle compared to other occupational tasks and less consequential than the duration, magnitude and mode of load carriage. However, the magnitude and position of hand loads can significantly alter gait kinematics and posture [128, 144, 145, 147, 148, 151].

Movements of the torso, pelvis, and lower extremities change systematically with external load levels and carrying modes when walking [143, 146]. Kinematic adjustments for maintaining posture and stability during walking are reflected in temporal and kinematic gait parameters, and rotational movement coordination between the torso and pelvis [143, 154]. Using data from body-worn inertial sensors, a recent study by Lim et al. [126] confirmed systematic differences in thoracic and pelvic sway and movement coordination based on load level between two-handed anterior and side carry. Specifically, in that study, carrying hand-loads that weighed 4.5 kg, 9.1 kg, and 13.6 kg in two-handed anterior vs. side carrying modes were associated with significant differences in coronal and transverse thoracic-pelvic coordination measured using relative phase angles after adjusting for stride length and gait speed. The present study aims to leverage information about changes in gait kinematic patterns for estimating the duration, relative magnitude and mode

of load carriage using inertial sensing and predictive modeling.

Predictive modeling or machine-learning (ML) techniques have been used in combination with wearable sensor data to extract contextual task information beyond just quantifying posture. For example, activity recognition is an area of active research where data from body-worn inertial sensors are used for classifying daily activities [118, 119], detecting gait events [160, 180, 181], and predicting safety critical events such as falls [120, 121, 122]. The application of such techniques to occupational ergonomics is still lagging. A few ergonomics studies have combined predictive modeling with the wearable sensor data in activity recognition to classify manual material handling tasks [78], assembly tasks [182], and patient handling activities [183], and to detect states of fatigue from gait kinematics during walking [184, 185, 186]. Lee [187] applied linear discriminant analysis (LDA) to gait kinematics data obtained from a 3-D optical motion capture system to distinguish between unloaded versus loaded gait with participants wearing a vest weighing 12.5 kg. Their study showed potential for using gait kinematics to classify carrying load condition but was limited to a single carrying mode and load magnitude. Collectively all of these previous studies suggest the possibility for leveraging information about postural adaptations during load carriage obtained by inertial sensors combined with predictive modeling techniques to create new algorithmic approaches for assessing physical exposures from load carriage *in situ*.

The aim of this paper was to develop and assess a statistical prediction algorithm as proof-of-concept that uses gait kinematics calculated from body-worn inertial sensor data for classifying hand-load carrying mode and load level. The statistical prediction algorithm implemented in this study incorporates a priori biomechanical knowledge about the effects of load carriage on human gait patterns to inform the data segmentation process, computing and selecting of predictor variables, and the structure of the statistical model. These steps are discussed in the context of leveraging ML techniques for ergonomics exposure assessment.

## 4.2 Methods

### 4.2.1 Study Participants

Nine healthy men were recruited from the university community for the study. Participants had ages ranging from 18 to 25 years with an average ± standard deviation (SD) of 22.0 ± 3.0 years, stature of 1.75 ± 0.05 m, weight of 77.11 ± 9.98 kg, and BMI of 24.87 ± 2.84 kg/m$^2$. Participants were screened for pre-existing back injuries or chronic pain with a body discomfort questionnaire adapted from the body mapping exercise by NIOSH ([165] for more details). All participants were right-handed and right-footed when tested with the questionnaire adapted from the Edinburgh handedness inventory [188]. Prior to the study, participants completed a written informed consent approved by the university's institutional review board.

### 4.2.2 Experiment Procedures

A pre-experimental session was conducted to determine each participants' MAWC [178], which was later used to set the normalized load levels in the main experiment. For the measurement of one-handed MAWC, participants were asked to carry a 2.3 kg box with their right hand and walk 5 m back and forth. The box had dimensions of 152.4 mm width x 177.8 mm depth x 127 mm height, and one handle on the top (Figure 4.1-a). The weight of the box could be increased in increments of 2.3 kg. A method of limits discussed in [189] was used for determining the maximum acceptable weight that the participant could carry without perceiving unusual tiredness, weakness, overheating, or breathlessness. The procedure was repeated to measure a two-handed MAWC by using a box with dimensions of 177.8 mm width x 228.6 mm depth x 203.3 mm height held anteriorly with both hands using handles located on the side (Figure 4.1-d).

During the main experiment, participants carried a weighted box down a levelled corri-

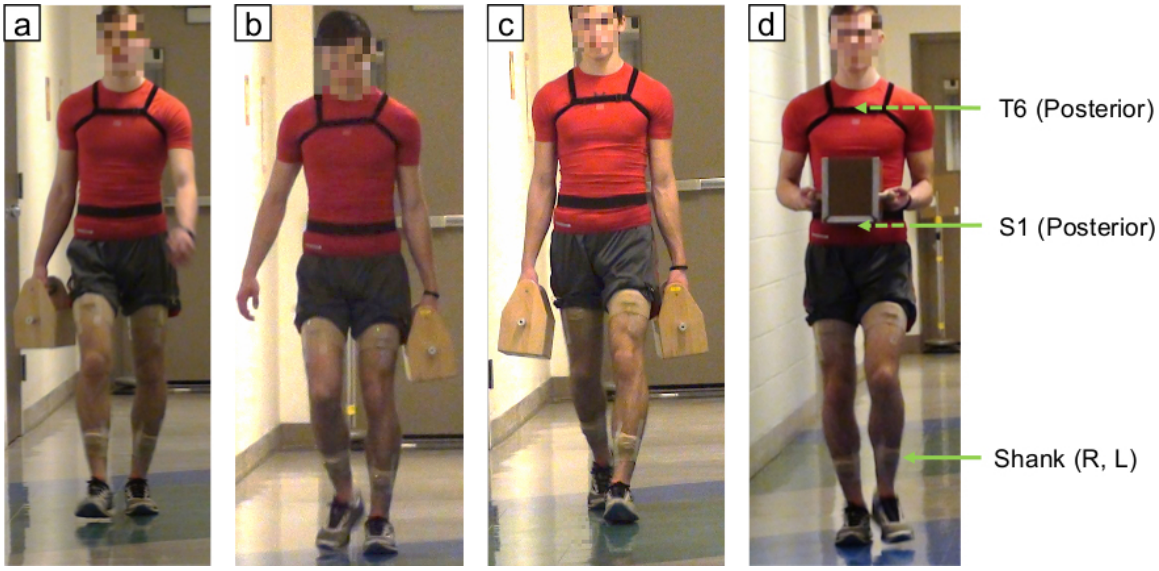



Figure 4.1: Images showing the four carrying modes performed in this study: (a) one-handed right hand carry (1H-R), (b) one-handed left hand carry (1H-L), (c) two-handed side carry (2H-Side), (d) two-handed anterior carry (2H-Anterior) along with the location of four inertial sensors attached on the body at T6, S1, and shank (R, L).

dor (26.2 m length x 1.6 m width) for a distance of 24 m in four carrying modes commonly used in occupational settings (Figure 4.1), viz., one-handed right hand carry (1H-R), one-handed left hand carry (1H-L), two-handed side carry (2H-Side), and two-handed anterior carry (2H-Anterior), in addition to a no-load (i.e., empty-handed reference) condition. Two levels of box weights were carried in each mode, namely, 50% MAWC and 75% MAWC. The one-handed MAWC for each participant was used to calculate the normalized load levels of 50% and 75% for the one-handed conditions (i.e., 1H-R and 1H-L). Likewise, the two-handed anterior MAWC was used to calculate the 50% and 75% normalized load levels for the 2H-Anterior and 2H-Side carrying modes. Hand load was equally divided between the right and left boxes in the 2H-Side carry.

Two no-load walk trials were performed first, and subsequently each participant performed two consecutive trials of eight loaded conditions (= 4 carrying modes x 2 load levels) in random order. Walking speed was self-selected to observe the natural adaptation in walking patterns due to different load carriage conditions. Two-minute rest breaks

between each walk trial were given to participants to minimize carry-over effects of fatigue.

### 4.2.3 Instrumentation

Four commercial inertial sensors (Opal, APDM Inc, Portland, OR, USA) were attached on the participant at the sixth thoracic vertebra (T6), the first sacral vertebra (S1), and superior aspect of the right and left shank midway between the lateral femoral and malleolar epicondyles (Figure 4.1-d). Sensor placement was informed by the need for computing specific predictor variables. Sensors attached on the right and left shank were used for detecting key gait events (e.g., heel strike and toe-off) and subsequent temporal gait parameters [160]. Sensors placed on the T6 and S1 were used for calculating torso and pelvis postural sway and thoracic-pelvic coordination measures [124] that were related to the objectives of this study. Velcro straps were used to secure the sensors located at T6 and S1, and double-sided hypoallergenic tape and medical wrap were used to attach the sensors to shank (R, L). One of the sensor axes (i.e., x-axis) was attached aligned with the proximal-distal axis of the body segment and pointing downward.

The inertial sensors recorded 3-D accelerometer, gyroscope, and magnetometer sensor data at a sampling frequency of 80 Hz. Accelerometer and gyroscope data were filtered using a second-order low-pass zero-lag Butterworth filter with a cut-off frequency of 2-Hz. Gyroscope data (angular velocity in radians/s) was integrated to obtain angular displacement, and subsequently filtered using a second-order high-pass filter with a cut-off frequency of 0.75 Hz to reduce the effect of drift [166].

### 4.2.4 Algorithm to Classify Carrying Mode and Load Level

A statistical classification algorithm was developed with six general steps described in the following section (Figure 4.2). Four carrying modes (i.e., 1H-R, 1H-L, 2H-Side, 2H-Anterior) and no-load and two load levels, 50% MAWC vs. 75% MAWC, were the target outcome variables for each walking trial.

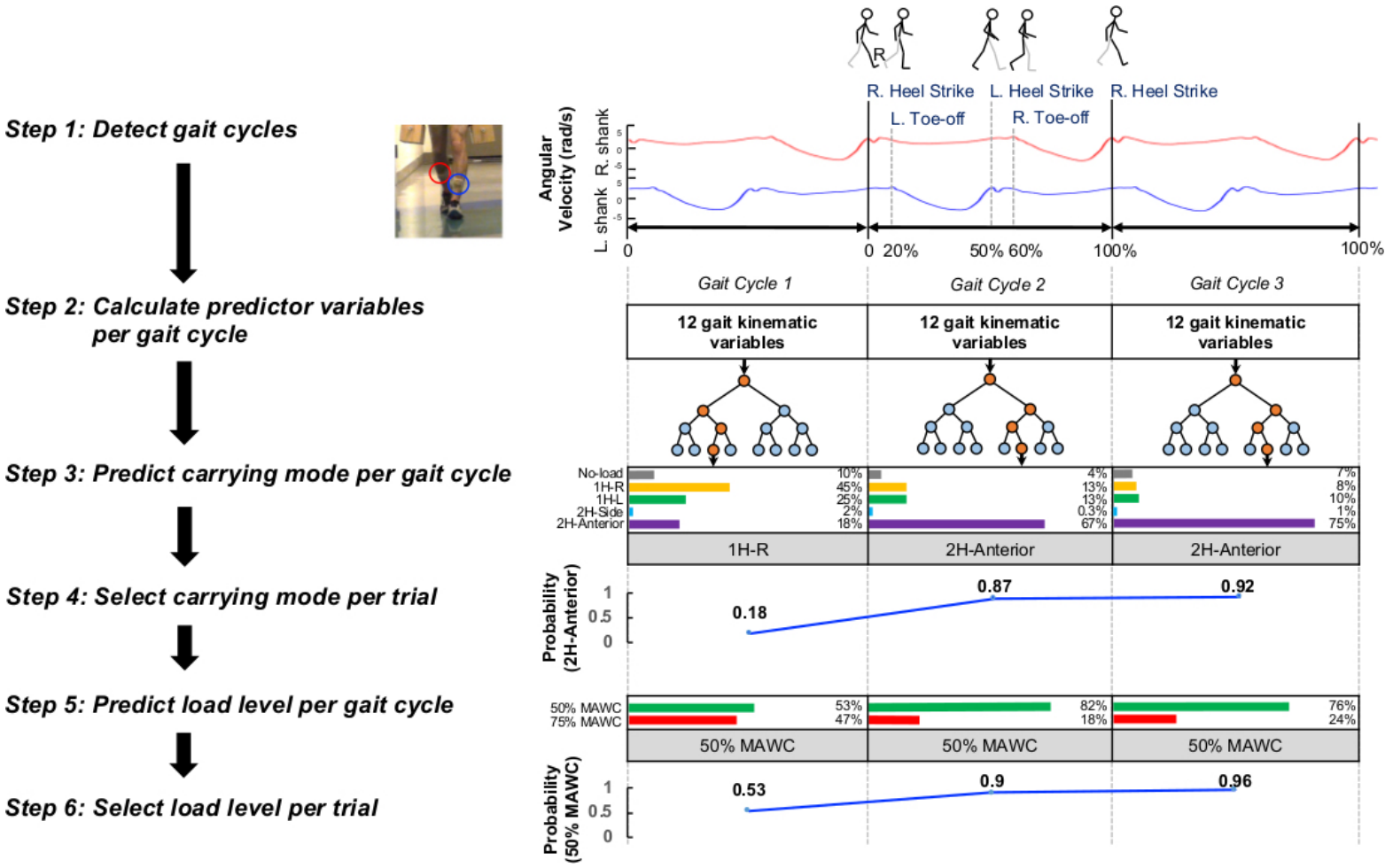



Figure 4.2: Overview of the carrying mode and load level classification algorithm developed in the study. The right panel shows example classification results for three consecutive gait cycles at a two-handed anterior carry with 50% MAWC load condition.

#### 4.2.4.1 Step 1: Detect Gait Cycles

Individual gait cycles were detected using a custom gait detection algorithm adapted from [160] and described in detail by Lim and D'Souza [126]. To summarize this process, first, gait events signifying heel strike and toe-off were detected from the angular velocity (rad/s) data obtained from the sensors on the right and left shank (Figure 4.2). Second, gait cycles were denoted by finding the sequence of the following events: right heel strike $\rightarrow$ left toe-off $\rightarrow$ left heel strike $\rightarrow$ right toe-off $\rightarrow$ next right heel strike. The algorithm was implemented in MATLAB (MATLAB R2016b, The MathWorks Inc., Natick, MA, USA).

#### 4.2.4.2 Step 2: Calculate Predictor Variables

Sixteen gait parameters were calculated over each gait cycle, namely, seven temporal gait measures, six torso and pelvis postural sway and three thoracic-pelvic coordination measured in the transverse, sagittal, and coronal planes, respectively (Table 4.1). Thoracic-pelvic coordination was measured as the relative phase angle of rotational movement between the torso and pelvis segments [143, 152]. This particular set of variables were considered based on preliminary work on 2H-Anterior load carriage [124]. Swing, left leg (%) and stance, left leg (%) durations were highly correlated with the initial double support (%) duration with a Pearson's correlation coefficient of $|R| > 0.8$. Swing, right leg (%) and stance, right leg (%) durations were also highly correlated with the terminal double support (%) duration. Thus, four temporal parameters, i.e., stance, right and left leg (%) and swing, right and left leg (%) were excluded from further analysis to avoid multi-collinearity, reducing the final set of predictor variables to twelve.

#### 4.2.4.3 Step 3: Predict Carrying Mode per Gait Cycle

A two-stage hierarchical model was implemented comprising a first stage classification model for predicting carrying mode (*Step 3* in Figure 4.2), and a second stage classification

Table 4.1: List and definitions of gait parameters calculated from the inertial sensor data for each gait cycle. Excluding stance right and left leg (%) and swing right and left leg (%), all of the remaining 12 parameters were used as predictors in the classification model.

| Parameter | | Definition |
|---|---|---|
| **Temporal parameters (7 nos.)** | | |
| 1 | Gait cycle duration (sec) | Duration of one gait cycle (one right plus left step duration). |
| 2,3 | Stance, Right and Left Leg (%) | Percentage of the gait cycle for when the right or left foot is on the ground. |
| 4,5 | Swing, Right and Left Leg (%) | Percentage of the gait cycle for when the right or left foot is not on the ground. |
| 6 | Initial double support (%) | Percentage of the gait cycle for when both feet are on the ground after a right foot heel-strike. |
| 7 | Terminal double support (%) | Percentage of the gait cycle for when both feet are on the ground after a left foot heel-strike. |
| **Torso and pelvis postural sway (6 nos.)** | | |
| 8~13 | ROM at T6 and S1 in the transverse, sagittal, and coronal planes (deg.) | Range of rotation angle at torso and pelvis in transverse, sagittal, and coronal planes: Max (integrated angular velocity) - min (integrated angular velocity) |
| **Thoracic-pelvic coordination (3 nos.)** | | |
| 14~16 | Mean relative phase angle between T6 and S1 in the transverse, sagittal, and coronal planes (deg.) | Average (pelvic phase angle - thoracic phase angle) in transverse, sagittal, and coronal planes. Phase angle (t) = arctan (normalized angular velocity (t) /normalized integrated angular velocity (t)) |

model for predicting the load level (*Step 5* in Figure 4.2). The design of the hierarchical structure was informed by prior studies demonstrating that the mode of load carriage influences alterations in gait kinematics significantly more than changes in the load levels within the same carrying mode [146, 151]. The random forest technique [190] was chosen as the classification algorithm for both stages because it produced the highest prediction accuracy in a preliminary study on estimating the carrying mode and load level compared to other common multiclass classification algorithms such as classification and regression trees, multinomial logistic regression, linear discriminant analysis, and support vector machines. Random forest is a nonparametric machine-learning technique based on a decision tree that grows recursive binary partitioning at the nodes of the tree. Hundreds of decision trees are grown by random selection of a subset of predictor variables each time. The prediction results across all trees are averaged to obtain the final consensus prediction. In this study, prediction was performed over 500 trees for each gait cycle with a selection of four predictor variables each time. This step was implemented using the randomForest package v.4.6-12 [191] in R v.3.3.1 (R core team).

#### 4.2.4.4 Step 4: Select Carrying Mode per Trial

Classification results from each gait cycle within a walk trial were used to decide the final classification result for the walk trial. In this algorithm, predictions in *Steps 3* and *5* were performed independently for each gait cycle; however, under the assumption that the carrying mode and load level does not change within a walk trial, probabilities of the current gait cycle data belonging to a specific carrying mode were updated based on the prior gait cycles using the method of Bayesian inference [192]. Assume that a prediction model ($M$) is developed based on the current gait cycle data ($Y$). When data on new gait cycle ($Y^*$) is obtained, the posterior distribution can be updated using Baye's theorem as follows:

$$p(M|Y^*) = c * p(Y^*|M) * p(M) \tag{4.1}$$

where $p(M|Y^*)$ is the posterior distribution updated by the new data ($Y^*$), $p(Y^*|M)$ is the probability that the new data belongs to each class given the prediction model, and $p(M)$ is the prior probability before updating the new data. A normalizing constant, $c$, ensures that the posterior probabilities of all classes add up to one. Using this method, the classification results from prior gait cycles were cumulatively used to update the classification result of the current gait cycle until the last gait cycle identified in a walk trial. The carrying mode with the highest posterior probability at the final gait cycle within the walk trial was selected as the final prediction outcome for the carrying mode.

#### 4.2.4.5 Step 5: Predict Load Level per Gait Cycle

*Steps 5* and *6* were performed to classify the load level within each predicted carrying mode. While one model was developed for *Step 3*, four separate models were developed in *Step 5* for each carrying mode excluding the no-load condition. Separate load level prediction models were built based on a priori knowledge that the important kinematic parameters to distinguish load levels differ by carrying mode [146, 151]. Gait data from each walk trial

was subjected to one of four classification models for predicting the load level depending on the carrying mode that was predicted in *Step 4*. Load levels were predicted for each gait cycle in the walk trial.

#### 4.2.4.6 Step 6: Select Load Level per Trial

Similar to *step 4*, Bayesian inference was used to update the classification result of the load level within a walk trial.

### 4.2.5 Evaluating Model Performance

The performance of the prediction model was evaluated using 10-fold cross-validation tests. All walk trials were split into ten roughly equal-sized subsamples or folds ($k$ = 1,2,...,10). In each iteration, one subsample ($k$) was selected as the validation data for testing the model, and the remaining $k$ -1 subsamples were used for training the model [193]. This test was iterated $k$ times until all subsamples were used as a validation set. Gait cycles from the same walk trial were grouped when partitioning, so that all of the gait cycles from the same walk trial were included in the same subsample.

An identical test was performed for the classification algorithm without the Bayesian update (*Step 4* and *6*) as a comparison to investigate the benefit of applying the Bayesian inference to the algorithm. In this model, the final classification result for the walk trial was decided by averaging the classification results from individual gait cycles within the walk trial.

Three performance measures were computed:

- Average prediction accuracy = [# true positives + # true negatives] / [# total walk trials],
- Precision = [# true positives] / [# true positives + # false positives]), and
- Sensitivity = [# true positives] / [# total positives].

### 4.2.6 Interpreting the Classification Model

The relative importance (%) of predictor variables in each model was calculated to investigate the importance of each predictor variable in predicting the response variable [194]. In a random forest model, variable importance is measured as the impurity of data after it is split at each node. The Gini impurity Index, a common measure of the node impurity, is computed by averaging impurity at a data partition across all classes of the response variable [195]. A larger decrease in the Gini index represents a larger decrease in impurity at a data partition and a greater importance of the predictor variable in the classification model. The magnitude of the Gini index can differ by models, so it is a common practice to calculate a normalized index as the relative importance (%) by giving the most important variable a score of 100% in each model.

## 4.3 Results

A total of 162 walk trials were performed across all participants (9 participants x 9 conditions per participant x 2 walk trials per condition). Excluding three interrupted walk trials during the data collection, 159 walk trials were used for building and testing the algorithm. A total of 2028 gait cycles were recorded across all participants with an average $\pm$ standard deviation (SD) of 12.8 $\pm$ 1.5 (range: 9 to 17) gait cycles in each repetition of the walk trials.

Across all participants the average $\pm$ SD for the MAWC (kg) in the one-handed condition was 32.5 $\pm$ 7.9 kg and in the two-handed condition was 31.0 $\pm$ 4.5 kg, respectively. Load levels for the walk trials were set to 50% and 75% of the participant's one-handed and two-handed MAWC value. Average $\pm$ SD values of normalized MAWCs were 17.4 $\pm$ 3.9 (50% MAWC) and 24.4 $\pm$ 6.3 (75% MAWC) for the one-handed conditions, and 16.6 $\pm$ 2.3 (50% MAWC) and 23.2 $\pm$ 3.53 (75% MAWC) for the two-handed conditions.

### 4.3.1 Bayesian Inference Update vs. Averaging

Applying Bayesian inference in *Steps 4* and *6* outperformed the averaging approach in terms of the prediction accuracy. The model with the Bayesian inference correctly classified the carrying mode in 96.9% of the walk trials and load level in 93.1% of the walk trials, resulting in an average overall prediction accuracy of 91.8%. In comparison, the averaging approach correctly classified the carrying mode in 95.3% and load level in 72.7% of the walk trials, resulting in an average overall prediction accuracy of 72.2%, which was 19.6% lower compared to the Bayesian approach.

Figure 4.3 depicts an example model prediction for a walk trial in a 2H-Anterior carry consisting of fifteen consecutive gait cycles. The Bayesian inference approach showed convergence in the posterior probability after four gait cycles in the example described in Figure 4.3. Across all conditions an average $\pm$ SD of 4.5 $\pm$ 1.5 gait cycles were needed to correctly classify carrying mode with a posterior prediction over 90%. Since the Bayesian approach demonstrated a clear advantage in prediction performance, we limit the subsequent analysis and discussion to this approach.

### 4.3.2 Model Performance

#### 4.3.2.1 Carrying Mode Classification

Table 4.2 presents the confusion matrix for the prediction model along with the precision and sensitivity values from the 10-fold cross-validation test. The prediction accuracy for classifying the carrying mode was 96.9%. The precision of the no-load, 2H-Side, and 2H-Anterior conditions were 100% while it was lower in the 1H-R and 1H-L at 91.4% and 94.3% respectively. Sensitivity was also highest for the no-load, 2H-Side and 2H-Anterior conditions at 100%, compared to 1H-R and 1H-L at 94.1% and 91.7% respectively. Five walk trials were misclassified in carrying mode between the 1H-R and 1H-L conditions, and interestingly were all at the load level of 75% MAWC.

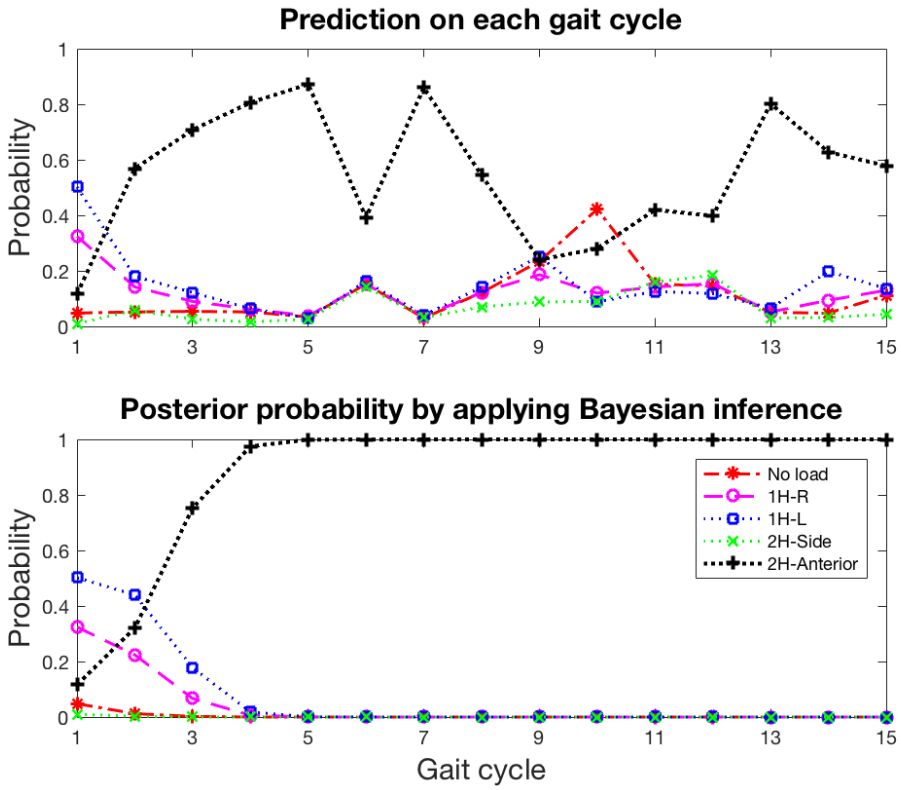



Figure 4.3: Example results from the random forest classification to predict carrying mode for fifteen consecutive gait cycles from a two-handed anterior carry walk trial without (top-panel) and with (bottom-panel) Bayesian inference applied. In each gait cycle, the mode with the highest predicted probability is labeled as the classification result for that gait cycle. In this example, without Bayesian inference applied (top-panel) 3 of the 15 gait cycles were misclassified as either 1H-L (gait cycle #1) or no-load (gait cycle #9 and #10). In the bottom graph, Bayesian inference was applied to the same data and updated the posterior probability of the gait cycle based on prior gait cycles cumulatively. The probability of the data predicted as the correct class (i.e., two-handed anterior carry in this case) exceeded 0.9 after four gait cycles and converged to 1.0 in subsequent cycles.

Table 4.2: Confusion matrix showing the classification result for carrying modes from each walk trial data: No-load = empty-handed reference condition, 1H-R = one-handed right carry, 1H-L = one-handed left carry, 2H-Side = two-handed side carry, 2H-Anterior = two-handed anterior carry.

| | | Predicted Carrying Mode | | | | | Total Walk Trials | Sensitivity |
|---|---|---|---|---|---|---|---|---|
| | | **No-load** | **1H-R** | **1H-L** | **2H-Side** | **2H-Anterior** | | |
| | **No-load** | 18 | 0 | 0 | 0 | 0 | 18 | 100% |
| **Actual** | **1H-R** | 0 | 32 | 2 | 0 | 0 | 34 | 94.1% |
| **Carrying** | **1H-L** | 0 | 3 | 33 | 0 | 0 | 36 | 91.7% |
| **Mode** | **2H-Side** | 0 | 0 | 0 | 36 | 0 | 36 | 100% |
| | **2H-Anterior** | 0 | 0 | 0 | 0 | 35 | 35 | 100% |
| **Total Walk Trials** | | 18 | 35 | 35 | 36 | 35 | 159 | |
| **Precision** | | 100% | 91.4% | 94.3% | 100% | 100% | | |

To further investigate the misclassified cases, posterior probabilities of the target carrying mode for individual walk trials were plotted by gait cycle (Figure 4.4). Consistent with Table 4.2, there were no misclassified cases for the no-load, 2H-Side, and 2H-Anterior conditions. The posterior probabilities in these conditions (n = 89 walk trials) converged to 1.0 typically after 4 to 5 gait cycles even though the initial probability at the first gait cycle was very low ($p < 0.5$) in many cases. On the other hand, the posterior probabilities for multiple walk trials in the 1H-R and 1H-L conditions did not converge to 1.0 and fluctuated throughout the walk trial.

#### 4.3.2.2 Load Level Classification

The average prediction accuracy for classifying the load level across all carrying modes was 93.1% (n = 148 of 159 walk trials), which was 3.8% lower than the classification of carrying mode. Table 4.3 summarizes the confusion matrices for the models by carrying mode and along with the precision and sensitivity values from the cross-validation test. Prediction accuracies within each carrying mode were 91.4% for 1H-R, 91.4% for 1H-L, 94.4% for 2H-Side, and 91.4% for 2H-Anterior. Among the carrying modes, the model for 2H-Side had the highest prediction accuracy with just 1 out of 18 walk trials misclassified between the 50% MAWC and 75% MAWC load levels each.

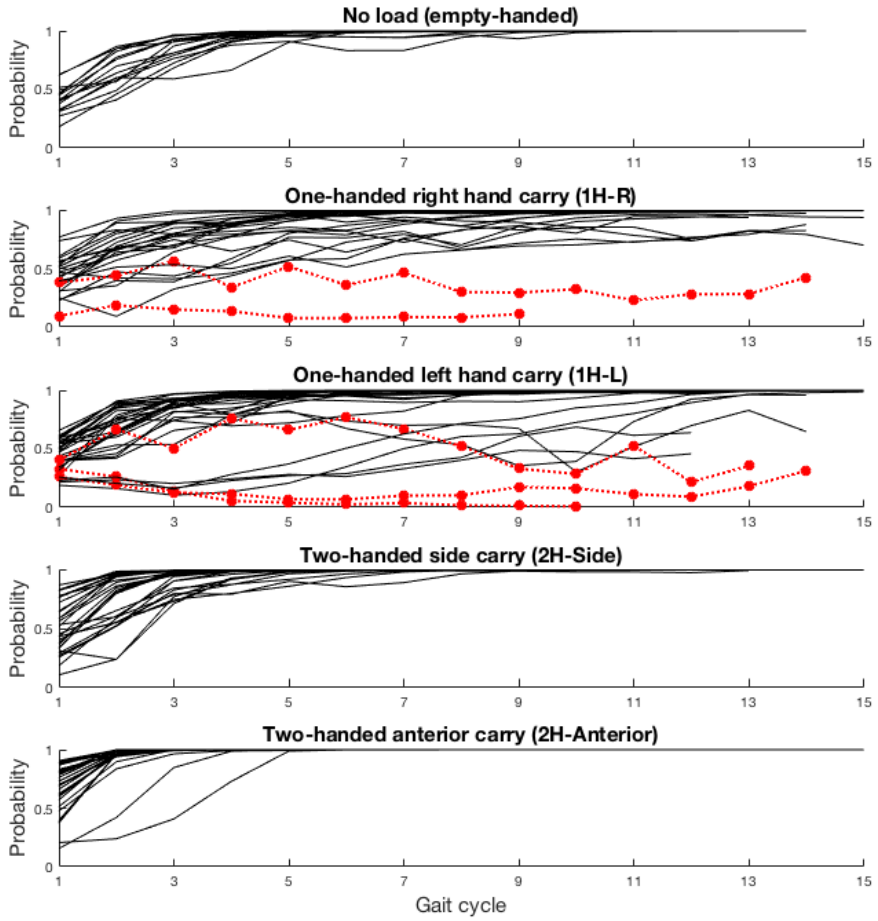



Figure 4.4: Posterior probabilities of the target carrying mode in each walk trial depicted by gait cycles. Misclassified classes are marked as red dotted lines.

Table 4.3: Confusion matrices summarizing the classification results for load level for each predicted carrying mode.

**1. One-handed right carry (1H-R)**

| | | Predicted Load Level | | Total Walk Trials | Sensitivity |
|---|---|---|---|---|---|
| | | **50% MAWC** | **75% MAWC** | | |
| **Actual Load Level** | **50% MAWC** | 16 | 2 | 18 | 88.9% |
| | **75% MAWC** | 1 | 16 | 17 | 94.1% |
| **Total Walk Trials** | | 17 | 18 | 35 | |
| **Precision** | | 94.1% | 88.9% | | |

**2. One-handed left carry (1H-L)**

| | | Predicted Load Level | | Total Walk Trials | Sensitivity |
|---|---|---|---|---|---|
| | | **50% MAWC** | **75% MAWC** | | |
| **Actual Load Level** | **50% MAWC** | 16 | 2 | 18 | 88.9% |
| | **75% MAWC** | 1 | 16 | 17 | 94.1% |
| **Total Walk Trials** | | 17 | 18 | 35 | |
| **Precision** | | 94.1% | 88.9% | | |

**3. Two-handed side carry (2H-Side)**

| | | Predicted Load Level | | Total Walk Trials | Sensitivity |
|---|---|---|---|---|---|
| | | **50% MAWC** | **75% MAWC** | | |
| **Actual Load Level** | **50% MAWC** | 17 | 1 | 18 | 94.4% |
| | **75% MAWC** | 1 | 17 | 18 | 94.4% |
| **Total Walk Trials** | | 18 | 18 | 36 | |
| **Precision** | | 94.4% | 94.4% | | |

**4. Two-handed anterior carry (2H-Anterior)**

| | | Predicted Load Level | | Total Walk Trials | Sensitivity |
|---|---|---|---|---|---|
| | | **50% MAWC** | **75% MAWC** | | |
| **Actual Load Level** | **50% MAWC** | 16 | 2 | 18 | 88.9% |
| | **75% MAWC** | 1 | 16 | 17 | 94.1% |
| **Total Walk Trials** | | 17 | 18 | 35 | |
| **Precision** | | 94.1% | 88.9% | | |

#### 4.3.2.3 Variable Importance

Figure 4.5 shows the relative importance (%) of the predictor variables in each classification model. Thoracic-pelvic coordination in the coronal plane was the most important predictor in the classification model for carrying mode, followed by postural sway of the pelvis in the coronal plane and transverse thoracic-pelvic coordination in a distant second and third, respectively (Figure 4.5, panel A). For 1H-R, gait cycle duration and thoracic-pelvic coordination in the coronal plane were nearly equally most important predictors for classifying the load level (Figure 4.5, panel B-1). However, unlike the classification model for carrying mode with one dominant predictor variable, the load level classification model for 1H-R also indicated terminal double support, torso and pelvis postural sway in the coronal plane, and torso postural sway in the transverse plane as relatively important (i.e., > 75%). Coronal plane measures of torso and pelvis postural sway and thoracic-pelvic coordination were the three most important predictors in the load level classification model for 1H-L compared to the rest of the predictor variables (Figure 4.5, panel B-2). Pelvis postural sway in the sagittal plane was the most important predictor when classifying the load level in the 2H-Side carry (Figure 4.5, panel B-3). Pelvis postural sway in the transverse plane and coronal plane were the second and third most important predictors. Pelvic postural sway in the transverse and coronal planes were both equally important when predicting the load level in the 2H-Anterior carry, followed by torso postural sway in the coronal plane (Figure 4.5, panel B-4).

## 4.4 Discussion

Wearable sensing technology combined with predictive modeling has the potential to advance the science of field-based exposure assessment by providing information about work content beyond just quantifying worker postures. This study assessed the potential for classifying carrying mode and load level using gait kinematics calculated from the iner-

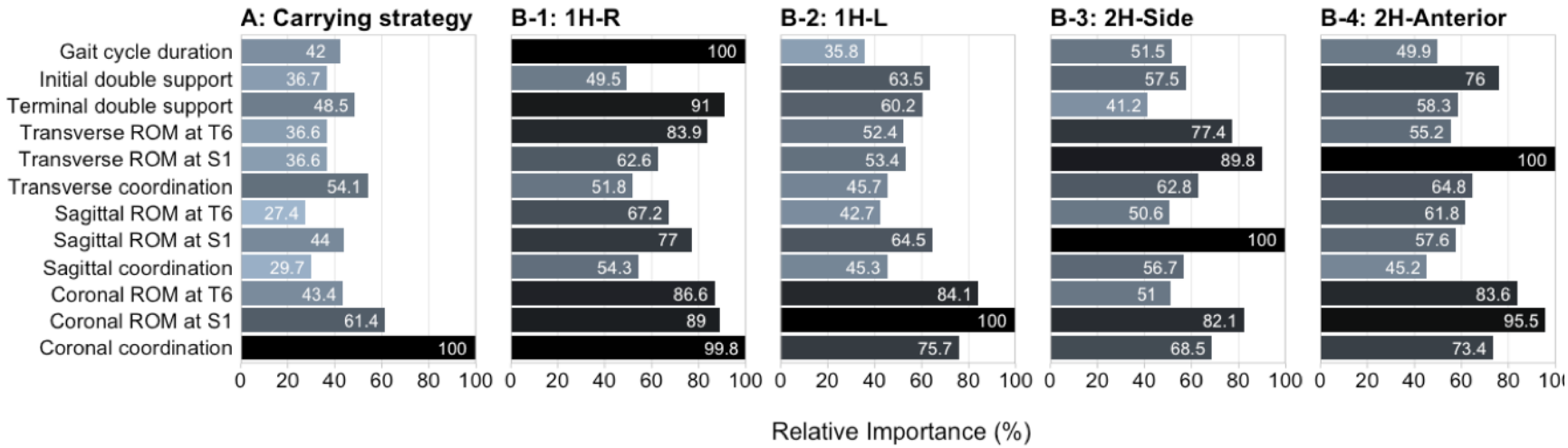



Figure 4.5: Relative importance (%) of the predictor variables computed as the mean decrease in the Gini index relative to the maximum (100%) for each of the five classification models, namely, for carrying mode (panel A) and for load level (panels B-1 to B-4).

tial sensor-derived data. As an initial investigation, the study was intentionally limited to a small homogeneous participant sample (n = 9) with gait data recorded at self-selecting walking speeds over multiple walk trials and conditions, namely 159 walk trials and 2028 gait cycles in total, to build and assess the statistical model. Thoracic and pelvic ROM and thoracic-pelvic coordination were important predictors in classifying carrying mode and relative load level compared to unloaded gait. The accuracy of statistically classifying carrying mode and load levels were 96.9% and 93.1%, respectively. Use of the Bayesian inference for updating probabilities with the incoming gait cycles improved the overall prediction accuracy by 19.6% with 4 to 5 gait cycles needed to converge on the classification result.

### 4.4.1 Methodological Contributions

Biomechanical exposures during physical work are typically characterized by three main dimensions [6], i.e., intensity (magnitude or amount of the forces and loads which are also a function of task and posture), frequency (repetition), and duration (the time the physical activity is performed). The algorithm presented provides information on all three dimensions of physical exposures during load carriage. The gait detection algorithm (*Step 1*) used in this study implements a robust detection of the start and end of walking, so the duration of the walking (either unloaded or loaded) can be accurately estimated. The load level classification (*Step 5 & 6*) predicts the relative intensity of the load carried, the measurement of which can be obtrusive in work settings that involve carrying loads of different magnitudes (e.g., construction work, distribution centers). The carrying mode classification (*Step 3 & 4*) combined with the load level classification (*Step 5 & 6*) quantifies the frequency of load carriage by categorizing the task in terms of its mode and load level.

Developing a successful prediction algorithm requires knowledge of the underlying system or domain when deciding on the structure of the statistical model (e.g., single-stage vs. multi-stage), segmenting the data, and selecting predictor variables or features within

the data segment [193]. The current study incorporated biomechanical information about the association between human gait kinematics and load carriage to develop and assess the statistical prediction model, which had direct bearing on model performance. We discuss key aspects of the model development and assessment in the subsequent sections.

#### 4.4.1.1 Data Segmentation and Choice of Predictor Variables

Statistical prediction with continuous time series data requires that the data be re-structured into segments. The methods of segmenting a continuous stream of sensor data influences the performance of the prediction model and thus needs consideration [196]. To be useful, the method of data segmentation needs to represent the data such that the prediction error of all segments across time is minimized [197]. A common approach to segmenting time series data uses sliding windows with a fixed sliding width (e.g., [78]). Other approaches include a top-down approach of splitting time-series data into partitions by decreasing the segment length iteratively until the prediction error is below a user-specified threshold [197], and a bottom-up algorithm that starts from the finest possible partition of the time-series data and increases the length of the segment iteratively. Unlike the latter two iterative approaches, use of a sliding window is the most popular form in online applications since the segmentation can be performed while the data is streaming. Another online approach involves segmenting data based on pre-defined events, as was the case in this study.

In this study, inertial sensor data were segmented by first detecting gait cycles, which represents a meaningful segmentation of the data stream. For a given carrying mode and load magnitude, gait cycle duration for a person shows little variability over short bouts of walking; however, the cycle duration can vary significantly between participants and across load carry conditions for the same person [143, 174]. For example, in the present study gait cycle duration ranged between 0.93s to 1.16s across all participants and carrying conditions. If a fixed window of average gait cycle, for example 1s, was used for data

segmentation instead of the proposed adaptive algorithm, the kinematic variables calculated within a segment would be less representative of the gait patterns relative to a data segment that captures a complete gait cycle. Another advantage of the proposed data segmentation method is that it can be used in online applications in near-real-time. Once a gait cycle is detected from an incoming data stream, predictor variables for the gait cycle can be computed and used as input to the classification algorithm. The delay in the classification output would be just over one gait cycle ($\sim$1s). The detection of an exact start and end of gait cycles resolves an issue of underestimating the task duration reported in previous studies on classifying manual material handling tasks [78]. In that study, task durations were underestimated by about 14% when classifying tasks using inertial sensor data that were segmented by sliding window of fixed duration. The detection of gait events and subsequent data segmentation based on gait cycles used in the current study would produce a more accurate estimate of duration of load carriage compared to a sliding window of fixed duration.

Choice of the predictor variables, which requires computing (i.e., extracting) and selecting features from sensor data, is also an important step towards building a simpler, comprehensible model while ensuring adequate prediction accuracy [198]. Predictor variables need to represent the main characteristics of a data segment, so that it contains important cues for distinguishing levels of outcome variables [196]. Use of domain specific features such as step detection, step variance, and vertical and horizontal acceleration of the sensor segment were found to increase prediction performance when classifying physical activities such as walking, running, cycling, and resting compared to using only time- and frequency-domain features [199]. Kim and Nussbaum [78] used descriptive statistics on whole-body joint angles to classify manual material-handling tasks. The present study used temporal, and thoracic and pelvic kinematic gait parameters as predictor variables. As opposed to using raw sensor data, the use of such domain specific features could significantly reduce the number of feature vectors used in a classification algorithm and also

increase prediction accuracy.

#### 4.4.1.2 Structure of the Model

A two-stage hierarchical model structure was implemented in this study where the carrying mode was classified first followed by classification of load levels within mode. Without the hierarchical structure, nine classes or categories would need to be predicted (i.e., 4 carrying modes x 2 load levels, and 1 no-load condition). With the same number of test datasets, increasing the number of target classes often increases the possibility of misclassification and lowers prediction accuracy. Reducing a k-class problem to a set of k two-class problems by building a separately trained binary classification model for each of the k problems is a common approach to deal with the multiclass classification [200]. However, this approach does not provide guidance about which the two classes need to be paired or the effect of having different pairs on model performance. Considering that classification problems in occupational settings may have a high number of potential outcome classes such as task type (e.g., lifting, pushing, pulling, carrying, etc.) and intensity level (e.g., forceful exertions) [32], multiclass classification models would be more common than two-class classification.

Implementing a hierarchical structure in classification models with multiple target classes has three advantages. First, implementation of the hierarchical model significantly improves the prediction accuracy compared to classifying the combination of different task conditions at one time. In our preliminary testing with the same test dataset, the multiclass prediction model with no hierarchical structure resulted in a prediction accuracy of 48.0%, which was 43.8% lower than the proposed hierarchical model. In a different study aimed at classifying the handle height and force intensity level in a pushing task, the hierarchically structured model produced a 50.0% greater prediction accuracy compared to the multiclass prediction model [123]. In both cases, the hierarchy of the models was built with an empirical understanding of the relative influence of different task vari-

ables [124, 124, 146, 151, 201].

A second advantage of having a hierarchical model structure is the opportunity for optimizing the predictor variable set in each model. The analysis of variable importance (Figure 4.5) suggests that the important variables in each model differ across classification models. This information can be used to reduce the number of predictor variables in each model thereby decreasing model complexity and computational effort, and increasing model interpretability.

Third, the hierarchical structure allows prediction performance assessment at every level of the hierarchy independently. In addition, the algorithms that occur in the lower level do not affect the performance of the algorithms that occur in the upper levels [202].

#### 4.4.1.3 Model Interpretability

The random forest method used in this study is flexible in modeling relationships between multiple predictors and outcome classes, without requiring any a priori assumptions about the type of relationships, e.g., linear vs. nonlinear. This flexibility lends to high prediction accuracy as was evident in this study, but comes at some expense of interpretability, i.e., it is difficult to quantify how any individual predictor is associated with the outcome. The primary means for interpreting a random forest model uses the average decrease in the Gini Index as an indicator of the relative importance of predictor variables. Our results on important predictor variables are supported by findings from previous studies that demonstrate that changes in gait from hand-load carriage are evident in the measures of thoracic and pelvic postural sway and thoracic-pelvic coordination [129, 143, 154, 203].

The relative importance of thoracic and pelvic sway and intersegment coordination differed across all five prediction models (Figure 4.5). Specifically, 2H-Side carriage increases angular momentum and moment of inertial in the coronal and transverse planes [203]. With this increase, postural stability is maintained by an increased but anti-phasic sway (i.e., counter-rotation) of the pelvis in the coronal, transverse, and sagittal planes with increas-

ing loads relative to unloaded gait [124]. Similar contributions of thoracic and pelvic sway and intersegment coordination in the coronal plane were also identified in the 1H-R and 1H-L side carry. However, the load prediction models for 1H right vs. left side carry showed differences in relative importance of other temporal gait parameters, namely, gait cycle duration and terminal double support. These differences may be due to bilateral asymmetries in strength and gait, and is a topic of further investigation.

Restricted arm movements and close coupling between the torso and pelvis during 2H-Anterior load carriage is associated with increased pelvic sway in the coronal and sagittal planes, and a decrease in pelvic sway in the transverse plane relative to unloaded gait [129, 203]. Consequently, movement coordination between the thoracic-pelvic segments is more in-phase or synchronized in the coronal and transverse planes with increasing load relative to unloaded gait [148, 173].

### 4.4.2 Study Limitations

Certain limitations of this laboratory study are worth emphasizing in order to contextualize the study findings and implications for practice. Given its focus on model development and assessment, the study sample comprised of a relatively small and homogenous sample of healthy, young male participants. Further investigation is needed to test the generalizability of the model across the spectrum of worker demographics on known sources of variability in gait such as age [204], gender [205], obesity [206, 207] and strength [208, 209]. The present study found that a minimum of 4 to 5 gait cycles needed to converge on a prediction result. This finding suggests that in subsequent studies the amount of data collected from each participant can be economized in lieu of a larger and more diverse sample.

For jobs that might involve long duration of manual load carriage, cumulative fatigue from load carriage may induce alterations in gait [175, 176, 210]. Prior studies have associated fatigue with increased variability in step length, step width, and mediolateral trunk accelerations while walking, and increased double support duration during load carriage.

[147] reported hip and torso ROM to increase while carrying a backpack load immediately following a fatiguing treadmill exercise. Age is also reported to moderate the effects of fatigue on gait [175, 176]. To minimize the confounding effects of fatigue, the present study introduced two-minute rest breaks between each walk trial of 24 m distance. However, subsequent studies will need to account for the effects of cumulative fatigue from long duration exposures to load carriage on thoracic and pelvic ROM and coordination.

The proposed model also requires that load magnitudes be normalized to individual carrying capacity determined using either biomechanical strength or psychophysical criteria. This may be a limitation in certain work settings that do not have a steady cohort of workers that can be assessed. Additional study is also needed to consider more diverse task conditions that are representative of applied settings (e.g., size and form-factor of the load carried, location of handles, and weight distribution of the load) and over extended periods before the proposed algorithm can be used as a field evaluation tool for manual load carriage work.

### 4.4.3 Application and Relevance

Quantifying physical exposures to load carriage can be challenging in non-routinized work settings where load intensity, duration and frequency vary between workers and within worker across time. The present study represents an initial step towards the development of a real-time exposure assessment tool that leverages wearable inertial sensing and predictive modeling for use in occupational settings. Multiple previous studies have used inertial sensors to classify between different types of activities (e.g., walking vs. sitting), however few studies have delved into predicting task demands within a specific activity (i.e., relative changes between load within the same task). The present study is novel in this regard. A key contribution of this study was the reliance on a biomechanical understanding of the effects of load carriage on pelvic and thoracic movement and coordination into a practical framework for predicting carrying mode and relative load conditions. From a practical

standpoint, our findings have direct implications for attachment locations of inertial sensors. Leveraging subtle movement patterns of the torso and pelvic implies that the sensors be closely attached to the skin on these segment as opposed to worn on top of loose clothing, helmet, or gloves. Newer forms of wearable sensing embedded in smart clothing may help overcome these potential usability concerns [112].

Extending the proposed approach to include other tasks that are of interest in ergonomics exposure assessment such as lifting-lowering and push-pull exertions will require task-specific models that capture intrinsic kinematic adaptations to task demands. For example, findings by [211] indicating that thoracic-pelvic coordination in the sagittal plane is influenced by lifting mode (i.e., freestyle, flexed and neutral spine) [211] can be leveraged to develop and assess predictive models of lifting modes using body worn inertial sensors. These task specific models can be envisioned as modules nested within an overarching activity classification model. This framework aligns with our proposed approach of a multi-stage hierarchical model structure led by classification by task type (e.g., lifting, pushing, pulling, carrying, etc.), followed by models that classifying mode and intensity within task type to account for the large number of potential outcome classes in occupational settings.

## 4.5 Conclusion

This chapter presents an algorithmic framework for combining wearable inertial sensing, gait kinematics, and statistical prediction for classifying carrying modes and load levels during manual load carriage. Overall, the algorithm was sensitive in discerning loaded from unloaded walk conditions within 4 to 5 consecutive gait cycles. Prediction accuracy and the relative importance of thoracic and pelvic measures as predictors were found to differ by models for carrying mode and load level. The few misclassified trials occurred largely in the 1H-R and 1H-L side carrying modes. Further investigation is needed to test the generalizability of the model across the spectrum of worker demographics and load

carrying conditions. The present study also provides practical information about locations for inertial sensor placement and the type and amount of data required for distinguishing carrying modes and relative load levels for use in subsequent studies of higher ecological validity and increased generalizability.

Applying statistical classification techniques to movement analysis requires an understanding of machine learning theory, signal processing, and feature extraction. By emphasizing model development and assessment, this study also attempts to explain aspects of classification and predictive modeling towards encouraging the application of these statistical techniques to ergonomics practice.

The present study was a proof-of-concept. The subsequent Chapter 5 extends the presented statistical classification model to diverse conditions of load carriage and lifting-lowering, and in a diverse cohort of participants.

# CHAPTER 5

# Investigating Generalized Algorithms for Statistical Classification of Load Carriage and Lifting-Lowering Exposures

The previous Chapters 3 and 4 operationalized information about the effects of load carriage on inertial sensor-derived gait kinematics, specifically torso and pelvis postural sway and thoracic-pelvic coordination into a novel statistical classification model of hand-loads and carrying modes [124, 125]. However, the analyses was limited to a homogeneous sample of young men. This chapter extends the statistical classification model to different tasks conditions in load carriage and lifting-lowering, which represent two common MMH tasks associated with an increased risk of low back disorders. A diverse sample 15 men and 12 women participated in a laboratory study simulating load carriage and lifting-lowering task. Separate classification models were developed for predicting binary load levels (i.e., low: 0 to 4.5 kgs. vs. high: 13.5 to 22.7 kgs.) in manual load carriage, lifting, and lowering using inertial-sensor derived kinematic measures as predictors. Classification accuracy for carrying mode was 80.2% and for load levels averaged 88.7% across carrying modes. Average accuracy of the model for classifying lifting height (floor vs. lift), mode (one vs. two-handed), and load levels were 97.7%, 93.9%, and 84.2%, respectively. Corresponding classification accuracy for lowering height, mode, and load levels were 97.4%, 92.8%, and 83.7%, respectively. Collectively, these findings demonstrate the potential for combining

wearable inertial sensing with statistical prediction to quantify biomechanical exposures in manual material handling work.

## 5.1 Introduction

Prolonged exposure to manual load carriage is a known risk factor for low back disorders [2, 130]. Measuring the carrying mode, duration, repetition, and magnitude of hand loads longitudinally is an essential step for assessing the biomechanical impacts to the musculoskeletal system and identifying strategies for intervention. Quantifying biomechanical exposures from load carriage are particularly challenging in non-routinized work (e.g., construction, warehousing). Using data from body-worn inertial sensors, the previous study presented a statistical classification model that leveraged subtle yet systematic kinematic adaptations in thoracic and pelvic sway and movement coordination to predict normalized load levels in two-handed and one-handed load carriage. However, the study was limited to a homogeneous sample of young men.

Prior studies have reported gait kinematics to be influenced by age [204, 209], gender [205], obesity [206, 207] and functional strength [208, 209]. For instance, gait kinematics are associated with gender during unloaded walking and manual load carriage [174]. Martin & Nelson [174] reported that spatiotemporal gait parameters (e.g., stride length, swing duration) showed greater sensitivity to load magnitude in women compared to men. These differences in gait kinematics due to anthropometry could potentially affect the performance of algorithms developed in Chapter 4. This has practical concerns if such prediction algorithms either systematically under- or over-estimate the predicted load level differently for people of different anthropometry.

### 5.1.1 Lifting-lowering and Low Back Disorder Risk

Manual lifting-lowering is another common MMH task associated with an increased risk of occupationally-related low back disorders [212, 213, 214]. Identifying lifting-lowering

tasks that pose higher disorder risk is an important step toward developing effective intervention strategies. However, multiple factors besides load magnitude affect the level of low back disorder risk from lifting, which complicates the assessment of biomechanical exposures to lifting. For instance, prior studies have documented that increases in the magnitude of lifting frequency, duration, load moment arm characterized by the horizontal and vertical lifting height, trunk lateral velocity, trunk twisting velocity, and trunk sagittal angle significantly increased the risk of LBD [215, 216]. Assessing spinal loads and low back disorder risk associated with lifting and lowering is even more challenging in non-repetitive work conditions where the magnitude, repetition and duration of load moments change over time.

A proper lifting-lowering movement is characterized by the ability to maintain dynamic balance and use minimal effort to achieve a smooth, uninterrupted and controlled movement while keeping the object as close to the body as possible. Movement dynamics in the torso, and angular hip and knee kinematics during lifting and lowering are influenced by lifting conditions (e.g., object load, squat vs. stoop lifting, vertical location of the object from the floor, angle of asymmetry). For example, increasing load magnitude (i.e., from 9.1 to 41.7 kg) was associated with a decrease in peak sagittal velocity and acceleration and increase in peak lateral acceleration of the torso [217]. Load magnitudes during lifting-lowering tasks also affect movement coordination between segments such as between lumbar and pelvis angular displacement, and hip and knee flexion/extension angles. Hu et al. demonstrated that lumbar-pelvic angular coordination measured as the mean relative phase angle decreased (i.e., movement was more synchronous) when lifting a load of 9.1 kg vs. a no-load movement [218].

Prior researchers have attempted to leverage these relationships between lifting load magnitude and kinematics into statistical prediction algorithms. A recent study by Brandt et al. [77] report on statistical classification using a Linear Discriminant Analysis to separate low vs. high risk lifting motions defined using guidelines from The Danish Working

Environment Authority [219]. The study simulated low vs. high risk lifting by manipulating load magnitude (i.e., 16, 18, 20, 22, and 24 kgs.), horizontal distance between the load and the lifter (i.e., forearm distance vs. 0.75 times arm distance), and symmetricity of the lifting (symmetric lifting vs. asymmetric lifting where the load was located to the right side of the lifter). The LDA-based algorithm classified low vs. high-risk lifts with an accuracy of 72.7% - 78.1% using as predictors the RMS activity of the upper trapezius and erector spinae muscles from surface electromyography and RMS accelerations from accelerometers located at T1 and L5 [77]. As a preliminary investigation, this study was also a cohort of young male participants. The generalizability of algorithms to classify lifting mode or load levels across a diverse spectrum of users remains unexplored.

Similar to load carriage, differences in lifting and lowering kinematics across person variables including gender, body mass, and prior health status. Boston et al. [220] reported that individuals low back pain displayed decreased hip-knee coordination (e.g., temporal parameters such as midpoints and risetimes) during repetitive lifting compared to an asymptomatic control group. Body Mass Index (BMI) has been also discussed as a factor affecting lifting kinematics, with a less smooth motion or higher RMS amplitude of jerk measured at the upper back from accelerometry among individuals with a lower BMI (BMI $< 30$ kg/m$^2$) vs. higher BMI (BMI $\geq 30$ kg/m$^2$) [221]. Akin to load carriage, the large diversity in anthropometry across workers could affect the accuracy of predictive modeling algorithms that use lifting-lowering kinematics as predictors.

The aim of this study was to develop and assess statistical classification algorithms that use kinematic variables calculated from body-worn inertial sensor data as predictors for classifying load magnitudes in common MMH tasks, namely load carriage, lifting, and lowering. To improve model generalizability across people, the data collection involved a diverse sample of participants differing in age, gender, and strength capabilities. Within the algorithm for each task, the study compared prediction accuracy using predictors in their original form vs. normalized to individual anthropometry. The statistical classification

algorithms implemented incorporate a priori biomechanical knowledge about the effects of external loads on movement kinematics to compute and select predictor variables for each MMH task, and the hierarchical structure of the statistical model.

## 5.2 Methods

### 5.2.1 Study Participants

The study recruited 27 healthy participants (15 men and 12 women) sampled on age and gender to obtain a sample diverse in age, gender, and strength capabilities. Participants were screened for pre-existing back injuries or chronic pain with a body discomfort questionnaire adapted from the body mapping exercise by NIOSH ([165] for more details). 88.9% of the participants (24 out of 27) were right-handed when tested with the questionnaire adapted from the Edinburgh handedness inventory [188]. Prior to the study, participants completed a written informed consent approved by the university's institutional review board.

#### 5.2.1.1 Participant Anthropometry

Static anthropometry and functional strength for each participant was measured at the onset. Static anthropometry dimensions included stature, hip breath, knee height, and body mass measured using a standing anthropometer, caliper, and weighing scale. Functional low back strength was measured as the adjusted torso lift strength using the procedure developed by Stobbe [222]. Table 5.1 summarizes the anthropometry of study participants.

Table 5.1: Average (standard deviation) age, stature, body mass, BMI, and low-back lifting strength for the study sample stratified by gender and age category (N = 27).

| Gender | Age category | N | Age, years | Stature, m | Mass, kg | BMI, kg/m$^2$ | Low-back strength, N |
|---|---|---|---|---|---|---|---|
| Men | 18-29 | 4 | 36.1 (9.7) | 1.76 (0.05) | 67.3 (9.5) | 21.7 (2.6) | 817.1 (96.1) |
| | 30-39 | 6 | | 1.83 (0.07) | 87.2 (9.8) | 26.0 (3.0) | 786.4 (118.7) |
| | 40-55 | 5 | | 1.79 (0.05) | 75.5 (10.9) | 23.6 (2.9) | 670.6 (134.5) |
| Women | 18-29 | 5 | 30.9 (10.0) | 1.68 (0.05) | 67.7 (15.3) | 23.8 (4.1) | 483.3 (90.2) |
| | 30-39 | 4 | | 1.67 (0.07) | 79.2 (14.9) | 28.1 (3.2) | 506.3 (63.8) |
| | 40-55 | 3 | | 1.70 (0.06) | 70.6 (7.8) | 24.5 (1.8) | 513.8 (177.1) |
| | Total | 27 | 33.8 (10.0) | 1.75 (0.08) | 75.4 (13.1) | 24.7 (3.4) | 641.6 (178.9) |

## 5.2.2 Experiment Procedures

### 5.2.2.1 Simulated MMH Tasks

Figure 5.1 summarizes the overall experiment procedure for the simulated MMH tasks. Initially reference measurements were recorded in a static posture and in dynamic reference movements at baseline. For the static measure, the average body posture angles from 30 seconds of quiet standing were subtracted from the dynamic postural angles obtained during the subsequent work tasks. Next, two types of dynamic reference movements were measured: (i) Unloaded (empty-handed) walking trials were performed twice to obtain the baseline walking patterns from each participant, (ii) Unloaded bending and rising movements were performed with participants reaching to floor height and knee height from standing, with two repetitions each.

**Load Carriage:** A laboratory experiment was conducted that required participants to carry a weighted box down a levelled corridor (12 m length x 1.5 m width) for a distance of 10 m in four carrying modes commonly used in occupational settings, namely, one-handed right hand carry (1H-R), one-handed left hand carry (1H-L), two-handed side carry (2H-Side), and two-handed anterior carry (2H-Anterior) (refer to Figure 4.1 in Chapter 4). Four levels of box weights were evaluated in each mode: no-load (i.e., unloaded reference

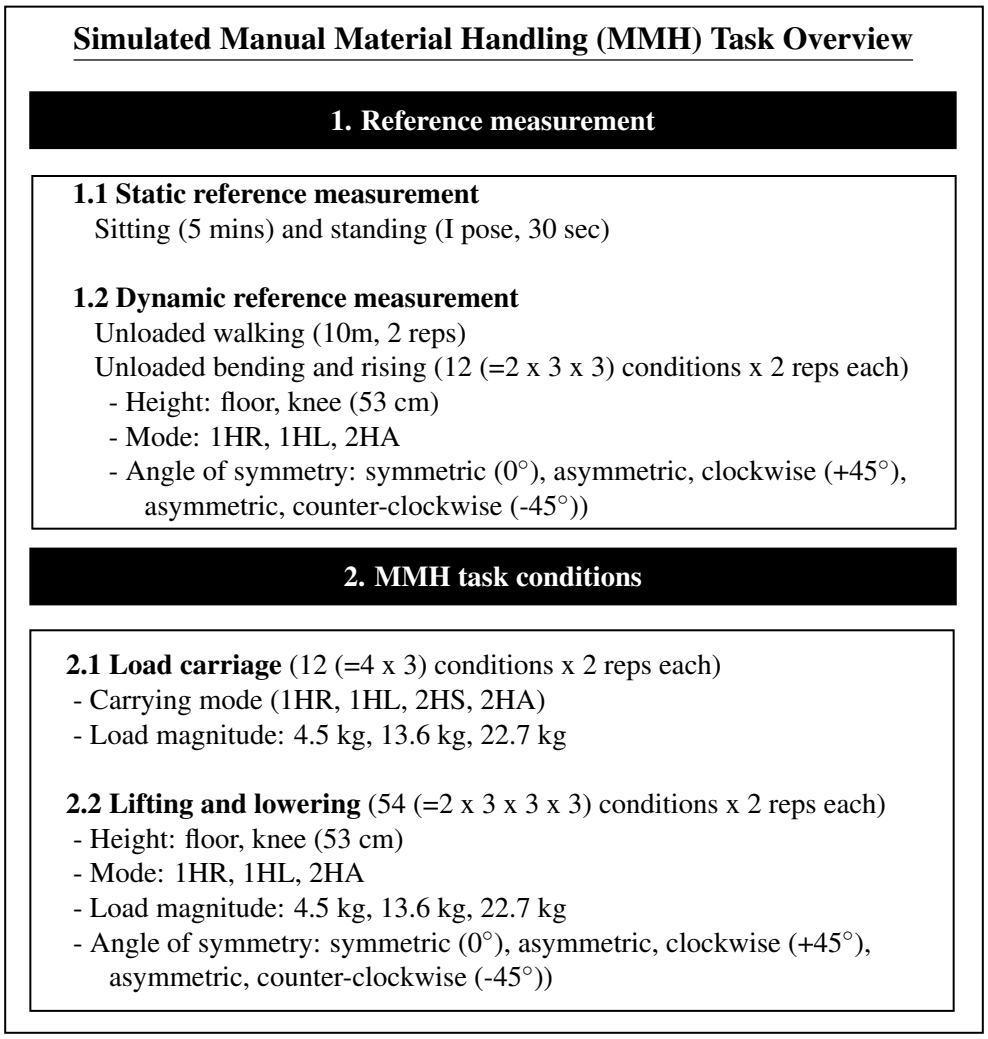



Figure 5.1: Overview of the experiment procedures for simulated MMH tasks.

condition), 4.5 kg (10 lbs), 13.6 kg (30 lbs), and 22.7 kg (50 lbs). The box dimensions were identical to the boxes used in the previous Chapter 4. The load was equally divided between the right and left hand in the 2H-Side carry.

Each participant performed two consecutive trials of 12 load carrying conditions (= 4 carrying modes x 3 load levels) in random order. Walking speed was self-selected to observe the natural adaptation in walking patterns due to different load carriage conditions. Two-minute rest breaks between each walk trial were given to participants to minimize carry-over effects of fatigue.

**Lifting and Lowering:** Each participant performed lifting and lowering motions at a self-selected speed. Four task parameters were manipulated to simulate different lifting-lowering conditions and geometric aspects of the workplace that influence lifting-lowering posture and internal loads [3, 213], namely,

- Lifting-lowering height: floor vs. average knee height (53 cm),
- Mode: 1H-R, 1H-L, and 2H-Anterior
- Load magnitude: 0 kg. (no-load), 4.5 kgs., 13.6 kgs., and 22.7 kgs.
- Symmetricity: -45°, 0°, and 45° (Figure 5.2)

During lifting-lowering, participants were instructed to keep their feet shoulder width apart, stationary, and symmetric while performing the lifting and lowering. Two consecutive repetitions of 54 lifting and lowering motion trials (= 2 heights x 3 hand modes x 3 load levels x 3 symmetricity levels) were performed, with task conditions presented in counterbalanced order.

### 5.2.3 Instrumentation

Kinematic data were continuously recorded using four commercial inertial sensors (Biostamp RC, mc10 Inc., Lexington, MA, USA) during the reference measurements and

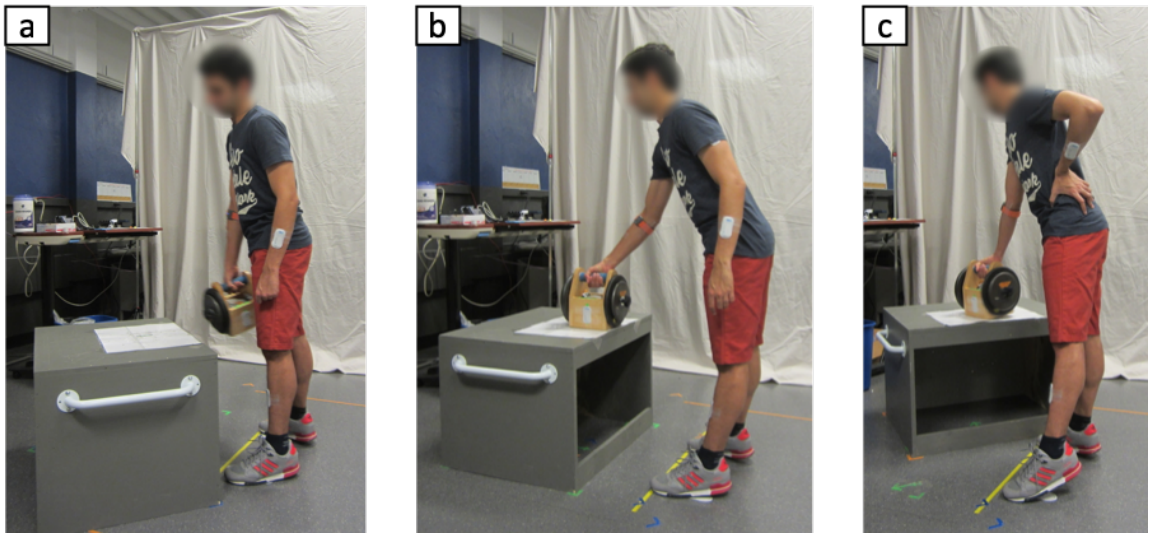



Figure 5.2: Sample images in a 1-handed right lifting condition at knee height depicting the three different symmetricity conditions evaluated in the experiment: (a) asymmetric, counter-clockwise (-45 deg.), (b) symmetric, and (c) asymmetric, clockwise (+45 deg.). The distance between the center of the original box location to the middle of the participants' right and left anterior shoe-tip was a constant 40 cm.

simulated load carriage, lifting, and lowering trials. Two inertial sensors were attached over the sixth thoracic vertebra (T6) and the first sacral vertebra (S1). A third sensor was positioned along the superior aspect of the right thigh midway between the hip and lateral femoral epicondyles, and the fourth sensor was on the superior aspect of the right shank midway between the lateral femoral and malleolar epicondyles (Figure 5.3). Sensor data pre-processing was described in Chapter 3 in detail.

### 5.2.4 Algorithm to Classify Carrying Mode and Load Level

A statistical algorithm was developed for classifying carrying mode and load level following the six general steps described in Figure 4.2 in Chapter 4, namely, (i) detect gait cycles, (ii) compute predictor variables, (iii) predict carrying mode per gait cycle, (iv) perform a Bayesian update to identify one carrying mode per trial, (v) predict load level per gait cycle, and (vi) select load level per trial. Four carrying modes (i.e., 1H-R, 1H-L, 2H-Side,

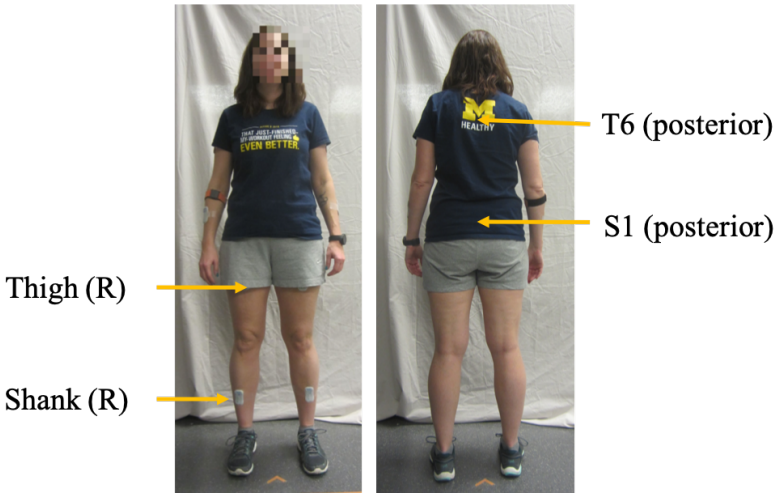



Figure 5.3: Images showing the four inertial sensors attached on the body at T6, S1, thigh (Right), and shank (Right).

2H-Anterior) and no-load and two load levels, i.e., Low (4.5 kg) vs. High (13.6 kg and 22.7 kg), were the target outcome variables for each walking trial.

Gait parameters calculated from the inertial sensor data included six measures of torso and pelvis postural sway, six measures of peak linear acceleration at torso and pelvis, and six measures of thoracic-pelvic coordination in the form of average and RMS relative phase angles in the coronal, transverse, and sagittal planes (Table 4.1 for more details). Additionally, spectral analysis (i.e., discrete Fourier transform) was performed to calculate an Index of Harmonicity (IH) of the individual time-series of the pelvic and thoracic rotations (Equation 5.1). IH is a measure of the relative contribution of the fundamental oscillating component to the observed coordination patterns [223]. An IH of 1.0 indicates that a time-series data is perfectly harmonic. Six measures of IH were computed, namely, for torso and pelvis angular displacement in the coronal, transverse, and sagittal planes, respectively. Three prior consecutive gait cycles and the current gait cycle (total of four consecutive gait cycles) were used to calculate the IH of the current gait cycle, while the IH of initial three

gait cycles were calculated only with the gait cycles up to the current gait cycle.

$$IH = \frac{P_0}{\sum_{t=0}^{5} P_i} \tag{5.1}$$

where:

$P_0$ = Power spectral density of the fundamental frequency (first harmonic),

$\sum_{t=0}^{5} P_i$ = Cumulative sum of power spectral density of the fundamental frequency and the first five superharmonics.

#### 5.2.4.1 Generalized Classification Algorithm

To account for inherent individual differences in gait patterns, three different models without and with data normalization were developed and assessed. The model with the highest classification accuracy in identifying load carriage mode and load level was interpreted as the most generalizable model.

(1) **Original model (*Original*)**: eighteen kinematic parameters (six measures of torso and pelvis postural sway, six measures of peak torso and pelvis acceleration, and six measures of thoracic-pelvic coordination) and six IH measures were included in this model in their original form, i.e., without normalization.

(2) **Normalized model relative to unloaded gait (*Rel-NL*)**: Six torso and pelvis postural sway measures and six peak torso and pelvis acceleration measures were expressed as the percent change from each individual's average unloaded gait parameters using Equation 5.2. Coordination and IH measures were included without normalization.

$$X_{(i)relative}(\%) = \frac{X_{(i)} - \overline{X}_{noload}}{\overline{X}_{noload}} * 100 \tag{5.2}$$

where:

$X_{(i)\ relative}$ = Percent change in gait parameter at gait cycle $i$,

$X_{(i)}$ = Gait parameter at gait cycle $i$,

$\overline{X}_{no\ load}$ = Average gait parameter across gait cycles in a no-load condition for each participant.

(3) **Normalized model relative to anthropometry (*Rel-Anthro*)**: eight gait parameters were normalized to each individual's anthropometry. Torso and pelvis postural sway and peak acceleration measures in transverse plane were normalized by each individual's hip breadth (401.6 $\pm$ 32.6 mm, range: 334.0 - 460.0 mm) while the same four measures in coronal plane were normalized by each individual's functional low-back strength (265.8 $\pm$ 909.7 N, range: 265.8 N to 909.7 N). Remaining measures were included without normalization.

### 5.2.5 Algorithm to Classify Lifting-Lowering Height, Hand Mode, and Load Level

#### 5.2.5.1 Classification Model Structure

Lowering (or bending if empty-handed) and lifting (or rising if empty-handed) phases were detected using a custom lifting-lowering detection algorithm described in Appendix F. A hierarchical three-stage statistical algorithm was developed for classifying lifting intensity level sequentially, i.e., height (floor vs. knee), hand mode (i.e., 1H: 1H-R or 1H-L vs. 2H-Anterior), and load level (i.e., Low: no-load and 4.5 kg vs. High: 13.6 kg and 22.7 kg), as depicted in Figure 5.4. Separate models were developed for lifting and lowering, and for each stage (i.e., H, M1 and M2, and L1 to L4; circles in Figure 5.4) based on the underlying hypothesis that the effects of load magnitude differs by the height and mode of lifting-lowering. Trials from three symmetricity conditions were aggregated, however symmetricity was not an outcome of the classification.

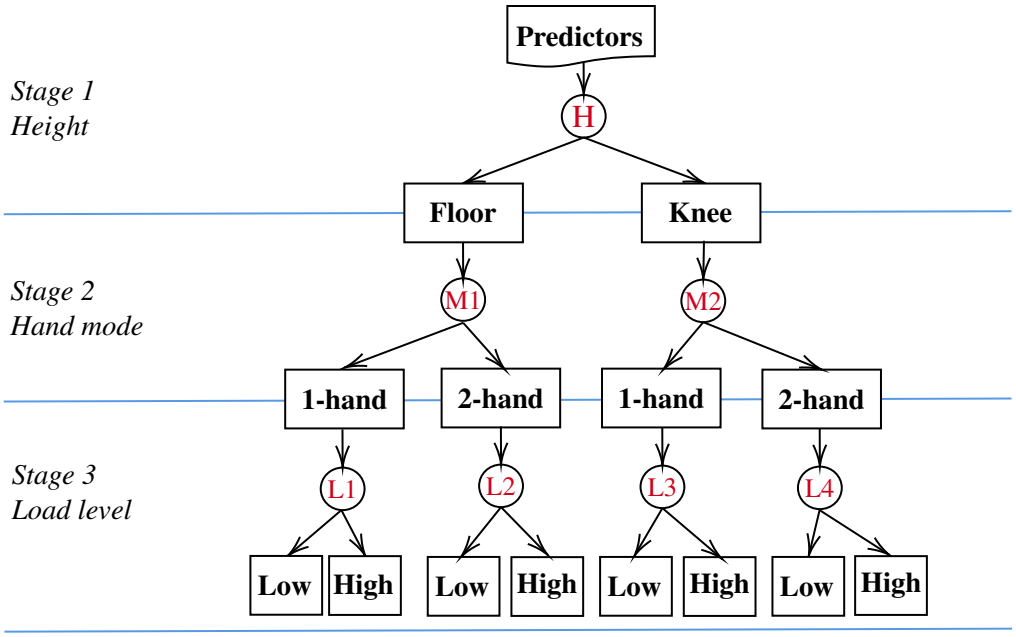



Figure 5.4: Hierarchical structure of the classification model for lifting and lowering intensity. Separate classification models were developed for each stage. For example, model-H for classifying height condition (floor vs. knee) and model M1 was developed for classifying hand mode (1H vs. 2H) for a predicted lifting height at floor-level. Load magnitudes of 0 kg (no-load) and and 4.5 kg were categorized as a Low load level, while the 13.6 kg and 22.7 kg load magnitudes were categorized as a High load level.

#### 5.2.5.2 Predictor Variables

A comprehensive review of the lifting literature (e.g., [220, 221, 224, 225]) identified 23 kinematic variables associated with different tasks variables (e.g., load magnitude, distance, mode) and used as potential predictors in this study. The 23 potential predictors consisted of two temporal parameters of the lifting phases, seven measures of postural ROM, three measures of peak postural angles, three measures of peak angular velocity, three measures of peak acceleration, two measures of jerk RMS, and three measures of intersegment coordination (Table 5.2). Inclination angles corresponding to sagittal flexion-extension and lateral bending in Table 5.2 were calculated from inertial sensor data using the sensor fusion algorithm with a modified linear Kalman filter presented by Chen at al. [226]. Postural angles during the reference standing posture were subtracted from the dynamic postural an-

gles calculated at each time frame of the lifting-lowering task, and the range (max - min) of angle values was calculated to obtain the ROM. Predictor variables were selectively chosen for each model based on a variable selection process. First, importance of variables in each model was tested using the Random Forests-based variable selection method implemented in the statistical package VSURF v.1.0.4 [227] in R v.3.3.1 (R core team). Second, pairwise correlation analysis was performed to identify pairs of highly correlated variables within the selected variable set for each model identified from the previous step. For variable pairs that were highly correlated (i.e., $|R| > 0.8$), the variable of lower importance was discarded to avoid multi-collinearity. Table 5.2 lists the final selection of predictor variables with a check-mark (✓) corresponding to the classification model.

#### 5.2.5.3 Generalized Classification Algorithm

Similar to carrying classification algorithms, three algorithms with and without normalized predictors were tested for lifting and lowering task.

(1) **Original model (*Original*)**: Lifting and lowering parameters in Table 5.2 were used in their original for, i.e., without normalization.

(2) **Normalized model relative to unloaded bending and rising (*Rel-NL*)**: lifting and lowering parameters were expressed as the percent change from each persons average no-load rising (or bending) parameters using Equation 5.2, where $X_{(i)relative}$ is the percent change in lifting parameter at $i$, $X_{(i)}$ is the measured lifting parameter at $i$, and $\overline{X}_{noload}$ is the average lifting-lowering parameter across two repetition of symmetric empty-handed rising (or bending) for each participant.

(3) **Normalized model relative to unloaded bending-rising and anthropometry (*Rel-NL & Anthro*)**: Lifting-lowering duration was divided by each individual's stature. Postural ROM and peak angular velocity measures were normalized by the average

Table 5.2: List and definitions of kinematic parameters calculated from the inertial sensor data for each lifting and lowering phase. Lifting-lowering parameters were selectively used in different classification models, namely, models H, M1, M2, L1 to L4 in Figure 5.4) and identified by a ✓ .

| Parameter | | Definition | Classification Models | | | | | | |
|---|---|---|---|---|---|---|---|---|---|
| | | | Height | Hand Mode | | Load Level | | | |
| | | | H | M1 | M2 | L1 | L2 | L3 | L4 |
| **Temporal parameters (2 nos.)** | | | | | | | | | |
| 1 | Lifting or lowering duration (sec) | Duration of lifting or lowering phase | | | | ✓ | ✓ | ✓ | ✓ |
| 2 | Hip-knee midpoint difference (%) | Midpoint = normalized time (100%) at which half of the change has occured [220, 221, 224] during lifting or lowering. Hip-knee midpoint difference = Hip midpoint - knee midpoint. This measures the coordination between hip and knee regardless of the changes in the absolute lifting/lowering time | | | | ✓ | ✓ | | |
| **Postural ROM (7 nos.)** | | | | | | | | | |
| 3 | ROM at torso, sagittal flexion (°) | Range of sagittal flexion angle measured at T6 | | ✓ | | | | | |
| 4 | ROM at pelvis, sagittal flexion (°) | Range of sagittal flexion angle measured at S1 | | | ✓ | | | | ✓ |
| 5 | ROM at lumbar, sagittal flexion (°) | Range of sagittal flexion angle measured as (torso flexion - pelvis flexion) | | | | | | | ✓ |
| 6 | ROM at hip, sagittal flexion (°) | Range of sagittal flexion angle measured as (180°- pelvis inclination - right thigh inclination) | | ✓ | | | | | |
| 7 | ROM at knee, sagittal flexion (°) | Range of sagittal flexion angle measured as (180°- right thigh inclination - right shank inclination) | | | ✓ | | | | |
| 8 | ROM at torso, lateral bending (°) | Range of lateral bending angle measured at T6 | | ✓ | | | | | |
| 9 | ROM at pelvis, lateral bending (°) | Range of lateral bending angle measured at S1 | | | | | | ✓ | |
| **Peak postural angles (3 nos.)** | | | | | | | | | |
| 10 | Peak sagittal flexion at torso (°) | Maximum sagittal flexion angle measured at T6 | ✓ | | | | | | ✓ |
| 11 | Peak sagittal flexion at hip (°) | Maximum sagittal flexion angle measured as (180°- pelvis inclination - right thigh inclination) | ✓ | | | | ✓ | | |
| 12 | Peak sagittal flexion at knee (°) | Maximum sagittal flexion angle measured as (180°- right thigh inclination - right shank inclination) | ✓ | | ✓ | | | | |
| **Peak torso and pelvis angular velocity (3 nos.)** | | | | | | | | | |
| 13 | Peak angular velocity at torso in the sagittal plane (°/s) | Maximum angular velocity measured at T6 in the sagittal plane | | | ✓ | | | | |
| 14 | Peak angular velocity at torso in the coronal plane (°/s) | Maximum angular velocity measured at T6 in the coronal plane | | | | ✓ | | ✓ | |
| 15 | Peak angular velocity at pelvis in the coronal plane (°/s) | Maximum angular velocity measured at S1 in the coronal plane | | | | ✓ | | ✓ | |

**Table 5.2 – continued from previous page**

| Parameter | | Definition | Classification Models | | | | | | |
|---|---|---|---|---|---|---|---|---|---|
| | | | Height | Hand Mode | | Load Level | | | |
| | | | H | M1 | M2 | L1 | L2 | L3 | L4 |
| **Peak torso and pelvis acceleration (3 nos.)** | | | | | | | | | |
| 16 | Peak acceleration at torso in the vertical plane (°/s$^2$) | Maximum linear acceleration measured at T6 in the vertical plane | | | | ✓ | ✓ | ✓ | ✓ |
| 17 | Peak acceleration at pelvis in the vertical plane (°/s$^2$) | Maximum linear acceleration measured at S1 in the vertical plane | | | | ✓ | ✓ | | |
| 18 | Peak acceleration at pelvis in the coronal plane (°/s$^2$) | Maximum linear acceleration measured at S1 in the coronal plane | | | | | | ✓ | |
| **Jerk RMS (2 nos.)** | | | | | | | | | |
| 19 | Jerk RMS at torso (°/s$^3$) | RMS amplitude of jerk calculated as the first derivative of T6 acceleration during the lifting and lowering. A lower jerk is an indicative of a smoother lifting pattern [221, 225]. | | | | | ✓ | | |
| 20 | Jerk RMS at pelvis (°/s$^3$) | RMS amplitude of jerk calculated as the first derivative of S1 acceleration during the lifting and lowering. | | | | ✓ | ✓ | ✓ | ✓ |
| **Postural coordination (3 nos.)** | | | | | | | | | |
| 21 | Mean thoracic-pelvic coordination in the sagittal plane (°) | Mean relative phase angle between T6 and S1 (pelvic phase angle - thoracic phase angle) in the sagittal plane. Phase angle (t) = arctan (normalized angular velocity (t)/normalized integrated angular velocity (t). | | | | | | ✓ | ✓ |
| 22 | Mean hip-knee coordination in the sagittal plane (°) | Mean relative phase angle between hip and knee (hip phase angle - knee phase angle) in the sagittal plane. | | | | ✓ | ✓ | | ✓ |
| 23 | RMS hip-knee coordination in the sagittal plane (°) | RMS relative phase angle between hip and knee (hip phase angle - knee phase angle) in the sagittal plane. | | | | ✓ | | | |

low back moment calculated for lifting and lowering duration based on participant's estimated upper body mass (i.e., Head, arms, and trunk; HAT), torso inclination (from the T6 inertial sensor), and stature, i.e., the low back moment from postural load alone, and not external hand load which was considered as unknown.

### 5.2.6 Evaluating Model Performance

The performance of the load carriage, lifting, and lowering intensity classification algorithms were evaluated separately using hold-out validation tests repeated 20 times. In each iteration, data from 2 randomly selected participants were set aside for model assessment, while data from the remaining 25 participants were used for training the model. Average prediction accuracy, sensitivity, and precision measures were computed as follows for assessing and comparing models across normalization technique:

- Average prediction accuracy = [# true positives + # true negatives] / [# total walk trials],
- Sensitivity = [# true positives] / [# total positives], and
- Precision = [# true positives] / [# true positives + # false positives]).

## 5.3 Results

### 5.3.1 Model Performance: Carrying Mode and Load Level

A total of 702 walk trials were obtained across all participants (27 participants x (No-load + 12 loaded conditions per participant) x 2 walk trials per condition). A total of 4994 gait cycles were recorded across all participants with an average $\pm$ SD of 7.1 $\pm$ 1.0 gait cycles (range: 5 to 11) in each repetition of the walk trials.

Table 5.3 summarizes the average classification accuracies (%) from the 20 hold-out validation tests stratified by the three different generalized algorithms, namely, *Original*,

Table 5.3: Summary of the carrying mode and load level classification accuracy (%) comparing three different generalized algorithms. Results from the twenty repetitions of the hold-out validation tests were averaged for each model (N=27).

| **Models** | **Classification accuracy (%)** | | |
|---|---|---|---|
| | ***Original*** | ***Rel-NL*** | ***Rel-Anthro*** |
| M1: Mode | 74.5 | 80.2 | 75.7 |
| L1: Load, @1H-R | 89.4 | 91.8 | 86.5 |
| L2: Load, @1H-L | 90.5 | 91.4 | 89.8 |
| L3: Load, @2H-Side | 85.4 | 86.6 | 83.4 |
| L4: Load, @2H-Anterior | 86.5 | 85.1 | 83.2 |

*Rel-NL*, and *Rel-Anthro*. Overall, the *Rel-NL* algorithm outperformed the *Original* and *Rel-Anthro* models in discerning different modes and load levels in load carriage except for the load prediction model for 2H-Anterior (model L4 in Table 5.3).

For further insight into the *Rel-N* algorithm, Table 5.4 and Table 5.5 present the confusion matrices for the classification of carrying mode and load level respectively. Sensitivity and precision of each model in this algorithm is also graphically summarized in Figure 5.5. The classification model for mode (model M) yielded low sensitivities of 67.5% and 63.3% for separating the 1H-R and 1H-L from other carrying modes, respectively. Among models for classifying load level, sensitivity of low load level was degraded at model L3 and L4 implying high rate of false negatives, or that the model overestimated the loads as high in about 1/3rd of cases in the 2H-Side and 2H-Anterior conditions. Precision of all load level classification models exceeded 84.0% indicating that models performed well at avoiding false positives.

### 5.3.2 Model Performance: Lifting and Lowering Height, Hand Mode, and Load Level

A total of 3120 trials were obtained for the lifting and lowering task across all participants (26 participants x (6 unloaded + 54 loaded conditions per participant) x 2 trials per condition) after excluding one participant's data due to instrumentation error. Table 5.6 sum-

Table 5.4: Confusion matrix summarizing the classification result for carrying modes across all of the walk trials in the *Rel-NL* model (N=27), where No-load = empty-handed reference condition, 1H-R = one-handed right carry, 1H-L = one-handed left carry, 2H-Side = two-handed side carry, 2H-Anterior = two-handed anterior carry.

**M1: Mode**

| | | Predicted Carrying Mode | | | | | Total Walk Trials | Sensitivity |
|---|---|---|---|---|---|---|---|---|
| | | No-load | 1H-R | 1H-L | 2H-Side | 2H-Anterior | | |
| | **No-load** | 75 | 0 | 1 | 3 | 1 | 80 | 93.8% |
| **Actual** | **1H-R** | 0 | 162 | 51 | 26 | 1 | 240 | 67.5% |
| **Carrying** | **1H-L** | 0 | 27 | 152 | 54 | 7 | 240 | 63.3% |
| **Mode** | **2H-Side** | 2 | 16 | 5 | 215 | 2 | 240 | 89.6% |
| | **2H-Anterior** | 0 | 2 | 0 | 8 | 230 | 240 | 95.8% |
| **Total Walk Trials** | | 77 | 207 | 209 | 306 | 241 | 1040 | |
| **Precision** | | 97.4% | 78.3% | 72.7% | 70.3% | 100% | | |

Table 5.5: Confusion matrices summarizing the classification results for load level for each predicted carrying load level in *Rel-NL* model (N=27): Low = 4.5 kg, High = 13.6 kg and 22.7 kg.

**L1: Load, @1H-R**

| | | Predicted Load Level | | Total Walk Trials | Sensitivity |
|---|---|---|---|---|---|
| | | Low | High | | |
| **Actual Load Level** | **Low** | 50 | 11 | 61 | 82.0% |
| | **High** | 6 | 140 | 146 | 95.9% |
| **Total Walk Trials** | | 56 | 151 | 207 | |
| **Precision** | | 89.3% | 92.7% | | |

**L2: Load, @1H-L**

| | | Predicted Load Level | | Total Walk Trials | Sensitivity |
|---|---|---|---|---|---|
| | | Low | High | | |
| **Actual Load Level** | **Low** | 56 | 11 | 67 | 83.6% |
| | **High** | 7 | 135 | 142 | 95.1% |
| **Total Walk Trials** | | 63 | 146 | 209 | |
| **Precision** | | 88.9% | 92.5% | | |

**L3: Load, @2H-Side**

| | | Predicted Load Level | | Total Walk Trials | Sensitivity |
|---|---|---|---|---|---|
| | | Low | High | | |
| **Actual Load Level** | **Low** | 67 | 31 | 98 | 68.4% |
| | **High** | 10 | 198 | 208 | 95.2% |
| **Total Walk Trials** | | 77 | 229 | 306 | |
| **Precision** | | 87.0% | 86.5% | | |

**L4: Load, @2H-Anterior**

| | | Predicted Load Level | | Total Walk Trials | Sensitivity |
|---|---|---|---|---|---|
| | | Low | High | | |
| **Actual Load Level** | **Low** | 53 | 29 | 82 | 64.6% |
| | **High** | 7 | 152 | 159 | 95.6% |
| **Total Walk Trials** | | 60 | 181 | 241 | |
| **Precision** | | 88.3% | 84.0% | | |

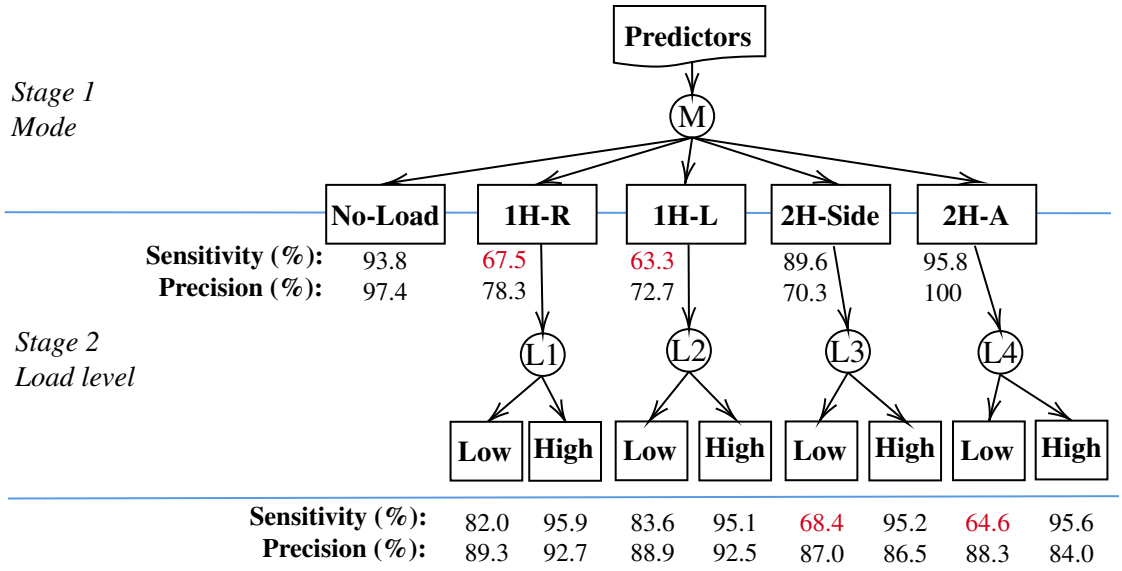



Figure 5.5: Graphical representation of the classification model for load carriage mode and load level for the algorithm with highest prediction accuracy (i.e., *Rel-NL*). Numbers next to each box represent sensitivity (%, above) and precision (%, below) in distinguishing that outcome class from the parent model (i.e., circles labelled M, L1 to L4). Sensitivity and precision values below 70% are indicated in red.

marizes the classification accuracy (%) across different generalized algorithms for lifting and lowering, separately. The three generalized algorithms performed similarly in terms of classification accuracy for both, lifting and lowering. The algorithm with *Original* variables was selected due to is simplicity.

For further insight into the classification algorithm with *Original* variables, Table 5.7 and Table 5.8 present the confusion matrices for lifting and lowering by height, hand mode, and load level classification models. Sensitivity and precision were calculated for the *Original* lifting and lowering algorithm are also summarized in Figure 5.6. Classification models for height (model H) and hand mode (models M1 and M2) showed higher sensitivity and precision compared to the classification models for load level (models L1 to L4). In the algorithm for the lowering task, model for classifying load level in the 1H-L condition (i.e., model L2) yielded low precision value (< 70%) in identifying low load level.

Table 5.6: Summary of the lifting and lowering height, hand mode, and load level classification accuracy (%) comparing three different generalized algorithms. Results from twenty repetitions of the hold-out validation tests were averaged for each model (N=26).

**1. Lifting**

| **Models** | **Classification accuracy (%)** | | |
|---|---|---|---|
| | ***Original*** | ***Rel-NL*** | ***Rel-NL & Anthro*** |
| H: Height | 97.7 | 97.8 | 97.8 |
| M1: Hand mode, @floor height | 92.5 | 88.2 | 85.3 |
| M2: Hand mode, @knee height | 95.3 | 95.2 | 92.3 |
| L1: Load, @1-handed, floor height | 84.7 | 82.0 | 81.1 |
| L2: Load, @2-handed, floor height | 86.3 | 83.0 | 82.5 |
| L3: Load, @1-handed, knee height | 85.8 | 83.8 | 83.1 |
| L4: Load, @2-handed, knee height | 79.8 | 78.2 | 79.7 |

**2. Lowering**

| **Models** | **Classification accuracy (%)** | | |
|---|---|---|---|
| | ***Original*** | ***Rel-NL*** | ***Rel-NL & Anthro*** |
| H: Height | 97.4 | 97.9 | 98.0 |
| M1: Hand mode, @floor height | 90.5 | 91.9 | 87.2 |
| M2: Hand mode, @knee height | 95.0 | 95.3 | 94.1 |
| L1: Load, @1-handed, floor height | 83.5 | 79.1 | 78.1 |
| L2: Load, @2-handed, floor height | 78.1 | 75.6 | 74.9 |
| L3: Load, @1-handed, knee height | 89.5 | 85.2 | 85.3 |
| L4: Load, @2-handed, knee height | 83.6 | 82.6 | 82.7 |

## 5.4 Discussion

Quantifying physical exposures in MMH tasks can be challenging in non-routinized work settings where load magnitudes, repetitions, and task durations differ between workers and within worker across time. This study developed and assessed statistical algorithms for predicting categorical intensity level of load carriage, and lifting and lowering tasks in a cohort of women and men across a broad spectrum of age, body mass, and functional strength.

### 5.4.1 Statistical Classification of Carried Load Intensity

The statistical algorithm for classifying carried load level implemented a two-stage hierarchical model structure, similar to the previous chapter 4, where the carrying mode was classified first followed by classification of load levels within mode. However, the present study improves upon the preliminary load classification algorithm in the previous chapter

Table 5.7: Confusion matrices summarizing the classification results for height, hand mode, and load level for lifting using the classification algorithm with *Original* variables (N = 26), where 1H = 1-handed right and left combined, 2H = 2-handed anterior, Low = no-load and 4.5 kg, and High = 13.6 kg and 22.7 kg. load magnitudes.

**H: Height**

| | | Predicted Height Level | | Total Lifting Trials | Sensitivity |
|---|---|---|---|---|---|
| | | Floor | Knee | | |
| Actual Load Level | Floor | 2826 | 80 | 2906 | 97.2% |
| | Knee | 54 | 2800 | 2854 | 98.1% |
| Total Lifting Trials | | 2880 | 2880 | 5760 | |
| Precision | | 98.1% | 97.2% | | |

**M1: Hand mode, @floor height**

| | | Predicted Hand Mode | | Total Lifting Trials | Sensitivity |
|---|---|---|---|---|---|
| | | 1H | 2H | | |
| Actual Hand Mode | 1H | 1812 | 109 | 1921 | 94.3% |
| | 2H | 108 | 851 | 959 | 88.7% |
| Total Lifting Trials | | 1920 | 960 | 2880 | |
| Precision | | 94.4% | 88.6% | | |

**M2: Hand mode, @knee height**

| | | Predicted Hand Mode | | Total Lifting Trials | Sensitivity |
|---|---|---|---|---|---|
| | | 1H | 2H | | |
| Actual Hand Mode | 1H | 1850 | 65 | 1915 | 96.6% |
| | 2H | 70 | 895 | 965 | 92.7% |
| Total Lifting Trials | | 1920 | 960 | 2880 | |
| Precision | | 96.4% | 93.2% | | |

**L1: Load, @1-handed, floor height height**

| | | Predicted Load Level | | Total Lifting Trials | Sensitivity |
|---|---|---|---|---|---|
| | | Low | High | | |
| Actual Load Level | Low | 825 | 159 | 984 | 83.8% |
| | High | 135 | 801 | 936 | 85.6% |
| Total Lifting Trials | | 960 | 960 | 1920 | |
| Precision | | 85.9% | 83.4% | | |

**L2: Load, @2-handed, floor height height**

| | | Predicted Load Level | | Total Lifting Trials | Sensitivity |
|---|---|---|---|---|---|
| | | Low | High | | |
| Actual Load Level | Low | 397 | 47 | 442 | 89.4% |
| | High | 85 | 433 | 518 | 83.6% |
| Total Lifting Trials | | 480 | 480 | 960 | |
| Precision | | 82.3% | 90.2% | | |

**L3: Load, @1-handed, knee height height**

| | | Predicted Load Level | | Total Lifting Trials | Sensitivity |
|---|---|---|---|---|---|
| | | Low | High | | |
| Actual Load Level | Low | 837 | 150 | 987 | 84.8% |
| | High | 123 | 810 | 933 | 86.8% |
| Total Lifting Trials | | 960 | 960 | 1920 | |
| Precision | | 87.2% | 84.4% | | |

**L4: Load, @2-handed, knee height height**

| | | Predicted Load Level | | Total Lifting Trials | Sensitivity |
|---|---|---|---|---|---|
| | | Low | High | | |
| Actual Load Level | Low | 392 | 106 | 498 | 78.7% |
| | High | 88 | 374 | 462 | 81.0% |
| Total Lifting Trials | | 480 | 480 | 9660 | |
| Precision | | 81.7% | 77.9% | | |

Table 5.8: Confusion matrices summarizing the classification results for height, hand mode, and load level for lowering using the classification algorithm with *Original* variables (N = 26), where 1H = 1-handed right and left, 2H = 2-handed anterior, Low = no-load and 4.5 kg, and High = 13.6 kg and 22.7 kg. load magnitudes.

**H: Height**

| | | Predicted Height Level | | Total Lifting Trials | Sensitivity |
|---|---|---|---|---|---|
| | | Floor | Knee | | |
| Actual Load Level | Floor | 2816 | 88 | 2904 | 97.0% |
| | Knee | 64 | 2792 | 2856 | 97.8% |
| Total Lifting Trials | | 2880 | 2880 | 5760 | |
| Precision | | 97.8% | 96.9% | | |

**M1: Hand mode, @floor height**

| | | Predicted Hand Mode | | Total Lifting Trials | Sensitivity |
|---|---|---|---|---|---|
| | | 1H | 2H | | |
| Actual Hand Mode | 1H | 1763 | 117 | 1880 | 93.8% |
| | 2H | 157 | 843 | 1000 | 84.3% |
| Total Lifting Trials | | 1920 | 960 | 2880 | |
| Precision | | 91.8% | 87.8% | | |

**M2: Hand mode, @knee height**

| | | Predicted Hand Mode | | Total Lifting Trials | Sensitivity |
|---|---|---|---|---|---|
| | | 1H | 2H | | |
| Actual Hand Mode | 1H | 1830 | 55 | 1885 | 97.1% |
| | 2H | 90 | 905 | 995 | 91.0% |
| Total Lifting Trials | | 1920 | 960 | 2880 | |
| Precision | | 95.3% | 94.3% | | |

**L1: Load, @1-handed, floor height height**

| | | Predicted Load Level | | Total Lifting Trials | Sensitivity |
|---|---|---|---|---|---|
| | | Low | High | | |
| Actual Load Level | Low | 802 | 158 | 960 | 83.5% |
| | High | 158 | 802 | 960 | 83.5% |
| Total Lifting Trials | | 960 | 960 | 1920 | |
| Precision | | 83.5% | 83.5% | | |

**L2: Load, @2-handed, floor height height**

| | | Predicted Load Level | | Total Lifting Trials | Sensitivity |
|---|---|---|---|---|---|
| | | Low | High | | |
| Actual Load Level | Low | 335 | 65 | 400 | 83.8% |
| | High | 145 | 415 | 560 | 74.1% |
| Total Lifting Trials | | 480 | 480 | 960 | |
| Precision | | 69.8% | 86.5% | | |

**L3: Load, @1-handed, knee height height**

| | | Predicted Load Level | | Total Lifting Trials | Sensitivity |
|---|---|---|---|---|---|
| | | Low | High | | |
| Actual Load Level | Low | 861 | 102 | 963 | 89.4% |
| | High | 99 | 858 | 957 | 89.7% |
| Total Lifting Trials | | 960 | 960 | 1920 | |
| Precision | | 89.7% | 89.4% | | |

**L4: Load, @2-handed, knee height height**

| | | Predicted Load Level | | Total Lifting Trials | Sensitivity |
|---|---|---|---|---|---|
| | | Low | High | | |
| Actual Load Level | Low | 380 | 57 | 437 | 87.0% |
| | High | 100 | 423 | 523 | 80.9% |
| Total Lifting Trials | | 480 | 480 | 9660 | |
| Precision | | 79.2% | 88.1% | | |

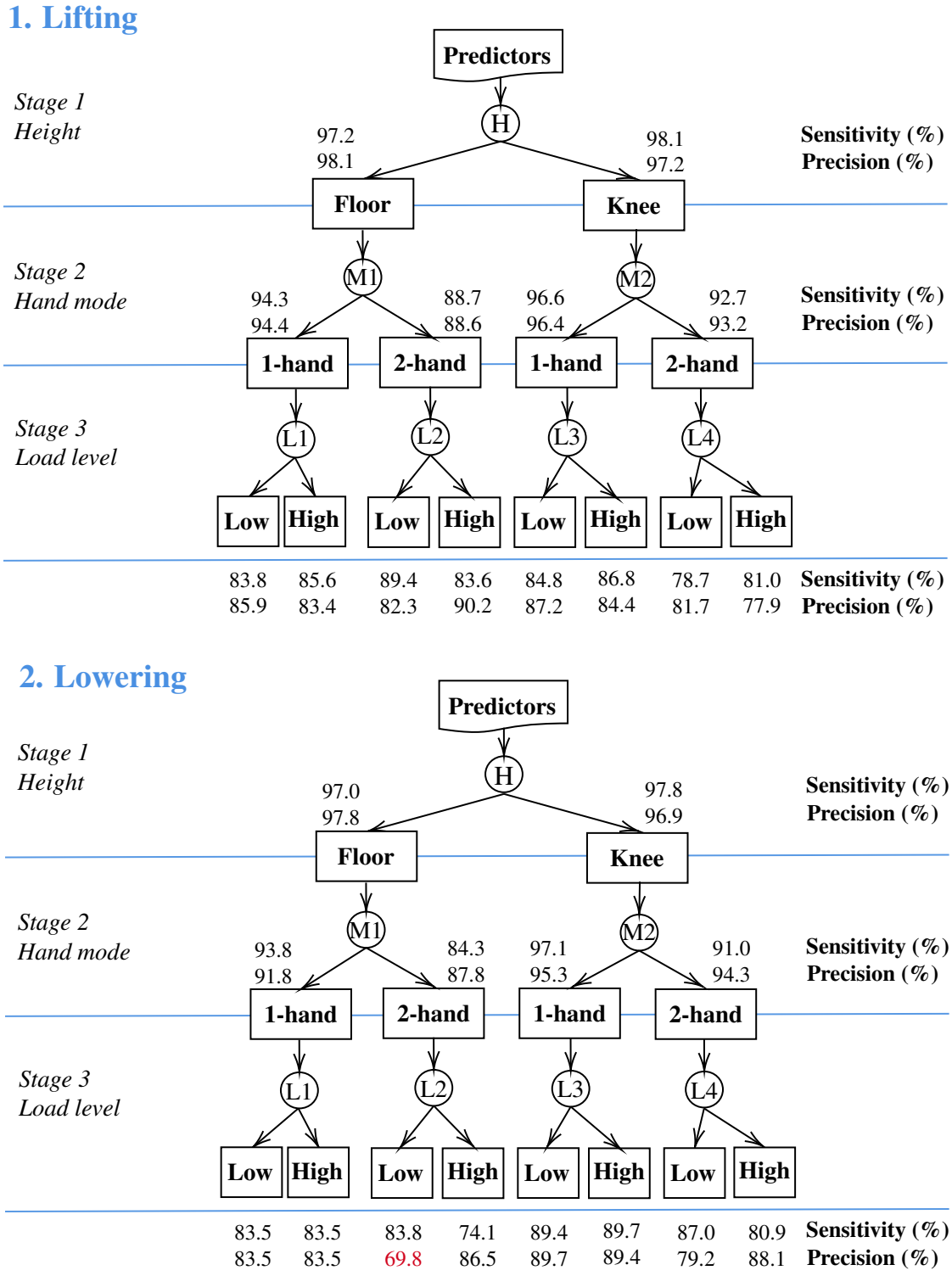



Figure 5.6: Graphical representation of the lifting and lowering classification results in terms of sensitivity and precision from the algorithm using *Original* variables. Numbers near each box represent sensitivity (%, top) and precision (%, bottom) in distinguishing that class from the preceding model (denoted using circles). Sensitivity or precision values below 70% are colored in red.

in two important aspects. First, the present study recorded gait data from a more diverse study sample to build and assess the statistical model, compared to the previous chapter 4 that was limited to a small homogeneous participant sample (N = 9 men). Second, the present study predicted load levels in terms of a range of absolute load magnitudes (i.e., low load: 0 to 4.5 kgs, high load: 13.6 to 22.7 kgs) which is easier to interpret compared to the previously developed algorithm which relied on load magnitudes normalized to individual carrying capacity (e.g., 50% maximum acceptable weight carried; MAWC).

To address the large variability between participant anthropometry and effects of different absolute load magnitudes this study also compared different approaches to normalizing the model predictors. The performance of load carriage mode and load level classification algorithm marginally increased when the postural sway and acceleration measures were normalized to no-loaded gait kinematics (i.e., the *Rel-NL* model) compared to either using normalized by anthropometry (*Rel-Anthro*) or using measures in their original form without normalizing (*Original*). Similar to the preliminary algorithm, thoracic and pelvic range of motion and thoracic-pelvic coordination remained important predictors in classifying carrying mode and relative load level. In the *Rel-NL* model, the accuracy of classifying carrying mode was 80.2% and load levels averaged across the 4 modes was 88.7%, compared to 96.9% and 93.1% in the previous chapter 4, respectively. The notable decrease in classifying mode was largely due to decreased sensitivity in identifying the 1H-R and 1H-L modes. This issue may be addressed by inclusion of predictors related to bilateral asymmetry to improve sensitivity in separating the 1H-R and 1H-L modes, or in some applications combining both these modes in to one outcome class (i.e., 1H-Side vs. 2H-Side vs. 2H-Anterior).

### 5.4.2 Statistical Classification of Lifting and Lowering Intensity

The classification algorithm for load level during lifting-lowering implemented a three-stage hierarchical model structure where the lifting height was classified first followed by

hand mode, and then classification of load levels within mode. There was no noticeable difference between different generalized algorithms in the lifting and lowering classification algorithms suggesting kinematic patterns across participants did not differ substantially. The algorithm with variables in their *Original* form was picked due to its simplicity. The accuracy of classifying **lifting** height, mode, and load levels were 97.7%, 93.9%, and 84.2%, respectively. The accuracy of classifying **lowering** height, mode, and load levels were 97.4%, 92.8%, and 83.7%, respectively. Overall the algorithm was accurate in predicting height and mode; however, the algorithm displayed some confusion in identifying low load condition during lowering (i.e., evident in the decreased precision for low load in Figure 5.6).

### 5.4.3 Study Limitations

A few key limitations of the current study are worth discussing. One limitation stems from the fact that the tasks were standardized in a laboratory environment with well-defined task onset and offset events. Improving the applicability of the presented algorithm to applied settings would require procedures to also detect task onset and offset to construct a timeline of the task with fine resolution or time increments. The gait detection algorithm (*Step 1*) used in this study implements a robust detection of the start and end of walking, so the duration of the walking (either unloaded or loaded) can be accurately estimated. Similarly algorithms for detecting lifting and lowering would be needed. This issue is addressed in the next Chapter 6.

Second, the algorithm only considered outcome classes for load levels representing low loads (0 to 4.5 kg) and high loads (13.6 kg to 22.7 kg). To ensure continuity in possible load magnitudes, a medium load condition, e.g., 9.1 kg (20 lbs.) could be added to address the scenario where the load magnitude during lifting-lowering or carrying was neither low nor high. For example, although not included in model development, a total of 936 trials were also recorded using a load of 9.1 kgs representing a medium load for each lifting and

lowering task across all participants (N = 26). Figure 5.7 plots the probability obtained from the classification algorithm for each trial belonging to the predicted high load level in one example scenario, namely a 1-handed floor lift. For a binary outcome (e.g. low vs. high load) the decision boundary is typically set at a probability of 0.5, i.e., any trial with a resultant probability greater than 0.5 is classified as high load while a probability lower than 0.5 is classified as low. In Figure 5.7, measurements from the medium load level condition were spread over the range of 0 and 1.0. To ensure continuity in possible load magnitudes, an intermediate range of probabilities, $0.375 \leq p \leq 0.625$ (shown as red vertical lines in Figure 5.7) was defined to categorize measurements as belonging to a medium load level, if not predicted strongly as a low ($p < 0.375$) or high ($p > 0.625$) load level. While presented a initial solution, further improvements to the algorithm could leverage specific statistical techniques (e.g., ROC curves) to determine an optimal range of probabilities for such medium load levels.

This study did not address the effects of cumulative fatigue on gait and lifting-lowering kinematics from long duration exposures. Each trial was randomized to avoid any carry-over effect of fatigue and also the total duration of the simulated MMH tasks was shorter (i.e.,$\sim$ 1 1/2 hours) compared to manual handler's regular work shift ($\sim$ 8 hours). Participants were also selected based on their prior and current health condition with only asymptomatic healthy participants without a prior history of back surgery and asymptomatic of back pain were included. Further studies are needed to improve the applicability of the algorithm to occupational settings.

### 5.4.4 Contributions and Implications for Practice

Wearable sensing technology combined with predictive modeling has the potential to advance the science of field-based exposure assessment by providing information about work content beyond just quantifying worker postures. The present study is unique in its ap-

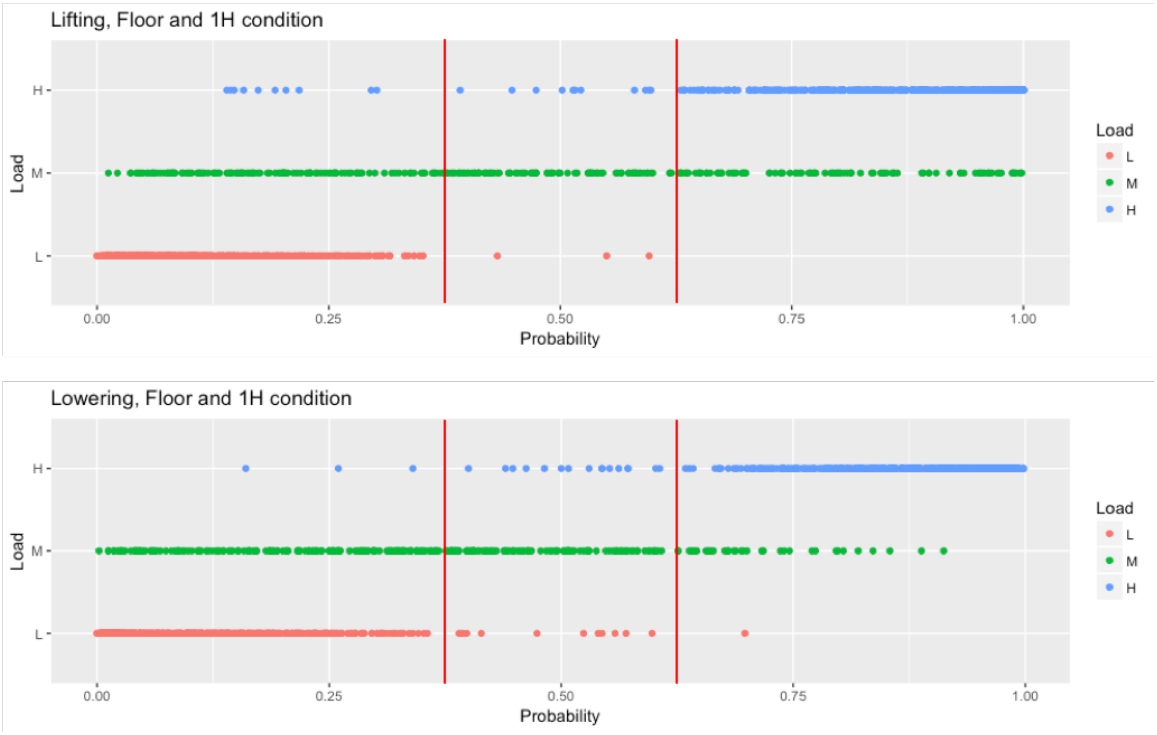



Figure 5.7: Probability of each measurement belonging to the high load level in a two-class random forest model (Low vs. High), when lifting (top panel) and lowering (bottom panel) from/to floor height in a one-handed hand mode. Two decision boundaries (0.375 and 0.625, red lines) were drawn to create a medium load level between the low ($p < 0.375$) and high ($p > 0.625$) level outcome classes.

proach to quantifying external loads by combining wearable inertial sensing and predictive modeling. The algorithm presented can potentially be used in applied settings where the magnitude of hand loads vary throughout a work-shift or is difficult to directly measure in field settings. In such situations, the predicted load levels combined with postural data can be used as inputs to a biomechanical model to estimate cumulative physical exposures (e.g., spinal loads, joint moments) towards quantifying the risk of occupationally-relevant low back disorders.

Multiple previous studies have used inertial sensors and predictive modeling to classify different types of activities (e.g., walking vs. sitting [67, 75, 78, 79]), however few studies have delved into predicting task intensity within a specific activity (i.e., relative changes in load within the same task). Studies that have focused on estimating lifting intensity

relied on some form of force measurement in addition to inertial sensing, such as EMG [77] and insole pressure sensors [25]. The present study is novel in that the developed algorithm does not rely on direct force measurement, but instead leverages biomechanical relationships between external loads on movement kinematics and intersegment coordination during manual load carriage and lifting-lowering. This information helped inform and reduce the number of feature vectors used in developing classification algorithm and potentially increase prediction accuracy, compared to using raw (unprocessed) sensor data directly.

Limiting the number and types of body worn sensors is a critical aspect of wearability in applied settings. The current study investigated the ability to classify task intensities (e.g., load level, lifting height) using four commercial wearable measurement systems. Three sensors (T6, S1, along with right shank for gait detection) were used for classifying load carriage, and four sensors (T6, S1, and right thigh and shank) for lifting-lowering. This marks a stark improvement over prior studies that have used ANNs to identify MMH task types (not load levels) relying on up to 17 body-worn inertial sensors [78]. New forms of wearable sensing embedded in smart clothing, e.g., [112], will further improve the wearability and potential acceptability of wearable inertial sensing in occupational settings.

## 5.5 Conclusion

This chapter presented algorithms for combining wearable inertial sensing and statistical prediction to classify intensity level during load carriage, and lifting and lowering tasks. The prediction models were developed and assessed in a cohort of women and men across a broad spectrum of age, body mass, and functional strength. Separate classification models were developed for predicting binary load levels (i.e., low: 0 to 4.5 kgs. vs. high: 13.5 to 22.7 kgs) in manual load carriage, lifting, and lowering using inertial-sensor derived kinematic measures as predictors, with classification accuracy exceeding 80% in all levels

of the model. Collectively, these findings demonstrate the potential for combining wearable inertial sensing with statistical prediction to quantify biomechanical exposures in manual material handling work.

The algorithms presented can potentially be used in applied settings where the magnitude of hand loads vary throughout a work-shift or is difficult to directly measure in field settings. In such situations, the predicted load levels combined with postural data could be used as inputs to a biomechanical model to estimate cumulative physical exposures (e.g., spinal loads, joint moments) towards quantifying the potential risk of occupationally-relevant low back disorders. Further investigation is also needed to test the generalizability of the model across different MMH work conditions. Towards this objective, the subsequent Chapter 6 extends the presented statistical classification algorithm into a framework for quantifying continuous biomechanical exposures in a simulated non-repetitive MMH job involving continuous load carriage and lifting-lowering.

# CHAPTER 6

# Inertial Sensor-Based Biomechanical Exposure Assessment: Preliminary Framework Implementation

The previous Chapter 5 addressed statistical classification of load levels during load carriage and lifting-lowering in a study cohort diverse in age, BMI, and functional strength. However, the analyses were limited to standalone carrying, lifting, and lowering tasks (i.e., each task repetition was performed in a discrete manner independent of other tasks). This chapter incorporated the developed algorithms into a framework implementation for inertial sensor-based biomechanical exposure assessment to analyze continuous material handling job cycles with different load magnitudes representing more realistic non-routinized work conditions. Algorithms for detecting MMH tasks (i.e., start-end of load carriage, lifting, lowering) using deterministic thresholds, and statistical classification models for predicting load levels during carriage, lifting, and lowering (developed in Chapter 5) were combined to estimate cumulative spinal compressive loads as a measure of low back disorder risk using a simple biomechanical link-segment analysis. A preliminary implementation of the framework was assessed in a laboratory study by comparing detected task types, durations, and predicted load levels to corresponding measures obtained from video-based observa-

tional analysis.

## 6.1 Introduction

Prior studies have documented a biomechanical pathway between lifting and carrying heavy loads and the increased risk of low back disorders [2, 130, 215, 216]. The cumulative trauma model provides one explanation for why musculoskeletal disorders are often work-related stemming from repeated and long duration of forceful exertions performed throughout the workday. The cumulative trauma model assumes injury results from the accumulated effect of transient external loads that in isolation may be not exceed internal tissue tolerances. Exposures from repetitive and/or prolonged duration cause cumulative compressive and shear loading on the spine such that the internal tolerances of tissues are eventually exceeded. Strong associations between biomechanical factors (e.g., load magnitude, load moment or load location, duration and repetitions) and the risk of low back disorder are evident in non-routine jobs including patient handling [7, 8, 9, 10], material handling in construction sites [11], distribution centers and ware-housing operations [12], and team lifting [13]. Thus, assessing the risk of work-related cumulative trauma disorders requires cumulative measures of biomechanical exposures.

Contemporary uses of inertial sensing in assessing biomechanical exposures during manual tasks have largely focused on postural analysis including the quantification of intensity (i.e., deviations from neutral, angular speed of movements), repetitions (frequency), and duration (i.e., sustained non-neutral postures) of postures in manual tasks (Chapter 2). However, this approach lacks information about the other biomechanical factors associated with work-related low back disorder risk, including the type of task being performed and the location and magnitude of loads handled, which are essential in order to identify problematic tasks and introduce targeted interventions. Not surprisingly, field-studies with inertial sensing also include other forms of direct measurements (e.g., EMG [77], pressure mapping insoles [25], instrumented shoes [26], instrumented gloves [27]) or observational

methods (e.g., [19]) to quantify biomechanical risk factors related to external forces and/or loads. The previous chapters 4 and 5 and a few other studies (e.g., [75, 76, 77, 78]) demonstrate the potential for leveraging predictive modeling methods to estimate the type of work task and intensity from wearable sensor data.

The aim of this study was to implement and assess an algorithmic framework for biomechanical exposure assessment that leverages kinematic information obtained from body-worn inertial sensor. The framework uses continuous inertial sensor data for detecting the type of MMH tasks (i.e., load carriage, lifting, and lowering), task duration, and subsequently predicting task conditions within each detected task. Detected task type, task start-end times, and predicted task conditions were used for estimating spinal compression forces across time as a proxy measure of work-related low back disorder risk. Task detection and classification performance was assessed in a laboratory experiment comprising two simulated MMH job cycles differing in load intensity, namely, low (4.5 kg) and high (22.7 kg) loads handled. Algorithm output were compared with *true* "gold standard" data obtained from a video-based task analysis as reference to examine the number of correct task detection, error in detecting task start times and task durations, and prediction accuracy in classifying task condition (i.e., carry mode and load level for load carriage; height, hand mode, and load level for lifting and lowering).

## 6.2 Methods

### 6.2.1 Study Participants

Eight healthy participants (4 men and 4 women) were recruited for the study. Table 6.1 summarizes the anthropometry for each study participant. Participants were screened for pre-existing back injuries or chronic pain with a body discomfort questionnaire adapted from the body mapping exercise by NIOSH ([165] for more details). Prior to the study, participants completed a written informed consent approved by the university's institutional

review board.

Table 6.1: Gender, age, stature, body mass, BMI, and low-back lifting strength for each of the 8 participants in the study sample.

| Part ID | Gender | Age, years | Stature, m | Mass, kg | BMI, kg/m$^2$ | Low-back lifting strength, N |
|---|---|---|---|---|---|---|
| P1 | M | 22 | 1.82 | 67.4 | 20.4 | 656.1 |
| P2 | M | 34 | 1.83 | 96.6 | 28.9 | 909.7 |
| P3 | M | 45 | 1.76 | 75.5 | 24.3 | 616.1 |
| P4 | M | 44 | 1.85 | 80.3 | 23.4 | 734.0 |
| P5 | F | 20 | 1.74 | 91.3 | 30.3 | 411.5 |
| P6 | F | 32 | 1.63 | 67.9 | 25.6 | 521.6 |
| P7 | F | 43 | 1.64 | 61.8 | 23.0 | 265.8 |
| P8 | F | 46 | 1.70 | 76.8 | 26.5 | 668.3 |

### 6.2.2 Experiment Procedures

The experiment required participants to perform 2 cycles of a simulated job comprising combinations of three MMH tasks including load carriage, lifting, and lowering. Low vs. high intensity job cycles were simulated by carrying, lifting, and lowering a load of 4.5 kg vs. 22.7 kg, respectively. Table 6.2 summarizes the task sequence and detailed task condition performed for each job cycle. Two lifting zones were positioned at the end of levelled corridor (10 m length x 1.5 m width) equipped with movable platform 53 cm high ($\sim$ average knee height). Figure 6.1 depicts the experiment layout. Participants were allowed to self-select the work pace, and adopt preferred foot placements during lifting and lowering (i.e., participants did not have to position their feet in specific locations relative to the load) as long as the specific lifting mode (e.g., one vs. two handed) was followed and the tasks transitioned from one to the next (i.e., no breaks within a job cycle).

### 6.2.3 Instrumentation and Data Segmentation

During the simulated job cycles, kinematic data were continuously recorded using four commercial inertial sensors with a sampling frequency of 80 Hz (BiostampRC, mc10 Inc.,

Table 6.2: Task sequence and conditions performed in two simulated job cycles comprising carrying, lifting, and lowering performed either at low load intensity (4.5 kg load) or high intensity (22.7 kg load).

| | | **Intensity** | | | | | |
|---|---|---|---|---|---|---|---|
| | | **Low** | | | **High** | | |
| **#** | **Task** | **Hand Mode** | **Load Level** | **Height** | **Hand Mode** | **Load Level** | **Height** |
| 1 | Lift | 2H-Anterior | 4.5 kg | Knee | 2H-Anterior | 22.7 kg | Knee |
| 2 | Carry | 2H-Anterior | 4.5 kg | - | 2H-Anterior | 22.7 kg | - |
| 3 | Lower | 2H-Anterior | 4.5 kg | Floor | 2H-Anterior | 22.7 kg | Floor |
| 4 | Walk | - | No-load | - | - | No-load | - |
| 5 | Lift | 1H-R | 4.5 kg | Floor | 1H-L | 22.7 kg | Knee |
| 6 | Carry | 1H-R | 4.5 kg | - | 1H-L | 22.7 kg | - |
| 7 | Hold (10 sec) | 1H-R | 4.5 kg | - | 1H-L | 22.7 kg | - |
| 8 | Carry | 1H-R | 4.5 kg | - | 1H-L | 22.7 kg | - |
| 9 | Lower | 1H-R | 4.5 kg | Floor | 1H-L | 22.7 kg | Floor |

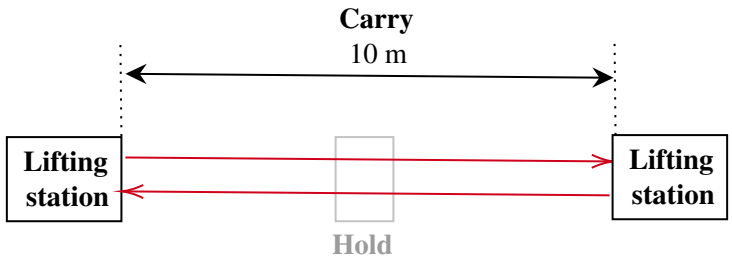



Figure 6.1: Plan view of the experiment set-up for performing simulated continuous MMH job cycles described in Table 6.2.

Lexington, MA, USA) attached at the sixth thoracic vertebra (T6), the first sacral vertebra (S1), the superior aspect of the right shank midway between the lateral femoral and malleolar epicondyles, and the thigh midway between the hip and lateral femoral epicondyles (Figure 5.3).

### 6.2.4 Algorithmic Framework for the Inertial Sensor-Based Biomechanical Exposure Assessment

A framework for inertial sensor-based biomechanical exposure assessment was developed by combining algorithms for threshold-based MMH task detection, statistical prediction of load carriage and lifting-lowering task condition, and computation of spinal compression force ($F_c$) by task condition. The framework was implemented in MATLAB R2016b (The MathWorks Inc., Natick, MA, USA). Figure 6.2 depicts a graphical overview of the framework, with the subsequent sections describing each component in detail.

#### 6.2.4.1 MMH Task Detection

Initially, each channel of continuous inertial sensor data (namely raw triaxial accelerometer and gyroscope signal data) was segmented using a moving sliding-window of 1 second width (80 frames) with 50% overlap. This raw data was used as an input to the MMH task detection algorithm (Figure 6.2). The next step involved detecting for each time-window if the person was ambulatory or stationary based on the swing phase of gait. Angular velocity data from the sensor located at the right shank was used to detect a swing motion of the right leg within each 1-sec time-window. If leg swing was detected, the window was coded as "ambulatory" and the loop continued until the last swing phase is detected in subsequent windows. Consecutive time-windows with detected swing phase were processed for continuous gait cycle detection and extraction of gait parameters per gait cycle using the algorithm previously presented in Chapter 3 and Appendix C.

Time-windows for which a leg swing was not detected, were examined for a lower-

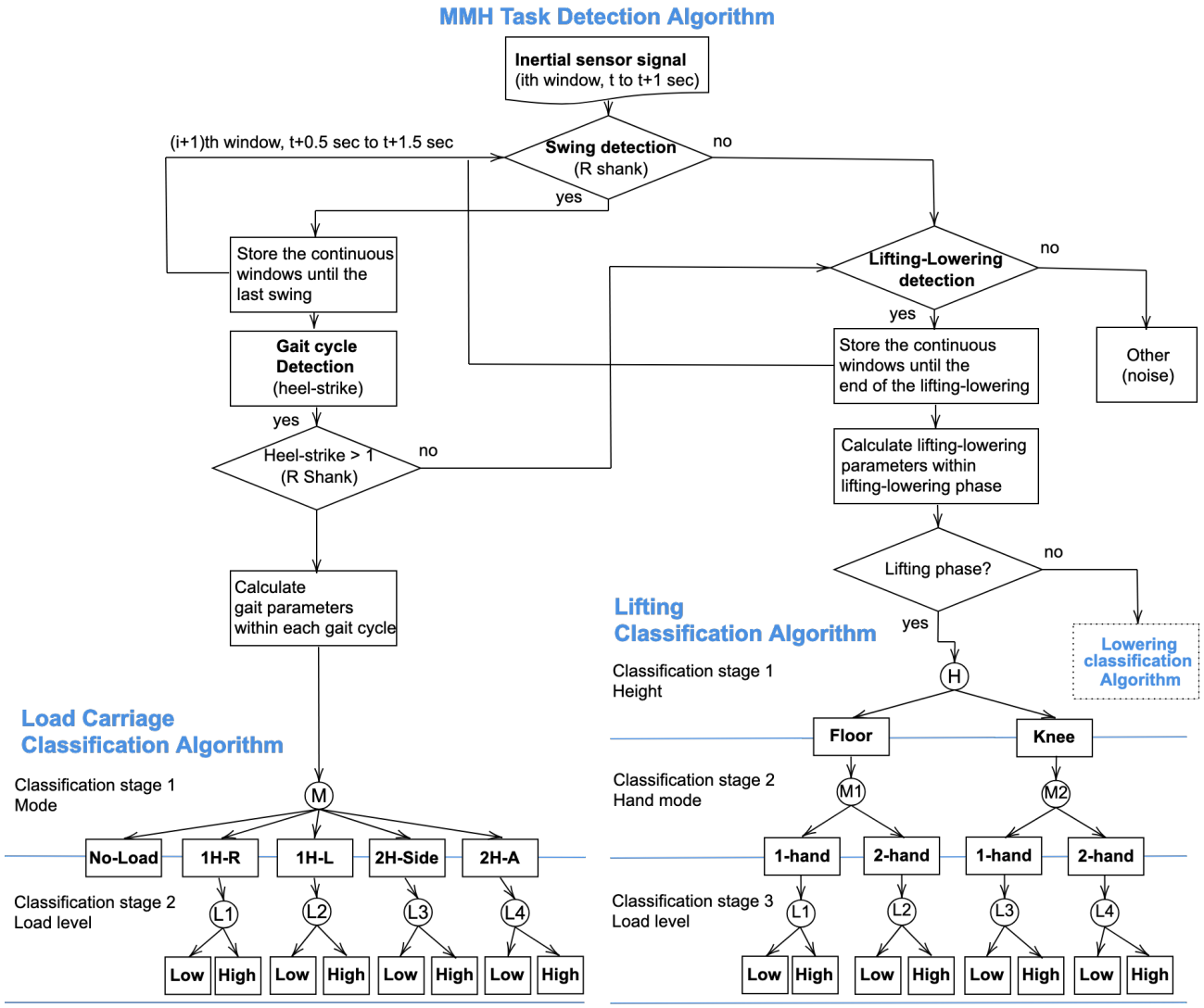



Figure 6.2: Flowchart showing the algorithmic framework for the MMH task detection and task condition classification.

ing (torso flexion) or lifting/rising (torso extension) motion using information about torso angular velocity and displacement obtained from the inertial sensor at T6 as described in the algorithm presented in Appendix F. Consecutive time-windows were coded as lifting-lowering. Once the start of the lifting (or empty-handed bending) was detected, three time-windows (2-sec of data) immediately before and after the detected lifting were used to refine the start and end time of the lifting-lowering task. The algorithm then separated lifting (or rising if empty-handed) and lowering (or torso bending if empty-handed) phases (Appendix F), followed by computing of kinematic parameters described in Chapter 5.

For the present study, time-windows that were neither detected as ambulatory nor lifting-lowering were labeled as 'other (noise)', and excluded from further classification.

#### 6.2.4.2 Statistical Classification of Task Condition and Load Level

Kinematic parameters calculated by task were used as predictor variables in the corresponding classification algorithm for load carriage, lifting, and lowering. Details of the predictor variables, variable selection, and structure of the classification algorithm were presented in Chapter 5 and not covered here in interest of brevity.

Outcome classes in the classification algorithm for load carriage included:

- **Mode**: No-load, 1H-R, 1H-L, 2H-Side, 2H-Anterior,
- **Load level**: Low (0 to 4.5 kgs.) vs. High (13.6 to 22.7 kgs.).

Outcome classes in the classification algorithm for lifting (similar classes for lowering) included:

- **Lifting-lowering height**: floor vs. knee height,
- **Mode**: 1H vs. 2H,
- **Load level**: Low (0 to 4.5 kgs.) vs. High (13.6 to 22.7 kgs.).

#### 6.2.4.3 Computing Low-back Compression Force, $F_c$

Spinal compression force ($F_c$) at the L5/S1 intervertebral disc was calculated as a composite measure of work-related low back disorder risk resulting from cumulative trauma. The computation used a simple quasi-static biomechanical link-segment model to estimate the spinal compression force for each window using on information about:

- **Posture**: the torso and pelvis sagittal flexion angles measured at T6 and S1 locations,
- **Load location**: horizontal moment arm based on torso length and flexion angle during lifting and lowering,
- **Load magnitude**: mid-value of the predicted load level, namely 2.3 kgs. for low, and 28.1 kgs. for high load levels,
- **Person-specific anthropometry**: stature and body mass.

Detailed formulation of the biomechanical analysis is described in Appendix G. For illustrative purposes, spinal compression forces obtained from the algorithm were plotted by job cycle as a function of time, and as a cumulative exposure distribution (i.e., amplitude probability distribution function; APDF). To convey relative risk, the spinal compression forces were compared to the NIOSH-recommended Action limit of 3.4kN and Maximum Permissible limit of 6.4kN [228].

#### 6.2.4.4 Assessing the Framework Implementation

Task information obtained from a video-based task analysis of the job cycles performed by all 8 participants was used as reference "gold standard" data for assessing performance of the framework implementation. Job cycles performed in the experiment were video-recorded using two cameras located at each end of the lifting stations in side views, and a third camera capturing a frontal view of the walking trial. The 3 video files were time-synchronized and imported into the software program ELAN v5.1 (The Language Archive;

Figure 6.3) for manual annotation of the start and end of each MMH task, and the specific task conditions performed.

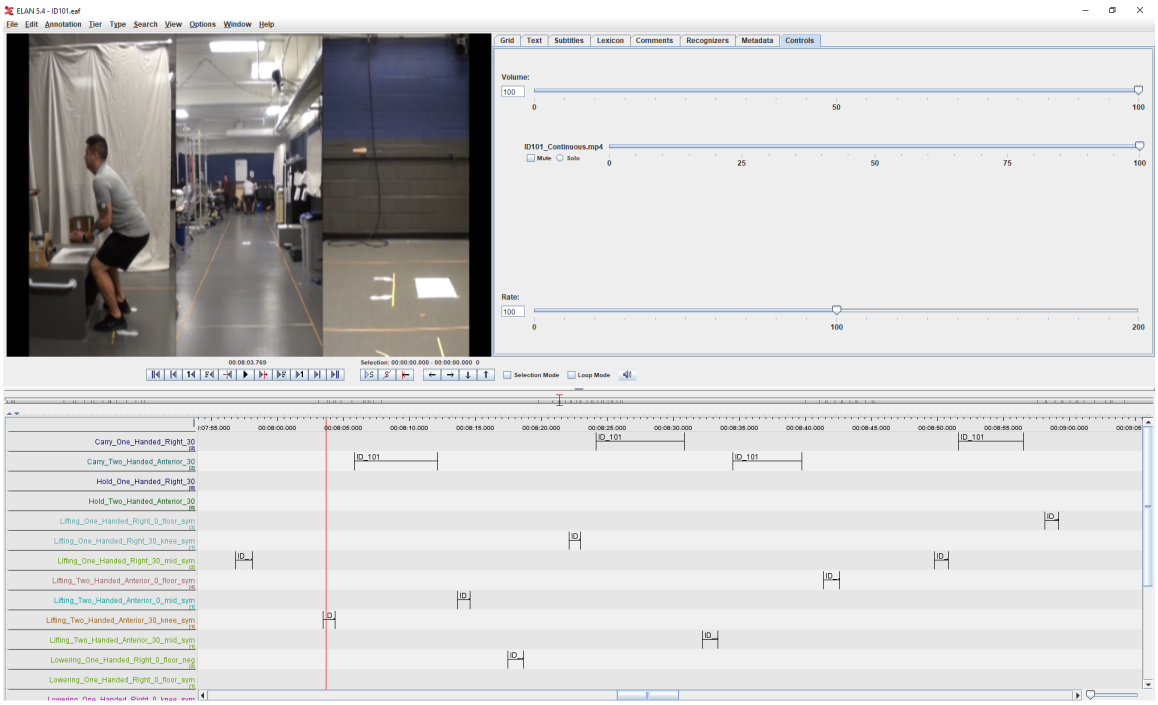



Figure 6.3: Example screenshot of the Elan software used for annotating the start and end of MMH tasks and task conditions. Upper left videos show the participant performing a two-handed lifting task at knee height.

### 6.2.5 Statistical Analysis

Task start and end time, task type, and specific task condition (i.e., carrying mode and load level for load carriage; height, hand mode, and load level for lifting and lowering) obtained from the framework implementation and video-based task analysis were tabulated and compared. Performance measures included the number of correct task detections (categorical outcome), error in detecting the task start time (i.e., detected vs. true), error in detecting the task duration time (detected vs. true), and prediction accuracy in task condition (i.e., load carriage: carry mode and load level; lifting-lowering: height, hand mode, and load level).

## 6.3 Results

### 6.3.1 Exemplar Output from a Low vs. High Intensity Job Cycle

Figure 6.4 and Figure 6.5 depict exemplar output from the implemented framework (Figure 6.2) for a low vs. high intensity continuous job cycle, respectively, using inertial sensor data obtained from one sample participant (Part ID: P3). Step 1 (top-panel) depicts the outcome from the task detection algorithm in identifying carrying, lifting, and lowering from each 1-sec time-window compared to the reference value from the video analysis. In Step 2, task conditions were predicted within the detected range of time-windows. In the figure, correct classification of load level are shown in green, while misclassifications highlighted in red. In Step 3, spinal compression force, $F_c$, was calculated as a function of time from information about the participant's anthropometry (body mass, stature), postural angle (i.e., torso sagittal flexion angle) per time window, estimated task duration, and predicted task conditions.

Table 6.3 summarizes performance for the task detection and classification of task condition from the same 2 job cycles described in Figure 6.4 and Figure 6.5. Correct classification of load level are shown in green, while misclassifications highlighted in red. In this particular example, fewer misclassifications occured in the low intensity (2 of 11) vs. high intensity job cycle (4 of 11). Origin height for lifting-lowering were correctly classified with the exception of two misclassifications in the high intensity job cycle.

Figure 6.6 summarizes the estimated $F_c$ as a cumulative exposure distribution. Differences between *true* vs. *predicted* $F_c$ were compared at $50^{th}$ and $90^{th}$ percentiles. For the example depicted, the *predicted* and *true predicted* $F_c$ were similar at the $50^{th}$ percentile in both low and high intensity job cycles. However, the *predicted* and *true* $F_c$ showed some differences in the $90^{th}$ percentile. In the low intensity job cycle, the *true* $F_c$ was lower by 0.2 kN compared to the *predicted* $F_c$, indicating an underestimation of $F_c$ due to misclassifications. On the other hand, the *true* $F_c$ was higher by 0.2 kN compared to the *true* $F_c$

in the high intensity job cycle, indicating an overestimation of $F_c$. The dark shaded area labelled 'External' in Figure 6.6 depicts the cumulative $F_c$ that could be attributed to the external hand loads obtained from the load classification algorithm, beyond the 'Internal' postural load obtained from inertial sensor based torso postures alone. In the low intensity job cycle, the effect of the additional information from the estimated 'External' loads was minimal. However, the difference in spinal loading from 'External' vs. 'Internal' loads increased as the load magnitudes in material handling increased (i.e., handling 22.7 kg of load) implying a concomitant increase in low back trauma and disorder risk.

### 6.3.2 Aggregate Performance Across Low vs. High Intensity Job Cycles

A total of 67 load carriages, 64 lifting, and 64 lowering tasks were performed across all participants and job cycles. Table 6.4 summarizes the performance measures obtained by comparing the results from the implemented framework to the *true* value obtained from video analysis.

### 6.3.3 MMH Task Detection

In total, 97% (65 of 67) of the load carriage tasks performed were detected. The task detection algorithm for load carriage had an average delay of $0.42 \pm 0.98$ sec in detecting the start of the load carriage across all carrying modes and load conditions. Duration of load carriage was consistently underestimated by an average of $0.98 \pm 1.15$ sec.

Lifting and lowering were detected in 89.1% and 90.6% of the cases, respectively. Unlike load carriage, both lifting and lowering onset times were detected in advance by an average of $0.12 \pm 0.30$ sec and $0.24 \pm 0.33$ sec than the *true* on average. Lifting and lowering durations were underestimated by $0.05 \pm 0.49$ sec and $0.24 \pm 0.58$ sec on average compared to *true*.

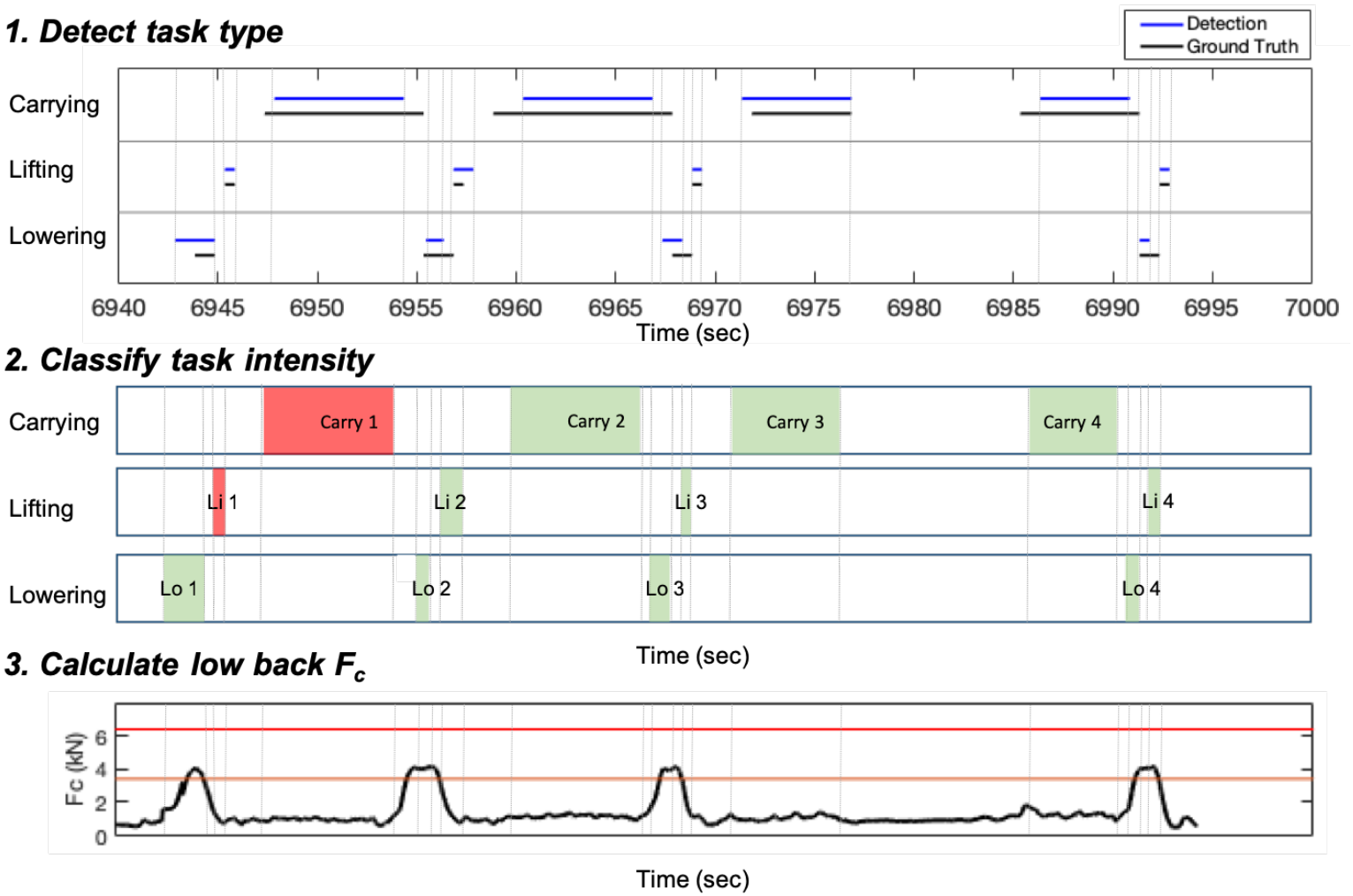



Figure 6.4: An example MMH task detection and task condition classification results for a low intensity job cycle. For Step 2 on classifying task intensity (middle panel) blocks colored red indicate misclassified load levels. Li = Lifting. Lo = Lowering.

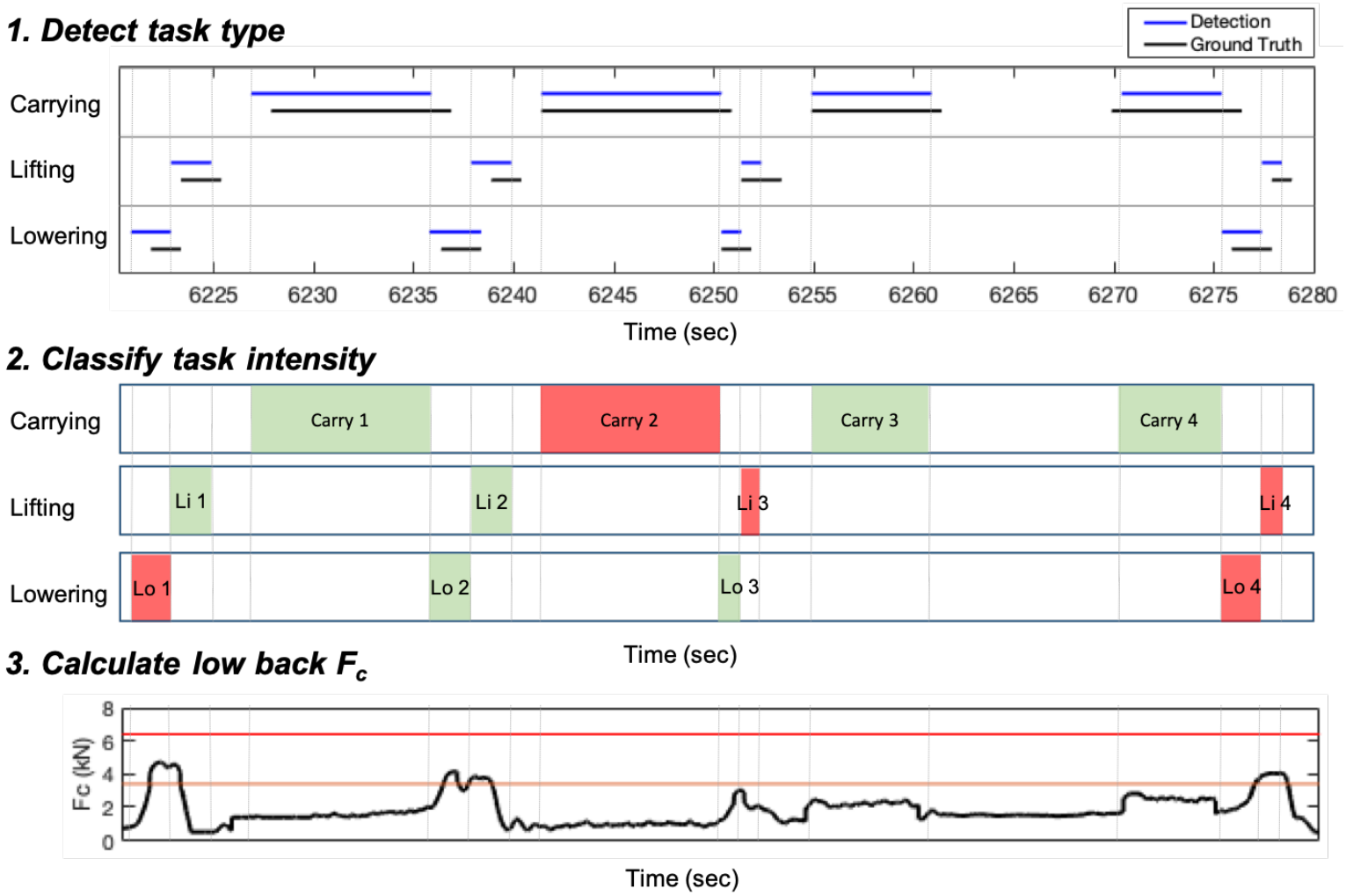



Figure 6.5: An example MMH task detection and task condition classification results for a high intensity job cycle. For Step 2 on classifying task intensity (middle panel) blocks colored red indicate misclassified load levels. Li = Lifting. Lo = Lowering.

Table 6.3: Example task detection and task condition classification results for low (refer to Figure 6.4) vs. high (refer to Figure 6.5) intensity job cycles. Correct classifications are indicated in green, while misclassified conditions are highlighted in red with the *true* task condition in parenthesis.

**1. Low intensity job cycle**

| Task # | Detection | Error in task start time (sec) | Error in task duration (sec) | Height | Mode | Load Level |
|---|---|---|---|---|---|---|
| Carry 1 | ✓ | 0.5 | -1.5 | - | 2H-Anterior | High (True = Low) |
| Carry 2 | ✓ | 1.5 | -2.5 | - | No-Load | - |
| Carry 3 | ✓ | -0.5 | 0.5 | - | 2H-Anterior (True = 1H-R) | Low |
| Carry 4 | ✓ | 1 | -1.5 | - | 1H-Right | Low |
| Li 1 | ✓ | 0 | 0 | Knee | 2H | High (True = Low) |
| Li 2 | ✓ | 0 | 0.5 | Floor | 1H (True = 2H) | Low |
| Li 3 | ✓ | 0 | 0 | Floor | 1H | Low |
| Li 4 | ✓ | 0 | 0 | Floor | 2H (True = 1H) | Low |
| Lo 1 | ✓ | -1 | 1 | Knee | 2H | Low |
| Lo 2 | ✓ | 0 | -0.5 | Floor | 1H (True = 2H) | Low |
| Lo 3 | ✓ | -0.5 | 0 | Floor | 1H | Low |
| Lo 4 | ✓ | 0 | -0.5 | Floor | 1H | Low |

**2. High intensity job cycle**

| Task # | Detection | Error in task start time (sec) | Error in task duration (sec) | Height | Mode | Load Level |
|---|---|---|---|---|---|---|
| Carry 1 | ✓ | -0.5 | -0.5 | - | 2H-Anterior | High |
| Carry 2 | ✓ | 0 | -1 | - | 1H-Left (True = No-Load) | - |
| Carry 3 | ✓ | 0 | -0.5 | - | 1H-Left | High |
| Carry 4 | ✓ | 0.5 | -2 | - | 1H-Left | High |
| Li 1 | ✓ | 0 | -0.5 | Floor (True = Knee) | 1H (True = 2H) | High |
| Li 2 | ✓ | -0.5 | 0.5 | Floor | 2H | Low |
| Li 3 | ✓ | 0 | -1 | Knee | 1H | Low (True = High) |
| Li 4 | ✓ | -0.5 | 0 | Floor | 1H | High (True = Low) |
| Lo 1 | ✓ | -1 | 0.5 | Floor (True = Knee) | 1H (True = 2H) | High (True = Low) |
| Lo 2 | ✓ | -0.5 | 0.5 | Floor | 1H (True = 2H) | High |
| Lo 3 | ✓ | 0 | -0.5 | Knee | 1H | Low |
| Lo 4 | ✓ | -0.5 | 0 | Floor | 1H | Low (True = High) |

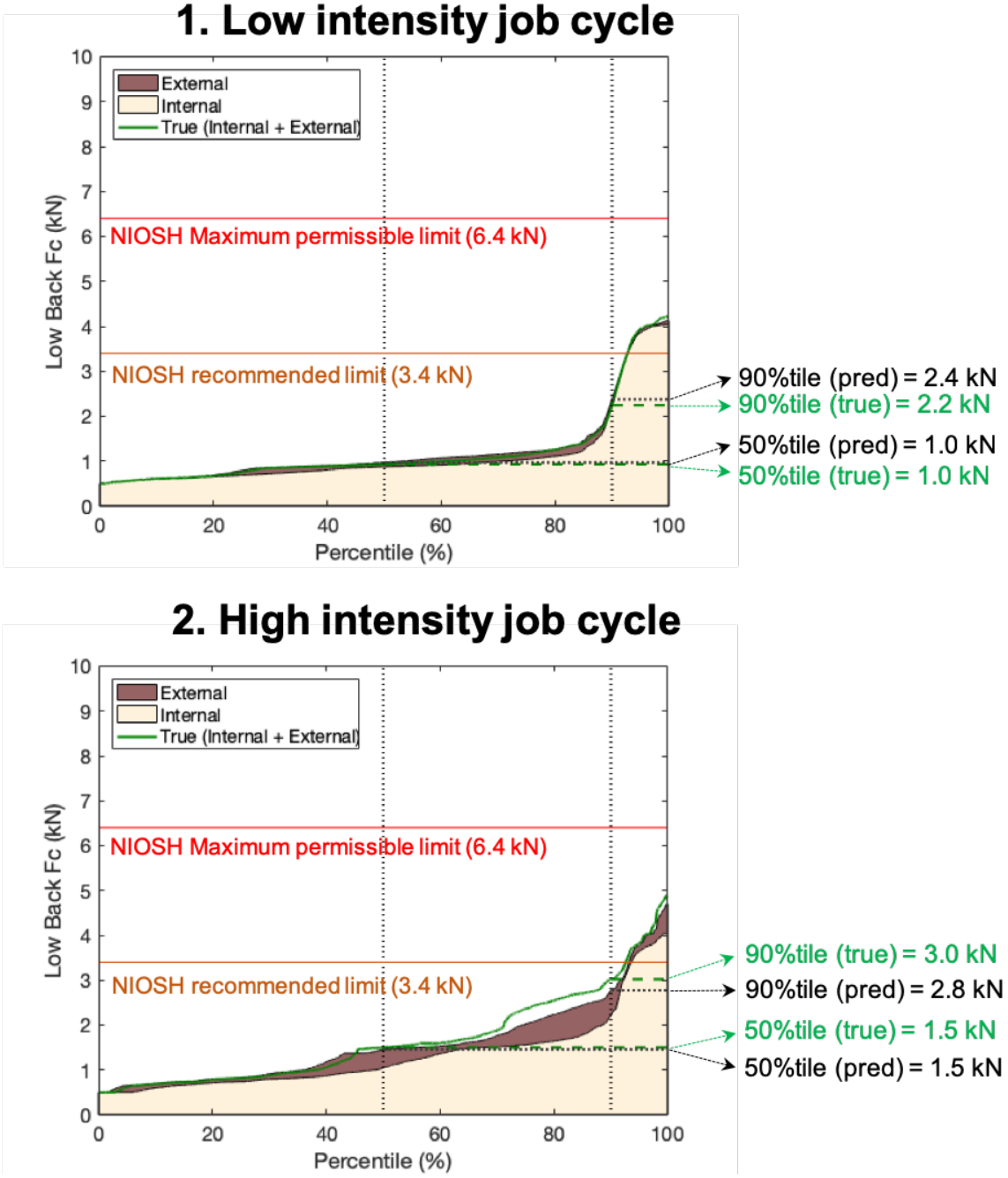



Figure 6.6: Cumulative spinal compression force, $F_c$, estimated for low (top) vs. high (bottom) intensity job cycle. "Internal" corresponds to $F_c$ attributed to the postural load due to mass of the head, arms and torso. "External" corresponds to $F_c$ attributed to the predicted external load. *True* corresponds to $F_c$ computed using reference data from video analysis, i.e., without misclassifications.

Table 6.4: Summary performance measures of the Load carriage, lifting, and lowering detection and task condition classification (N=8).

| True carrying condition | | Carry | Carry start time (sec) | | Carry duration (sec) | | Classification accuracy (%) | |
|---|---|---|---|---|---|---|---|---|
| **Mode** | **Load** | **detection (%)** | **Error (Mean ± SD)** | **MAE** | **Error (Mean ± SD)** | **MAE** | **Mode** | **Load** |
| No–Load | - | 18 of 19 (94.7) | 0.86 ± 1.50 | 1.03 | -1.61 ± 1.58 | 1.67 | 12 of 18 (66.7) | - |
| 1H-R | Low | 16 of 16 (100) | 0.47 ± 0.67 | 0.66 | -0.88 ± 0.79 | 1 | 11 of 16 (68.8) | 16 of 16 (100) |
| 1H-L | High | 15 of 16 (93.8) | 0.13 ± 0.52 | 0.47 | -0.53 ± 0.88 | 0.73 | 15 of 15 (100) | 15 of 15 (100) |
| 2H-Anterior | Low | 8 of 8 (100) | 0.25 ± 0.53 | 0.38 | -1.12 ± 0.58 | 1.12 | 8 of 8 (100) | 5 of 8 (62.5) |
| | High | 8 of 8 (100) | 0.06 ± 0.78 | 0.56 | -0.44 ± 1.02 | 0.94 | 8 of 8 (100) | 8 of 8 (100) |
| | **Total** | 65 of 67 (97.0) | 0.42 ± 0.98 | 0.67 | -0.98 ± 1.15 | 1.13 | 54 of 65 (83.1) | 56 of 65 (86.2) |

| True lifting condition | | | Lifting | Lift start time (sec) | | Lift duration (sec) | | Classification accuracy (%) | | |
|---|---|---|---|---|---|---|---|---|---|---|
| **Height** | **Mode** | **Load** | **detection (%)** | **Error (Mean ± SD)** | **MAE** | **Error (Mean ± SD)** | **MAE** | **Height** | **Mode** | **Load** |
| Knee | 1H | High | 6 of 8 (75.0) | -0.17 ± 0.26 | 0.17 | -0.38 ± 0.35 | 0.38 | 6 of 6 (100) | 0 of 6 (0) | 4 of 6 (66.7) |
| | 2H | Low | 7 of 8 (87.5) | -0.21 ± 0.27 | 0.21 | -0.12 ± 0.69 | 0.62 | 5 of 7 (71.4) | 5 of 7 (71.4) | 5 of 7 (71.4) |
| | | High | 7 of 8 (87.5) | -0.21 ± 0.27 | 0.21 | -0.12 ± 0.749 | 0.5 | 7 of 7 (100) | 7 of 7 (100) | 4 of 7 (57.1) |
| Floor | 1H | Low | 23 of 24 (95.8) | -0.02 ± 0.35 | 0.24 | -0.15 ± 0.65 | 0.4 | 20 of 23 (87.0) | 12 of 23 (52.2) | 8 of 23 (34.8) |
| | 2H | Low | 14 of 16 (87.5) | -0.18 ± 0.25 | 0.18 | -0.12 ± 0.47 | 0.31 | 14 of 14 (100) | 12 of 14 (85.7) | 4 of 14 (28.6) |
| | | **Total** | 57 of 64 (89.1) | -0.12 ± 0.30 | 0.21 | -0.05 ± 0.49 | 0.33 | 52 of 57 (91.2) | 36 of 57 (63.2) | 25 of 57 (43.9) |

| True lowering condition | | | Lowering | Lower start time (sec) | | Lower duration (sec) | | Classification accuracy (%) | | |
|---|---|---|---|---|---|---|---|---|---|---|
| **Height** | **Mode** | **Load** | **detection (%)** | **Error (Mean ± SD)** | **MAE** | **Error (Mean ± SD)** | **MAE** | **Height** | **Mode** | **Load** |
| Knee | 1H | Low | 6 of 8 (75.0) | -0.33 ± 0.26 | 0.33 | 0 ± 0.32 | 0.17 | 6 of 6 (100) | 0 of 6 (0) | 1 of 6 (16.7) |
| | 2H | Low | 15 of 16 (93.8) | -0.10 ± 0.39 | 0.23 | -0.20 ± 0.62 | 0.53 | 13 of 15 (86.7) | 13 of 15 (86.7) | 5 of 15 (33.3) |
| Floor | 1H | Low | 16 of 16 (100) | -0.25 ± 0.26 | 0.25 | -0.16 ± 0.40 | 0.28 | 14 of 16 (87.5) | 15 of 16 (93.8) | 5 of 16 (31.3) |
| | | High | 7 of 8 (87.5) | -0.29 ± 0.39 | 0.29 | -0.07 ± 0.35 | 0.21 | 6 of 7 (85.7) | 0 0f 7 (0) | 4 of 7 (57.1) |
| | 2H | Low | 8 of 8 (100) | -0.38 ± 0.35 | 0.38 | -0.12 ± 0.58 | 0.5 | 7 of 8 (87.5) | 7 0f 8 (87.5) | 4 of 8 (50.0) |
| | | High | 6 of 8 (75.0) | -0.25 ± 0.27 | -0.25 | -0.17 ± 0.41 | 0.33 | 6 of 6 (100) | 5 of 6 (83.3) | 6 of 6 (100) |
| | | **Total** | 58 of 64 (90.6) | -0.24 ± 0.33 | 0.28 | -0.24 ± 0.58 | 0.45 | 52 of 58 (89.7) | 40 of 58 (69.0) | 25 of 58 (43.1) |

### 6.3.4 MMH Task Condition Classification

The classification accuracy for load carriage mode and load level were 83.1% and 86.2%, respectively. These values were comparable to corresponding values from the algorithm development phase in Chapter 5, namely, 80.2% for carrying mode and 88.7% for load levels averaged across the 4 modes.

Height classification accuracy in lifting and lowering were 91.2% and 89.4%, which were 6.5% and 8% lower, respectively, compared to corresponding values from development phase in Chapter 5.

Classification accuracy for mode and load levels were substantially lower compared to the development phase. Specifically, classification accuracy for identifying 1H lifting and lowering was particularly poor ranging from 0% to 52.2%, with most of these modes categorized as 2H. The misclassification in 1H mode also decreased the accuracy in predicting load levels at the next stage, ranging from 16.7% to 66.7% across conditions.

In contrast, classification accuracy for identifying 2H lifting and lowering mode were consistently high, ranging from 71.4% to 100% across conditions. However, a substantial number of the 2H lifting and lowering tasks at the low load levels were misclassified as the high load condition (accuracy ranging from 28% to 71.4%), suggesting that the algorithm overestimated load level in 2H lifting-lowering.

## 6.4 Discussion

This study implemented an initial framework for assessing biomechanical exposures in manual load carriage, lifting and lowering by leveraging continuous inertial sensor-based kinematic information and predictive modeling. Importantly, the study demonstrates the potential for combining wearable sensing technology with predictive modeling to advance field-based exposure assessment by providing information about work content beyond just quantifying worker postures.

A quantitative evaluation of the implemented framework indicated promising results for detecting load carriage tasks and classifying the carrying mode and load level. Performance in the lifting and lowering task were comparatively less remarkable in classifying load level. However results for lifting-lowering in the 2H mode were more encouraging than the 1H mode, and provide some impetus for further refinement. Two avenues for improvement are proposed. The first pertains to inclusion of predictors related to bilateral asymmetry to improve sensitivity in separating the 1H-R and 1H-L modes. Second, a more sophisticated approach to creating normalized models specific to individual anthropometry may be warranted. The previous Chapter 5 conducted a preliminary study in this regard, though used a very simple approach to normalizing predictor variables by stature. Admittedly, the present evaluation was conducted with only two load levels. Further testing using a range of different load magnitudes may provide better insights into systematic bias (i.e., over vs. under-estimation of load levels) and opportunities for refining the algorithm.

The gait detection algorithm (*Step 1*) used in this study implemented a robust approach to detection of the start and end of ambulation. The estimated start times and durations of ambulation (either unloaded or loaded) were accurate within a mean absolute error of 1 second. The duration of individual lifting and lowering motions were generally very short (< 1s) and thus the start times and durations have less relevance. Despite the short durations, 89.1% of the lifting motions and 90.6% of the lowering motions were correctly detected, i.e., about 10% of the lifting-lowering motions were missed.

This study also attempted to combine the obtained task-specific information into a cumulative measure of biomechanical exposure in the form of cumulative spinal compression force. The example cases presented showed demonstrable effects of predicted low vs. high load intensity on cumulative spinal loads. Similar comparisons could be conducted by task type, time intervals, and across workers. The algorithm presented can potentially be used in applied settings where the magnitude of hand loads vary throughout a work-shift or is difficult to directly measure in field settings.

## 6.5 Conclusion

This study is the first of its kind to estimate external loads and cumulative biomechanical exposures using inertial-sensor based kinematic data alone. Comparative studies have all relied on some form of observational or direct measurement approach to quantify the magnitude of loads handled. Observation methods can be time and cost prohibitive when applied to non-routinized work. Force measurement instrumentation such as pressure mapping insoles [25], instrumented force shoes [26], instrumented gloves [27], and electromyography [77] are costly and can potentially interfere with worker movements and work performance. While the current study might underperform in terms of accuracy of load prediction compared to studies that use direct force measurement, it also uses a lot less information with much less instrumentation. This might be particularly appealing in applied settings where the magnitude of hand loads vary throughout a work-shift or is difficult to directly measure in field settings. It is likely that new forms of inertial sensing embedded in clothing, e.g., [112], will further improve the wearability and potential acceptability of wearable inertial sensing in occupational settings.

# CHAPTER 7

# Conclusion

## 7.1 Summary of Findings

This research explored several emerging applications and opportunities afforded by body-worn inertial sensing technology for quantifying biomechanical exposures and low back disorder risk in non-repetitive MMH jobs. It also demonstrated the potential for combining wearable inertial sensing and predictive modeling techniques to improve the accuracy of biomechanical exposure assessment in ergonomics applications.

The principal findings of this research can be summarized in the context of the three objectives outlined in Chapter 1:

**Objective 1: Quantify empirical relationships between the effects of hand load and mode in manual load carriage on inertial sensor-based posture kinematics.**
Chapter 3 had nine participants perform walk trials at self-selected speeds while carrying hand loads in two modes (two-handed side vs. anterior) at four load levels (empty-handed, 4.5 kg, 9.1 kg, and 13.6 kg). Six temporal gait parameters, six postural sway parameters, and three measures of thoracic-pelvic coordination were calculated from data recorded by six body-worn inertial sensors for 540 gait cycles. Results demonstrated that gait patterns characterized by inertial sensor-derived temporal and kinematic gait parameters changed systematically by the mode of load carriage and load magnitude, after adjusting for gait cycle duration and stride length. Collectively, the findings indicated that inertial-sensor based

posture and gait kinematics were jointly influenced by magnitude and mode of manual load carriage.

**Objective 2: Develop and assess a statistical prediction algorithm that uses posture kinematics calculated from body-worn inertial sensors to classifying material handling mode and load level.**

Chapters 4 and 5 presented statistical models to classify different task conditions in load carriage and lifting-lowering, which represent two common MMH tasks associated with an increased risk of low back disorders. Separate classification models were developed for predicting binary load levels (i.e., low: 0 to 4.5 kgs. vs. high: 13.5 to 22.7 kgs) in manual load carriage, lifting, and lowering using inertial-sensor derived kinematic measures as predictors. Collectively, the findings indicated that subtle adaptations in posture and movement kinematics can provide useful information to typify different modes and intensity levels in load carriage and lifting-lowering. Importantly, these two chapters demonstrated the potential for combining wearable inertial sensing with statistical prediction to quantify biomechanical exposures in MMH work.

**Objective 3: Implement and empirically assess an algorithmic framework for quantifying biomechanical exposures during load carriage and lifting-lowering by leveraging outcomes from Objectives 1 and 2, including, inertial sensing and predictive modeling techniques.**

Chapter 6 implemented an initial algorithmic framework for assessing biomechanical exposures in manual load carriage, lifting and lowering by leveraging continuous inertial sensor-based kinematic information and predictive modeling. The algorithm also combined task-specific information to estimate cumulative spinal compression force as a measure of low back disorder risk. A quantitative evaluation of the implemented framework indicated promising results for detecting load carriage tasks and classifying the carrying mode and load level. Performance in the lifting and lowering task were comparatively less remarkable in classifying load level. However results for lifting-lowering in the 2H mode were

more encouraging than the 1H mode, and provide impetus for further refinement. Overall, the study demonstrated the possibility for combining wearable inertial sensing and predictive modeling techniques to improve the accuracy of biomechanical exposure assessment in ergonomics applications.

## 7.2 Theoretical Contributions

This research makes theoretical contributions in three main areas:

(1) This research improves our understanding about the biomechanical effects of transient loads of different magnitudes during MMH on posture and gait kinematics, particularly movement coordination between thoracic and pelvic segments. For example, with regards to load carriage, prior studies have investigated the effects of carrying mode and hand load on temporal and kinematic gait parameters but while participant walked at precise speeds on a treadmill. This research examined effects under self-selected speeds on leveled ground in order to obtain the natural adaptation in walking patterns due to different load carriage conditions. Subtle yet statistically significant changes in temporal parameters from the external loads were observed. Importantly, the effects of carrying mode and load magnitude on gait were more evident in the measure of postural sway and thoracic-pelvic coordination, which served as the basis for classifying load carrying mode and load levels in a statistical prediction algorithm (Figure 7.1).

(2) Quantifying physical exposures to load carriage can be challenging in non-routinized work settings where load intensity, duration and frequency vary between workers and within worker across time. A key contribution of this research was an algorithmic framework that combines biomechanical and empirical findings, wearable inertial sensing, and predictive modeling to quantify biomechanical exposures associated

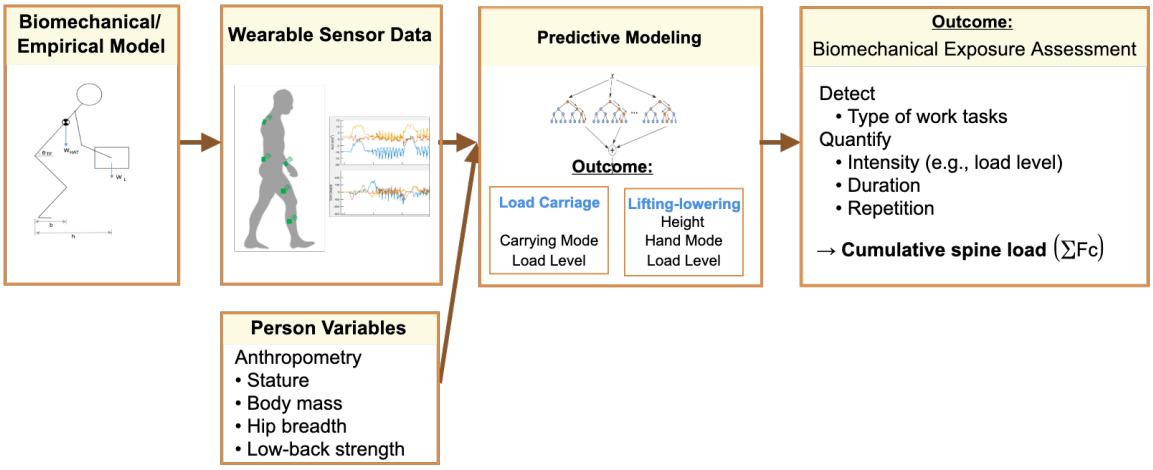



Figure 7.1: Revised conceptual framework depicting the inertial sensor-based biomechanical exposure assessment investigated in the research.

with low back disorder risk in non-repetitive MMH work. The algorithm was novel in that it did not rely on direct force measurement, but instead leveraged biomechanical relationships between external loads on movement kinematics and intersegment coordination during manual load carriage and lifting-lowering. This information helped to inform and also reduce the number of feature vectors used in developing classification algorithm and potentially increased prediction accuracy, compared to using raw (unprocessed) sensor data directly. The algorithm presented can potentially be used in applied settings where the magnitude of hand loads vary throughout a work-shift or is difficult to directly measure in field settings. In such situations, the predicted load levels combined with postural data can be used as inputs to a biomechanical model to estimate cumulative physical exposures (e.g., spinal loads, joint moments) towards quantifying the risk of occupationally-relevant low back disorders.

(3) This research demonstrated the potential for leveraging wearable inertial sensing and predictive modeling techniques to improve the accuracy of quantifying biomechanical exposures in ergonomics applications. Analysis of inertial sensor data has largely been limited to characterizing the intensity, repetitions and duration of postures. The

ability to extract information about work content from motion data is underutilized. Likewise, the application of predictive modeling techniques in ergonomics remains underexplored. A few of the studies reviewed [67, 75, 76] used commercial software to detect different work postures. The presented research substantially expands the applications and opportunities afforded by body-worn inertial sensing technology and predictive modeling techniques in ergonomics.

## 7.3 Limitations and Future Research Direction

Certain limitations of this dissertation research are worth discussing, particularly in the context of directions for future research.

- ***Task duration***: This research did not address the effects of cumulative fatigue on gait and lifting-lowering kinematics from long duration exposures. For example, in jobs that might involve long duration of manual load carriage, cumulative fatigue from load carriage may induce alterations in gait [175, 176, 210]. Prior studies have associated fatigue with increased variability in step length, step width, and mediolateral trunk accelerations while walking, and increased double support duration during load carriage. Qu et al. [147] reported hip and torso range of motion to increase while carrying a backpack load immediately following a fatiguing treadmill exercise. Further research is need to examine the effects of fatigue development from MMH on performance of the algorithm developed in this research, and perhaps even incorporate features to detect the onset of fatigue.

- ***Type of MMH tasks***: As a proof of concept, the MMH tasks investigated in this research was limited to the load carriage, lifting, and lowering. Other tasks such as cart pushing, pulling, 1- and 2-handed force exertions are also known to be associated with the increased risk of low back disorders. Further studies addressing these MMH tasks could help increase the generalizability of the algorithms developed to applied

settings.

- ***MMH task simulation in the lab environment vs. field-based assessment***: The work tasks simulated in this research were designed to capture realistic work conditions and to observe natural adaptations in kinematics with different task conditions (e.g., height of the load, hand-mode, and load levels). Participants were allowed to adopt their own walking speed, work pace, and foot placements throughout the continuous job cycle simulation in Chapter 6. However, the performance of the algorithm can be still affected by certain external factors (e.g., slope of the floor, object size dimensions, object center of mass, weather) or internal changes (e.g., cumulative fatigue from MMH tasks) not discussed as the scope of this dissertation, and can potentially affect the kinematics of the workers, which then may affect the performance of statistical classification algorithms. Field-based studies are needed to examine the generalizability and feasibility of the presented algorithms to applied work settings, particularly in non-repetitive jobs (e.g., patient handling and transport, construction, warehousing and delivery).

- ***Load level prediction***: This dissertation categorized load level of each task by grouping the conditions into low intensity (0 to 4.5 kg) vs. high intensity (13.6 to 22.7 kg) conditions. Improved resolution of load level estimation can have direct practical values by providing more fine and accurate load estimation than just categorizing two levels. This can be achieved by applying different methods. For example, use of regression models instead of classification models can provide continuous estimation of external load. Further investigation of the selection and normalizing of kinematic predictors could help to improve classifying accuracy.

- ***Parity in exposure assessment***: On a broader note, while the scientific literature (especially in human factors and ergonomics) is witnessing a proliferation of studies using statistical prediction (i.e., machine learning, deep learning), few studies explic-

itly examine potential issues of classification parity, algorithmic fairness and bias. A lack of attention to these issues could erode user trust and undermine the potential benefits of such novel techniques for improving worker health and safety. Examples of algorithmic bias from other domains such as social media, journalism, and banking have sparked tremendous interest in developing fair machine-learning algorithms [229, 230]. It is important that the ergonomics community also become cognizant of these issues and work towards productive solutions particularly as machine learning techniques gain popularity in ergonomics practice. Chapter 5 introduced a few preliminary approaches to normalizing predictor variables in order to adjust for between-subject differences. However, further research is need to minimize between-subject effects with an eye towards ensuring classification parity across key worker demographics (e.g., gender, age) prior to algorithm deployment in applied settings.

- ***Real-time assessment and feedback***: Wearable inertial sensing with wireless connectivity present unprecedented opportunity for real-time assessment and subsequent feedback about biomechanical exposures either to workers directly (e.g., using vibrotactile feedback [47]) or to managers and supervisors (e.g., [49]). However, the algorithms developed in this dissertation were not yet implemented as a real-time assessment tool. Research is needed to better understand use-cases for such real-time feedback capability, and the content and modality of real-time information provided.

## 7.4 Concluding Remarks

The overall goal of this research was to create and validate inertial sensor-based biomechanical exposure assessment framework by combining wearable inertial sensing technologies and predictive modeling. This research presented a novel method of MMH task detection and task condition classification algorithms combined as a framework for assessing cumulative low-back exposures during load carriage, lifting, and lowering across different

task conditions. The research makes important contributions towards our theoretical understanding of (1) adaptations in gait and posture resulting from transient loads and task conditions, and (2) the potential for leveraging biomechanical information in the building of accurate and interpretable statistical classification algorithms (e.g., data segmentation, choice of predictor variables, and predictor normalization) for use in ergonomics applications. This research also contributes to ergonomics practice by providing a framework implementation for combining biomechanical information and empirical findings, wearable inertial sensing, and predictive modeling to quantify physical exposures associated with low back disorder risk in non-repetitive MMH work.

# APPENDIX A

# Summary of studies in the literature review.

Table A.1: Summary of studies in the literature review.

| Study | Ref. | Study sample | n | Lab vs. Field (site) | Type of occupational activities measured | # of sensors | Analysis | Assessment |
|---|---|---|---|---|---|---|---|---|
| 1 | [89] | N/A | N/A | Field | Repetitive upper limb task, prolonged awkward postures (e.g., holding a bent-arm position) | 4 | Descriptive | Relative |
| 2 | [91] | Healthy individuals (various occupations) | 21 | Field (various) | Work day activities (e.g., computer use, writing, driving, register work, etc.) | 2 | Inferential | |
| 3 | [92] | Dental hygienists | 12 | Field (dentistry) | Prophylactic and periodontal treatment (e.g., scaling using an ultrasonic device, using turbines for polishing, manual scaling with hand instruments, all the other auxiliary tasks) | 3 | Descriptive | Relative |
| 4 | [58] | Female dental hygienists | 16 | Lab | Reaching task (i.e., target located in the sagittal plane at a horizontal distance of 80% of arm length and height of 50% of arm length above shoulder height), flossing task in a simulated workstation | 1 | | |
| 5 | [65] | Typists | 8 | Lab | Typing task | 1 | | |
| 6 | [83] | Patient care unit worker | 50 | Field (patient care unit) | Nursing task during one work-shift | 2 | Descriptive | Absolute |
| 7 | [84] | Patient care unit worker (40 nurses, 10 pc assistants) | 50 | Field (patient care unit) | Nursing task during one work-shift | 2 | Inferential | Absolute |
| 8 | [70] | Male meat cutters | 20 | Field (meat-processing plants in Sweden) | Meat cutting in the split-carcass system, the sixth-part system, and the line-production system | 4 | Descriptive | Relative |
| 9 | [49] | N/A | N/A | Field (distribution center in fashion industry, warehouse in an assembly line) | Manual material handling at warehouses (i.e., refilling, picking, packing) | 17 | Descriptive | Absolute |
| 10 | [93] | Baggage handlers | 44 | Field (6 airports) | Baggage handling job | 2 | Inferential | Relative |
| 11 | [71] | N/A | 2 | Lab | Reach task with three isolated joint motions: elbow f/e, shoulder f/e, shoulder ab/ad, and cross body reach task | 3 | Descriptive | Relative |
| 12 | [55] | N/A | N/A | Lab | Sit to stand | 1 | | |
| 13 | [94] | Construction workers | ~80 | Field (construction site) | Construction tasks (e.g., heavy lifting) | 8 | Inferential | Relative |
| 14 | [77] | Male office workers | 26 | Lab | Symmetric and right-handed asymmetric lifting | 2 | Predictive | |
| 15 | [75] | Male fishermen | 4 | Field (on two steel trawlers - fishing boat) | Fishing activities | 1 | Predictive | Relative |
| 16 | [76] | Patient with chronic low back pain | 1 | Field (city Hall) | Maintenance and repair jobs, messenger jobs (i.e., sorting mail, prepaying postage, distributing mail) | 3 | Predictive | Relative |
| 17 | [62] | Healthy individuals | 12 | Lab | Simulated painting work, computer work, furniture polishing work, and arms rest with elevated or supported | 4 | | |

**Table A.1 – continued from previous page**

| Study | Ref. | Study sample | n | Lab vs. Field (site) | Type of occupational activities measured | # of sensors | Analysis | Assessment |
|---|---|---|---|---|---|---|---|---|
| 18 | [60] | Healthy individuals | 8 | Lab | Walking at speeds 2,3, and 4 km/h, sitting, standing, and swinging | 2 | | |
| 19 | [72] | Parlor workers (milkers) | 9 | Field (five large-herd diary operations: two parallel parlors, two herringbone parlors, and one rotary parlor) | Full-shift exposures at milking parlor | 2 | Descriptive | Relative |
| 20 | [95] | Employees | 158 (phase 1), 48 (phase 2) | Lab & Field (various) | Traditional washer assembly line work (fixed-cycle), new washer line during its start-up operations (non-fixed cycle), and managerial/technical support work | 1 | Inferential | Relative |
| 21 | [44] | N/A | N/A | Lab | Manual material handling | N/A | | |
| 22 | [231] | Healthy men | 10 | Lab | Symmetric lifting of 8.5 kg crate, asymmetric lifting with 45 deg. to the right of the sagittal plane, and left-right lateral trunk flexion | 3 | | |
| 23 | [41] | Healthy men | 9 | Lab | Symmetric, asymmetric, and fast symmetric trunk bending | 17 | | |
| 24 | [59] | Healthy men | 10 | Lab | Knee abduction/adduction movement, and walking (30m) | 2 | | |
| 25 | [46] | Healthy men | 40 | Lab | Static reaching, lifting of 5 kg at 9 different anterior-right positions and at 5 different heights (i.e., 0, 30, 60, 90, and 120 cm from the floor) | 3 | Predictive | |
| 26 | [96] | Workers (various occupations) | 604 | Field (43 types of workplace) | Various type of works including breaks | 3 | Descriptive | Relative |
| 27 | [80] | Paper mill workers | 28 | Field (Swedish paper mill) | Operating paper machines, testing paper quality, transporting and packaging paper rolls, and monitoring/controlling production | 3 | Predictive | |
| 28 | [97] | Personal support workers, healthcare | 27 | Field (7 long-term care facilities) | Patient support work activities (e.g., patient handling tasks, lifting tasks) | 1 | Descriptive | Relative |
| 29 | [42] | Personal support workers, healthcare | 20 | Field (7 long-term care facilities) | Patient support work activities (e.g., patient handling tasks, lifting tasks) | 1 | Descriptive | Relative |
| 30 | [98] | Firefighters | 24 | Lab (environmental chamber, Firefighting Activities Station) | Firefighting activities (climbing stairs, moving a hose line, search a room, pulling down the ceiling), walking on a treadmill | 3 | Inferential | Relative |
| 31 | [51] | Dentists | 24 | Field (dentistry) | Dentistry work (e.g. sitting office work, sitting treatment of lower/upper jaw, standing office work, standing treatment of lower/upper jaw, waiting, and x-ray) | 4 | Inferential | Relative |

**Table A.1 – continued from previous page**

| Study | Ref. | Study sample | n | Lab vs. Field (site) | Type of occupational activities measured | # of sensors | Analysis | Assessment |
|---|---|---|---|---|---|---|---|---|
| 32 | [99] | Dentists | 12 | Field (dentistry) | Dentistry work | 4 | Inferential | Relative |
| 33 | [43] | Healthy individuals | 14 | Lab | Manual material handling tasks (i.e., symmetric lifting and lowering to/from ground height/knuckle height, asymmetrical lifting and lowering, carrying, pushing/pulling) | 17 | | |
| 34 | [78] | Healthy individuals | 10 | Lab | Manual material handling tasks (i.e., lifting/lowering from the ground/knuckle, pushing and pulling, carrying, walking) | 17 | Predictive | |
| 35 | [73] | Blue-collar workers | 682 | Field (manufacturing, cleaning, and transportation workers) | Work activities | 3 | Inferential | Absolute |
| 36 | [56] | Healthy individuals | 20 | Lab | 5m timed up and go (TUG) | 6 | | |
| 37 | [100] | Operators | 5 | Field (automotive plant) | Assembly of indicators, assembly of tachometers, final assembly (e.g., materials handling, soldering, screw driving, transport, packaging) | 3 | Descriptive | Relative |
| 38 | [52] | 24 electricians (12 Brazilian, 12 Norwegian, all M, mean age 38 and 33 years) | 24 | Field (construction site) | Electrician's task (i.e., planning tasks, supporting tasks, and wiredraw tasks) | 4 | Descriptive | Relative |
| 39 | [101] | Firefighters | 20 | Field (5 outdoor stations simulating the firefighting) | Simulated outdoor firefighting activities (i.e., crossing a stream, walk in the woods, log walk, hill climb, and over/under logs) | 4 | Inferential | Relative |
| 40 | [82] | N/A | N/A | Lab | Manual screw driving task | 2 | Predictive | Absolute |
| 41 | [48] | N/A | N/A | Lab & Field | 80 s quiet standing (lab study), standing (field study) | 1 | | |
| 42 | [232] | Officer workers | 34 | Field (Department of health and human services office) | Typical desk-based work | 1 | | |
| 43 | [79] | Healthy individuals | 10 | Lab | Supermarket cashiers' everyday operation | 3 | Predictive | Absolute |
| 44 | [102] | Residential healthcare workers | 21 | Field (residential home) | Patient care | 1 | Descriptive | Absolute |
| 45 | [103] | Healthcare workers | 108 | Field | Nursing tasks | 1 | Inferential | Absolute |
| 46 | [50] | Healthy individuals | 12 | Lab | Manual material handling tasks (i.e., move boxes from conveyer to a platform with 3 different set-up) | 17 | | |
| 47 | [104] | Cleaners | 18 | Lab & Field (lab and lecture room) | Clearing tasks at a normal pace (i.e., mopping the floor, sweeping, empting the garbage bin, changing its plastic bag, and cleaning the rows of desks and blackboards) | 1 | Inferential | Relative |
| 48 | [105] | Registered nurses | 36 | Field (Hospital) | Nursing tasks | 3 | Inferential | Relative |

**Table A.1 – continued from previous page**

| Study | Ref. | Study sample | n | Lab vs. Field (site) | Type of occupational activities measured | # of sensors | Analysis | Assessment |
|---|---|---|---|---|---|---|---|---|
| 49 | [61] | Healthy men | 36 | Lab | Manual material handling (i.e., move 4.5 kg plastic crates from a waist-high material feeder to one of six unloading areas) | 2 | | |
| 50 | [57] | Healthy men | 6 | Lab | Simulated milking cluster attachment task (cyclical task) | 3 | | |
| | | Dairy workers | 10 | Field (Milking parlors of three large-herd diary operations) | Milking tasks | 4 | | |
| 51 | [63] | Healthy individuals | 20 | Field (examination room) | Physical examination (ROM examination) | 13 | | |
| 52 | [106] | Healthy individuals | 10 | Lab | Buzz-wire test involving upper arm movement while seated | 4 | Inferential | Relative |
| 53 | [45] | Healthy individuals | 60 | Lab | Sagittal-symmetric manual material handling task (i.e., lowering and lifting) | 4 | | |
| 54 | [107] | Gynecologists | 4 | Field (Hospital, operating room) | Vaginal procedures performed for pelvic organ prolapse | 4 | Inferential | Relative |
| 55 | [233] | Aircraft cabin cleaners | 19 | Field (open storage room, inside/outside of the aircraft) | Semi-standardized activity (i.e., lying, sitting, standing, walking, walking on stairs, running all performed for min 30 secs) and non-standardized activity (normal level of movement complexity and very complex movements performed for relatively short duration and at a high tempo) | 2 | | |
| 56 | [64] | Healthy individuals | 20 | Lab | Sitting and standing | 5 | | |
| 57 | [85] | Healthy office workers (study 1 and 2), school teachers (study 2) | 4 (study 1), 24 (study 2) | Field (office) | Office work including sedentary computer work and sitting desk work | 1 | Inferential | Relative |
| 58 | [40] | Workers with the history of back strain and pain | 126 | Field (various sites including forestry, wood and projects, transportation, warehousing, and construction) | Various activities depending on worker's occupation | 1 | | |
| 59 | [47] | N/A | N/A | Lab | Lifting tasks | 7 | Descriptive | |
| 60 | [53] | Healthy individuals | 12 | Lab | Manual tasks (i.e., turning levers, removing fuses, screw/unscrewing, putting the screws using a ladder) | 8 | Inferential | Absolute |
| 61 | [74] | 374 blue-collar workers (age: 18-65) | 374 | Field (various) | Blue-collar work tasks (various) | 2 | Inferential | Relative |

**Table A.1 – continued from previous page**

| Study | Ref. | Study sample | n | Lab vs. Field (site) | Type of occupational activities measured | # of sensors | Analysis | Assessment |
|---|---|---|---|---|---|---|---|---|
| 62 | [90] | Blue-collar workers (e.g., cleaning, manufacturing, transport) | 657 | Field (various) | Blue-collar work tasks (various) and leisure activities | 2 | Inferential | Relative |
| 63 | [108] | Female nurses | 50 | Field (hospitals) | Patient transfer tasks with and without the use of assistive device | 2 | Inferential | Relative |
| 64 | [86] | Officer workers | 40 | Field (office) | Office work involving sedentary behavior | 1 | Inferential | Relative |
| 65 | [68] | Recreational runners | 25 | Field (N/A) | Repetitive upper limb task, prolonged awkward postures (e.g., holding a bent-arm position) | 1 | Inferential | Relative |
| 66 | [67] | Officer workers | 38 | Field (office) | Work day activities (e.g., computer use, writing, driving, register work, etc.) | 1 | Predictive | Relative |
| 67 | [54] | Surgeons (6 primarily console tasks, 4 primarily assisting tasks) | 10 | Field (operation room) | Prophylactic and periodontal treatment (e.g., scaling using an ultrasonic device, using turbines for polishing, manual scaling with hand instruments, all the other auxiliary tasks) | 5 | Inferential | Relative |

# APPENDIX B

# Type of commercial inertial sensors

Table B.1 lists the make, model, and technical specifications of commercially-available inertial sensors typically used in ergonomics research studies. The Biostamp RC (mc10 Inc., Lexington, MA) and and Opal (APDM, Inc., Portland, OR) sensors were used in this research.

Table B.1: Example commercial inertial sensors used across different studies with product specifications.

| | **Sensor Type** | | | |
|---|---|---|---|---|
| | **BiostampRC** | **GT3X+** | **MVN** | **Opal** |
| **Manufacturer** | mc10, Inc. | Actigraph, Inc. | Xsens, Inc. | APDM, Inc. |
| **Components of each sensor module** | | | | |
| Accelerometer (range, G) | triaxial (±16) | triaxial (±6) | triaxial (±16) | triaxial (±16) |
| Gyroscope (range, °/s) | triaxial (±2000) | - | triaxial (±2000) | triaxial (±2000) |
| Magnetometer (range, Gauss) | - | - | triaxial (±1.9) | triaxial (±8) |
| **Dimensions (L x W x H, cm)** | 6.6 x 3.4 x 0.45 | 3.3 x 4.6 x 1.5 | 4.7 x 3 x 1.3 | 4.8 x 3.6 x 1.3 |
| **Weight (g)** | 7 | 19 | 16 | 25 |
| **Battery life** | < 3 hours | < 31 days | < 6 hours | < 12 hours |
| **Memory capacity** | 32MB | < 42.5 days | N/A | 8GB |
| **Sampling rate (Hz)** | 15-250 | 30-100 | 60-100 | 20-128 |
| **Sensor attachment** | Directly on skin | Strap | Strap or suit | Strap |
| **Additional sensing modes** | EGC, sEMG | ambient light sensor | - | - |
| **Example citations** | [167] | [86, 90] | [43, 50] | [54, 71] |

# APPENDIX C

# Computing temporal gait parameters from angular velocity of the shank and thigh recorded by inertial sensors

Temporal gait parameters used in the present study were calculated as the time duration between right and left heel-strike and toe-off events and expressed as a percentage (%) of each gait cycle Figure C.1. Detection of heel-strike and toe-off gait events were performed as the first step in a custom algorithm (modified from Aminian et al. [160]). One gait cycle was composed of the sequence of the following events: 1) right heel-strike, 2) left toe-off, 2) left heel-strike, 4) right toe-off, and 5) next right heel-strike. Sagittal angular velocity (rad/s) from inertial sensors on the right and left shank were used to find the signature peaks for each event separately Figure C.1. The procedure is outlined below:

***Step 1*: Detect mid-swing**

Mid-swings were detected by finding the global minimum peaks (Points A in Figure C.1) in the sagittal angular velocity (rad/s) data. To detect the valid global minima representing the mid-swing, Aminian et al. [160] applied a multi-resolution wavelet decomposition. In this paper, we applied two search criteria in terms of the amplitude of the peak and time duration between peaks. First, an amplitude threshold of -1.75 rad/s determined from preliminary testing was applied to identify the global minimum peaks of interest (i.e.,

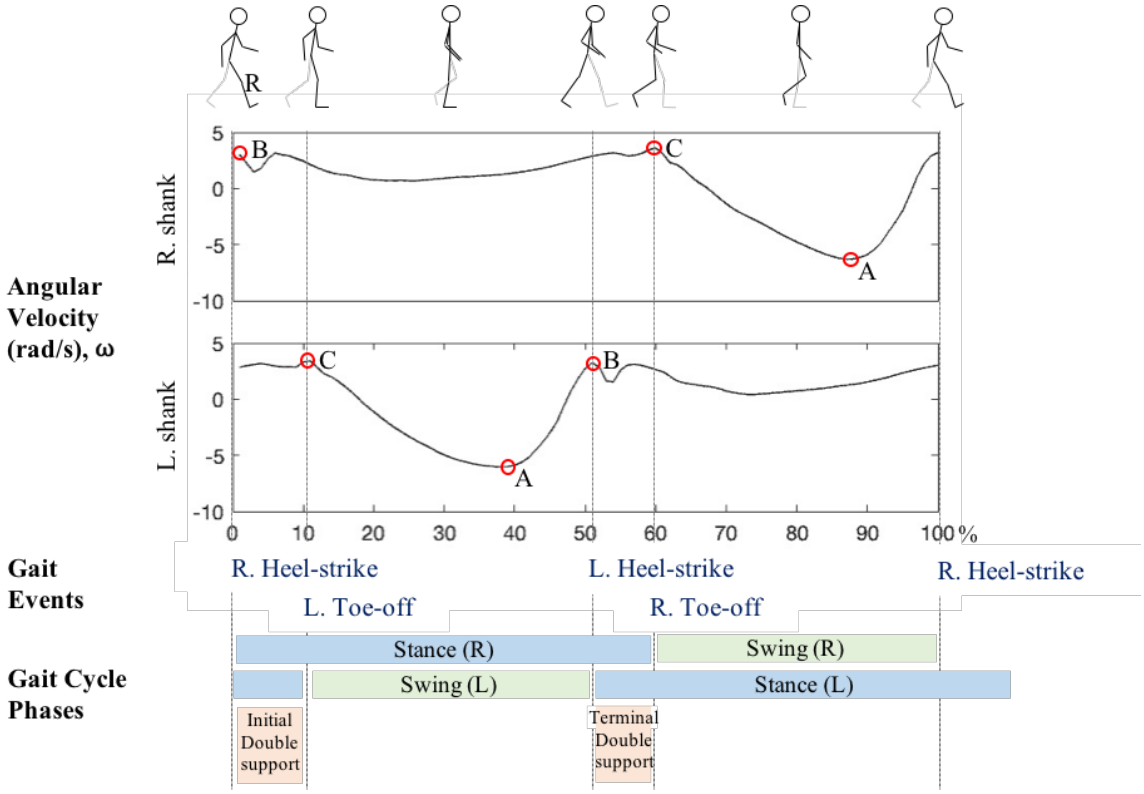



Figure C.1: Graphical overview of the algorithm for detecting temporal gait events, applied to right and left legs separately. Sample profile of the sagittal angular velocity (rad/s) from the right and left shank sensors are depicted for one complete gait cycle (100%) recorded during empty-handed condition.

Points A in Figure C.1) while avoiding Points D after the heel-strike and the minimum peaks during the stance phase (i.e., Points E in Figure C.1). Second, a time threshold of 0.63s was used for the minimum time difference between consecutive global minima to ensure rejection of points D and E in Figure C.1.

***Step 2*: Estimating average gait cycle duration**

Time duration between consecutive mid-swings were calculated to estimate the average gait cycle duration ($\overline{T'}$) using equation C.1.

$$\overline{T'} = \frac{\sum_0^N (T(A)_{i+1} - T(A)_i)}{N} \tag{C.1}$$

where, $T(A)_i$ is an array containing the timeframes for the $i^{th}$ instance of a mid-swing Point A, $N$ is the number of gait cycles detected, and $i = 0$ to $N$.

***Step 3*: Detect heel-strike**

Heel-strikes were detected by finding the local maxima (Points B in Figure C.1) within the range of [$T(A)_i$ + 0.25s, $T(A)_i + \overline{T'}$]. Multiple peaks may be detected within this time range so the search was refined in Step 5.

***Step 4*: Detect Toe-off**

Toe-offs were detected by finding the local maxima (Points C in Figure C.1) within the range of [$T(A)_i$ - $\overline{T'}$, $T(A)_i$ - 0.05s].

***Step 5*: Refine heel-strike**

Heel-strikes were refined amongst the detected heel-strikes from Step 3 by setting the search range of [$T(A)_i$, $T(C)_{i+1}$], where $T(C)_{i+1}$ is the timeframe for i+1 instance of Point C. The first local peak after the mid-swing was selected as the heel-strike.

***Step 6*: Pair heel-strike and toe-off events for each leg**

Heel-strikes and toe-offs detected were paired if the time duration between heel-strike ($T(B)_i$) to toe-off ($T(C)_i$) was within [0.1s, 2.5s]. This pairing starts from the first heel-strike and toe-off in the time series and continued until the last heel-strike. Any heel-strike that does not meet this criterion was discarded.

***Step 7*: Complete the gait cycle by aligning the paired heel-strikes and toe-offs from both legs**

In order to complete the gait cycles, paired heel-strike and toe-off events from both legs were aligned in the following time sequence: right heel-strike $\rightarrow$ left toe-off $\rightarrow$ left toe-off $\rightarrow$ left heel-strike $\rightarrow$ right toe-off $\rightarrow$ next right heel-strike.

***Step 8*: Compute temporal durations between detected gait events**

Six temporal parameters were computed as the time difference between reference gait events (Figure C.1, bottom panel) and expressed as a percentage (%) of a gait cycle duration.

# APPENDIX D

# Estimating stride length from angular velocity of the right shank and thigh recorded by inertial sensors

Stride lengths were estimated using the sagittal angular velocity (rad/s) data from the right thigh ($\omega_{Thigh}$) and right shank ($\omega_{Shank}$) sensors and right thigh length ($l_1$, trochanter height - knee height) and right shank length ($l_2$, knee height). The calculation was performed in a custom algorithm implemented in MATLAB R2016b (The MathWorks Inc., Natick, MA, USA). Leg movement during stance and swing phases were modeled as an inverted double pendulum and double pendulum [160], respectively, as depicted in Figure D.1. During the right stance phase, the right shank and thigh rotate forward by pivoting the right foot on the ground. Although the foot has not moved forward, the body has moved forward by distance $d_1$. During the right swing phase the right foot steps forward by distance $d_2$. Total stride length can be estimated as the sum of $d_1$ and $d_2$ assuming bilateral symmetry, i.e., that right and left step lengths are equal. Stride lengths were calculated for each gait cycle $k$ following the steps:

***Step 1*: Calculate the distance $d_1$ moved during the stance phase**

The distance moved during the right stance phase ($d_1$) was estimated from the trigonometric relations. The angular rotation of the right thigh ($\alpha$) and right shank ($\beta$) were estimated by

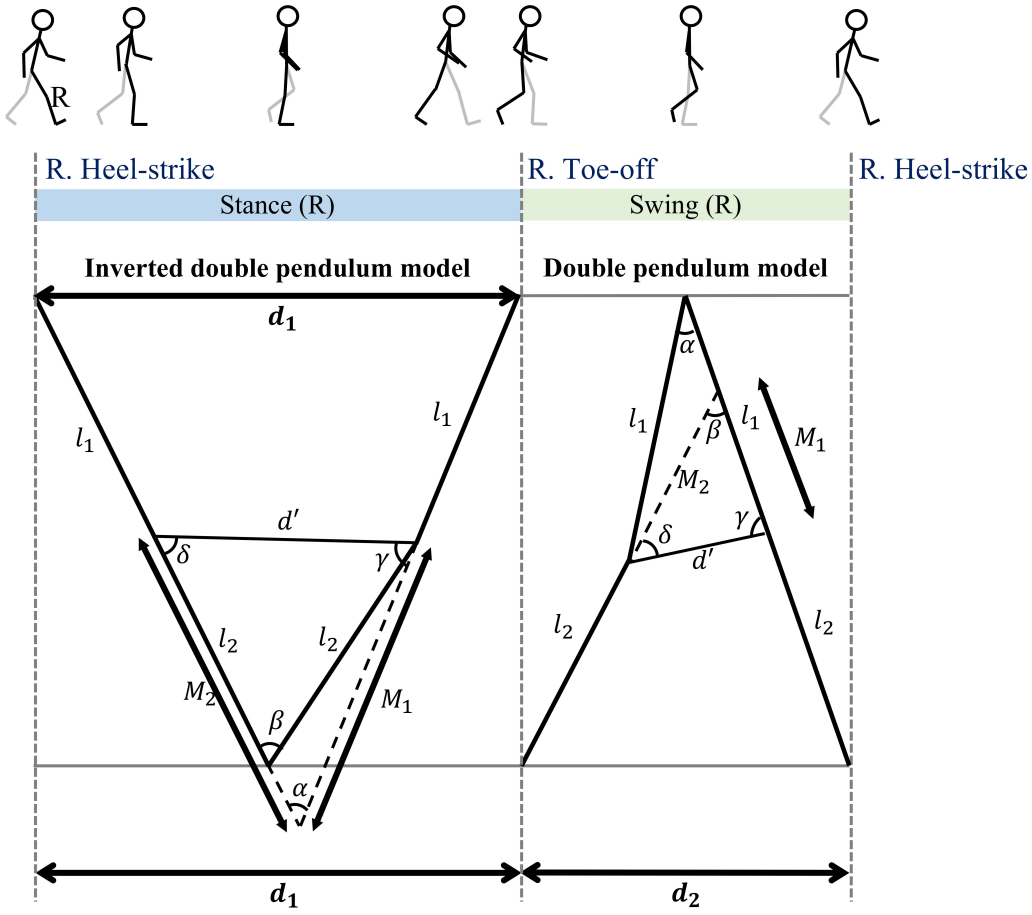



Figure D.1: Graphical summary of the double pendulum model (adapted from Aminian et al.) used for estimating the stride lengths from sagittal angular velocity (rad/s) data of the right shank and right thigh during right stance and swing phases separately.

integrating $\omega_{Thigh}$ and $\omega_{Shank}$, within each gait cycle, respectively. For each gait cycle $k$, we calculated $d_1(k)$ as follows:

$$d_1(k) = \sqrt{(l_1 + M_2(k))^2 + (l_1 + M_1(k))^2 - (l_1 + M_2(k))(l_1 + M_1(k)) \cos\alpha(k)}, \quad \text{(D.1)}$$

where:

$$\alpha(k) = \int_{R.Heel-strike(k)}^{R.Toe-off(k)} \omega_{Thigh}(t)dt, \quad \text{(D.2)}$$

$$\beta(k) = \int_{R.Heel-strike(k)}^{R.Toe-off(k)} \omega_{Shank}(t)dt, \quad \text{(D.3)}$$

$$M_1(k) = \frac{sin\delta(k)}{sin\alpha(k)} d'(k), \quad \text{(D.4)}$$

$$M_2(k) = \frac{sin\gamma(k)}{sin\alpha(k)} d'(k), \quad \text{(D.5)}$$

with:

$$\gamma(k) = \frac{\pi - \alpha(k)}{2}$$

$$\delta(k) = \frac{\pi + \alpha(k) - 2\beta(k)}{2} \quad \text{(D.6)}$$

$$d'(k) = l_2(k) \sqrt{2(1 - cos\beta(k))}$$

***Step 2*: Calculate the distance ($d_2$) moved during the swing phase**

The distance moved during the right swing phase ($d_2$) was estimated as follows:

$$d_2(k) = \sqrt{(l_2 + M_1(k))^2 + (l_2 + M_2(k))^2 - (l_2 + M_1(k))(l_2 + M_2(k)) \cos\beta(k)}, \quad \text{(D.7)}$$

where:

$$\alpha(k) = \int_{R.Toe-off(k)}^{R.Heel-strike(k)} \omega_{Thigh}(t)dt, \quad \text{(D.8)}$$

$$\beta(k) = \int_{R.Toe-off(k)}^{R.Heel-strike(k)} \omega_{Shank}(t)dt, \quad \text{(D.9)}$$

$$M_1(k) = \frac{sin\delta(k)}{sin\beta(k)} d'(k), \quad \text{(D.10)}$$

$$M_2(k) = \frac{sin\gamma(k)}{sin\beta(k)} d'(k), \quad \text{(D.11)}$$

with:

$$\gamma(k) = \frac{\pi - \beta(k)}{2}$$

$$\delta(k) = \frac{\pi - 2\alpha(k) + \beta(k)}{2} \quad \text{(D.12)}$$

$$d'(k) = l_2(k)\sqrt{2(1 - cos\alpha(k))}$$

***Step 3*: Combining $d_1$ and $d_2$**

Stride length is the total distance moved during one gait cycle $k$:

$$Stride\ length(k) = d_1(k) + d_2(k) \quad \text{(D.13)}$$

# APPENDIX E

# Algorithm for calculating the mean thoracic-pelvic relative phase angle

Mean relative phase angle [152] was calculated using the angular velocity (rad/s) data obtained from the torso ($\omega_{T6}$) and pelvis ($\omega_{S1}$) sensors. Additionally, angular displacement (rad, $\theta$) was calculated by integrating the angular velocity data across time within each gait cycle. The algorithm is outlined below along with an example obtained during no-load condition depicted in Figure E.1.

***Step 1*: Calculate normalized angular velocity and angular displacement**

Normalized angular velocity and angular displacement were obtained by rescaling the amplitudes of the data to the range [-1, 1] within each normalized (%) gait cycle separately for each sensor.

***Step 2*: Calculating phase angle**

Phase angles of the torso and pelvis segments ($\phi$) were calculated separately by following the equation E.1.

$$\phi(t) = arctan(\omega(t)/\theta(t)) \tag{E.1}$$

where $\omega$(t) represents the normalized angular velocity time series, $\theta$(t) the normalized

angular displacement, at t = 0, ..., 100%.

***Step 3*: Calculate relative phase angle**

Relative phase angle between torso and pelvis was obtained following the equation E.2.

$$\Delta\phi(t) = \phi_{T6}(t) - \phi_{S1}(t) \tag{E.2}$$

***Step 4*: Calculate mean relative phase angle**

Mean relative phase angle, which was the dependent measure used in the present study, was computed as the average of the relative phase angle over one gait cycle.

$$\Delta\overline{\phi} = \frac{\sum_{t=0}^{N} \Delta\phi(t)}{N} \tag{E.3}$$

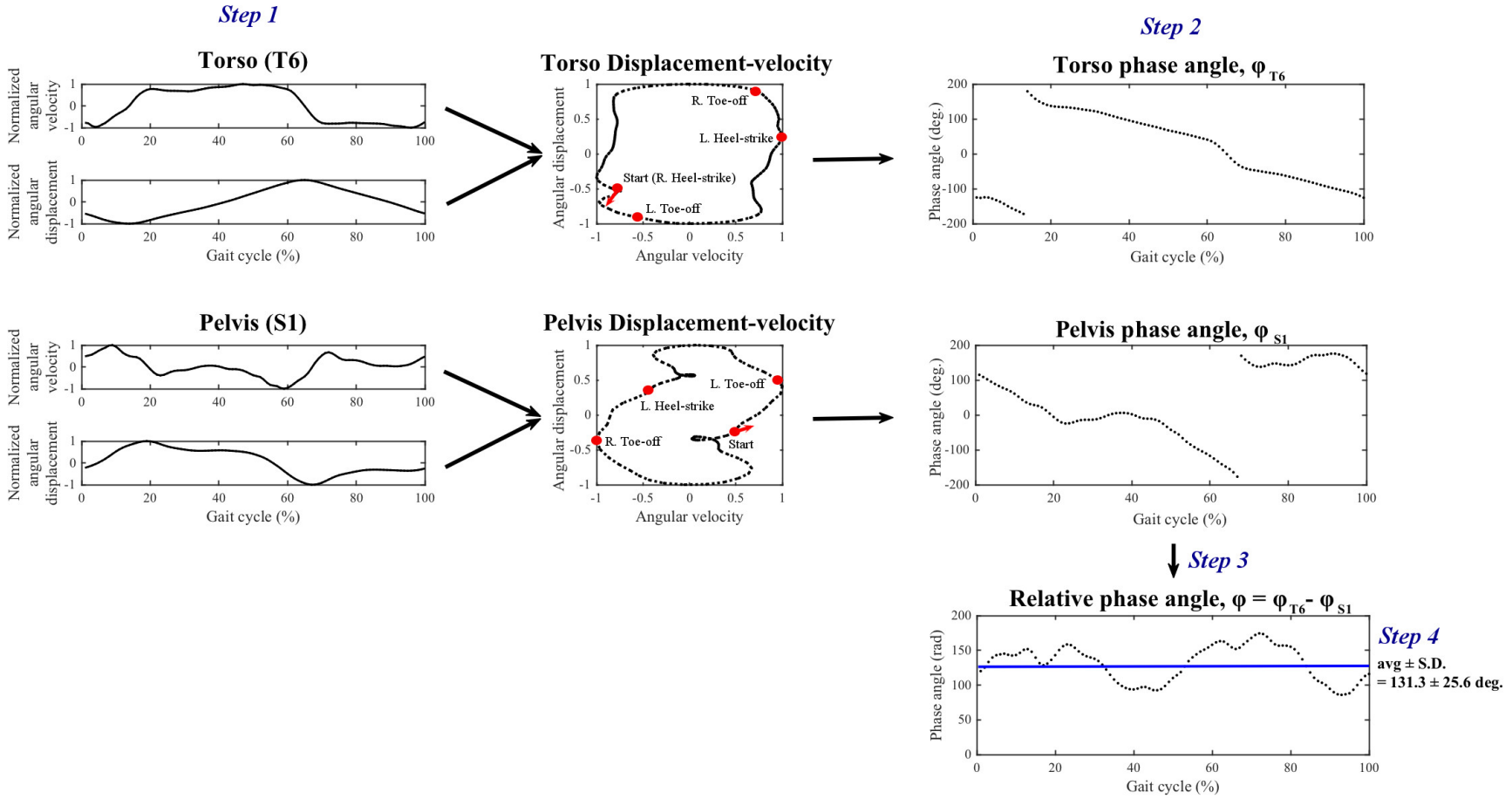



Figure E.1: Overview of the algorithm for computing mean thoracic-pelvic relative phase angle using one exemplar participant data from the no-load condition in the coronal plane.

# APPENDIX F

# Detecting lowering and lifting from thoracic angular displacement and velocity recorded by inertial sensor located at T6

Lifting-lowering parameters used in the present study were calculated for detected lowering (or bending if empty-handed) and lifting (or rising if empty-handed) phases. Detection of lowering and lifting were performed in a custom algorithm implemented in MATLAB R2016b (The MathWorks Inc., Natick, MA, USA). One lifting-lowering task was composed of the sequence of the following events: 1) start-lowering, 2) end-lowering or start-lifting, which assumed to be happening at the same time, and 3) end-lifting. Sagittal angular displacement (°) and velocity (°/s) from inertial sensors attached on the T6 was used to find the signature peaks for each event. The procedure is outlined below:

***Step 1*: Detect end-lowering or start-lifting**

End of the lowering and start of the lifting were assumed to be coincident in time. End-lowerings were detected by finding the global maximum peaks (Point A in Figure F.1 in the sagittal torso flexion angle (°). To detect the valid global maximum representing the end-lowering, an amplitude threshold of 30% of the maximum reference bending angle (°) averaged over two repetitions of knee height lowering of each participant was applied (Point A in Figure F.1).

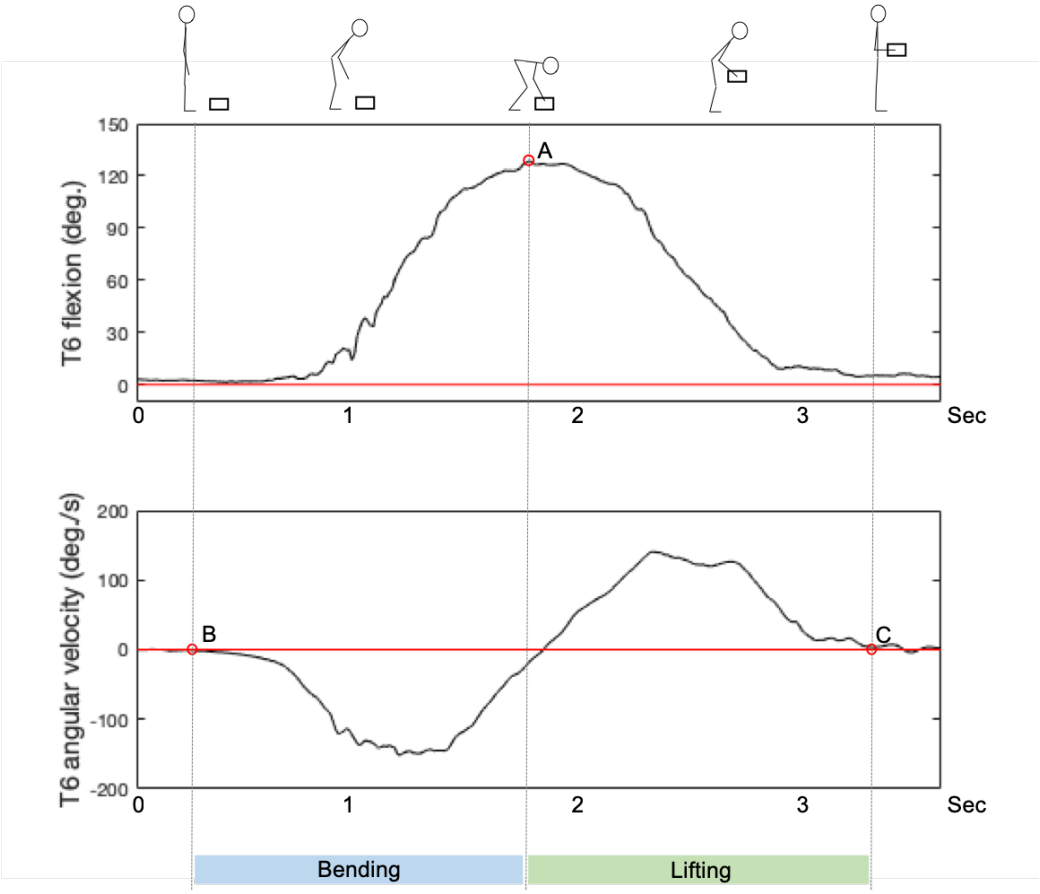



Figure F.1: Graphical overview of the algorithm for detecting start and end of lowering and lifting phases. Sample profile of the sagittal angle (°) and angular velocity (°/s) from the upper back (T6) sensor are depicted for one complete bending and lifting trial recorded during a two-handed anterior lifting condition.

***Step 2*: Detect start-lowering**

Start-lowerings (Point B in Figure F.1) were detected by finding the last negative-going zero-crossing of the sagittal torso flexion angular velocity (°/s) within the range of [$T(A)_i$ - 3s, $T(A)_i$], where $T(A)_i$ is the time for the $i^{th}$ instance of a end-lowering Point A.

***Step 3*: Detect end-lifting**

End-liftings (Point C in Figure F.1) were detected by finding the the first negative-going zero-crossing of the sagittal torso flexion angular velocity (°/s) within the range of [$T(A)_i$, $T(A)_i$ + 3s].

# APPENDIX G

# Algorithm for calculating low back compression force ($F_c$)

Low back compression forces ($F_c$) calculated in the present study used both body postural angles (i.e., torso flexion angle in the sagittal plane measured at T6) obtained from the inertial sensor data as well as the information from detected task type and predicted task conditions.

**Assumptions:**

- Segment length was calculated as a fraction of individual stature using proportionality constants developed by Drillis and Contini [234]. Hip height from the floor was calculated as 53% of stature. Lower arm length was estimated as 14.6% of stature.
- The location of the CoM of the upper body (i.e., Head, arms, and trunk; HAT) from the hip was estimated by 62.6% of (Stature - Hip height) [235].
- Hand load of 2.3 kg and 18.1 kg were used in the calculation for the predicted load level of low (i.e., no-load or 4.5 kg) and high (i.e., 13.6 kg or 22.7 kg), respectively.
- The moment arm from the center of the hand load to the L5/S1 ($h$) is estimated based on the location of the box the person is carrying, lifting, or lowering.

- The moment arm '$E$' of the back extensor muscle at L5/S1 was set to a constant value of 6.5 cm based on findings by Chaffin et al. [236].

- The sacral cutting plane angle '$\alpha$' was assumed to be the same as the torso flexion ($\theta_{TF}$) angle.

**Formulation:** The compression force at the L5/S1 intervertebral disc at each time frame was computed by following Equation G.1 to G.7. Low-back biomechanical model is depicted in Figure G.1.

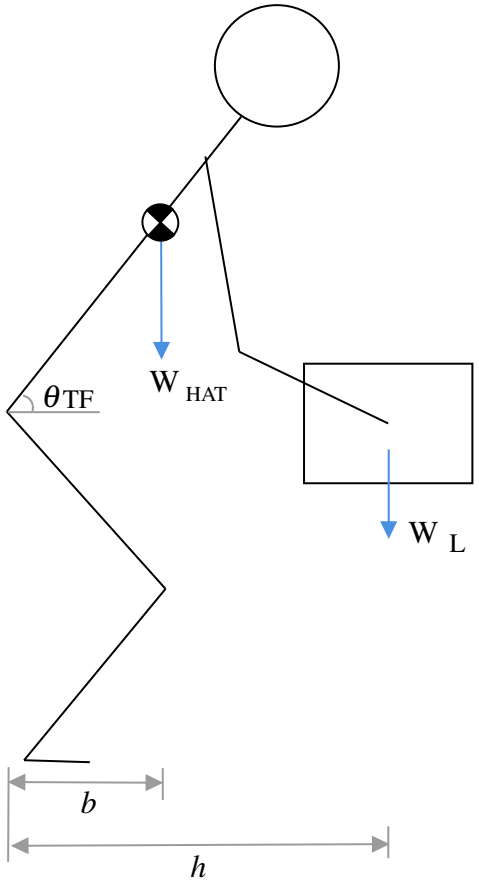



Figure G.1: Low-back biomechanical model based on inverse kinematics for calculating low-back compression forces ($F_c$) as a function of posture, internal ($W_{HAT}$) and external ($W_L$) loads and corresponding moment arms, $b$ and $h$.

The spinal load due to mass of the head, arms, and torso ($F_{HAT}$) is calculated as:

$$F_{HAT} = (W_{HAT} * b)/E \tag{G.1}$$

where:

$$\begin{aligned} W_{HAT} &= 0.678 * m_{Body} * 9.81, \\ b &= 0.626 * (Stature - HipHeight) * cos(\theta_{TF}) \end{aligned} \tag{G.2}$$

The spinal load due to mass of the hand load ($F_L$) is calculated as:

$$F_L = (W_L * h)/E \tag{G.3}$$

where:

$$W_L = \begin{cases} \text{true load * 9.81} & \text{, for } \textit{true} \\ \text{2.3 kg * 9.81} & \text{, if predicted as low load} \\ \text{18.1 kg * 9.81} & \text{, if predicted as high load} \end{cases} \tag{G.4}$$

and,

$$h = \begin{cases} 0 & \text{, if predicted or true carrying mode was one-handed or 2H-Side carry} \\ \text{Stature * 0.146} & \text{, if predicted or true carrying mode was 2H-Anterior} \\ \text{(Stature - Hip Height)} * cos(\theta_{TF}) + 25.4 * sin(\theta_{TF}) & \text{, for } \textit{lifting-lowering} \end{cases} \tag{G.5}$$

$F_M$ is the spinal load due to activation of the low back extensor muscle and calculated as:

$$F_M = F_{HAT} + F_L \tag{G.6}$$

Finally, $F_c$ is the low-back compression forces at the L5/S1 intervertebral disc and calculated as:

$$F_c = -cos(\theta_{TF}) * F_{HAT} - cos(\theta_{TF}) * F_L - F_M \tag{G.7}$$

Figure G.2 depicts a two-handed anterior load carriage when the person is upright. In this example, the moment arm from the center of the HAT to the L5/S1 disc is zero ($b = 0$), so the $F_c$ becomes:

$$F_c = -cos(\theta_{TF}) * F_L - F_L \tag{G.8}$$

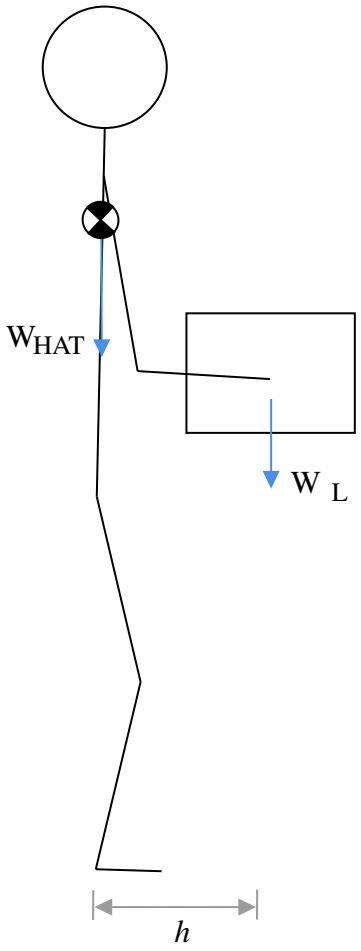



Figure G.2: Low-back biomechanical model based on inverse kinematics for calculating low-back compression forces ($F_c$) when the torso is in upright posture during two-handed anterior carry of load.

# BIBLIOGRAPHY


[1] Marras, W. S., Lavender, S. A., Leurgans, S. E., Fathallah, F. A., Ferguson, S. A., Gary Allread, W., and Rajulu, S. L., "Biomechanical risk factors for occupationally related low back disorders," *Ergonomics*, Vol. 38, No. 2, 1995, pp. 377–410.

[2] Putz-Anderson, V., Bernard, B. P., Burt, S. E., Cole, L. L., Fairfield-Estill, C., Fine, L. J., Grant, K. A., Gjessing, C. C., Jenkins, L., and Hurrell Jr, J. J., "Musculoskeletal disorders and workplace factors," *National Institute for Occupational Safety and Health (NIOSH)*, Vol. 104, 1997.

[3] Punnett, L., Fine, L. J., Keyserling, W. M., Herrin, G. D., and Chaffin, D. B., "Back disorders and nonneutral trunk postures of automobile assembly workers," *Scandinavian journal of work, environment & health*, 1991, pp. 337–346.

[4] Keyserling, W. M., Brouwer, M., and Silverstein, B. A., "A checklist for evaluating ergonomic risk factors resulting from awkward postures of the legs, trunk and neck," *International Journal of Industrial Ergonomics*, Vol. 9, No. 4, 1992, pp. 283–301.

[5] David, G., "Ergonomic methods for assessing exposure to risk factors for work-related musculoskeletal disorders," *Occupational medicine*, Vol. 55, No. 3, 2005, pp. 190–199.

[6] Winkel, J. and Mathiassen, S. E., "Assessment of physical work load in epidemiologic studies: concepts, issues and operational considerations," *Ergonomics*, Vol. 37, No. 6, 1994, pp. 979–988.

[7] Jensen, R. C., "Epidemiology of work-related back pain," *Top Acute Care Trauma Rehabil*, Vol. 2, No. 3, 1988, pp. 1–15.

[8] Videman, T., Nurminen, T., Tola, S., Kuorinka, I., Vanharanta, H., and Troup, J., "Low-back pain in nurses and some loading factors of work." *Spine*, Vol. 9, No. 4, 1984, pp. 400–404.

[9] Garg, A. and Owen, B., "Reducing back stress to nursing personnel: an ergonomic intervention in a nursing home," *Ergonomics*, Vol. 35, No. 11, 1992, pp. 1353–1375.

[10] Knibbe, N. E. and Knibbe, H. J., "Postural load of nurses during bathing and showering of patients: Results of a laboratory study," *Professional Safety*, Vol. 41, No. 11, 1996, pp. 37.

[11] Liira, J. P., Shannon, H. S., Chambers, L. W., and Haines, T. A., "Long-term back problems and physical work exposures in the 1990 Ontario Health Survey." *American Journal of Public Health*, Vol. 86, No. 3, 1996, pp. 382–387.

[12] Waters, T. R., Putz-Anderson, V., and Baron, S., "Methods for assessing the physical demands of manual lifting: a review and case study from warehousing," *American Industrial Hygiene Association Journal*, Vol. 59, No. 12, 1998, pp. 871–881.

[13] Sharp, M. A., Rice, V. J., Nindl, B. C., and Williamson, T. L., "Effects of team size on the maximum weight bar lifting strength of military personnel," *Human factors*, Vol. 39, No. 3, 1997, pp. 481–488.

[14] Gold, J. E., Park, J.-S., and Punnett, L., "Work routinization and implications for ergonomic exposure assessment," *Ergonomics*, Vol. 49, No. 1, 2006, pp. 12–27.

[15] Mathiassen, S. E., "Diversity and variation in biomechanical exposure: what is it, and why would we like to know?" *Applied ergonomics*, Vol. 37, No. 4, 2006, pp. 419–427.

[16] Silverstein, B. A., Fine, L. J., and Armstrong, T. J., "Hand wrist cumulative trauma disorders in industry," *British journal of industrial medicine*, Vol. 43, No. 11, 1986, pp. 779–784.

[17] Paquet, V., Punnett, L., Woskie, S., and Buchholz, B., "Reliable exposure assessment strategies for physical ergonomics stressors in construction and other non-routinized work," *Ergonomics*, Vol. 48, No. 9, 2005, pp. 1200–1219.

[18] Buchholz, B., Paquet, V., Punnett, L., Lee, D., and Moir, S., "PATH: a work sampling-based approach to ergonomic job analysis for construction and other non-repetitive work," *Applied ergonomics*, Vol. 27, No. 3, 1996, pp. 177–187.

[19] Karhu, O., Kansi, P., and Kuorinka, I., "Correcting working postures in industry: a practical method for analysis," *Applied ergonomics*, Vol. 8, No. 4, 1977, pp. 199–201.

[20] McAtamney, L. and Corlett, E. N., "RULA: a survey method for the investigation of work-related upper limb disorders," *Applied ergonomics*, Vol. 24, No. 2, 1993, pp. 91–99.

[21] Hignett, S. and McAtamney, L., "Rapid entire body assessment (REBA)," *Applied ergonomics*, Vol. 31, No. 2, 2000, pp. 201–205.

[22] Radwin, R. G. and Lin, M. L., "An analytical method for characterizing repetitive motion and postural stress using spectral analysis," *Ergonomics*, Vol. 36, No. 4, 1993, pp. 379–389.

[23] Marras, W., Fathallah, F., Miller, R., Davis, S., and Mirka, G., "Accuracy of a three-dimensional lumbar motion monitor for recording dynamic trunk motion characteristics," *International Journal of Industrial Ergonomics*, Vol. 9, No. 1, 1992, pp. 75–87.

[24] Hansson, G., Asterland, P., Holmer, N. g., and Skerfving, S., "Validity and reliability of triaxial accelerometers for inclinometry in posture analysis," *Medical and Biological Engineering and Computing*, Vol. 39, No. 4, 2001, pp. 405–13.

[25] Cordero, A. F., Koopman, H., and Van Der Helm, F., "Use of pressure insoles to calculate the complete ground reaction forces," *Journal of biomechanics*, Vol. 37, No. 9, 2004, pp. 1427–1432.

[26] Faber, G. S., Kingma, I., and van DieÃńn, J. H., "Bottom-up estimation of joint moments during manual lifting using orientation sensors instead of position sensors," *Journal of biomechanics*, Vol. 43, No. 7, 2010, pp. 1432–1436.

[27] Castro, M. C. F. and Cliquet, A., "A low-cost instrumented glove for monitoring forces during object manipulation," *IEEE Transactions on Rehabilitation Engineering*, Vol. 5, No. 2, 1997, pp. 140–147.

[28] Theado, E., Knapik, G., and Marras, W., "Modification of an EMG-assisted biomechanical model for pushing and pulling," *International Journal of Industrial Ergonomics*, Vol. 37, No. 11, 2007, pp. 825–831.

[29] Bergmann, J. H., Mayagoitia, R. E., and Smith, I. C., "A portable system for collecting anatomical joint angles during stair ascent: a comparison with an optical tracking device," *Dyn Med*, Vol. 8, 2009, pp. 3.

[30] Barbour, N. and Schmidt, G., "Inertial sensor technology trends," *IEEE sensors journal*, Vol. 1, No. 4, 2001, pp. 332–339.

[31] Scott, K. A. and Browning, R. C., "Occupational physical activity assessment for chronic disease prevention and management: A review of methods for both occupational health practitioners and researchers," *J Occup Environ Hyg*, Vol. 13, No. 6, 2016, pp. 451–63.

[32] Schall Jr., M. C., Sesek, R. F., and Cavuoto, L. A., "Barriers to the Adoption of Wearable Sensors in the Workplace: A Survey of Occupational Safety and Health Professionals," *Human factors*, 2018, pp. 0018720817753907.

[33] Lim, S. and D'Souza, C., "A Systematic Review of Inertial Sensing-Based Approaches to Ergonomic Exposure Assessment," in preparation.

[34] Pedley, M., "Tilt sensing using a three-axis accelerometer," *Freescale semiconductor application note*, Vol. 1, 2013, pp. 2012–2013.

[35] Luinge, H. J., *Inertial sensing of human movement*, Twente University Press Enschede, 2002.

[36] Abyarjoo, F., Barreto, A., Cofino, J., and Ortega, F. R., *Implementing a sensor fusion algorithm for 3D orientation detection with inertial/magnetic sensors*, Springer, 2015, pp. 305–310.

[37] Foxlin, E., "Inertial head-tracker sensor fusion by a complementary separate-bias Kalman filter," *Virtual Reality Annual International Symposium, 1996., Proceedings of the IEEE 1996*, IEEE, pp. 185–194.

[38] Liberty Mutual Insurance, https://www.libertymutualgroup.com/about-liberty-mutual-site/research-institute-site/Pages/Workplace-Safety-Index.aspx, 2017, [Online; accessed 04-09-2019].

[39] Moher, D., Liberati, A., Tetzlaff, J., Altman, D. G., and Group, P., "Reprint-preferred reporting items for systematic reviews and meta-analyses: the PRISMA statement," *Physical therapy*, Vol. 89, No. 9, 2009, pp. 873–880.

[40] Teschke, K., Trask, C., Johnson, P., Chow, Y., Village, J., and Koehoorn, M., "Measuring posture for epidemiology: Comparing inclinometry, observations and self-reports," *Ergonomics*, Vol. 52, No. 9, 2009, pp. 1067–1078.

[41] Faber, G. S., Chang, C. C., Kingma, I., Dennerlein, J. T., and van Dieen, J. H., "Estimating 3D L5/S1 moments and ground reaction forces during trunk bending using a full-body ambulatory inertial motion capture system," *J Biomech*, Vol. 49, No. 6, 2016, pp. 904–912.

[42] Holmes, M. W. R., Hodder, J. N., and Keir, P. J., "Continuous assessment of low back loads in long-term care nurses," *Ergonomics*, Vol. 53, No. 9, 2010, pp. 1108–1116.

[43] Kim, S. and Nussbaum, M. A., "Performance evaluation of a wearable inertial motion capture system for capturing physical exposures during manual material handling tasks," *Ergonomics*, Vol. 56, No. 2, 2013, pp. 314–326.

[44] Faber, G., Chang, C. C., Kingma, I., and Dennerlein, J. T., "A novel wearable measurement system for ambulatory assessment of joint loading in the occupational setting," *Work-a Journal of Prevention Assessment & Rehabilitation*, Vol. 41, 2012, pp. 5527–5528.

[45] Shojaei, I., Vazirian, M., Croft, E., Nussbaum, M. A., and Bazrgari, B., "Age related differences in mechanical demands imposed on the lower back by manual material handling tasks," *Journal of Biomechanics*, Vol. 49, No. 6, 2016, pp. 896–903.

[46] Gholipour, A. and Arjmand, N., "Artificial neural networks to predict 3D spinal posture in reaching and lifting activities; Applications in biomechanical models," *Journal of Biomechanics*, Vol. 49, No. 13, 2016, pp. 2946–2952.

[47] Valero, E., Sivanathan, A., BoschÃl', F., and Abdel-Wahab, M., "Musculoskeletal disorders in construction: A review and a novel system for activity tracking with body area network," *Applied Ergonomics*, Vol. 54, 2016, pp. 120.

[48] Nocerino, E., Ackermann, S., Del Pizzo, S., Menna, F., and Troisi, S., "Low-cost human motion capture system for postural analysis onboard ships," *SPIE*, Vol. 8085, SPIE, Bellingham, WA,United States.

[49] Battini, D., Persona, A., and Sgarbossa, F., "Innovative real-time system to integrate ergonomic evaluations into warehouse design and management," *Computers & Industrial Engineering*, Vol. 77, 2014, pp. 1–10.

[50] Robert-Lachaine, X., Mecheri, H., Larue, C., and Plamondon, A., "Validation of inertial measurement units with an optoelectronic system for whole-body motion analysis," *Medical & Biological Engineering & Computing*, Vol. 55, No. 4, 2017, pp. 609–619.

[51] Jonker, D., Rolander, B., and Balogh, I., "Relation between perceived and measured workload obtained by long-term inclinometry among dentists," *Applied ergonomics*, Vol. 40, No. 3, 2009, pp. 309–315.

[52] Moriguchi, C. S., Carnaz, L., Veiersted, K. B., Hanvold, T. N., Haeg, L. B., Hansson, G.-Ã., and Coury, H. J. C. G., "Occupational posture exposure among construction electricians," *Applied Ergonomics*, Vol. 44, No. 1, 2013, pp. 86.

[53] Vignais, N., Miezal, M., Bleser, G., Mura, K., Gorecky, D., and Marin, F., "Innovative system for real-time ergonomic feedback in industrial manufacturing," *Applied Ergonomics*, Vol. 44, No. 4, 2013, pp. 566.

[54] Yu, D., Dural, C., Morrow, M. M., Yang, L., Collins, J. W., Hallbeck, S., Kjellman, M., and Forsman, M., "Intraoperative workload in robotic surgery assessed by wearable motion tracking sensors and questionnaires," *Surg Endosc*, Vol. 31, No. 2, 2017, pp. 877–886.

[55] Bonnet, S. and Heliot, R., "Magnetometer-based approach for studying human movements," *Ieee Transactions on Biomedical Engineering*, Vol. 54, No. 7, 2007, pp. 1353–1355.

[56] Lebel, K., Boissy, P., Nguyen, H., and Duval, C., "Inertial measurement systems for segments and joints kinematics assessment: towards an understanding of the variations in sensors accuracy," *Biomedical Engineering Online*, Vol. 16, 2017.

[57] Schall Jr., M. C., Fethke, N. B., Chen, H., Oyama, S., and Douphrate, D. I., "Accuracy and repeatability of an inertial measurement unit system for field-based occupational studies," *Ergonomics*, Vol. 59, No. 4, 2016, pp. 591–602.

[58] Amasay, T., Latteri, M., and Karduna, A. R., "In Vivo Measurement of Humeral Elevation Angles and Exposure Using a Triaxial Accelerometer," *Human Factors*, Vol. 52, No. 6, 2010, pp. 616.

[59] Favre, J., Jolles, B. M., Aissaoui, R., and Aminian, K., "Ambulatory measurement of 3D knee joint angle," *Journal of Biomechanics*, Vol. 41, No. 5, 2008, pp. 1029–1035.

[60] Dejnabadi, H., Jolles, B. M., and Aminian, K., "A new approach to accurate measurement of uniaxial joint angles based on a combination of accelerometers and gyroscopes," *Ieee Transactions on Biomedical Engineering*, Vol. 52, No. 8, 2005, pp. 1478–1484.

[61] Schall Jr., M. C., Fethke, N. B., Chen, H., and Gerr, F., "A comparison of instrumentation methods to estimate thoracolumbar motion in field-based occupational studies," *Appl Ergon*, Vol. 48, 2015, pp. 224–31.

[62] Dahlqvist, C., Hansson, G.-Ã., and Forsman, M., "Validity of a small low-cost triaxial accelerometer with integrated logger for uncomplicated measurements of postures and movements of head, upper back and upper arms," *Applied Ergonomics*, Vol. 55, 2016, pp. 108.

[63] Schiefer, C., Kraus, T., Ellegast, R. P., and Ochsmann, E., "A technical support tool for joint range of motion determination in functional diagnostics - an inter-rater study," *Journal of Occupational Medicine and Toxicology*, Vol. 10, 2015.

[64] Stenlund, T. C., ÃŰhberg, F., LundstrÃűm, R., Lindroos, O., HÃd'ger, C., and Rehn, B., "Inter- and intra-tester reliability when measuring seated spinal postures with inertial sensors," *International Journal of Industrial Ergonomics*, Vol. 44, No. 5, 2014, pp. 732.

[65] Ambusam, S., Omar, B., Joseph, L., Meng, S. P., and Padzil, F. A. M., "Is a triaxial accelerometer a reliable device to measure head excursion?" *Technology and Health Care*, Vol. 23, No. 5, 2015, pp. 691–697.

[66] Pedersen, S. J., Kitic, C. M., Bird, M.-L., Mainsbridge, C. P., and Cooley, P. D., "Is self-reporting workplace activity worthwhile? Validity and reliability of occupational sitting and physical activity questionnaire in desk-based workers," *BMC Public Health*, Vol. 16, 2016.

[67] Wick, K., Faude, O., Schwager, S., Zahner, L., and Donath, L., "Deviation between self-reported and measured occupational physical activity levels in office employees: effects of age and body composition," *International Archives of Occupational and Environmental Health*, Vol. 89, No. 4, 2016, pp. 575–582.

[68] Whitfield, G. P., Pettee Gabriel, K. K., and Kohl, H. W., "Assessing Sitting across Contexts: Development of the Multicontext Sitting Time Questionnaire," *Research Quarterly for Exercise and Sport*, Vol. 84, No. 3, 2013, pp. 323–328.

[69] Village, J., Trask, C., Luong, N., Chow, Y., Johnson, P., Koehoorn, M., and Teschke, K., "Development and evaluation of an observational Back-Exposure Sampling Tool (Back-EST) for work-related back injury risk factors," *Applied ergonomics*, Vol. 40, No. 3, 2009, pp. 538–544.

[70] Arvidsson, I., Balogh, I., Hansson, G.-Ã., Ohlsson, K., ÃĚkesson, I., and Nordander, C., "Rationalization in meat cutting - Consequences on physical workload," *Applied Ergonomics*, Vol. 43, No. 6, 2012, pp. 1.

[71] Bertrand, P., Reyes, S., and Newman, D., "Pressure and kinematic in-suit sensors: Assessing human-suit interaction for injury risk mitigation," *The Institute of Electrical and Electronics Engineers, Inc. (IEEE) Conference Proceedings.*, 2016, pp. 1–10.

[72] Douphrate, D. I., Fethke, N. B., Nonnenmann, M. W., Rosecrance, J. C., and Reynolds, S. J., "Full shift arm inclinometry among dairy parlor workers: A feasibility study in a challenging work environment," *Applied Ergonomics*, Vol. 43, No. 3, 2012, pp. 604.

[73] Lagersted-Olsen, J., Thomsen, B. L., Holtermann, A., Sogaard, K., and Jorgensen, M. B., "Does objectively measured daily duration of forward bending predict development and aggravation of low-back pain? A prospective study," *Scandinavian Journal of Work Environment & Health*, Vol. 42, No. 6, 2016, pp. 528–537.

[74] Villumsen, M., Madeleine, P., JØrgensen, M. B., Holtermann, A., and Samani, A., "Social support modifies association between forward bending of the trunk and low-back pain: Cross-sectional field study of blue-collar workers," *Scandinavian Journal of Work Environment & Health*, Vol. 42, No. 2, 2016, pp. 125–134.

[75] Breidahl, T., Christensen, M., Jepsen, J. R., and Omland, O., "The influence of vessel movements on the energy expenditure of fishermen in relation to activities and occupational tasks on board," *International Maritime Health*, Vol. 66, No. 4, 2015, pp. 196–202.

[76] Busser, H. J., de Korte, W. G., Glerum, E. B., and van Lummel, R. C., "Method for objective assessment of physical work load at the workplace," *Ergonomics*, Vol. 41, No. 10, 1998, pp. 1519–1526.

[77] Brandt, M., Madeleine, P., Samani, A., Jakobsen, M. D., Skals, S., Vinstrup, J., and Andersen, L. L., "Accuracy of identification of low or high risk lifting during standardised lifting situations," *Ergonomics*, Vol. 61, No. 5, 2018, pp. 710–719.

[78] Kim, S. and Nussbaum, M. A., "An evaluation of classification algorithms for manual material handling tasks based on data obtained using wearable technologies," *Ergonomics*, Vol. 57, No. 7, 2014, pp. 1040–1051.

[79] Peppoloni, L., Filippeschi, A., Ruffaldi, E., and Avizzano, C. A., "(WMSDs issue) A novel wearable system for the online assessment of risk for biomechanical load in repetitive efforts," *International Journal of Industrial Ergonomics*, Vol. 52, 2016, pp. 1–11.

[80] Heiden, M., Garza, J., Trask, C., and Mathiassen, S. E., "Predicting Directly Measured Trunk and Upper Arm Postures in Paper Mill Work From Administrative Data, Workers' Ratings and Posture Observations," *Annals of Work Exposures and Health*, Vol. 61, No. 2, 2017, pp. 207–217.

[81] Borg, G. A., "Psychophysical Bases of Perceived Exertion," *Medicine and Science in Sports and Exercise*, Vol. 14, No. 5, 1982, pp. 377–381.

[82] Nath, N. D., Akhavian, R., and Behzadan, A. H., "Ergonomic analysis of construction worker's body postures using wearable mobile sensors," *Appl Ergon*, Vol. 62, 2017, pp. 107–117.

[83] Arias, O. E., Umukoro, P. E., Stofell, S., Dennerlein, J. T., and Sorensen, G., "Association between Trunk Flexion and Physical Activity in Patient Care Unit Workers," *Proceedings of the Human Factors and Ergonomics Society Annual Meeting*, Vol. 56, SAGE Publications Sage CA: Los Angeles, CA, pp. 1188–1191.

[84] Arias, O. E., Umukoro, P. E., Stoffel, S. D., Hopcia, K., Sorensen, G., and Dennerlein, J. T., "Associations between trunk flexion and physical activity of patient care workers for a single shift: A pilot study," *Work*, Vol. 56, No. 2, 2017, pp. 247–255.

[85] Straker, L., Campbell, A., Mathiassen, S. E., Abbott, R. A., Parry, S., and Davey, P., "Capturing the Pattern of Physical Activity and Sedentary Behavior: Exposure Variation Analysis of Accelerometer Data," *Journal of Physical Activity & Health*, Vol. 11, No. 3, 2014, pp. 614–625.

[86] Waters, C. N., Er, P. L., Chu, A. H. Y., Ng, S. H. X., Chia, A., Yee Wei, L., and Muller-Riemenschneider, F., "Assessing and understanding sedentary behaviour in office-based working adults: a mixed-method approach," *BMC Public Health*, Vol. 16, 2016.

[87] Uiterwaal, M., Glerum, E., Busser, H., and Van Lummel, R., "Ambulatory monitoring of physical activity in working situations, a validation study," *Journal of medical engineering & technology*, Vol. 22, No. 4, 1998, pp. 168–172.

[88] Skotte, J., Korshøj, M., Kristiansen, J., Hanisch, C., and Holtermann, A., "Detection of physical activity types using triaxial accelerometers," *Journal of physical activity and health*, Vol. 11, No. 1, 2014, pp. 76–84.

[89] Alvarez, D., Alvarez, J. C., Gonzalez, R. C., and Lopez, A. M., "Upper limb joint angle measurement in occupational health," *Comput Methods Biomech Biomed Engin*, Vol. 19, No. 2, 2016, pp. 159–70.

[90] Villumsen, M., Madeleine, P., Jørgensen, M. B., Holtermann, A., and Samani, A., "The variability of the trunk forward bending in standing activities during work vs. leisure time," *Applied Ergonomics*, Vol. 58, 2017, pp. 273.

[91] Acuna, M. and Karduna, A. R., "Wrist activity monitor counts are correlated with dynamic but not static assessments of arm elevation exposure made with a triaxial accelerometer," *Ergonomics*, Vol. 55, No. 8, 2012, pp. 963–970.

[92] Åkesson, I., Balogh, I., and Hansson, G.-Å., "Physical workload in neck, shoulders and wrists/hands in dental hygienists during a work-day," *Applied Ergonomics*, Vol. 43, No. 4, 2012, pp. 803–811.

[93] Bergsten, E. L., Mathiassen, S. E., Kwak, L., and Vingard, E., "Daily Shoulder Pain Among Flight Baggage Handlers and its Association With Work Tasks and Upper Arm Postures on the Same Day," *Annals of Work Exposures and Health*, Vol. 61, No. 9, 2017, pp. 1145–1153.

[94] Brandt, M., Madeleine, P., Ajslev, J. Z., Jakobsen, M. D., Samani, A., Sundstrup, E., Kines, P., and Andersen, L. L., "Participatory intervention with objectively measured physical risk factors for musculoskeletal disorders in the construction industry: study protocol for a cluster randomized controlled trial," *BMC Musculoskelet Disord*, Vol. 16, 2015, pp. 302.

[95] Estill, C. F., MacDonald, L. A., Wenzl, T. B., and Petersen, M. R., "Use of accelerometers as an ergonomic assessment method for arm acceleration-a large-scale field trial," *Ergonomics*, Vol. 43, No. 9, 2000, pp. 1430–45.

[96] Hansson, G.-A., Balogh, I., Ohlsson, K., Granqvist, L., Nordander, C., Arvidsson, I., Aakesson, I., Unge, J., Rittner, R., Stroemberg, U., and Skerfving, S., "Physical workload in various types of work: Part II. Neck, shoulder and upper arm," *International Journal of Industrial Ergonomics*, Vol. 40, No. 3, 2010, pp. 267–281.

[97] Hodder, J. N., Holmes, M. W. R., and Keir, P. J., "Continuous assessment of work activities and posture in long-term care nurses," *Ergonomics*, Vol. 53, No. 9, 2010, pp. 1097–1107.

[98] Horn, G. P., Kesler, R. M., Motl, R. W., Hsiao-Wecksler, E. T., Klaren, R. E., Ensari, I., Petrucci, M. N., Fernhall, B., and Rosengren, K. S., "Physiological responses to simulated firefighter exercise protocols in varying environments," *Ergonomics*, Vol. 58, No. 6, 2015, pp. 1012–1021.

[99] Jonker, D., Rolander, B., Balogh, I., Sandsjo, L., Ekberg, K., and Winkel, J., "Rationalisation in public dental care - impact on clinical work tasks and mechanical exposure for dentists - a prospective study," *Ergonomics*, Vol. 56, No. 2, 2013, pp. 303–313.

[100] Möller, T., Mathiassen, S. E., Franzon, H., and Kihlberg, S., "Job enlargement and mechanical exposure variability in cyclic assembly work," *Ergonomics*, Vol. 47, No. 1, 2004, pp. 19–40.

[101] Moser, D. J., Graham, R. B., Stevenson, J. M., and Costigan, P. A., "Subjective and objective analysis of three water pump systems carried by forest firefighters," *Work-a Journal of Prevention Assessment & Rehabilitation*, Vol. 47, No. 1, 2014, pp. 45–53.

[102] Ribeiro, D. C., Sole, G., Abbott, J. H., and Milosavljevic, S., "Cumulative postural exposure measured by a novel device: a preliminary study," *Ergonomics*, Vol. 54, No. 9, 2011, pp. 858–865.

[103] Ribeiro, D. C., Milosavljevic, S., and Abbott, J. H., "Effectiveness of a lumbopelvic monitor and feedback device to change postural behaviour: a protocol for the ELF cluster randomised controlled trial," *BMJ Open*, Vol. 7, No. 1, 2017, pp. e015568.

[104] Samani, A., Holtermann, A., Søgaard, K., Holtermann, A., and Madeleine, P., "Following ergonomics guidelines decreases physical and cardiovascular workload during cleaning tasks," *Ergonomics*, Vol. 55, No. 3, 2012, pp. 295.

[105] Schall Jr., M. C., Fethke, N. B., and Chen, H., "Working postures and physical activity among registered nurses," *Applied Ergonomics*, Vol. 54, 2016, pp. 243.

[106] Shafti, A., Lazpita, B. U., Elhage, O., Wurdemann, H. A., and Althoefer, K., "Analysis of comfort and ergonomics for clinical work environments," *Conf Proc IEEE Eng Med Biol Soc*, Vol. 2016, 2016, pp. 1894–1897.

[107] Singh, R., Carranza Leon, D. A., Morrow, M. M., Vos-Draper, T. L., Mc Gree, M. E., Weaver, A. L., Woolley, S. M., Hallbeck, S., and Gebhart, J. B., "Effect of chair types on work-related musculoskeletal discomfort during vaginal surgery," *Am J Obstet Gynecol*, Vol. 215, No. 5, 2016, pp. 648.e1–648.e9.

[108] Vinstrup, J., Madeleine, P., Jakobsen, M. D., Jay, K., and Andersen, L. L., "Patient Transfers and Risk of Back Injury: Protocol for a Prospective Cohort Study With Technical Measurements of Exposure," *Jmir Research Protocols*, Vol. 6, No. 11, 2017.

[109] Fathallah, F. A., Marras, W. S., and Parnianpour, M., "An assessment of complex spinal loads during dynamic lifting tasks," *Spine*, Vol. 23, No. 6, 1998, pp. 706–716.

[110] Wahlström, J., Bergsten, E., Trask, C., Mathiassen, S. E., Jackson, J., and Forsman, M., "Full-shift trunk and upper arm postures and movements among aircraft baggage handlers," *Annals of Occupational Hygiene*, Vol. 60, No. 8, 2016, pp. 977–990.

[111] Standard, B., "Safety of machinery: Human physical performance," *BS EN*, 2005, pp. 1005–4.

[112] Mokhlespour Esfahani, M. I. and Nussbaum, M. A., "A"Smart"Undershirt for Tracking Upper Body Motions: Task Classification and Angle Estimation," *IEEE Sensors Journal*, Vol. 18, 2018, pp. 7650–7658.

[113] Beeler, N., Roos, L., Delves, S. K., Veenstra, B. J., Friedl, K., Buller, M. J., and Wyss, T., "The Wearing Comfort and Acceptability of Ambulatory Physical Activity Monitoring Devices in Soldiers," *IISE Transactions on Occupational Ergonomics and Human Factors*, Vol. 6, No. 1, 2018, pp. 1–10.

[114] Mokhlespour Esfahani, M. I., Nussbaum, M. A., and Kong, Z., "Using a Smart Textile System for Classifying Occupational Manual Material Handling Tasks: Evidence from Lab-based Simulations," *Ergonomics*, , No. just-accepted, 2019, pp. 1–25.

[115] Burdorf, A., Rossignol, M., Fathallah, F. A., Snook, S. H., and Herrick, R. F., "Challenges in assessing risk factors in epidemiologic studies on back disorders," *American journal of industrial medicine*, Vol. 32, No. 2, 1997, pp. 142–152.

[116] Chung, A. Z. and Shorrock, S. T., "The research-practice relationship in ergonomics and human factorsâĂŞsurveying and bridging the gap," *Ergonomics*, Vol. 54, No. 5, 2011, pp. 413–429.

[117] Dempsey, P. G. and Mathiassen, S. E., "On the evolution of task-based analysis of manual materials handling, and its applicability in contemporary ergonomics," *Applied Ergonomics*, Vol. 37, No. 1, 2006, pp. 33–43.

[118] Oshima, Y., Kawaguchi, K., Tanaka, S., Ohkawara, K., Hikihara, Y., Ishikawa-Takata, K., and Tabata, I., "Classifying household and locomotive activities using a triaxial accelerometer," *Gait Posture*, Vol. 31, No. 3, 2010, pp. 370–4.

[119] Ravi, N., Dandekar, N., Mysore, P., and Littman, M. L., "Activity Recognition from Accelerometer Data." *AAAI*, Vol. 3, 2005, pp. 1541–1546.

[120] Bagala, F., Becker, C., Cappello, A., Chiari, L., Aminian, K., Hausdorff, J. M., Zijlstra, W., and Klenk, J., "Evaluation of accelerometer-based fall detection algorithms on real-world falls," *PloS one*, Vol. 7, No. 5, 2012, pp. e37062.

[121] Schwickert, L., Becker, C., Lindemann, U., Marechal, C., Bourke, A., Chiari, L., Helbostad, J., Zijlstra, W., Aminian, K., and Todd, C., "Fall detection with body-worn sensors," *Zeitschrift fur Gerontologie und Geriatrie*, Vol. 46, No. 8, 2013, pp. 706–719.

[122] Wu, G. and Xue, S., "Portable preimpact fall detector with inertial sensors," *IEEE Transactions on Neural Systems and Rehabilitation Engineering*, Vol. 16, No. 2, 2008, pp. 178–183.

[123] Lim, S. and D'Souza, C., "Statistical Prediction of Hand Force Exertion Levels in a Simulated Push Task using Posture Kinematics," *Proceedings of the Human Factors and Ergonomics Society Annual Meeting*, Vol. 61, SAGE Publications Sage CA: Los Angeles, CA, 2017, pp. 1031–1035.

[124] Lim, S. and D'Souza, C., "Inertial Sensor-based Measurement of Thoracic-Pelvic Coordination Predicts Hand-Load Levels in Two-handed Anterior Carry," *Proceedings of the Human Factors and Ergonomics Society Annual Meeting*, Vol. 62, SAGE Publications Sage CA: Los Angeles, CA, 2018, pp. 798–799.

[125] Lim, S. and D'Souza, C., "Statistical prediction of load carriage mode and magnitude from inertial sensor derived gait kinematics," *Applied Ergonomics*, Vol. 76, 2019, pp. 1–11.

[126] Lim, S. and D'Souza, C., "Measuring effects of two-handed side and anterior load carriage on gait kinematics using wearable inertial sensors," under review.

[127] Orr, R. M. and Pope, R. R., "Load Carriage: An Integrated Risk Management Approach," *The Journal of Strength & Conditioning Research*, Vol. 29, 2015, pp. S119–S128.

[128] Park, K., Hur, P., Rosengren, K. S., Horn, G. P., and Hsiao-Wecksler, E. T., "Effect of load carriage on gait due to firefighting air bottle configuration," *Ergonomics*, Vol. 53, No. 7, 2010, pp. 882–891.

[129] Anderson, A., Meador, K., McClure, L., Makrozahopoulos, D., Brooks, D., and Mirka, G., "A biomechanical analysis of anterior load carriage," *Ergonomics*, Vol. 50, No. 12, 2007, pp. 2104–2117.

[130] Knapik, J., Harman, E., and Reynolds, K., "Load carriage using packs: a review of physiological, biomechanical and medical aspects," *Applied ergonomics*, Vol. 27, No. 3, 1996, pp. 207–216.

[131] Dalen, A., Nilsson, J., and Thorstensson, A., *Factors influencing a prolonged foot march*, 1978.

[132] LaFiandra, M., Holt, K. G., Wagenaar, R. C., and Obusek, J. P., "Transverse plane kinetics during treadmill walking with and without a load," *Clinical Biomechanics*, Vol. 17, No. 2, 2002, pp. 116–122.

[133] Nottrodt, J. W. and Manley, P., "Acceptable loads and locomotor patterns selected in different carriage methods," *Ergonomics*, Vol. 32, No. 8, 1989, pp. 945–957.

[134] Matsuo, T., Hashimoto, M., Koyanagi, M., and Hashizume, K., "Asymmetric load-carrying in young and elderly women: Relationship with lower limb coordination," *Gait & posture*, Vol. 28, No. 3, 2008, pp. 517–520.

[135] Neumann, D. A., Cook, T. M., Sholty, R. L., and Sobush, D. C., "An electromyographic analysis of hip abductor muscle activity when subjects are carrying loads in one or both hands," *Physical Therapy*, Vol. 72, No. 3, 1992, pp. 207–217.

[136] DeVita, P., Hong, D., and Hamill, J., "Effects of asymmetric load carrying on the biomechanics of walking," *Journal of biomechanics*, Vol. 24, No. 12, 1991, pp. 1119–1129.

[137] Cook, T. M. and Neumann, D. A., "The effects of load placement on the EMG activity of the low back muscles during load carrying by men and women," *Ergonomics*, Vol. 30, No. 10, 1987, pp. 1413–1423.

[138] McGill, S. M., Marshall, L., and Andersen, J., "Low back loads while walking and carrying: comparing the load carried in one hand or in both hands," *Ergonomics*, Vol. 56, No. 2, 2013, pp. 293–302.

[139] Marras, W. S. and Granata, K. P., "Changes in trunk dynamics and spine loading during repeated trunk exertions," *Spine (Phila Pa 1976)*, Vol. 22, No. 21, 1997, pp. 2564–70.

[140] Rose, J. D., Mendel, E., and Marras, W. S., "Carrying and spine loading," *Ergonomics*, Vol. 56, No. 11, 2013, pp. 1722–1732.

[141] Zhang, X. A., Ye, M., and Wang, C. T., "Effect of unilateral load carriage on postures and gait symmetry in ground reaction force during walking," *Computer methods in biomechanics and biomedical engineering*, Vol. 13, No. 3, 2010, pp. 339–344.

[142] Rohlmann, A., Zander, T., Graichen, F., Schmidt, H., and Bergmann, G., "How does the way a weight is carried affect spinal loads?" *Ergonomics*, Vol. 57, No. 2, 2014, pp. 262–270.

[143] LaFiandra, M., Wagenaar, R. C., Holt, K. G., and Obusek, J. P., "How do load carriage and walking speed influence trunk coordination and stride parameters?" *Journal of biomechanics*, Vol. 36, No. 1, 2003, pp. 87–95.

[144] Goh, J. H., Thambyah, A., and Bose, K., "Effects of varying backpack loads on peak forces in the lumbosacral spine during walking," *Clinical Biomechanics*, Vol. 13, No. 1, 1998, pp. S26–S31.

[145] Hong, Y. and Cheung, C.-K., "Gait and posture responses to backpack load during level walking in children," *Gait & posture*, Vol. 17, No. 1, 2003, pp. 28–33.

[146] Kinoshita, H., "Effects of different loads and carrying systems on selected biomechanical parameters describing walking gait," *Ergonomics*, Vol. 28, No. 9, 1985, pp. 1347–1362.

[147] Qu, X. and Yeo, J. C., "Effects of load carriage and fatigue on gait characteristics," *Journal of biomechanics*, Vol. 44, No. 7, 2011, pp. 1259–1263.

[148] Majumdar, D., Pal, M. S., and Majumdar, D., "Effects of military load carriage on kinematics of gait," *Ergonomics*, Vol. 53, No. 6, 2010, pp. 782–791.

[149] Pau, M., Kim, S., and Nussbaum, M. A., "Does load carriage differentially alter postural sway in overweight vs. normal-weight schoolchildren?" *Gait & posture*, Vol. 35, No. 3, 2012, pp. 378–382.

[150] Cottalorda, J., Rahmani, A., Diop, M., Gautheron, V., Ebermeyer, E., and Belli, A., "Influence of school bag carrying on gait kinetics," *Journal of Pediatric Orthopaedics B*, Vol. 12, No. 6, 2003, pp. 357–364.

[151] Ghori, G. M. U. and Luckwill, R. G., "Responses of the lower limb to load carrying in walking man," *European journal of applied physiology and occupational physiology*, Vol. 54, No. 2, 1985, pp. 145–150.

[152] Burgess-Limerick, R., Abernethy, B., and Neal, R. J., "Relative phase quantifies interjoint coordination," *Journal of biomechanics*, Vol. 26, No. 1, 1993, pp. 91–94.

[153] Seay, J. F., Van Emmerik, R. E. A., and Hamill, J., "Low back pain status affects pelvis-trunk coordination and variability during walking and running," *Clinical biomechanics*, Vol. 26, No. 6, 2011, pp. 572–578.

[154] van Emmerik, R. E. A. and Wagenaar, R. C., "Effects of walking velocity on relative phase dynamics in the trunk in human walking," *Journal of biomechanics*, Vol. 29, No. 9, 1996, pp. 1175–1184.

[155] Whittle, M. W. and Levine, D., "Three-dimensional relationships between the movements of the pelvis and lumbar spine during normal gait," *Human Movement Science*, Vol. 18, No. 5, 1999, pp. 681–692.

[156] Graham, R. B., Smallman, C. L. W., Miller, R. H., and Stevenson, J. M., "A dynamical systems analysis of assisted and unassisted anterior and posterior hand-held load carriage," *Ergonomics*, Vol. 58, No. 3, 2015, pp. 480–491.

[157] Mayagoitia, R. E., Lotters, J. C., Veltink, P. H., and Hermens, H., "Standing balance evaluation using a triaxial accelerometer," *Gait & Posture*, Vol. 16, No. 1, 2002, pp. 55–59.

[158] Faber, G. S., Chang, C. C., Rizun, P., and Dennerlein, J. T., "A novel method for assessing the 3-D orientation accuracy of inertial/magnetic sensors," *J Biomech*, Vol. 46, No. 15, 2013, pp. 2745–51.

[159] Sabatini, A. M., "Estimating three-dimensional orientation of human body parts by inertial/magnetic sensing," *Sensors*, Vol. 11, No. 2, 2011, pp. 1489–1525.

[160] Aminian, K., Najafi, B., Büla, C., Leyvraz, P.-F., and Robert, P., "Spatio-temporal parameters of gait measured by an ambulatory system using miniature gyroscopes," *Journal of biomechanics*, Vol. 35, No. 5, 2002, pp. 689–699.

[161] Djuric, M., "Automatic recognition of gait phases from accelerations of leg segments," *Neural Network Applications in Electrical Engineering*, IEEE, pp. 121–124.

[162] Hanlon, M. and Anderson, R., "Real-time gait event detection using wearable sensors," *Gait & posture*, Vol. 30, No. 4, 2009, pp. 523–527.

[163] Jasiewicz, J. M., Allum, J. H. J., Middleton, J. W., Barriskill, A., Condie, P., Purcell, B., and Li, R. C. T., "Gait event detection using linear accelerometers or angular velocity transducers in able-bodied and spinal-cord injured individuals," *Gait & Posture*, Vol. 24, No. 4, 2006, pp. 502–509.

[164] Lee, S. W., Mase, K., and Kogure, K., "Detection of spatio-temporal gait parameters by using wearable motion sensors," *2005 IEEE Engineering in Medicine and Biology 27th Annual Conference*, IEEE, pp. 6836–6839.

[165] Cohen, A. L., Gjessing, C. C., Fine, L. J., Bernard, B. P., and McGlothlin, J. D., *Elements of ergonomics programs: a primer based on workplace evaluations of musculoskeletal disorders*, Vol. 97, DIANE Publishing, 1997.

[166] Williamson, R. and Andrews, B. J., "Detecting Absolute Human Knee Angle," *Medical and Biological Engineering and Computing*, Vol. 39, No. 3, 2001, pp. 294–302.

[167] Moon, Y., McGinnis, R. S., Seagers, K., Motl, R. W., Sheth, N., Wright Jr, J. A., Ghaffari, R., and Sosnoff, J. J., "Monitoring gait in multiple sclerosis with novel wearable motion sensors," *PLoS One*, Vol. 12, No. 2, 2017, pp. e0171346.

[168] Salarian, A., Russmann, H., Vingerhoets, F. J., Burkhard, P. R., and Aminian, K., "Ambulatory monitoring of physical activities in patients with Parkinson's disease," *IEEE Trans Biomed Eng*, Vol. 54, No. 12, 2007, pp. 2296–9.

[169] Wagenaar, R. C. and Beek, W. J., "Hemiplegic gait: a kinematic analysis using walking speed as a basis," *Journal of biomechanics*, Vol. 25, No. 9, 1992, pp. 1007–1015.

[170] Snijders, T. A. B. and Bosker, R. J., *Multilevel analysis: an introduction to basic and advanced multilevel modeling*, Sage, 1999.

[171] Elftman, H., "The function of the arms in walking," *Human biology*, Vol. 11, No. 4, 1939, pp. 529.

[172] Madinei, S. and Ning, X., "Effects of the weight configuration of hand load on trunk musculature during static weight holding," *Ergonomics*, Vol. 61, No. 6, 2018, pp. 831–838.

[173] Birrell, S. A. and Haslam, R. A., "The influence of rifle carriage on the kinetics of human gait," *Ergonomics*, Vol. 51, No. 6, 2008, pp. 816–826.

[174] Martin, P. E. and Nelson, R. C., "The effect of carried loads on the walking patterns of men and women," *Ergonomics*, Vol. 29, No. 10, 1986, pp. 1191–1202.

[175] Barbieri, F. A., Dos Santos, P. C. R., Lirani-Silva, E., Vitório, R., Gobbi, L. T. B., and Van Diëen, J. H., "Systematic review of the effects of fatigue on spatiotemporal gait parameters," *Journal of back and musculoskeletal rehabilitation*, Vol. 26, No. 2, 2013, pp. 125–131.

[176] Helbostad, J. L., Leirfall, S., Moe-Nilssen, R., and Sletvold, O., "Physical fatigue affects gait characteristics in older persons," *The Journals of Gerontology Series A: Biological Sciences and Medical Sciences*, Vol. 62, No. 9, 2007, pp. 1010–1015.

[177] Kelsey, J. L., Githens, P. B., White, A. A., Holford, T. R., Walter, S. D., O'Connor, T., Ostfeld, A. M., Weil, U., Southwick, W. O., and Calogero, J. A., "An epidemiologic study of lifting and twisting on the job and risk for acute prolapsed lumbar intervertebral disc," *Journal of Orthopaedic Research*, Vol. 2, No. 1, 1984, pp. 61–66.

[178] Cheng, T.-S. and Lee, T.-H., "Maximum acceptable weight of manual load carriage for young Taiwanese males," *Industrial health*, Vol. 44, No. 1, 2006, pp. 200–206.

[179] Gallagher, S. and Marras, W. S., "Tolerance of the lumbar spine to shear: a review and recommended exposure limits," *Clinical Biomechanics*, Vol. 27, No. 10, 2012, pp. 973–978.

[180] Coley, B., Najafi, B., Paraschiv-Ionescu, A., and Aminian, K., "Stair climbing detection during daily physical activity using a miniature gyroscope," *Gait Posture*, Vol. 22, No. 4, 2005, pp. 287–94.

[181] Sabatini, A. M., Martelloni, C., Scapellato, S., and Cavallo, F., "Assessment of walking features from foot inertial sensing," *IEEE Transactions on biomedical engineering*, Vol. 52, No. 3, 2005, pp. 486–494.

[182] Stiefmeier, T., Lombriser, C., Roggen, D., Junker, H., Ogris, G., and Tröster, G., "Event-based activity tracking in work environments," *International Forum on 3rd Applied Wearable Computing (IFAWC)*, VDE, 2006, pp. 1–10.

[183] Lin, F., Song, C., Xu, X., Cavuoto, L., and Xu, W., "Patient Handling Activity Recognition Through Pressure-Map Manifold Learning Using a Footwear Sensor," *Smart Health*, 2017.

[184] Baghdadi, A., Megahed, F. M., Esfahani, E. T., and Cavuoto, L. A., "A machine learning approach to detect changes in gait parameters following a fatiguing occupational task," *Ergonomics*, 2018, pp. 1–14.

[185] Janssen, D., Schöllhorn, W. I., Newell, K. M., Jäger, J. M., Rost, F., and Vehof, K., "Diagnosing fatigue in gait patterns by support vector machines and self-organizing maps," *Human movement science*, Vol. 30, No. 5, 2011, pp. 966–975.

[186] Zhang, J., Lockhart, T. E., and Soangra, R., "Classifying lower extremity muscle fatigue during walking using machine learning and inertial sensors," *Annals of biomedical engineering*, Vol. 42, No. 3, 2014, pp. 600–612.

[187] Lee, M., *Biomechanical adaptations of human gait due to external loads*, Thesis, 2008.

[188] Oldfield, R., "The assessment and analysis of handedness - the Edinburgh inventory." *Neuropsychologia*, Vol. 9, No. 1, 1971, pp. 97–113.

[189] Snook, S. H. and Ciriello, V. M., "The design of manual handling tasks: revised tables of maximum acceptable weights and forces," *Ergonomics*, Vol. 34, No. 9, 1991, pp. 1197–1213.

[190] Breiman, L., "Random forests," *Machine learning*, Vol. 45, No. 1, 2001, pp. 5–32.

[191] Liaw, A. and Wiener, M., "Classification and regression by randomForest," *R news*, Vol. 2, No. 3, 2002, pp. 18–22.

[192] Box, G. E. and Tiao, G. C., *Bayesian inference in statistical analysis*, Vol. 40, John Wiley & Sons, 2011.

[193] Hastie, T., Tibshirani, R., and Friedman, J., *The elements of statistical learning: Data Mining, Inference, and Prediction*, Springer, 2008.

[194] Boulesteix, A., Janitza, S., Kruppa, J., and KÃűnig, I. R., "Overview of random forest methodology and practical guidance with emphasis on computational biology and bioinformatics," *Wiley Interdisciplinary Reviews: Data Mining and Knowledge Discovery*, Vol. 2, No. 6, 2012, pp. 493–507.

[195] Strobl, C., Boulesteix, A.-L., Zeileis, A., and Hothorn, T., "Bias in random forest variable importance measures: Illustrations, sources and a solution," *BMC bioinformatics*, Vol. 8, No. 1, 2007, pp. 25.

[196] Avci, A., Bosch, S., Marin-Perianu, M., Marin-Perianu, R., and Havinga, P., "Activity recognition using inertial sensing for healthcare, wellbeing and sports applications: A survey," *Architecture of computing systems (ARCS), 2010 23rd international conference on*, VDE, pp. 1–10.

[197] Keogh, E., Chu, S., Hart, D., and Pazzani, M., "An online algorithm for segmenting time series," *Proceedings IEEE International Conference on Data Mining*, IEEE, pp. 289–296.

[198] Liu, H., Motoda, H., Setiono, R., and Zhao, Z., "Feature selection: An ever evolving frontier in data mining," *Feature Selection in Data Mining*, pp. 4–13.

[199] Bieber, G. and Peter, C., "Using physical activity for user behavior analysis," *Proceedings of the 1st international conference on PErvasive Technologies Related to Assistive Environments*, ACM, p. 94.

[200] Anand, R., Mehrotra, K., Mohan, C. K., and Ranka, S., "Efficient classification for multiclass problems using modular neural networks," *IEEE Transactions on Neural Networks*, Vol. 6, No. 1, 1995, pp. 117–124.

[201] Lim, S., Case, A., and D'Souza, C., "Comparative Analysis of Inertial Sensor to Optical Motion Capture System Performance in Push-Pull Exertion Postures," *Proceedings of the Human Factors and Ergonomics Society Annual Meeting*, Vol. 60, SAGE Publications Sage CA: Los Angeles, CA, pp. 970–974.

[202] Mathie, M., Celler, B. G., Lovell, N. H., and Coster, A., "Classification of basic daily movements using a triaxial accelerometer," *Medical and Biological Engineering and Computing*, Vol. 42, No. 5, 2004, pp. 679–687.

[203] Madinei, S. and Ning, X., "Effects of the Weight Configuration of Hand Load on Trunk Musculature during Static Weight Holding," *Ergonomics*, Vol. 61, No. 6, 2017, pp. 831–838.

[204] Ko, S.-u., Hausdorff, J. M., and Ferrucci, L., "Age-associated differences in the gait pattern changes of older adults during fast-speed and fatigue conditions: results from the Baltimore longitudinal study of ageing," *Age and ageing*, Vol. 39, No. 6, 2010, pp. 688–694.

[205] Mazzà, C., Iosa, M., Picerno, P., and Cappozzo, A., "Gender differences in the control of the upper body accelerations during level walking," *Gait & posture*, Vol. 29, No. 2, 2009, pp. 300–303.

[206] Cau, N., Cimolin, V., Galli, M., Precilios, H., Tacchini, E., Santovito, C., and Capodaglio, P., "Center of pressure displacements during gait initiation in individuals with obesity," *J Neuroeng Rehabil*, Vol. 11, 2014, pp. 82.

[207] Pamukoff, D. N., Dudley, R. I., Vakula, M. N., and Blackburn, J. T., "An evaluation of the heel strike transient in obese young adults during walking gait," *Gait & Posture*, Vol. 49, 2016, pp. 181–183.

[208] Lord, S. R., Lloyd, D. G., Nirui, M., Raymond, J., Williams, P., and Stewart, R. A., "The effect of exercise on gait patterns in older women: a randomized controlled trial," *The Journals of Gerontology Series A: Biological Sciences and Medical Sciences*, Vol. 51, No. 2, 1996, pp. M64–M70.

[209] Nigg, B., Fisher, V., and Ronsky, J., "Gait characteristics as a function of age and gender," *Gait & posture*, Vol. 2, No. 4, 1994, pp. 213–220.

[210] Yoshino, K., Motoshige, T., Araki, T., and Matsuoka, K., "Effect of prolonged free-walking fatigue on gait and physiological rhythm," *Journal of biomechanics*, Vol. 37, No. 8, 2004, pp. 1271–1280.

[211] Zehr, J. D., Howarth, S. J., and Beach, T. A., "Using relative phase analyses and vector coding to quantify Pelvis-Thorax coordination during lifting-A methodological investigation," *Journal of Electromyography and Kinesiology*, Vol. 39, 2018, pp. 104–113.

[212] Kuiper, J. I., Burdorf, A., Verbeek, J. H., Frings-Dresen, M. H., van der Beek, A. J., and Viikari-Juntura, E. R., "Epidemiologic evidence on manual materials handling as a risk factor for back disorders: a systematic review," *International Journal of Industrial Ergonomics*, Vol. 24, No. 4, 1999, pp. 389–404.

[213] Fathallah, F. A., Marras, W. S., and Wright, P. L., "Diurnal variation in trunk kinematics during a typical work shift." *Journal of spinal disorders*, Vol. 8, No. 1, 1995, pp. 20–25.

[214] Marras, W., "Occupational low back disorder causation and control," *Ergonomics*, Vol. 43, No. 7, 2000, pp. 880–902.

[215] Shannon, R. H., *Determination of efficient methods of lift by comparing trained and untrained male and female lifters*, Ph.D. thesis, Texas Tech University, 1978.

[216] Herrin, G., Chaffin, D., and Mach, R., "Criteria for Research on the Hazards of Manual Materials Handling, NIOSH Report," 1974.

[217] Davis, K. G. and Marras, W. S., "Assessment of the relationship between box weight and trunk kinematics: does a reduction in box weight necessarily correspond to a decrease in spinal loading?" *Human Factors: The Journal of the Human Factors and Ergonomics Society*, Vol. 42, No. 2, 2000, pp. 195–208.

[218] Hu, B., N. X. and Nussbaum, M. A., "The influence of hand load on lumbar-pelvic coordination during lifting task." *In Proceedings of the Human Factors and Ergonomics Society Annual Meeting*, Vol. 58, No. 1, 2014, pp. 1617–1621.

[219] Labor Inspection Authority, https://arbejdstilsynet.dk/da/regler/at-vejledninger/l/d-3-1-loft-traek-og-skub, 2005, [Online; accessed 04-25-2019].

[220] Boston, J. R., Rudy, T. E., Mercer, S. R., and Kubinski, J. A., "A measure of body movement coordination during repetitive dynamic lifting," *IEEE Transactions on Rehabilitation Engineering*, Vol. 1, No. 3, 1993, pp. 137–144.

[221] Sangachin, M. G. and Cavuoto, L. A., "Obesity-related changes in prolonged repetitive lifting performance," *Applied Ergonomics*, Vol. 56, 2016, pp. 19–26.

[222] Stobbe, T. J., "The Development of a Practical Strength Testing Program for Industry." 1983.

[223] Lamoth, C., Beek, P. J., and Meijer, O. G., "Pelvis-thorax coordination in the transverse plane during gait," *Gait & posture*, Vol. 16, No. 2, 2002, pp. 101–114.

[224] Rudy, T. E., Boston, J. R., Lieber, S. J., Kubinski, J. A., and Stacey, B. R., "Body motion during repetitive isodynamic lifting: a comparative study of normal subjects and low-back pain patients," *Pain*, Vol. 105, No. 1-2, 2003, pp. 319–326.

[225] Hogan, N. and Flash, T., "Moving gracefully: Quantitative theories of motor coordination," *Trends in Neurosciences*, Vol. 10, No. 4, 1987, pp. 170–174.

[226] Chen, H., Schall Jr, M. C., and Fethke, N., "Accuracy of angular displacements and velocities from inertial-based inclinometers," *Applied ergonomics*, Vol. 67, 2018, pp. 151–161.

[227] Genuer, R., Poggi, J.-M., and Tuleau-Malot, C., "VSURF: an R package for variable selection using random forests," *The R Journal*, Vol. 7, No. 2, 2015, pp. 19–33.

[228] NIOSH, *A Work Practices Guide for Manual Lifting*, No. 81, U.S. Dept. of health and Human Services (NIOSH), 1981.

[229] O'Neil, C., *Weapons of math destruction: How big data increases inequality and threatens democracy*, Broadway Books, 2017.

[230] Zemel, R., Wu, Y., Swersky, K., Pitassi, T., and Dwork, C., "Learning fair representations," *International Conference on Machine Learning*, 2013, pp. 325–333.

[231] Faber, G. S., Kingma, I., Bruijn, S. M., and van DieÃńn, J. H., "Optimal inertial sensor location for ambulatory measurement of trunk inclination," *Journal of biomechanics*, Vol. 42, No. 14, 2009, pp. 2406–2409.

[232] Pedersen, E. S. L., Danquah, I., Petersen, C., and Tolstrup, J., "Intra-individual variability in day-to-day and month-to-month measurements of physical activity and sedentary behaviour at work and in leisure-time among Danish adults," *BMC public health*, Vol. 16, No. 1, 2016, pp. 1222.

[233] Stemland, I., Ingebrigtsen, J., Christiansen, C. S., Jensen, B. R., Hanisch, C., Skotte, J., and Holtermann, A., "Validity of the Acti4 method for detection of physical activity types in free-living settings: comparison with video analysis," *Ergonomics*, Vol. 58, No. 6, 2015, pp. 953–965.

[234] Drillis, R., Contini, R., and Bluestein, M., *Body segment parameters*, New York University, School of Engineering and Science, 1969.

[235] Plagenhoef, S., *Patterns of human motion: A cinematographic analysis*, Prentice Hall, 1971.

[236] Chaffin, D. B., Andersson, G., and Martin, B. J., *Occupational biomechanics*, Wiley New York, 1999.